

**DOCTORAL THESIS**

# The Role of Heterogeneity in the Dynamics of Excitable Cell Networks

Stefano Scialla

TALLINN UNIVERSITY OF TECHNOLOGY  
DOCTORAL THESIS  
97/2025

# **The Role of Heterogeneity in the Dynamics of Excitable Cell Networks**

STEFANO SCIALLA



TALLINN UNIVERSITY OF TECHNOLOGY  
School of Science  
Department of Cybernetics

NATIONAL INSTITUTE OF CHEMICAL PHYSICS AND BIOPHYSICS  
Laboratory of Chemical Biology

**The dissertation was accepted for the defence of the doctoral degree in Applied Physics and Mathematics on 15 October 2025.**

**Supervisor:** Dr. Marco Patriarca,  
<sup>1</sup>National Institute of Chemical Physics and Biophysics  
Tallinn, Estonia  
<sup>2</sup>Department of Cybernetics, School of Science  
Tallinn University of Technology  
Tallinn, Estonia

**Co-supervisor:** Dr. Els Heinsalu,  
National Institute of Chemical Physics and Biophysics  
Tallinn, Estonia

**Opponents:** Prof. Marko Gosak,  
Department of Physics  
University of Maribor  
Maribor, Slovenia  
  
Prof. Pere Colet,  
Instituto de Física Interdisciplinar y Sistemas Complejos  
Campus Universitat de les Illes Balears  
Palma de Mallorca, Spain

**Defence of the thesis:** 18 December 2025, Tallinn

**Declaration:**

*Hereby I declare that this doctoral thesis, my original investigation and achievement, submitted for the doctoral degree at Tallinn University of Technology, has not been submitted for any academic degree elsewhere.*

Stefano Scialla

---

signature

Copyright: Stefano Scialla, 2025  
ISSN 2585-6898 (publication)  
ISBN 978-9916-80-425-4 (publication)  
ISSN 2585-6901 (PDF)  
ISBN 978-9916-80-426-1 (PDF)  
DOI <https://doi.org/10.23658/taltech.97/2025>  
Printed by Koopia Niini & Rauam

Scialla, S. (2025). *The Role of Heterogeneity in the Dynamics of Excitable Cell Networks* [TalTech Press]. <https://doi.org/10.23658/taltech.97/2025>

TALLINNA TEHNIKAÜLIKOOL  
DOKTORITÖÖ  
97/2025

# Heterogeensuse roll ergastatavate rakuvõrgustike dünaamikas

STEFANO SCIALLA





# Contents

List of Publications .....	8
Author's Contributions to the Publications .....	9
Abbreviations.....	11
INTRODUCTION.....	12
1 ELECTROPHYSIOLOGY AND HETEROGENEITY OF EXCITABLE CELLS AND PANCREATIC $\beta$ -CELLS .....	16
1.1 Electrophysiology of Excitable Cells .....	16
1.2 $\beta$ -Cells and Insulin Production Mechanism .....	17
1.3 Relevance of Cellular Heterogeneity .....	19
2 MODELING OF $\beta$ -CELLS.....	22
2.1 Models of Single $\beta$ -Cells .....	22
2.1.1 Chay-Keizer Model .....	22
2.1.2 Phantom Burster Model .....	22
2.1.3 Dual Oscillator Model .....	24
2.2 Modeling of $\beta$ -Cell Clusters.....	25
2.2.1 Dynamical Models of Electrically Coupled Cells .....	25
2.2.1.1 <i>Sherman and Rinzel Model</i> .....	26
2.2.1.2 <i>Saadati and Jamali Model</i> .....	27
2.2.2 Models Based on Percolation Theory .....	28
2.2.2.1 <i>Stamper, Jackson, and Wang Model</i> .....	29
3 MODELS OF COUPLED OSCILLATORS .....	31
3.1 FitzHugh-Nagumo Oscillator .....	31
3.2 Heterogeneity in Coupled Oscillator Networks .....	35
3.2.1 Cartwright Model.....	36
3.2.2 Diversity-Induced Resonance .....	36
3.2.3 Other DIR models .....	38
3.3 3D Model Based on Heterogeneous FHN Units .....	38
3.3.1 Choice of Model Parameters and Correlation with $\beta$ -Cell Physiology	39
3.3.2 Simulation Results and Estimate of Hub Percentage .....	41
3.3.3 Effect of Faster versus Slower Oscillations .....	43
3.3.4 Effect of Heterogeneity on Network Response to Varying Glucose Levels .....	43
4 HETEROGENEITY AND NOISE .....	46
4.1 Stochastic Resonance and Noise-Driven Resonance Phenomena .....	46
4.2 Role of Noise in Biological Systems.....	49
4.3 Diversity and Noise in Excitable Cell Networks .....	50
4.4 Interplay Between Diversity and Noise: A Quantitative Study .....	50
4.4.1 The Model .....	50
4.4.2 Qualitative Mean Field Analysis .....	51
4.4.3 Key Simulation Results and Discussion .....	54
4.4.4 Concluding Remarks.....	57

5	INHIBITORY EFFECTS OF DISORDER .....	58
5.1	Inverse Stochastic Resonance .....	58
5.2	Diversity Induced Decoherence .....	59
5.2.1	The Model .....	59
5.2.2	Analytic Study of the Effects of Diversity on SISR .....	61
5.2.2.1	Mean-Field Approximation. ....	61
5.2.2.2	Analysis of the Mean-Field Equations. ....	62
5.2.3	Numerical Simulations .....	64
5.2.4	Biological Relevance.....	66
6	UNDERSTANDING THE MECHANISM OF DIR .....	68
6.1	Dimer-Diffusion Resonance .....	68
6.2	Extension of DDR to a Polymer .....	70
6.2.1	Networks with Two Types of Oscillators.....	70
6.2.2	Networks with a Continuous Bias Distribution.....	73
6.3	DDR and Polymer Translocation in Networks of FHN Units .....	74
6.4	Final Considerations.....	75
7	SIMMETRY OF THE DIVERSITY DISTRIBUTION AS A DETERMINANT OF GLOBAL OSCILLATIONS .....	77
7.1	Model Framework.....	77
7.2	Mean-Field Analysis.....	78
7.3	Numerical Simulations .....	78
7.3.1	Symmetry Metrics.....	79
7.3.2	Half-normal Diversity Distributions.....	79
7.3.3	Normal Diversity Distributions.....	83
7.4	Two-Unit Reduction and Effective Potential .....	85
7.5	Discussion and Implications .....	87
	CONCLUSIONS .....	88
	List of Figures .....	92
	List of Tables .....	93
	References .....	94
	Acknowledgements .....	105
	Abstract.....	106
	Kokkuvõte .....	109
	Appendix 1.....	111
	Appendix 2 .....	121
	Appendix 3 .....	131
	Appendix 4 .....	139
	Appendix 5 .....	155

Curriculum Vitae .....	168
Elulookirjeldus.....	172

## List of Publications

The present Ph.D. thesis is based on the following publications that are referred to in the text by Roman numbers.

- I S. Scialla, A. Loppini, M. Patriarca, and E. Heinsalu, "Hubs, diversity, and synchronization in FitzHugh-Nagumo oscillator networks: Resonance effects and biophysical implications," *Phys. Rev. E*, vol. 103, p. 052211, 2021
- II S. Scialla, M. Patriarca, and E. Heinsalu, "The interplay between diversity and noise in an excitable cell network model," *EPL*, vol. 137, p. 51001, 2022
- III M. E. Yamakou, E. Heinsalu, M. Patriarca, and S. Scialla, "Diversity-induced decoherence," *Phys. Rev. E*, vol. 106, p. L032401, 2022
- IV M. Patriarca, S. Scialla, E. Heinsalu, M. E. Yamakou, and J. H. E. Cartwright, "Dynamical equivalence between resonant translocation of a polymer chain and diversity-induced resonance," *Chaos*, vol. 35, p. 073115, 2025
- V S. Scialla, M. Patriarca, E. Heinsalu, M. E. Yamakou, and J. H. E. Cartwright, "Effect of diversity distribution symmetry on global oscillations of networks of excitable units," *Phys. Rev. E*, vol. 112, p. 054201, 2025

## Author's Contributions to the Publications

- I In Ref. [I], I was the main author, wrote the simulation program, carried out the simulations and analysis of the results, prepared most of the figures, and wrote the manuscript.
- II In Ref. [II], I was the main and correspondent author, wrote the simulation program, carried out the simulations and analysis of the results, prepared most of the figures, and wrote the manuscript.
- III In Ref. [III], I contributed significantly to the ideation of the research project, provided fundamental input on the development of the mean-field approach and the analysis of the numerical results, and played an important role in the editing and revision of the manuscript.
- IV In Ref. [IV], I contributed significantly to the ideation of the research project, provided input on the analysis of the numerical results, and played an important role in the editing and revision of the manuscript.
- V In Ref. [V], I was the main and correspondent author, conceived the idea of the research project, wrote the simulation program, carried out the simulations and analysis of the results, prepared most of the figures, and wrote the manuscript.

## Approbation

I presented the results of the thesis at the following conferences:

1. S. Scialla, M. Patriarca, E. Heinsalu, M. E. Yamakou, and J. H. E. Cartwright. *Effect of diversity distribution symmetry on global oscillations of networks of excitable units*, Dynamics Days Europe 2025: 23–27 June 2025, Thessaloniki, Greece (contributed talk).
2. S. Scialla, M. Patriarca, E. Heinsalu, M. E. Yamakou, and J. H. E. Cartwright. *Asymmetry in the distribution of unit properties is the key factor determining the efficiency of collective oscillations in FitzHugh-Nagumo networks*, Conference on Complex Systems CCS 2024: 2–6 September 2024, Exeter, UK (contributed talk).
3. S. Scialla, A. Loppini, M. Patriarca, E. Heinsalu. *Hubs, diversity, and synchronization in FitzHugh Nagumo oscillator networks: Resonance effects and biophysical implications*, Conference on Complex Systems CCS 2021: 25–29 October 2021, Lyon, France (poster).
4. S. Scialla, M. Patriarca, E. Heinsalu. *Hubs, diversity, and noise in FitzHugh-Nagumo oscillator networks: Synchronization and Resonances*, SR 40 1981-2021 Forty Years of Stochastic Resonance: 13–15 September 2021, Perugia, Italy (contributed talk).

## Abbreviations

CR	Coherence Resonance
DDR	Dimer Diffusion Resonance
DID	Diversity-Induced Decoherence
DIR	Diversity-Induced Resonance
FHN	FitzHugh-Nagumo
ISR	Inverse Stochastic Resonance
SISR	Self-Induced Stochastic Resonance
SR	Stochastic Resonance

# INTRODUCTION

Understanding the collective dynamics of excitable systems has long been a central objective in the study of nonlinear phenomena, with important implications for physiology, neuroscience, and more in general complex systems. Among the most relevant biological instances of excitable media are pancreatic  $\beta$ -cells, whose ability to coordinate electrical activity across a network is critical to the regulation of insulin secretion and, as a consequence, to glucose homeostasis. Theoretical modeling of these systems not only helps develop a mechanistic interpretation of emergent behaviors, but also offers predictive insight into how variations at the cellular or network level may affect functionality, robustness, or pathological conditions. This thesis is situated at the intersection of dynamical systems theory, cellular modeling, and systems biology, investigating how the collective dynamics of coupled heterogeneous excitable units, particularly  $\beta$ -cell clusters, can be better understood through suitably simplified mathematical models [6–8].

Despite their simplicity, models such as the FitzHugh–Nagumo (FHN) oscillator have proven instrumental in capturing essential features of excitable cell dynamics [9–11]. In addition, various studies have validated the use of reduced models for elucidating the role of heterogeneity, coupling, and noise in excitable systems [12–16]. Yet, as explained in more detail below, many open questions remain about how these factors jointly influence collective properties such as synchronization, excitability, and resonance, as well as about the underlying mechanisms. The present thesis contributes to this discussion by systematically analyzing the impact of heterogeneity on network behavior across a range of topologies, both on its own and in combination with stochastic fluctuations. By leveraging models such as the FHN and quartic oscillators, it offers new insight into the network dynamics and key mechanisms.

## Motivation

The main aim of this thesis work is to advance the understanding of how heterogeneity shapes collective dynamics in excitable cell networks, with particular focus on biologically relevant systems such as pancreatic  $\beta$ -cell clusters.

The motivation for studying the role of heterogeneity in networks of excitable cells, and  $\beta$ -cells in particular, is multifold.  $\beta$ -cells play a central role in metabolic regulation through the secretion of insulin, a process that is tightly controlled by oscillatory electrical and calcium ion activity [17, 18]. To perform this crucial function,  $\beta$ -cells operate as a coordinated ensemble of heterogeneous units, exhibiting collective behaviors such as synchronization of bursting across islets [19]. These phenomena are believed to enhance the effectiveness and robustness of insulin release. Importantly, pathophysiological conditions such as type 2 diabetes are associated with disrupted  $\beta$ -cell synchronization, altered gap junctional coupling, and excessive heterogeneity in excitability [20, 21], making it essential to understand how these factors contribute to the normal and pathological states of the system. While detailed electrophysiological models of  $\beta$ -cells exist, their complexity often hinders the identification of general principles. In contrast, the simplified approach taken here enables a higher-level investigation into the dynamical regimes and mechanisms that underlie collective excitability. In addition to its biological and medical relevance, the modeling of diversity in networks of excitable units inspired by  $\beta$ -cell clusters can deepen our understanding of the collective dynamics of a wide range of heterogeneous excitable systems, thus bringing an even broader motivation for the present thesis.

## Objectives and Outline

The main objectives of the thesis are:

- To assess the ability of reduced-order models, particularly networks of FHN oscillators, to reproduce essential features of  $\beta$ -cell network behavior and to serve as tools for exploring the functional role of cellular variability.
- To determine how the effects of diversity on the collective behavior of networks of excitable units depend on key system parameters, such as the regime of excitability, the coupling strength between units, and the level of external noise, if present.
- To investigate the distinct roles of heterogeneity and noise in shaping the dynamics of such networks, and to disentangle their respective mechanisms of action using reduced mathematical models.
- To understand whether diversity can have not only constructive but also inhibitory effects, suppressing network synchronization under specific parameter regimes, which may have physiological relevance.
- To characterize the emergence of diversity-induced resonance (DIR) in heterogeneous networks modeling  $\beta$ -cell clusters, and to elucidate its underlying mechanisms and broader relevance by drawing analogies with analogous phenomena in mechanical systems.
- To investigate the role of the degree of symmetry of the diversity distribution in shaping the collective dynamics of networks of coupled excitable units, modeled by FHN equations.
- To explore the physiological relevance of the modeling results, particularly in relation to the organization, robustness, and dysfunction of collective activity in pancreatic islets and other heterogeneous excitable tissues.

The thesis is organized as follows:

- **Chapter 1** provides a summary of the electrophysiology of excitable cells, with a particular focus on  $\beta$ -cells and the biological structure of the pancreas. This is an essential background for the following chapters of the thesis and the publications produced during the doctoral project. The mechanisms of excitability and insulin production are presented both at the level of individual cells and in the context of cell-cell interactions within a cluster, emphasizing the biological relevance of cellular heterogeneity.
- **Chapter 2** offers an overview of the theoretical modeling of pancreatic  $\beta$ -cells. It begins with early models of single-cell electrophysiology and proceeds to describe progressively more advanced frameworks, including those for multicellular systems, which are classified according to their underlying assumptions and mathematical formalisms. This chapter sets the stage for the original contributions of the thesis by tracing the evolution of modeling approaches and highlighting their respective strengths and limitations.
- **Chapter 3** focuses on modeling approaches based on networks of coupled oscillators, providing a brief historical overview of their development and applications to biological systems. It introduces the FHN oscillator as a paradigmatic model of

excitable dynamics, providing a detailed account of its equations and bifurcation structure. The chapter then presents the concept of diversity-induced resonance (DIR), highlighting its relevance in the context of heterogeneous cell populations. Finally, it discusses the  $\beta$ -cell network model developed in the first publication of this doctoral work, outlining its main results and the insights it offers into the role of heterogeneity and network structure in shaping the collective behavior of  $\beta$ -cell clusters.

- **Chapter 4** investigates the interplay between heterogeneity and noise, highlighting the differences between these two types of disorder. Regimes are identified where small amounts of noise enhance synchronization, especially when combined with an optimal degree of heterogeneity. The potential relevance of these effects to biological systems and, in particular,  $\beta$ -cell networks is also discussed.
- **Chapter 5** investigates scenarios in which heterogeneity does not enhance but instead inhibits synchronization in excitable networks. The analysis focuses on identifying the conditions under which diversity suppresses collective behavior, particularly in a nontrivial regime where even minimal heterogeneity is sufficient to disrupt the resonance mechanism known as self-induced stochastic resonance (SISR). This chapter provides a counterpoint to earlier results and deepens the understanding of how disorder can also impair, rather than facilitate, network-level responses.
- **Chapter 6** explores a formal dynamical equivalence between DIR in networks of nonlinear oscillators and a physically distinct phenomenon: the resonant translocation of a polymer composed of nonlinear units along a periodic potential. By establishing this correspondence, the chapter offers mechanistic insights into the fundamental drivers of DIR, while extending its relevance to broader classes of physical systems.
- **Chapter 7** investigates how the symmetry of the diversity distribution affects global oscillations in networks of excitable units. Using FHN models and different network topologies, the chapter shows that symmetric distributions can induce collective oscillations even without oscillatory units. Two metrics are introduced to quantify symmetry and predict network behavior, and a reduced two-unit model offers mechanistic insight into the observed dynamics.

Chapters 3, 4, 5, 6, and 7 include cross-references to the corresponding publications that have originated from the doctoral work, designated by Roman numbers. These are:

- I. A study of the impact of diversity on a 3D network of FHN units used to model a  $\beta$ -cell cluster.
- II. An exploration of the interplay between noise and heterogeneity in  $\beta$ -cell networks.
- III. An analysis of diversity-induced effects on cell network coherence.
- IV. A study of the dynamical equivalence between polymer translocation and diversity-induced resonance, providing new insight into the mechanisms underlying the latter.
- V. An investigation into how the symmetry of the diversity distribution influences global oscillations in networks of excitable units.

While the thesis is based on the above-mentioned papers [I-V], not all of their content is reproduced in the main text. Instead, the thesis highlights the most important results, emphasizes their conceptual interconnections, and provides additional background on the biological and physical systems studied. The full texts of the papers, included as Appendices, are considered as an integral part of the thesis.

# 1 ELECTROPHYSIOLOGY AND HETEROGENEITY OF EXCITABLE CELLS AND PANCREATIC $\beta$ -CELLS

## 1.1 Electrophysiology of Excitable Cells

Each cell that forms the human body is enclosed within a membrane, which is made of lipid bilayers that typically have a low electrical conductivity. However, the cell membrane has several channels that selectively allow certain chemical species to pass through it, from the inside of the cell to the external environment or vice versa, while other species are prevented from being exchanged. Some of the most important species that can be exchanged are metal ions, in particular sodium ( $\text{Na}^+$ ), potassium ( $\text{K}^+$ ) and calcium ( $\text{Ca}^{2+}$ ) ions, as well as negative counterions such as chloride ( $\text{Cl}^-$ ) [22, 23].

Under resting conditions, the concentration of negative ions within the cell is higher than in the external environment, whereas the opposite occurs with positive ions, so that the interior of the cell has an excess of negative charge with respect to the outside. This means that the so called cell membrane potential is negative and usually presents values between -60 and -100 mV, depending on the cell type [22].

Some special cell types have the ability to respond to an external electric current, which usually comes from a neighbor cell, by sharply raising their membrane potential to neutral or positive values (*depolarization*), followed by a *repolarization* phase that reestablishes the negative membrane potential values associated with resting conditions. Cells that exhibit this ability to process electric signals are located, for instance, in the brain (neurons), heart (cardiomyocytes) and other muscles (myocytes), pancreas ( $\beta$ -cells), and uterus (myometrial cells) [24].

This property is called *excitability* and the corresponding cells are referred to as *excitable*. The response of excitable cells to an external signal is nonlinear, in the sense that it occurs only if the signal intensity is higher than a certain critical value or threshold, and once this condition is satisfied, the magnitude of the membrane potential increase, as well as the rate at which depolarization and repolarization take place, is always the same independently of the signal intensity [6, 22].

Looking at what happens microscopically in a neuron during the depolarization phase, the permeability of the cell membrane to  $\text{Na}^+$  ions increases, due to the opening of specific structures inside the membrane, named  *$\text{Na}^+$  ion channels*. This causes an influx of such ions from the external environment into the cell, resulting in an increase in positive charge until the membrane potential shifts from negative to positive. When the concentration increase of  $\text{Na}^+$  ions inside the cell is such that an equilibrium is achieved with the external environment, the influx of such ions stops and, at that point, the action potential reaches its maximum positive value, which determines the corresponding peak amplitude. What happens then is that  $\text{Na}^+$  ion channels close while  $\text{K}^+$  ion channels open, allowing an outward flux of positive ions ( $\text{K}^+$ ) this time from inside the cell to the external environment. This starts the repolarization phase, during which the membrane potential decreases until it returns to its negative value corresponding to the cell resting conditions [22, 23]. It should be noted that the relative importance of  $\text{Na}^+$ ,  $\text{K}^+$  and  $\text{Ca}^{2+}$  ions in determining membrane potential variations is different depending on cell types: In neurons, the effects of the exchange of  $\text{Na}^+$  and  $\text{K}^+$  ions are predominant, while in cardiomyocytes and pancreatic  $\beta$ -cells,  $\text{Ca}^{2+}$  ions assume greater relevance, as we shall see in more detail in Section 1.2 [25].

The sequence of membrane depolarization and repolarization is called *action potential*. Both the amplitude and the duration of the action potential can change significantly from one cell type to another. In particular, the duration can be as short as one millisecond

ond in the case of neurons, while it is of the order of hundreds of milliseconds in the case of cardiomyocytes [22]. The action potential represents a fundamental mechanism for the propagation of electrical signals in biological cell networks. When an action potential occurs in a cell, it produces an electrical impulse that can be transmitted to one or more neighboring cells, which in turn will generate an action potential. Thanks to this mechanism, neurons, cardiomyocytes,  $\beta$ -cells, etc., are able to synchronize their electrical oscillations and have coordinated activities, such as information transmission, mechanical contraction, insulin production, etc., which are crucial to ensure their functionality from a physiological standpoint [22, 26, 27].

From the above introductory description of the electrical activity of excitable cells, it should already be clear that networks made of these cells lend themselves to being studied and modeled as complex systems. Perhaps their most relevant features from this standpoint are:

1. **Emergence of collective behaviors.** For example, in the case of pancreatic  $\beta$ -cells, which are a key topic of this thesis work, it is well-known that single cells either do not have any electrical oscillations at all or, if they do oscillate, they present irregular oscillation patterns [28, 29]. Instead, when they are part of a cluster, such as in Langerhans islets,  $\beta$ -cells are capable of synchronized collective oscillations, which are essential for normal insulin production [21, 26]. Therefore, this is an emergent property of the cell network, which cannot be found in its individual constituents, i.e., single  $\beta$ -cells.
2. **Ability to self-organize.** Still taking  $\beta$ -cells as an example, it has been shown that the ability of clusters of these cells to have synchronized collective oscillations does not necessarily rely on the existence of specialized pacemaker cells. Modeling studies have demonstrated that synchronization can be achieved as a consequence of introducing into the network a certain degree of cell heterogeneity [30].
3. **Nonlinearity.** As mentioned above, the behavior of excitable cells, as well as their interactions in a network, follow a nonlinear dynamics, where relatively small changes in a given external signal can cause very large effects in terms of cell membrane potential variation and associated physiological responses, for instance mechanical contraction in the case of myocytes, or insulin secretion in the case of  $\beta$ -cells [25, 27].

## 1.2 $\beta$ -Cells and Insulin Production Mechanism

$\beta$ -Cells constitute one of the three main cell types hosted in the pancreas, i.e.,  $\alpha$ ,  $\beta$  and  $\delta$ -cells. They are responsible for the production of glucagon, insulin, and somatostatin, respectively, which are hormones involved in the control of glucose level in the blood. Insulin is released by  $\beta$ -cells when the hematic glucose level increases above a certain threshold, and is capable of inducing the absorption of glucose by various organs, mainly the liver, muscles and adipose tissues. Glucagon performs the opposite function, i.e., it is produced by  $\alpha$ -cells when the hematic glucose level becomes too low, and stimulates the release of glucose that has been stored in the liver and muscles under the form of glycogen, a highly branched polymer made of several thousands of glucose units [31]. Somatostatin, which is produced by  $\delta$ -cells, does not directly participate in glucose level regulation, however, it is capable of partially inhibiting the activity of both  $\alpha$  and  $\beta$ -cells, thus indirectly contributing to glucose control [32, 33].

$\alpha$ ,  $\beta$  and  $\delta$ -cells are arranged in clusters, named *islets of Langerhans*, which in the human body are approximately a million and are spread throughout the pancreas structure.

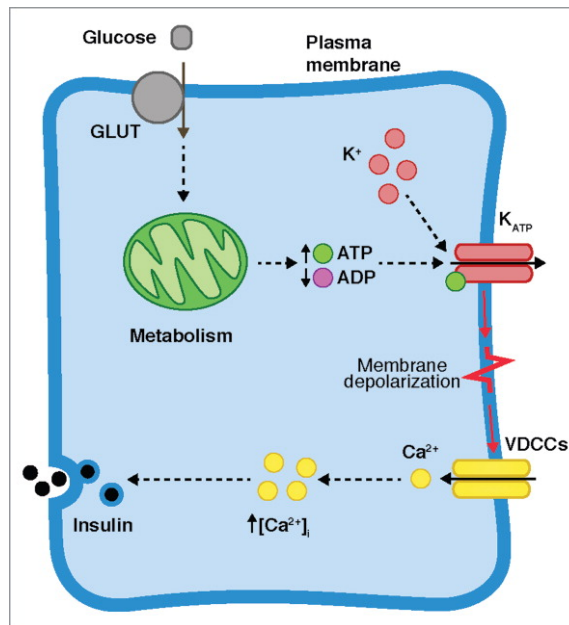


Figure 1: Schematic structure of a  $\beta$ -cell. [Reprinted from: Gerardo J Félix-Martínez and J Rafael Godínez-Fernández, *Mathematical models of electrical activity of the pancreatic  $\beta$ -cell: A physiological review*, *Islets*, 6:3, e949195 (2014). Copyright ©2014, The Authors. Published under the CC BY-NC license. <https://doi.org/10.4161/19382014.2014.949195>].

Each islet measures roughly 0.2 mm in diameter and hosts about a thousand  $\beta$ -cells [34]. This facilitates the theoretical modeling of  $\beta$ -cells, because a cluster of a thousand cells, which is an affordable size for today's computing power, is representative of a typical  $\beta$ -cell network in an islet of Langerhans and, therefore, has physiological relevance.

Fig. 1 summarizes in a simplified manner the current understanding of how a  $\beta$ -cell functions [18]. The production of insulin is triggered by an increase of the hematic glucose concentration and, for this reason, it is named *glucose-stimulated insulin secretion* (GSIS). The sequence of events that leads to insulin secretion begins with the transport of glucose from the bloodstream into the  $\beta$ -cell, operated by the so called *glucose transporters* (GLUT). Glucose, which is a relatively large hydrophilic molecule, cannot travel through the hydrophobic cell membrane by plain diffusion. This is why nature has developed dedicated protein structures that perform the crucial function of delivering it into the cell. Glucose transporters are present in every cell of our body, since all cells need to uptake glucose as a primary metabolic fuel and a key substrate for a wide range of biochemical reactions [35]. In the case of  $\beta$ -cells, in addition to this common function, glucose transport by GLUT is essential to provide an input signal to the cell that insulin must be produced, when the glucose level in the bloodstream becomes higher than a certain threshold.

The increased cell metabolism caused by glucose intake has the effect of converting a proportional amount of ADP (adenosine diphosphate) to ATP (adenosine triphosphate) in cell mitochondria. The higher ATP/ADP ratio triggers the closure of ATP-sensitive K<sup>+</sup> channels [36, 37], stopping the outward flux of K<sup>+</sup> ions and therefore causing a build-up of positive charges inside the cell. This results in a progressive depolarization, i.e., an increase of the membrane potential, up to a critical threshold value that triggers the opening of voltage-dependent Ca<sup>2+</sup> channels, allowing an influx of Ca<sup>2+</sup> ions from the exter-

nal environment into the cell. The consequent rise in intracellular  $\text{Ca}^{2+}$  ion concentration ultimately triggers insulin secretion [18], which is expelled through the cell membrane (exocytosis) and delivered to the bloodstream. The release of insulin into the bloodstream leads to a progressive decrease in hematic glucose concentration and a consequent slowdown in ATP production inside  $\beta$ -cells, until the ATP/ADP ratio reduces back to a point where ATP-sensitive  $\text{K}^+$  channels reopen, thus allowing  $\text{K}^+$  ions to exit the cell, starting a repolarization phase.

The synthetic pathway by which  $\beta$ -cells produce insulin is rather complex and occurs through the sequential formation of two precursor molecules, *preproinsulin* and *proinsulin*, which involves various functional domains of the cell [38]. Since the insulin synthetic process does not have an impact on the dynamics of electrical oscillations (at least in a first-order approximation), it is usually ignored in the mathematical modeling of  $\beta$ -cells. The focus of these models is, ultimately, on the ability to predict  $\text{Ca}^{2+}$  ion concentration fluctuations in the cytosol, knowing that this is the key factor triggering insulin exocytosis.

As mentioned in Sec. 1.1, cell-cell communication is critical for excitable cells to synchronize their electrical activity and, as a consequence, plays a key role in  $\beta$ -cells for the regulation of insulin production. This communication takes place mainly through specific channels in the cell membrane structure, named *gap junctions*, which are made up of assemblies of a particular protein, *connexin36* (abbreviated: *Cx36*), and mediate the transfer of cytoplasmic ions between neighboring cells, which are therefore electrically coupled [39]. Through this ion exchange mechanism, gap junctions allow intracellular  $\text{Ca}^{2+}$  ion concentration to oscillate in a coordinated manner across Langerhans islets in response to an increase in blood glucose level, thus stimulating collective insulin secretion from all  $\beta$ -cells at the same time. Through the same mechanism, gap junctions also allow the transmission of the signal that causes oscillations to stop when glucose concentration returns to its basal level [40]. As a further confirmation of the criticality of cell-cell communication enabled by gap junctions, age-related declines in insulin secretion have been shown to be associated with a reduced efficiency of electrical coupling between  $\beta$ -cells, leading to an increased susceptibility to type 2 diabetes [41].

The synchronized electrical oscillations of  $\beta$ -cells within a Langerhans islet exhibit a so called *bursting* pattern, characterized by the network generating rapid sequences of spikes, known as *bursts*, followed by a resting phase before the next burst begins. The period of these bursting oscillations, defined as the interval between the onset of two successive bursts, can range from less than a minute up to 5 minutes. An example of bursting patterns is illustrated in Fig. 2, which also shows the synchronization between membrane potential oscillations and fluctuations in intracellular  $\text{Ca}^{2+}$  ion concentration [30].

### 1.3 Relevance of Cellular Heterogeneity

By cellular *heterogeneity* we mean the existence of functionally and phenotypically distinct subpopulations within the same overall cell type. It is worth pointing out that the terms *heterogeneity* and *diversity* are commonly used as synonyms in the scientific literature to express this concept and, therefore, will be used interchangeably in this thesis.

Cellular heterogeneity is a fundamental feature of living organisms. It is increasingly recognized as essential for the robustness, adaptability, and specialization of tissues. In the immune system, for example, functional heterogeneity among T cells and macrophages enables context-dependent responses not only to infection and inflammation but also to sterile tissue injury, where immune cells contribute to both damage control and repair processes [42,43]. In the brain, diversity among neuronal and glial cell types underlies

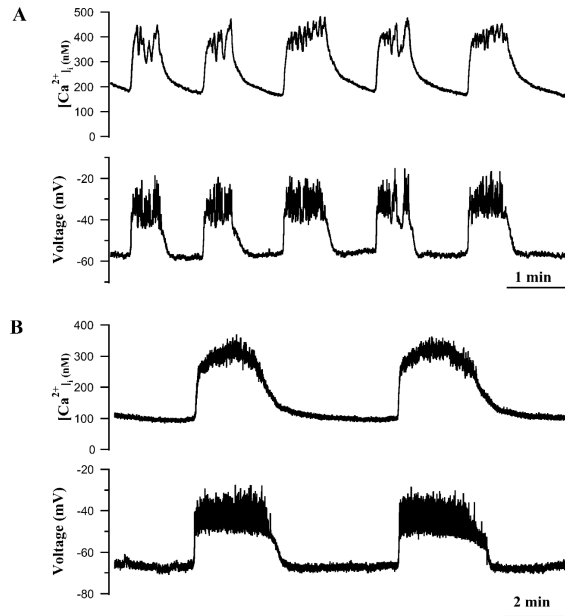


Figure 2: Typical profile of bursting oscillations in a faster (panel A) and slower (panel B) islet of  $\beta$ -cells. In each panel, cytosolic  $Ca^{2+}$  ion and membrane potential oscillations are plotted in the upper and lower graph, respectively. [Reprinted from *Biophysical Journal*, Vol 84 /Issue 5, Min Zhang, Paula Goforth, Richard Bertram, Arthur Sherman, Leslie Satin, *The  $Ca^{2+}$  Dynamics of Isolated Mouse  $\beta$ -Cells and Islets: Implications for Mathematical Models*, p. 2852-2870, Copyright 2003, with permission from Elsevier. <https://www.sciencedirect.com/science/article/pii/S0006349503700149>].

complex behaviors, information processing, and plasticity [44,45]. Hepatic zonation in the liver represents another form of spatial and metabolic heterogeneity, where hepatocytes differ according to their location in the lobule and perform region-specific metabolic functions [46,47]. Similarly, in the intestinal epithelium, stem cell heterogeneity ensures tissue renewal while maintaining responsiveness to injury and environmental changes [48, 49]. Understanding cellular heterogeneity has been significantly advanced by technologies such as single-cell RNA sequencing (scRNA-seq), which enable high-resolution profiling of gene expression patterns across individual cells [46, 48, 50, 51]. These insights have reshaped current views of tissue function and disease mechanisms, including cancer, autoimmunity, and metabolic disorders.

Heterogeneity is also highly relevant for pancreatic  $\beta$ -cells, which have traditionally been viewed as a uniform population, while relatively recent evidence reveals significant heterogeneity among them in terms of function, gene expression, and response to stimuli [52–54]. Understanding this heterogeneity is crucial for elucidating the pathological mechanisms behind diabetes and developing targeted therapies.

Functional differences among  $\beta$ -cells have been observed in their insulin secretion capacity, glucose sensitivity, and electrophysiological properties. For instance, studies have identified subpopulations of  $\beta$ -cells that respond differently to glucose stimulation [55, 56]. Some  $\beta$ -cells act as *hub* cells, coordinating the activity of neighboring cells to ensure synchronized insulin release. These hub cells exhibit higher connectivity and influence over the islet network, playing a pivotal role in the regulation of insulin secretion dynamics [57, 58].

Advances in single-cell RNA sequencing have revealed significant gene expression diversity among  $\beta$ -cells. Subpopulations differ in the expression of genes associated with insulin production, ion channel activity, mitochondrial metabolism, and stress response pathways [59]. Some  $\beta$ -cells appear to be designed for rapid insulin secretion, while others may have more protective or proliferative roles. Such diversity reflects a continuum of functional states that likely respond dynamically to physiological or pathological changes.

$\beta$ -cell heterogeneity also arises from differences in developmental origins and maturation states. During pancreatic development,  $\beta$ -cells differentiate at varying times and rates, leading to a spectrum of maturation statuses within the islet. Some cells exhibit markers of immature  $\beta$ -cells, while others display characteristics of fully mature, insulin-secreting cells [53]. This developmental heterogeneity may influence the overall functional capacity of the islet and its ability to respond to metabolic challenges.

In both type 1 and type 2 diabetes,  $\beta$ -cell heterogeneity plays a role in disease progression. Certain subpopulations may be more prone to autoimmune attack or metabolic dysfunction. For example,  $\beta$ -cells with lower insulin content or changes in how they are recognized by the immune system, may be preferentially targeted in type 1 diabetes [54]. In type 2 diabetes, variations in stress response pathways among  $\beta$ -cells can lead to differential survival and function under glucotoxic (hyperglycemic) conditions. Understanding these differences is critical for developing strategies to preserve or restore  $\beta$ -cell function in diabetic patients.

Recognizing  $\beta$ -cell heterogeneity has significant implications for diabetes treatment strategies. Efforts to generate  $\beta$ -cells from stem cells for transplantation must account for the need to replicate the diverse functional subtypes present in healthy islets. Additionally, therapies aimed at preserving or enhancing  $\beta$ -cell function may need to be tailored to target specific subpopulations to be effective [55, 59]. Personalized medicine approaches that consider  $\beta$ -cell heterogeneity could improve treatment outcomes for individuals with diabetes.

## 2 MODELING OF $\beta$ -CELLS

A key area of focus in this thesis work is the theoretical modeling of networks of pancreatic  $\beta$ -cells. Before reviewing the main mathematical models that have been developed over the past 40 years to mimic the electrical activity of  $\beta$ -cells, we shall provide a brief summary of their physiology, with particular reference to those aspects that are most relevant to insulin secretion. Then, the review of mathematical models will be divided into two categories: a) models of single  $\beta$ -cells, and b) models of  $\beta$ -cell clusters.

### 2.1 Models of Single $\beta$ -Cells

#### 2.1.1 Chay-Keizer Model

The Chay-Keizer model, introduced in 1983, is usually regarded as the first mathematical model capable of replicating the bursting oscillations of  $\beta$ -cells, as observed in experiments [60]. The model takes into account: voltage-regulated  $\text{Ca}^{2+}$  channels; voltage-regulated  $\text{K}^+$  channels;  $\text{Na}^+$  (and  $\text{Cl}^-$ ) leaks; and an external current that mimics the signal associated with the blood glucose level. It is based on a Hodgkin-Huxley-type formalism, meaning that the membrane current is the sum of contributions from all of the aforementioned ionic channels. This gives rise to the following equation:

$$C_m \frac{dV}{dt} = g_K(V_K - V) + 2g_{Ca}(V_{Ca} - V) + g_L(V_L - V) + I_{app} \quad (1)$$

where  $C_m$  represents the cell membrane capacitance and  $V$  is the membrane potential. On the right hand side, the first two  $g$  terms indicate the membrane conductance per unit area for  $\text{K}^+$  and  $\text{Ca}^{2+}$  ions respectively, with  $V_K$  and  $V_{Ca}$  being the corresponding resting potentials. The third  $g$  term, with the corresponding resting potential  $V_L$ , accounts for a general leak conductance that encompasses sodium and chloride ion leaks, which was supported by experimental evidence available when the Chay-Keizer model was developed. Finally,  $I_{app}$  represents an applied external current, which can be considered as the stimulus resulting from an increase in hematic glucose concentration.

In the Chay-Keizer model, bursting relies entirely on a single pacemaker variable, which is the intracellular  $\text{Ca}^{2+}$  ion concentration. However, subsequent experimental evidence contradicted this assumption, as measurements of intracellular  $\text{Ca}^{2+}$  ion concentration in  $\beta$ -cells, which became feasible a few years later, showed faster dynamics for this variable compared to model predictions [18, 61, 62]. Nevertheless, almost all  $\beta$ -cell models that were developed in subsequent years are derived from the minimal Chay-Keizer model. A wider range of bursting patterns was obtained in subsequent models by defining a different pacemaker variable, while using a mathematical approach analogous to that of the Chay-Keizer model [18].

#### 2.1.2 Phantom Burster Model

A key motivation for the development of this model [63] is the observation that clusters of pancreatic  $\beta$ -cells exhibit bursting oscillations with a wide range of periods. Specifically, while the bursting periods of isolated, individual  $\beta$ -cells are either very fast or very slow (in some cases there can even be no oscillations at all), the bursting periods observed in islets of Langerhans (which, as explained in Section 1.2, are clusters composed of about 1,000 cells) can assume a broad spectrum of intermediate values between these extremes. To capture this behavior, the authors of the Phantom Burster model developed a mathematical framework for  $\beta$ -cell electrical activity capable of producing a wide range of bursting oscillations. In their model, bursting is driven by the interaction of two oscillatory pro-

cesses: one with a relatively short time constant and another with a much longer time constant.

Depending on the chosen parameter regime, different dynamics emerge from this model. In one case, the faster of the two processes exerts primary control, producing fast bursting oscillations. In another, the slower process governs the behavior, giving rise to slow bursting. A third, more subtle regime arises when neither process independently dictates the bursting period. Instead, the interplay between the fast and slow processes produces oscillations with an intermediate period (see Fig. 3). Notably, this intermediate behavior does not require the existence of a separate process operating at that timescale; rather, it emerges as a consequence of the combined dynamics of the two original processes, a phenomenon referred to by the authors as *phantom bursting* [63].

As shown in Eqs. (2)-(8) [63], similarly to other models of  $\beta$ -cell activity, the Phantom Burster model is composed of a set of fast variables (the fast subsystem) that regulate spiking during the active phase of a burst, along with a slow negative feedback mechanism that modulates the initiation and termination of spiking.

$$\frac{dV}{dt} = -\frac{(I_{Ca} + I_K + I_{s_1} + I_{s_2} + I_L)}{C_m} \quad (2)$$

$$\frac{dn}{dt} = \frac{n_\infty(V) - n}{\tau_n} \quad (3)$$

$$\frac{ds_1}{dt} = \frac{s_{1\infty}(V) - s_1}{\tau_{s_1}} \quad (4)$$

$$\frac{ds_2}{dt} = \frac{s_{2\infty}(V) - s_2}{\tau_{s_2}} \quad (5)$$

$$I_{Ca} = g_{Ca}m_\infty(V)(V - V_{Ca}), \quad I_K = g_Kn(V - V_K) \quad (6)$$

$$I_{s_1} = g_{s_1}s_1(V - V_K), \quad I_{s_2} = g_{s_2}s_2(V - V_K) \quad (7)$$

$$I_L = g_L(V - V_L) \quad (8)$$

The fast subsystem includes two equations: one (Eq. (2)) governing the membrane potential,  $V$ , and another (Eq. (3)) describing the dynamics of the fast activation variable,  $n$ . In addition to these, the model incorporates two distinct negative feedback variables, labeled  $s_1$  and  $s_2$  in Eqs (4) and (5), respectively. The variable  $s_1$  operates on a timescale of tens of milliseconds, classifying it as a fast variable, whereas  $s_2$  evolves much more slowly, with a time constant on the order of minutes. Consequently,  $s_1$  is responsible for driving the fast oscillations,  $s_2$  governs the slow oscillations, and the interaction between  $s_1$  and  $s_2$  gives rise to intermediate oscillations in accordance with the phantom bursting mechanism outlined previously.

In Eqs. (6)-(8), the various ionic currents present in the first equation for the membrane potential are defined. Without delving too deeply into the detailed expressions of these currents, it can be observed that, similar to the Chay-Keizer model, we have a  $Ca^{2+}$  ion current ( $I_{Ca}$ ) and a  $K^+$  ion current ( $I_K$ ), while  $I_L$  is a leak current, with their respective resting potentials  $V_{Ca}$ ,  $V_K$ , and  $V_L$ . In addition, there are two further currents associated with the slow variables  $s_1$  and  $s_2$ , which are denoted as  $I_{s_1}$  and  $I_{s_2}$ , respectively. While these two currents were designated as potassium currents for the sake of specificity in the Phantom Burster model, their exact biophysical nature was not definitively established by the authors and may, in fact, be different [63].

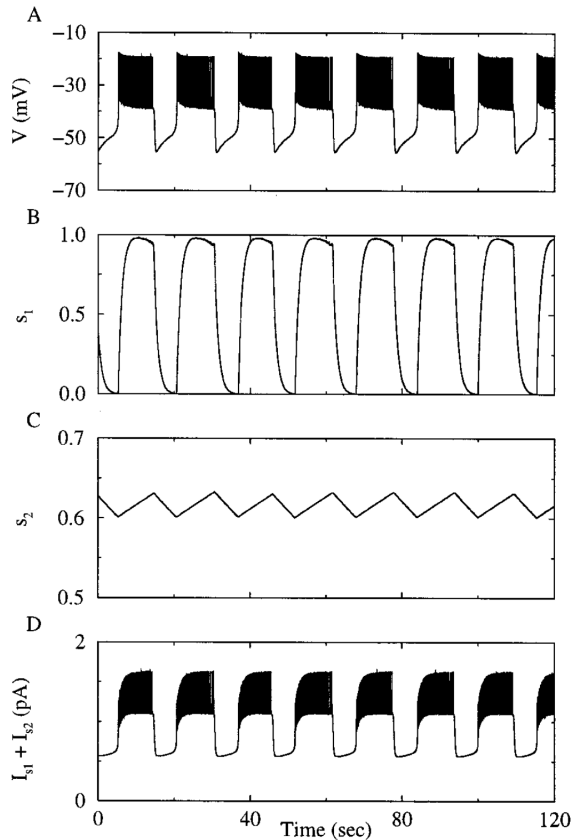


Figure 3: Bursting oscillations with intermediate period produced by the Phantom Bursting model. The bursts are generated by activity-dependent oscillations in both  $s_1$  and  $s_2$ . [Reprinted from *Biophysical Journal*, Vol 79 /Issue 6, Richard Bertram, Joseph Previte, Arthur Sherman, Tracie A. Kinard, Leslie S. Satin, *The Phantom Burster Model for Pancreatic  $\beta$ -Cells*, p. 2880-2892, Copyright 2000, with permission from Elsevier. <https://www.sciencedirect.com/science/article/pii/S0006349500765258>].

### 2.1.3 Dual Oscillator Model

A key reason for the introduction of the Dual Oscillator model [17, 25, 64] was the observation, enabled by increasingly sophisticated experimental techniques, that  $\beta$ -cells can exhibit not only oscillations with fast, slow, and intermediate periods, but also *compound oscillations*, where fast bursts of action potentials are grouped into episodes (see Fig. 4). Therefore, this model is able to generate all four types of oscillatory patterns.

The key hypothesis underlying the model is that the slow component of compound bursting is caused by glycolytic oscillations, i.e., periodic fluctuations in the concentration of metabolites produced by the biochemical reactions involved in glycolysis, whereas faster oscillations that are superimposed are produced by the electrical activity of  $\beta$ -cells. As far as  $\beta$ -cell electrical activity is concerned, although the details of the two formalisms are different, the Dual Oscillator framework can be considered analogous to the Phantom Burster model. As we have seen, the latter is able to generate bursting oscillation periods ranging from a few seconds to several minutes, however, it cannot produce compound bursting. In a simplified description, it is the addition of the slower glycolytic oscillations

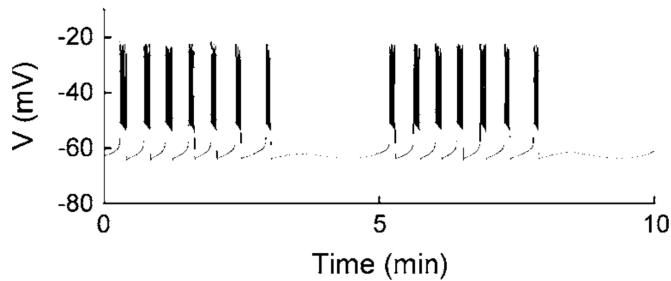


Figure 4: Example of compound bursting. [Reprinted from *Biophysical Journal*, Vol 92 /Issue 5, Richard Bertram, Leslie S. Satin, Morten Gram Pedersen, Dan S. Luciani, Arthur Sherman, *Interaction of Glycolysis and Mitochondrial Respiration in Metabolic Oscillations of Pancreatic Islets*, p. 1544-1555, Copyright 2007, with permission from Elsevier. <https://www.sciencedirect.com/science/article/pii/S0006349507709621>]

on top of the faster electrical ones that leads to compound bursting, and this is what the Dual Oscillator model is capable of representing.

The complete formalism of the Dual Oscillator model is rather complex and its detailed illustration is beyond the scope of the present thesis, which is focused on collective phenomena that arise in cell clusters, rather than on modeling single cell behavior. However, it is worth mentioning that this remains one of the models with the best ability to replicate the full range of  $\beta$ -cell oscillation patterns and, notably, has been capable of reproducing experimental observations that were made even after its introduction [18].

## 2.2 Modeling of $\beta$ -Cell Clusters

After providing a synthetic review of single  $\beta$ -cell models in Sec. 2.1, we will now go through some of the main mathematical models developed to represent multicellular systems, i.e.,  $\beta$ -cell clusters. The examples we will consider can be divided into three categories [32]: a) dynamical models of electrically coupled cells, b) models based on percolation theory, and c) models of coupled oscillators. Given the relevance of point c) to the research work presented in this thesis, it will be discussed in the next, dedicated chapter.

### 2.2.1 Dynamical Models of Electrically Coupled Cells

The most conceptually straightforward approach to develop a multicellular model is to build a system of coupled differential equations where all relevant parameters describing the electrical cell activity (such as membrane potential, cytosolic  $\text{Ca}^{2+}$  concentration, etc.) are taken into account as time-dependent variables [32]. This approach clearly allows the cell network to be described in as much detail and, consequently, with as much complexity as desired. However, the computational cost associated with solving a dynamical model consisting of hundreds or even thousands of individual cells, each described by tens of coupled differential equations, can become extremely high. In addition, due to the complexity of the system and the large number of variables involved, it can be difficult to understand the “general picture” of the synchronization mechanisms in terms of overall network dynamics.

In what follows, we will provide a few examples of some of the most relevant models of this kind that can be found in the literature, with no intent to be exhaustive, but just to share useful background information to help understand the reasons behind the choices made in the development of the new models that will be presented later in this thesis.

**2.2.1.1 Sherman and Rinzel Model.** A key question the authors of this model [65] tried to address was why individual  $\beta$ -cells often exhibit irregular spiking/bursting oscillations, whereas cell clusters are usually very regular and synchronized. Their central hypothesis to explain this difference was that stochastic fluctuations in single, isolated cells disrupt the bursts, whereas when cells are electrically coupled by conductance gap junctions, these fluctuations are shared among cells and hence dampened. The authors used the Chay-Keizer equations (see Sec. 2.1.1) to represent single  $\beta$ -cells in their multicellular model and developed the following system of coupled differential equations [65], where  $j = 1, 2, \dots, N$ , with  $N$  being the number of cells constituting the cluster:

$$C_m \frac{dV_j}{dt} = -I_{\text{ion}}(V_j, n_j) - \bar{g}_{\text{K-Ca}} p_j (V_j - V_K) - g_c \sum_{k \in \Omega_j} (V_j - V_k) \quad (9)$$

$$\frac{dn_j}{dt} = \lambda \left[ \frac{n_{\infty}(V_j) - n_j}{\tau_n(V_j)} \right] \quad (10)$$

$$\frac{dCa_j}{dt} = f [-\alpha I_{\text{Ca}}(V_j) - k_{\text{ca}} Ca_j] \quad (11)$$

In the above Eqs. (9)-(11), the independent variables are: the membrane potential,  $V_j$ ; the open fraction of voltage-gated  $\text{K}^+$  channels,  $n_j$ ; and the concentration of free intracellular  $\text{Ca}^{2+}$  ions,  $Ca_j$ .

In Eq. (9), the term  $I_{\text{ion}}(V_j, n_j)$  accounts for the sum of the electric currents related to the exchange of  $\text{Ca}^{2+}$  and  $\text{K}^+$  ions through the membrane;  $\bar{g}_{\text{K-Ca}}$  captures the conductance of the  $\text{K}^+$ - $\text{Ca}^{2+}$  channels ( $p_j$  is a stochastic term that mimics the irregular spiking observed in isolated cells); and  $g_c$  is the conductance of the gap junctions, which is assumed to be the same for all gap junctions and expresses the strength of the coupling between cell  $j$  and  $k$ . The sum in Eq. (9) is taken across the cells  $\Omega_j$  that are coupled to the  $j$ th cell, which are its nearest neighbors and depend on the specific topology used in the model.

In Eq. (10),  $\tau_n$  and  $\lambda$  are experimentally determined time constants, while  $n_{\infty}(V_j)$  is the value that  $n$  would eventually reach if the voltage  $V_j$  was kept constant indefinitely.

Finally, in Eq. (11),  $f$  is the fraction of free cytosolic  $\text{Ca}^{2+}$  ions;  $\alpha$  is a factor used to convert units of ionic current into units of concentration change over time; and  $k_{\text{ca}}$  expresses the rate of removal of free  $\text{Ca}^{2+}$  ions from the cytosol through various mechanisms [65].

It can be observed that Eqs. (9) and (10) describe the fast spike-generating dynamics, whereas Eq. (11) represents a slow process due to the small value of  $f$ . Thanks to the gap junction conductance,  $g_c$ , coupled cells can decrease (or eliminate) differences between their membrane potentials, which provides a synchronization mechanism for their electrical oscillations.

As shown in Fig. 5, the model produces irregular spiking for a single cell, as expected from the presence of the stochastic term  $p_j$  in Eq. (9). However, an increase in the number of cells leads to a progressive clustering of membrane potential spikes into bursts and the development of sawtooth oscillations in intracellular calcium levels [65]. Also, the oscillatory patterns generated for large cell numbers tend to resemble those corresponding to a single deterministic cell, i.e., the case where, in Eqs. (9)-(11),  $j = 1$  only, the coupling term in Eq. (9) is zero (because  $j = k = 1$ ), and the stochastic term  $p_j$  is constant and equal to 1.

The Sherman and Rinzel model has provided a significant contribution to the understanding of Langerhans islet physiology by offering a theoretical framework that demonstrates how gap junction coupling influences the synchronization of  $\beta$ -cells. It should be

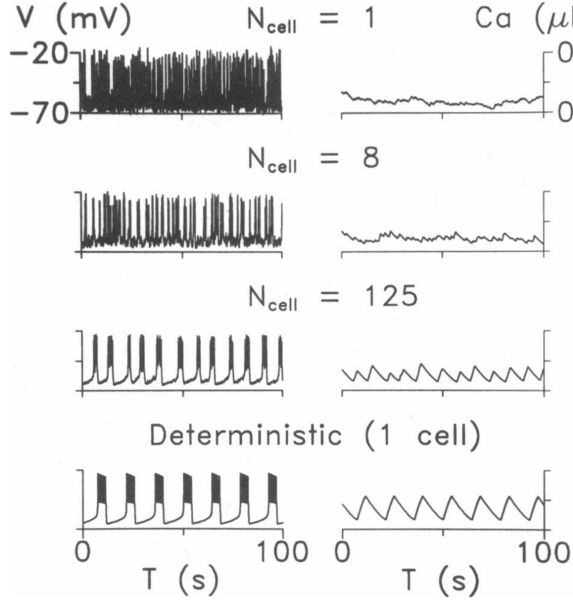


Figure 5: Membrane potential and  $\text{Ca}^{2+}$  ion concentration oscillations predicted by the Sherman and Rinzel model, as a function of the number of cells in the network. [Reprinted from *Biophysical Journal*, Vol 59 /Issue 3, A. Sherman, J. Rinzel, Model for synchronization of pancreatic beta-cells by gap junction coupling, p. 547-559, Copyright 1991, with permission from Elsevier. <https://www.sciencedirect.com/science/article/pii/S0006349591822718>]

pointed out that this model does not take into account heterogeneity, as all cells in the network are described as identical.

**2.2.1.2 Saadati and Jamali Model.** This is a relatively recent example of a dynamical model [66] characterized by the addition of more subtle effects besides electrical coupling linked to the diffusion of  $\text{Ca}^{2+}$  and  $\text{K}^+$  ions through gap junctions. Specifically, the model accounts for the effects on  $\beta$ -cell coordination of key metabolites, such as fructose 1,6-bisphosphate (FBP) and glucose 6-phosphate (G6P), which can diffuse through gap junctions in addition to ions.

Without going into the details of each equation used in this model, the diffusion of metabolites through gap junctions was introduced through a term

$$J_X^{jk} = \sum_{k \in \Omega_j} p_{c,X} (X_j - X_k), \quad (12)$$

where  $J_X^{jk}$  represents the flux of  $X = \text{FBP}$  or  $\text{G6P}$  through the gap junctions between cell  $j$  and cell  $k$ ,  $X_j$  and  $X_k$  are the respective cytosolic concentrations of metabolites (FBP or G6P),  $p_c$  is the gap-junctional permeability, and the sum is taken across the cells  $\Omega_j$  that are coupled to the  $j$ th cell, which are its nearest neighbors [32].

The results of simulations produced by this model show that electrical coupling has a greater impact on the synchronization of membrane potential oscillations than metabolic coupling. However, when the two mechanisms of electrical and metabolic coupling are combined, the outcome is a higher degree of synchronization compared to electrical coupling alone [66].

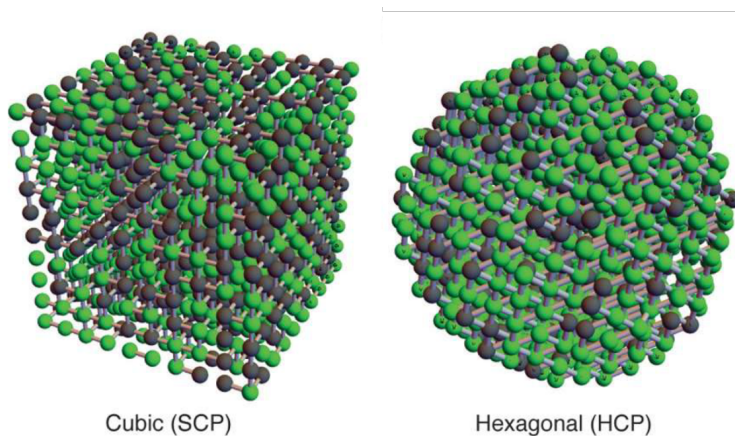


Figure 6: Three-dimensional structures used in multicellular models of pancreatic cells. Green and black cells represent active and inactive cells, respectively, as modeled using the discrete probabilistic approach based on percolation theory. Left: Simple Cubic Packing (SCP). Right: Hexagonal Cubic Packing (HCP). [Adapted from: G.J. Felix-Martinez, J.R. Godinez-Fernandez, A primer on modeling pancreatic islets: from models of coupled beta-cells to multicellular islet models, *Islets* 15, 2231609 (2023). Copyright ©2023, The Authors. Published under the CC BY-NC license. <https://doi.org/10.1080/19382014.2023.2231609>].

## 2.2.2 Models Based on Percolation Theory

In the framework of percolation theory, interconnected  $\beta$ -cells are modeled as a network, where each cell corresponds to a node, and connections between nodes represent functional coupling, meaning that if one cell is active, all its connected neighbors are considered active as well. Cell coupling is established through a probabilistic method, where each pair of cells has a probability  $p$  of being coupled, and a probability  $1 - p$  of remaining uncoupled. According to percolation theory, there exists a critical threshold  $p_c$ : when  $p < p_c$ , the network consists of small, disconnected clusters, whereas for  $p > p_c$ , a large, spanning cluster emerges that connects a significant portion of the network [32]. This represents a geometric phase transition: as the proportion of added elements reaches the critical threshold  $p_c$ , isolated, small clusters suddenly merge into larger, connected structures, referred to as spanning clusters. It is important to note that pancreatic islets function as miniorgans, consisting not only of insulin-producing  $\beta$ -cells, but also of  $\alpha$ -cells and  $\delta$ -cells, which secrete glucagon and somatostatin, respectively, i.e., two other essential hormones.  $\beta$ -cells make up approximately 50% to 70% of the total cell population, while the remaining cells are primarily  $\alpha$ -cells and  $\delta$ -cells. Since  $\alpha$ - and  $\delta$ -cells do not form functional couplings with  $\beta$ -cells, their occupied locations effectively become inaccessible to the  $\beta$ -cell network. In percolation theory terms, this results in a reduced probability of site availability (or site open probability) for  $\beta$ -cells. In healthy pancreatic islets, where  $\beta$ -cells constitute 50%–70% of the total cells, this implies a corresponding site open probability within that range [20].

Unlike full dynamical models of electrically coupled cells, these probabilistic models offer the benefit of avoiding exhaustive representations of all underlying cellular mechanisms, thereby reducing computational demands. However, this simplification can come at the cost of diminished physiological interpretability, particularly concerning the subcellular processes involved [32].

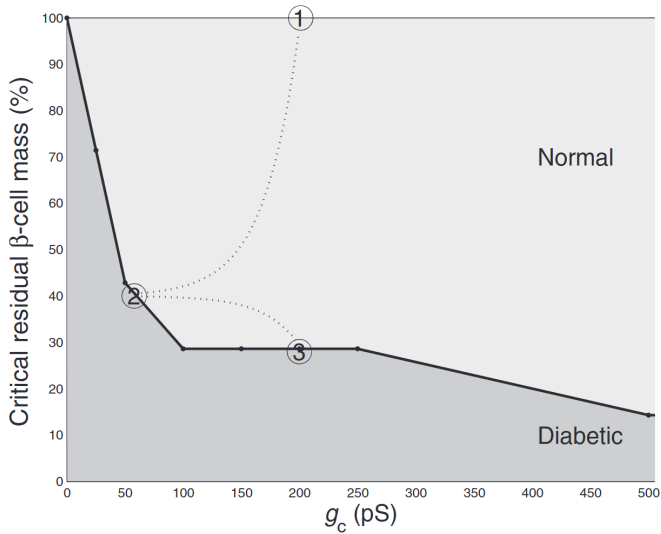


Figure 7: Residual beta-cell mass versus gap junction conductance. Reprinted figure with permission from [I. J. Stamper, Elais Jackson, and Xujing Wang. *Phys. Rev. E* **89**, 012719 (2014).] Copyright 2014 by the American Physical Society. <https://journals.aps.org/pre/abstract/10.1103/PhysRevE.89.012719>

**2.2.2.1 Stamper, Jackson, and Wang Model.** By applying percolation theory, the authors of this work [20] were able to show that proper islet function is fundamentally dependent on the connectivity of the  $\beta$ -cell network. Specifically, they highlighted the existence of a critical level of  $\beta$ -cell loss beyond which the network can no longer maintain site percolation, leading to a breakdown in connectivity. This threshold aligns closely with experimental and clinical findings that identify a similar degree of  $\beta$ -cell loss as the tipping point at which islet function fails in type 1 diabetes.

The authors modeled the structure of a pancreatic islet using a hexagonal close-packed lattice, for which percolation theory predicts a critical site open probability,  $p_c$ , of approximately 0.199. Since the typical site open probability for  $\beta$ -cell clusters ranges between 0.5 and 0.7 (see Sec. 2.2.2), this indicates that in healthy islets, the  $\beta$ -cell network exceeds the percolation threshold and thus forms a spanning, connected cluster. To fall below this critical threshold, about 72% of the  $\beta$ -cell in a healthy cluster would need to be lost. This level of cell loss aligns well with clinical data that identify a similar range as the point at which islet function begins to fail. Furthermore, the sharp, nonlinear shift from normal function to dysfunction can be effectively described as a phase transition within a dynamical system [20].

Interestingly, the model also accounts for the *honeymoon phenomenon*, which is a temporary restoration of islet function that often occurs shortly after treatment begins in type 1 diabetes patients.

In general, loss of  $\beta$ -cell synchronization can result from reduced site occupancy (due to cell death), weakened intercellular coupling (through impaired gap junctions), or both. Let us consider a healthy islet positioned at point 1 in a conceptual diagram (see Fig. 7), where  $\beta$ -cell mass and gap-junctional connectivity are fully intact [20]. As the disease progresses,  $\beta$ -cell destruction reduces site occupancy, and if this were the only factor, the system would follow a vertical path downward to point 3. Upon crossing the critical threshold, synchronization would collapse, leading to functional failure.

However, type 1 diabetes also involves factors like inflammation, oxidative stress, and hyperglycemia, which damage gap junctions and consequently reduce coupling strength. This shifts the path leftward to point 2, where the islet loses synchronization and function, even with a higher residual  $\beta$ -cell mass than at point 3.

Treatment, typically aimed at improving glycemic control and reducing inflammation, can partially restore the functionality of gap junctions. This improvement increases coupling strength, moving the system back to the right across the critical line and temporarily restoring synchronization and functionality, as seen in the honeymoon phase.

Despite this recovery, ongoing autoimmune destruction caused by type 1 diabetes continues to deplete  $\beta$ -cell mass. Eventually, the system declines again, passing below the critical threshold and resulting in permanent loss of function (point 3). This trajectory explains the transient nature of the honeymoon phase, which often lasts between several months and a couple of years, observed in many patients with type 1 diabetes after the onset of treatment [20].

### 3 MODELS OF COUPLED OSCILLATORS

In this modeling framework, the complex biological processes underlying  $\beta$ -cell function, such as membrane excitability, gap-junctional electrical coupling, and paracrine signaling, are not modeled in mechanistic detail. Instead, the collective behavior of the  $\beta$ -cell population is approximated using a simplified, abstract representation based on networks of coupled oscillators. Typical choices for these oscillators include the Kuramoto model, which focuses on phase interactions, and the FitzHugh-Nagumo model, which captures excitable dynamics with minimal complexity.

The principal advantage of this abstraction lies in its ability to reveal large-scale, emergent properties of the  $\beta$ -cell network without requiring full biophysical detail. For example, such models have been successfully employed to investigate the conditions under which synchronization arises among  $\beta$ -cells, to characterize the role of heterogeneity within the cell population, and to identify subsets of cells with disproportionately strong influence on the overall dynamics, the so-called *pacemaker* cells.

However, the trade-off for this conceptual simplicity is a reduced capacity to directly relate model behavior to specific intracellular pathways or molecular mechanisms. Cellular processes such as calcium handling, ion channel kinetics, and glucose metabolism are typically excluded or only implicitly represented. As a result, while coupled oscillator models are powerful tools for exploring the collective dynamics and coordination within islet cell populations, they are less suited for studies that aim to directly link electrophysiological behavior with biochemical signaling or metabolic regulation.

Nonetheless, this class of models is a very valuable part of the theoretical toolkit in the study of Langerhans islet and, more in general, excitable cell cluster physiology. By capturing essential dynamical features of cell interactions, they enable an understanding of phenomena at a complex systems level, which is very difficult to grasp within the plethora of variables and parameters used in full biophysical models. Obviously, this advantage is even more significant when accounting for cell heterogeneity, as the resulting complexity of full biophysical models can become overwhelming.

Before presenting some of the most relevant examples of multicellular models in this category, we first introduce the FitzHugh-Nagumo (FHN) oscillator, a commonly used non-linear system that serves as a foundational element in this modeling framework and plays a central role in the models developed in this thesis.

#### 3.1 FitzHugh-Nagumo Oscillator

The FHN oscillator was presented in 1961 by R. FitzHugh [9, 10] with the aim to provide a simplified two-dimensional version of the four-dimensional Hodgkin-Huxley model of the action potential of squid giant axons. It is named *FitzHugh-Nagumo* because it was further refined about a year later by Nagumo et al., who proved its equivalence to an electrical circuit [11].

Therefore, the FHN oscillator is originally a neuronal dynamics model and was soon broadly adopted for this purpose. In addition, it has been adapted into numerous variants of the original system and explored across several disciplines, owing to its structural simplicity and the ability to capture a wide range of dynamical behaviors [67].

Both the Hodgkin-Huxley and FHN models are excitable systems, exhibiting three phases of activity [67]:

**Resting state:** The system resides in a stable equilibrium, exhibiting no significant activity in the absence of external input.

**Excited state:** If the external input, or stimulus, surpasses a critical threshold, the sys-

tem is driven out of equilibrium, producing a fast and temporary response characteristic of excitation.

**Refractory period:** After this response, the system enters a recovery phase during which it is temporarily less sensitive to further stimuli and cannot be re-excited immediately.

Mathematically, the model consists of two main components [68]. The first is a voltage-like, fast variable whose dynamics includes a cubic nonlinearity. This nonlinearity enables the system to exhibit regenerative self-excitation through a mechanism of positive feedback, allowing rapid activation once a threshold is crossed. The second component is a recovery variable that evolves more slowly and follows a linear dynamics. This variable introduces a negative feedback that acts to stabilize the system and return it to its resting state after excitation.

The version of the FHN equations used in most of this thesis work is as follows [9, 10, 12, 1]:

$$\dot{x} = a \left( x - \frac{x^3}{3} + y \right), \quad (13a)$$

$$\dot{y} = -\frac{1}{a} (x + by - J), \quad (13b)$$

where  $x(t)$  denotes the fast variable corresponding to the cell membrane potential, while  $y(t)$  represents the slower recovery variable. The quantity  $J$  functions as an external stimulus current. The parameters  $a$  and  $b$  are proportional to the ratio of inductance to capacitance and to the electrical resistance of the cell membrane, respectively [12]. They are assumed to be positive,  $a > 0$  and  $b > 0$ , as this ensures that the behavior of the model is physically meaningful in its typical applications. As will be shown later, these parameters also play a critical role in determining both the period and the shape of the resulting oscillations.

The above system of equations possesses an equilibrium point, whose stability is governed by a critical threshold value  $\varepsilon$  of the external stimulus  $J$ . This threshold, which is where a Hopf bifurcation takes place, determines whether the system remains at rest or transitions into oscillatory behavior. To calculate  $\varepsilon$ , let us first impose the general condition for the occurrence of an equilibrium point, which is that both derivatives,  $\dot{x}$  and  $\dot{y}$ , are zero. This yields the following equations:

$$a \left( x_h - \frac{x_h^3}{3} + y_h \right) = 0, \quad (14a)$$

$$-\frac{1}{a} (x_h + by_h - J) = 0, \quad (14b)$$

where we have designated with  $x_h$  and  $y_h$  the coordinates of the specific equilibrium point we are looking for, where the Hopf bifurcation occurs.

We now extract  $y_h$  from Eq. (14a) and substitute it into Eq. (14b). From Eq. (14b), we can then extract the specific value of  $J$ , which we call  $J_h$ , corresponding to the equilibrium point where the Hopf bifurcation occurs, which by definition coincides with the threshold  $\varepsilon$ :

$$y_h = -x_h + \frac{x_h^3}{3}, \quad (15)$$

$$J_h = \varepsilon = x_h + by_h = x_h + b \left( -x_h + \frac{x_h^3}{3} \right) = x_h(1 - b) + \frac{bx_h^3}{3}. \quad (16)$$

For a Hopf bifurcation to take place at this equilibrium point, the conditions to be met are that the trace of the Jacobian matrix of the system of Eqs. (13) must be zero,  $\text{tr}(\mathcal{J}) = 0$ , and its determinant must be positive,  $\det(\mathcal{J}) > 0$ . The Jacobian matrix for the aforementioned system is defined as

$$\mathcal{J} = \begin{bmatrix} \frac{\partial f}{\partial x} & \frac{\partial f}{\partial y} \\ \frac{\partial g}{\partial x} & \frac{\partial g}{\partial y} \end{bmatrix}, \quad (17)$$

where

$$f(x, y) = a \left( x - \frac{x^3}{3} + y \right), \quad (18)$$

$$g(x, y) = -\frac{1}{a} (x + by - J). \quad (19)$$

Therefore, after calculating the derivatives, one obtains:

$$\mathcal{J} = \begin{bmatrix} a(1-x^2) & a \\ -\frac{1}{a} & -\frac{b}{a} \end{bmatrix}. \quad (20)$$

Upon imposing the condition  $\text{tr}(\mathcal{J}) = 0$  at the equilibrium point  $(x_h, y_h)$  where the Hopf bifurcation occurs, we get:

$$\text{tr}(\mathcal{J}) = a(1-x_h^2) - \frac{b}{a} = 0 \quad \Rightarrow \quad x_h^2 = 1 - \frac{b}{a^2}, \quad (21)$$

from which we take the positive solution:

$$x_h = \sqrt{1 - \frac{b}{a^2}}. \quad (22)$$

Let us now plug Eq. (22) into Eq. (16):

$$\begin{aligned} \varepsilon &= J_h = x_h(1-b) + \frac{bx_h^3}{3} = \\ &= \sqrt{1 - \frac{b}{a^2}} \left( 1 - b + \frac{b}{3} \left( 1 - \frac{b}{a^2} \right) \right) = \\ &= \sqrt{a^2 - b} \cdot \frac{1}{a} \cdot \left( \frac{3a^2(1-b) + b(a^2 - b)}{3a^2} \right) = \\ &= \frac{3a^2 - 2a^2b - b^2}{3a^3} \sqrt{a^2 - b}. \end{aligned} \quad (23)$$

Eq. (23) implies that we must assume  $a^2 - b > 0$ , i.e.,  $a^2 > b$ , since the Hopf bifurcation threshold  $\varepsilon$  must be real and positive to have physical meaning. From the way we have obtained  $\varepsilon$ , it follows that an equilibrium point of the FHN model described by Eqs. (13) is stable when  $|J| > \varepsilon$  and unstable when  $|J| < \varepsilon$  [12, 1]. This means that, when  $J < -\varepsilon$ , the system is in an excitable resting state (stable equilibrium point), where  $x(t)$  has a constant negative value. If the stimulus  $J$  exceeds the lower threshold, i.e.  $J > -\varepsilon$ , the system becomes oscillatory, exhibiting periodic spiking activity (unstable equilibrium point). However, if the external stimulus increases further and exceeds the upper threshold, i.e.  $J > \varepsilon$ ,

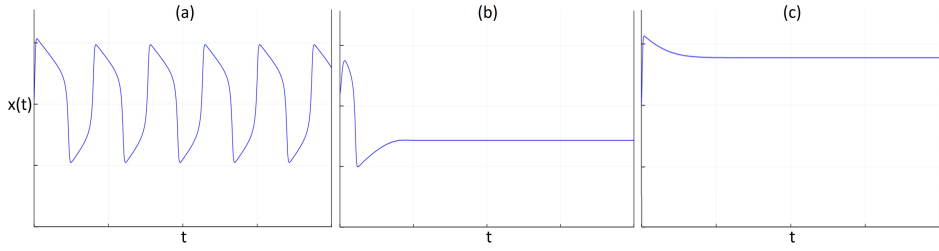


Figure 8: Plots of  $x(t)$  produced by the FHN model, corresponding to different ranges of  $J$  values (arbitrary units). (a)  $-\varepsilon < J < \varepsilon$  (periodic spiking activity). (b)  $J < -\varepsilon$  (resting state). (c)  $J > \varepsilon$  (excitation block state).

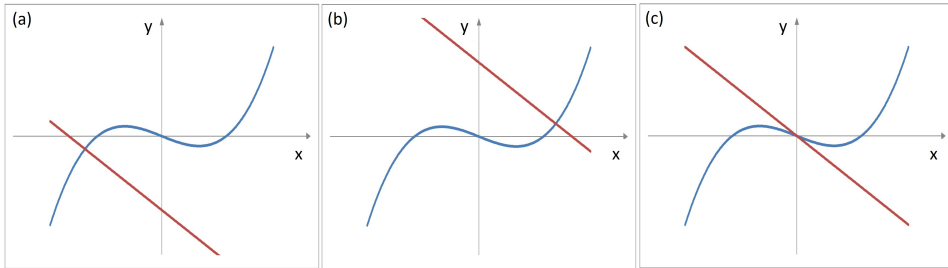


Figure 9: Plots of the nullclines corresponding to Eqs. (24a) (blue curves) and (24b) (brown curves). In panels (a) and (b), the intersection occurs on the left and right branch of the cubic nullcline, respectively, corresponding to stability. In panel (c), the intersection occurs on the middle branch of the cubic nullcline, corresponding to instability.

the equilibrium point becomes stable again, so the system enters an *excitation block* state, where oscillations are blocked by excitation [68] and the system is in fact resting but has a constant positive value of  $x(t)$ . This is illustrated in Fig. 8.

An important advantage of the FHN model is that its relative simplicity and two-dimensional nature allow the entire dynamics to be visualized in a single phase portrait, whereas the Hodgkin-Huxley model requires examining projections of trajectories in a four-dimensional phase space [68]. For example, the relative positions of the two nullclines of the FHN model help illustrate how the system responds to different values of  $J$ . The nullclines are obtained by setting  $\dot{x} = 0$  and  $\dot{y} = 0$  in Eqs. (13), and plotting  $y$  as a function of  $x$ :

$$y = -x + \frac{x^3}{3}, \quad (24a)$$

$$y = \frac{1}{b}(J - x). \quad (24b)$$

At the intersection of these two curves, by definition, both derivatives vanish, therefore the intersection geometrically represents an equilibrium point. As  $J$  varies, the linear nullcline shifts vertically, while its slope remains constant at  $-1/b$ . When  $|J| > \varepsilon$ , the intersection lies on either the left branch ( $J < -\varepsilon$ ) or the right branch ( $J > \varepsilon$ ) of the cubic nullcline. In both of these regions,  $|x| > 1$ , implying that the partial derivative with respect to  $x$  of the right-hand side of Eq. (13a) is negative,  $a(1 - x^2) < 0$ . This means negative feedback in the fast subsystem of the model, which supports stable equilibrium points in these two regions. In contrast, when  $|J| < \varepsilon$ , the intersection occurs on the middle branch of the

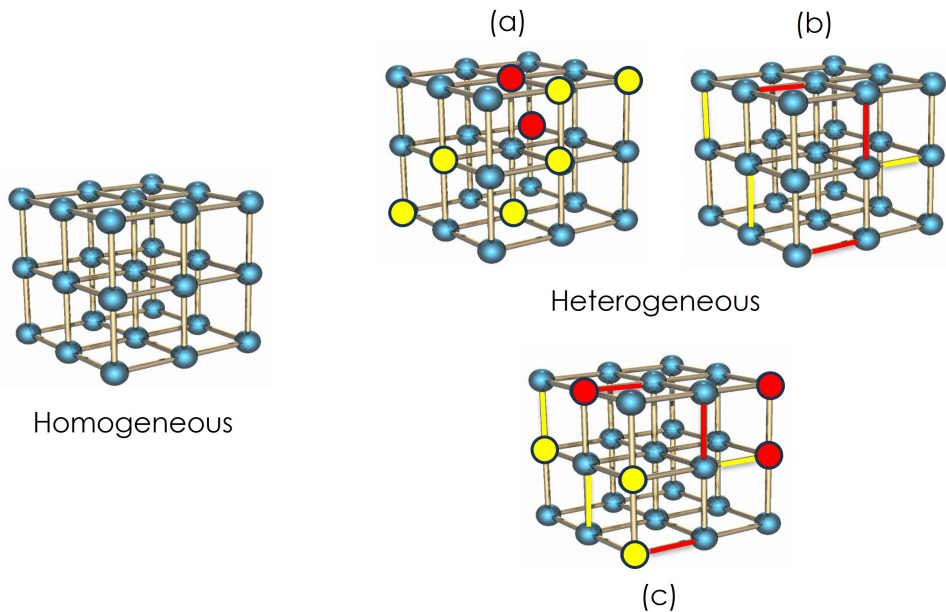


Figure 10: Examples of cubic lattice networks: on the left, homogeneous; on the right, heterogeneous (different types). Among the heterogeneous examples, (a) corresponds to variations in the parameter space of the network units; (b) to variations in the coupling strength (or type of coupling); (c) to variations in both the parameter space of the units and coupling.

cubic nullcline, where  $|x| < 1$  and  $a(1 - x^2) > 0$ . As a consequence, there is now positive feedback in the fast subsystem, leading to instability of the equilibrium points in this region. This is graphically shown in Fig. 9.

### 3.2 Heterogeneity in Coupled Oscillator Networks

As explained in Sec. 1.3, it is widely accepted that in several biological systems, cellular diversity plays an important constructive role, increasing the robustness, as well as the adaptability and sensitivity to external stimuli, of tissues, cell clusters, or more generally cell systems. It is remarkable that in complex systems physics, the same has been shown to be true in the case of coupled oscillator networks, where heterogeneity of the component units of the network can be responsible for the appearance of emergent properties, amplifying the network response to an external signal and/or strengthening its stability against external perturbations. This is one of the key reasons for using coupled oscillator networks as a basis to model excitable cell networks, especially when investigating the effects of cellular diversity on network synchronization.

Heterogeneity can be introduced in coupled oscillator network models by appropriately varying the parameter space of the system across the population of its units. The variation may concern either the parameters that define the dynamics of the units, or the coupling between units, or both. Fig. 10 provides a visual illustration of these possibilities in the case of a network with cubic lattice topology.

### 3.2.1 Cartwright Model

One of the earliest studies of this kind dates back to the year 2000, when Cartwright introduced a heterogeneous  $\beta$ -cell network model based on diffusively coupled FHN units [12]. In this model, two distinct types of FHN units are distributed across a network with a cubic lattice topology. Heterogeneity is introduced by randomly assigning to each unit one of two parameter values, specifically  $J_i = -v$  or  $J_i = +v$ , in the following equations:

$$\dot{x}_i = a \left[ x_i - x_i^3/3 + y_i + C \sum_{j \in \Omega_i} (x_j - x_i) \right], \quad (25a)$$

$$\dot{y}_i = -\frac{1}{a} (x_i + by_i - J_i). \quad (25b)$$

Eqs. (25) are derived from the previously shown FHN equations for an isolated oscillator, Eqs. (13), with the addition of a diffusive coupling term  $C \sum_{j \in \Omega_i} (x_j - x_i)$  to the first equation, where the sum is taken across the cells  $\Omega_i$  that are coupled to the  $i$ th cell, which are its six nearest neighbors in the cubic lattice. The coupling constant is assumed to be the same across all connections; thus, heterogeneity is introduced solely through variations in the parameter space that governs the dynamics of the individual FHN units. It should be noted that, in this study,  $v$  is a positive quantity chosen in such a way that  $v > \varepsilon$ , where  $\varepsilon$  is defined by Eq. (23). This means that each FHN unit in the network, taken individually, is in an excitable, non-oscillatory state; specifically, the units characterized by  $J_i = -v$  are in a resting state, while the ones with  $J_i = +v$  are in an excitation block state (see Sec. 3.1). Despite this, the study shows that by running numerical simulations on a network comprising  $4 \times 4 \times 4$  FHN elements, it is possible to observe strong and synchronized collective oscillations of the network for values of the coupling strength  $C$  above a certain threshold. These collective oscillations represent a remarkable case of emergent network property, considering that the parameters that define the dynamics of the individual units correspond to quiescent states. Instead, it can be shown that a homogeneous network with the same topology, which is composed of identical FHN units (all with  $J_i = -v$  or all with  $J_i = +v$ ) remains in a non-oscillatory state.

In this work [12], Cartwright also proposed using the above-described network of FHN units as a model for a  $\beta$ -cell cluster. Building on the analogy with the results obtained from his FHN network model, he highlighted that the presence of *hubs* or *pacemaker* cells in  $\beta$ -cell clusters is not necessary for the generation of global network oscillations, as such oscillations can emerge independently of the existence of intrinsically oscillatory units and instead arise as a collective effect driven by network heterogeneity.

### 3.2.2 Diversity-Induced Resonance

In the first two decades of the current century, various theoretical studies have documented similar effects to the one presented in Ref. [12], by investigating the dependence of collective oscillations of nonlinear oscillator networks on the heterogeneity of their dynamical parameters, as well as on the action of external forces/signals to which network elements may be subjected.

In this context, Tessone et al. [13] investigated two paradigmatic examples: a network of quartic oscillators and a network of FHN units, both characterized by diffusive, all-to-all coupling. Like in Cartwright's work, diversity was introduced by varying an additive parameter in the dynamical equations, i.e., the equivalent of  $J_i$  in Eqs. (25). However, in this case, the values  $J_i$  were extracted from a Gaussian distribution with a mean  $J_{av}$  and a standard deviation  $\sigma$ , where  $\sigma$  is a measure of the diversity of the network. Both systems

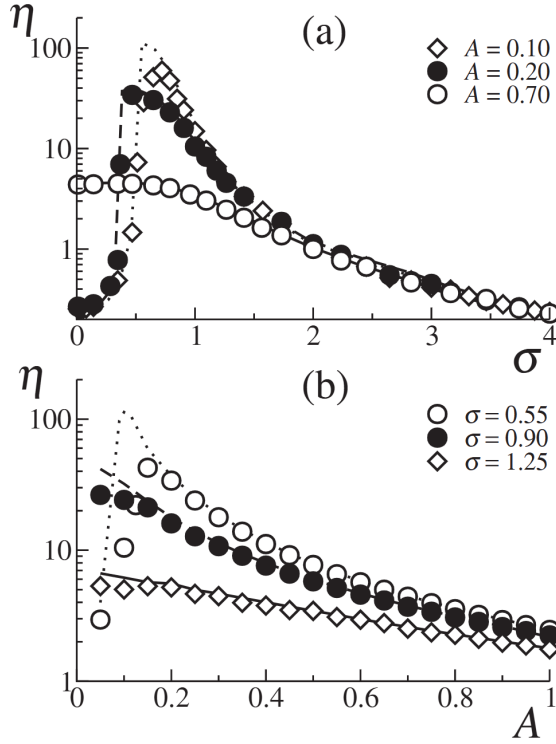


Figure 11: DIR in an ensemble of heterogeneous, globally coupled bistable oscillators with periodic external forcing of amplitude  $A$ . Panel (a): collective oscillatory activity  $\eta$  as a function of  $\sigma$  for different  $A$  values. Panel (b):  $\eta$  as a function of  $A$  for different  $\sigma$  values. Reprinted figure with permission from [C. Tessone, C. Mirasso, R. Toral, J. Gunton. *Phys. Rev. Lett.* **97**, 194101 (2006).] Copyright 2006 by the American Physical Society. <https://doi.org/10.1103/PhysRevLett.97.194101>

were subjected to sinusoidal external forcing through a term  $A \sin \omega t$ . Both the mean of the diversity distribution,  $J_{av}$ , and the amplitude of the external forcing,  $A$ , were chosen so that, in the absence of diversity (i.e. for  $\sigma = 0$ ), the external forcing alone would not be sufficient to push any of the network units from the region of excitability (non-oscillatory) into the oscillatory regime. This can be expressed by saying that all network units were *subthreshold* for  $\sigma = 0$ .

Upon increasing diversity, i.e. for  $\sigma > 0$ , some units may become *suprathreshold* when the external stimulus reaches its maximum intensity, if their diversity parameter  $J_i$  is large enough, meaning that they will become oscillatory. Due to the coupling term, the oscillatory units will *pull* at least some of the units that are still intrinsically in a quiescent state, making them oscillatory as well and producing a collective oscillatory effect.

As shown in Fig. 11(a), a plot of the collective oscillatory activity of the network as a function of  $\sigma$  exhibits a progressive increase up to a certain optimum value of  $\sigma$ , followed by a decline that tends to zero when  $\sigma$  becomes too large. The decline is due to the fact that, for large  $\sigma$  values beyond the optimum, the positions of the  $J_i$  values of each unit along the  $J$  axis are so scattered that several quiescent units, being very far away from the threshold, offer too much resistance, and the oscillatory units are not able to pull them any more (in the FHN case, this is further complicated by the fact that some units will even fall in the excitation block region). As a consequence, the plot shows a

relatively sharp resonance maximum corresponding to the optimum value of diversity, which is why this effect has been named *Diversity-Induced Resonance* (DIR) by the authors [13]. Fig. 11(b) shows the dependence of the collective oscillatory activity on the external forcing amplitude, for different values of  $\sigma$ . If we consider the external sinusoidal force as a signal and the oscillator network as a sensor for this signal, it is clear that an optimal level of diversity enables a higher sensitivity and a more efficient amplification of the network response to the signal.

Based on this reasoning, the authors speculated that cellular heterogeneity, which can be observed in several biological systems, may play a crucial role in the physiological efficiency of the latter, and that the degree of diversity might have been optimized by nature through evolution in order to achieve maximum sensitivity and functionality [13].

### 3.2.3 Other DIR models

A few months prior to the publication by Tessone et al. [13], Pazó and Montbrió [69] investigated a system composed of Morris-Lecar units that were organized into two distinct subpopulations: one consisting of identical excitable units and the other of identical oscillatory units. These units interacted through a global linear all-to-all coupling scheme. Their study also highlighted the presence of a “pulling” phenomenon, whereby the oscillatory subpopulation could induce oscillations in the excitable units, effectively entraining the entire network. This interaction emerged as the dominant mechanism causing the onset of collective oscillatory behavior within the network. Consequently, they found that the global dynamics of the system could be inferred from the relative abundance of oscillatory versus excitable units.

Comparable findings were reported two years later by Chuan-Sheng et al. [70], who analyzed a one-dimensional chain of heterogeneous FHN units with nearest-neighbor interactions, supplemented by a certain number of randomly added long-range links, referred to as “shortcuts”. In their model, most or all units operated below the excitation threshold and could be induced to oscillate either by increasing heterogeneity or through external stimulation. Their analysis demonstrated that the amplitude of global oscillations across the network could be maximized by tuning key parameters: specifically, by selecting an optimal level of heterogeneity, an appropriate coupling strength, and a favorable number of shortcuts. They likewise interpreted the generation of collective oscillatory behavior as being driven by a subset of intrinsically oscillatory elements that effectively entrain the excitable ones through network interactions.

## 3.3 3D Model Based on Heterogeneous FHN Units

In this work, Scialla et al. [1] focused on the long-standing question whether hubs, or pacemaker cells, in Langerhans islets are a permanently distinct subpopulation of  $\beta$ -cells or, vice versa, different  $\beta$ -cell subsets can behave like hubs or standard cells as a function of time and external factors, such as glucose concentration. To get some insights on this question, they modeled a Langerhans islet by a 3D system of coupled FHN units with the same cubic lattice topology as that used by Cartwright (see Sec. 3.2.1). The cubic lattice topology can be considered reasonably realistic in this context, because each unit of the cubic lattice has six nearest neighbors and it has been experimentally determined that  $\beta$ -cells in a Langerhans islet have six or seven adjacent cells on average [71, 72]. In addition, the cubic lattice used in their simulations comprised  $10^3$  FHN units ( $10 \times 10 \times 10$ ), which is also consistent with the average number of  $\beta$ -cells that form a Langerhans islet. Therefore, a central objective of this study was to determine whether the existence of hub cells and their main biophysical properties could be inferred from the overall dynamical be-

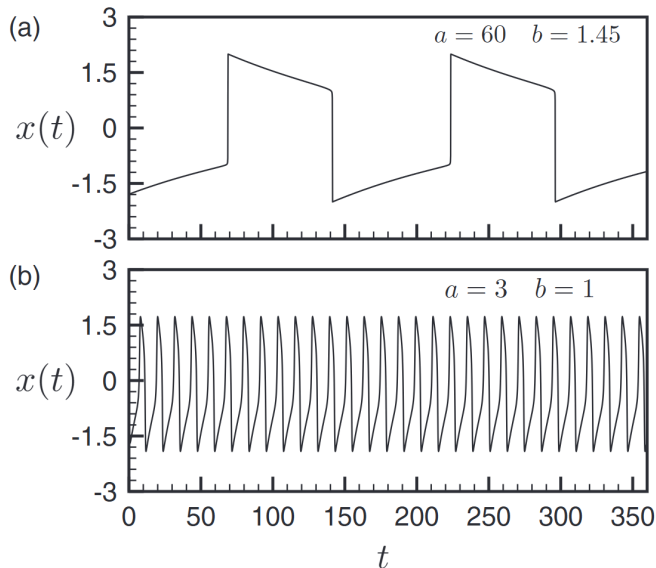


Figure 12: Oscillation  $x(t)$  of a single FHN element for different values of parameters  $a$ ,  $b$  and an external stimulus  $|J| < \epsilon$  [see Sec. 3.1], corresponding to the oscillatory regime. Reprinted figure with permission from [S. Scialla, A. Loppini, M. Patriarca, E. Heinsalu. *Phys. Rev. E* **103**, 052211 (2021)]. Copyright 2021 by the American Physical Society. <https://journals.aps.org/pre/abstract/10.1103/PhysRevE.103.052211>

havior of a network of coupled oscillators designed to replicate the electrical activity of a  $\beta$ -cell cluster.

### 3.3.1 Choice of Model Parameters and Correlation with $\beta$ -Cell Physiology

The dynamical equations used by Scialla et al. [1] to represent their model are the same as in the work by Cartwright [12], Eqs. (25), with some important differences in the choice of the parameter values. It should be noted that parameters  $a$  and  $b$  in Eqs. (25) determine, besides the value of  $\epsilon$  (see Eq. (23)), the shape of  $x(t)$  oscillations. In particular, the oscillation period  $T$  scales proportionally with the parameter  $a$ , so that increasing  $a$  results in longer periods. On the other hand, parameter  $b$  primarily influences the proportion of time the system spends at higher versus lower values of  $x(t)$  during each oscillatory cycle. This is illustrated in Fig. 12, showing a comparison between slower (Fig. 12(A)) and faster (Fig. 12(B)) oscillations, corresponding to different combinations of  $a$  and  $b$  values. In most of the simulations presented in their study, Scialla et al. used the combination  $a = 60$  and  $b = 1.45$ , corresponding to Fig. 12(A). When time is measured in seconds, this specific parameter combination produces an oscillatory waveform with a period of approximately  $T \approx 150$  s. The resulting waveform features a slightly longer duration of the low- $x(t)$  phase compared to the high- $x(t)$  phase, closely resembling the characteristic temporal pattern of bursting oscillations observed in  $\beta$ -cell clusters [30].

It should be apparent from looking at Fig. 12(A) that the fast action potential spikes superimposed on slower bursting oscillations, which are typical features of the electrical activity of  $\beta$ -cells (as shown previously in Fig. 2) are not explicitly represented in this model, which relies on a FHN formulation. Nonetheless, this work was focused on exploring the collective behavior and synchronization properties of oscillator networks that

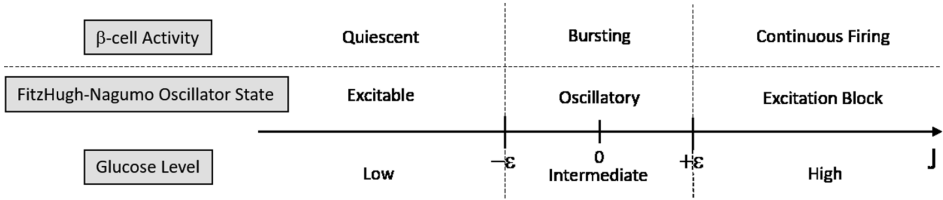


Figure 13: Correspondence between  $\beta$ -cell activity and FHN oscillator states. Reprinted figure with permission from [S. Scialla, A. Loppini, M. Patriarca, E. Heinsalu. *Phys. Rev. E* **103**, 052211 (2021)]. Copyright 2021 by the American Physical Society. <https://journals.aps.org/pre/abstract/10.1103/PhysRevE.103.052211>

serve as simplified representations of  $\beta$ -cell clusters, with particular attention to the effects of heterogeneity. Within this modeling context, the slower bursting component is of greater interest than the high-frequency spikes, primarily because of its established link to pulsatile insulin secretion, which is a process of fundamental physiological significance.

The other key parameter in Eqs. (25) is  $J_i$ , which determines whether the  $i$ th FHN unit is in an oscillatory state, corresponding to bursting activity (for  $|J_i| < \epsilon$ ), or in an excitable state (for  $|J_i| > \epsilon$ ), as explained in Sec. 3.1, where an expression to determine  $\epsilon$  from the values of  $a$  and  $b$  is also provided (see Eq. (23)). In this model,  $J$  is correlated to the glucose level  $G$  in the bloodstream through some function  $J = f(G)$ , so that  $J < -\epsilon$  corresponds to low glucose levels, where  $\beta$ -cells are in a quiescent state; the range  $-\epsilon < J < \epsilon$  corresponds to intermediate glucose levels, where  $\beta$ -cells are bursting; and  $J$  values above  $\epsilon$  are representative of high glucose levels, where  $\beta$ -cells are in a state of continuous firing (corresponding to excitation block), with  $x(t)$  constantly positive. This is illustrated in Fig. 13.

It is important to note that, since  $J$  in the FHN equations is a constant, this model treats the glucose level in the bloodstream as a constant. This assumption is consistent with most mathematical models that describe  $\beta$ -cell electrical activity and is supported by the relevant timescale separation: the bursting dynamics evolves much more rapidly than the slower physiological processes responsible for altering glucose levels, such as uptake by peripheral tissues and feedback from hepatic regulation.

To incorporate diversity within the network of coupled oscillators, the model assigns to each FHN unit a distinct sensitivity to the external input. Mathematically, this corresponds to associating a different value  $J_i$  with each oscillator  $i$ . From a physiological perspective, this reflects the assumption that individual  $\beta$ -cells within an islet exhibit varying sensitivities to glucose concentrations, a premise that aligns well with experimental findings on  $\beta$ -cell heterogeneity [73–75]. The  $J_i$  values were sampled from a Gaussian distribution characterized by a mean  $J_{av}$  and a standard deviation  $\sigma$ , the latter quantifying the degree of heterogeneity within the oscillator population [13]. As noted earlier, the mean value  $J_{av}$  corresponds to the average external stimulus and serves as a proxy for blood glucose concentration. Consequently, it can be modulated over a relatively wide range to reflect different physiological conditions. The authors performed model simulations corresponding to different  $J_{av}$  and  $\sigma$  values, as will be discussed later.

The coupling strength was fixed at  $C = 0.15$ , as this value yields an efficient level of interaction among network units: lower values lead to a marked reduction in the amplitude of global oscillations, while further increases in  $C$  do not make any difference. This choice is further justified and quantitatively illustrated in the following section. From a modeling standpoint, it represents a biologically plausible compromise, ensuring sufficiently effec-

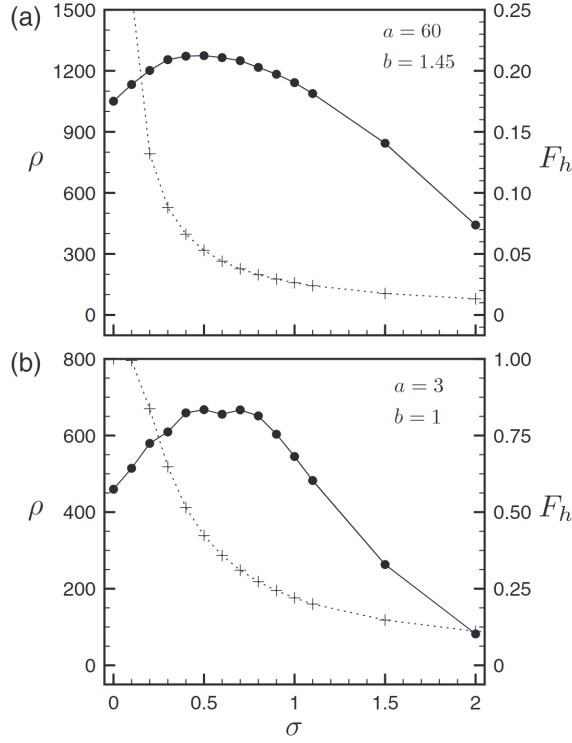


Figure 14: Global oscillatory activity  $\rho$  (dots, solid curve, left axis) defined in Eq. (26) and fraction of hubs  $F_h$  (crosses, dotted curve, right axis) defined in Eq. (5) as a function of population diversity  $\sigma$ , for different values of  $a$  and  $b$ ;  $J_{av} = 0$ . Reprinted figure with permission from [S. Scialla, A. Loppini, M. Patriarca, E. Heinsalu. *Phys. Rev. E* **103**, 052211 (2021)]. Copyright 2021 by the American Physical Society. <https://journals.aps.org/pre/abstract/10.1103/PhysRevE.103.052211>

tive coupling without exceeding realistic physiological limits.

### 3.3.2 Simulation Results and Estimate of Hub Percentage

After numerically solving the FHN Eqs. (25) with the above-mentioned topology and parameters, the global oscillatory activity of the network,  $\rho$ , was calculated from the expression:

$$\rho = \frac{1}{N} \sqrt{\frac{1}{t_f} \int_0^{t_f} dt [X(t) - \bar{X}]^2}, \quad (26)$$

where  $N = 10^3$  denotes the total number of units in the network,  $X(t)$  represents the collective oscillation obtained by summing all individual  $x_i(t)$  contributions, and  $\bar{X}$  is the time-averaged value of  $X(t)$  over the interval  $[0, t_f]$ . By definition, the quantity  $\rho$  corresponds to the root mean square amplitude of the global network oscillation  $X(t)$ , which exhibits periodic behavior. As a result,  $\rho$  remains effectively constant with respect to the choice of  $t_f$ , provided that  $t_f$  is sufficiently large to encompass multiple oscillation cycles. The authors verified that a value of  $t_f = 300$  time units satisfies this criterion in their numerical simulations.

The dependence of the global oscillatory activity  $\rho$  on the diversity parameter  $\sigma$  is illustrated in Fig. 14(a) (solid curve). The results reveal a pronounced resonance centered at  $\sigma = 0.5$ , caused by network diversity. The peak value of  $\rho$  observed at this optimal heterogeneity level is substantially higher than that obtained in the homogeneous case ( $\sigma = 0$ ), where all elements have identical dynamical states. The specific value of  $\sigma$  at which the resonance shows its maximum corresponds to the level of heterogeneity that optimizes collective oscillations within the network. Based on previous studies concerning the DIR effect [13, 69, 70], one can speculate that the enhancement arises, at least partially, from interactions between units that are intrinsically oscillatory—namely, those satisfying  $|J| < \varepsilon$ —and units that, in isolation, would not oscillate due to either being in a quiescent or excitation-block regime ( $|J| > \varepsilon$ ), but are nevertheless driven into oscillatory behavior through coupling and resonance mechanisms. However, based on Cartwright’s results [12] (see Sec. 3.2.1), we must assume that interactions between excitable units play a critical role as well, independently of the presence of oscillatory elements.

Following the introduction of heterogeneity through a Gaussian distribution of  $J_i$  values, and the subsequent analysis of global oscillatory behavior, it becomes a natural step to classify network elements according to their intrinsic dynamical regime. Specifically, oscillators for which  $|J| < \varepsilon$  fall within the oscillatory domain and can thus be interpreted as pacemaker units or “hubs” within the network. Conversely, elements with  $|J| > \varepsilon$  are considered non-hubs; although they are not intrinsically oscillatory, they may be recruited into active dynamics through their interactions with the rest of the network, with their responsiveness depending on how far their  $J_i$  values lie from the oscillatory threshold.

The proportion of hubs relative to non-hubs that corresponds to the maximum of the DIR provides an estimate of the most effective network composition, as it yields the highest level of global synchronization. This ratio can be quantified by evaluating the normalized Gaussian integral

$$F_h = \frac{1}{\sqrt{2\pi}\sigma} \int_{-\varepsilon}^{\varepsilon} dJ \exp \left[ -\frac{(J - \bar{J})^2}{2\sigma^2} \right], \quad (27)$$

which, by definition, gives the fraction of oscillators in the population whose  $J_i$  values lie within the interval  $|J| < \varepsilon$ , thus representing the proportion of hubs.

The behavior of  $F_h$  as a function of the diversity parameter  $\sigma$ , evaluated for  $a = 60$  and  $b = 1.45$ , is depicted in Fig. 14(a) (dotted curve). At the resonance peak located at  $\sigma = 0.5$ , the calculated hub fraction is  $F_h = 0.053$ , corresponding to approximately 5% of the total population. This value aligns well with experimental data obtained via optogenetic techniques [21, 76–78], which report typical hub fractions in the range of 1–10%. It is important to note that this prediction depends on the particular choice of model parameters  $a$  and  $b$  in Eqs. (25). The values of  $a$  and  $b$  corresponding to Fig. 14(a) were selected to reproduce the characteristic oscillation period of individual FHN units so as to match experimental observations of  $\beta$ -cell dynamics, as explained in Sec. 3.3.1. The parameter values corresponding to Fig. 14(b), which generate oscillations with a much shorter period, result in a different resonance profile and fraction of individually oscillatory units.

These findings indicate that the *in vivo* behavior of  $\beta$ -cells in Langerhans islets, when considered from the perspective of collective dynamics and network structure, is compatible with the intrinsic properties of a FHN oscillator network with cubic lattice topology and optimal heterogeneity. Additionally, as shown in Fig. 14, increasing  $\sigma$  beyond the resonance optimum leads to a monotonic decline in  $\rho$ . For instance, at  $\sigma = 2$ , where  $\rho$  is reduced to approximately one-third of its peak value, the corresponding hub fraction  $F_h$

drops to around 1%. This underscores the direct relationship between the proportion of intrinsically oscillatory units and the efficiency of collective oscillations, offering a potential mechanistic insight into how disruptions in the optimal hub/non-hub balance, such as those induced by pathological conditions, may impair coordinated activity in pancreatic islets.

### 3.3.3 Effect of Faster versus Slower Oscillations

For comparison purposes, the authors repeated the simulations using the alternative parameter set  $a = 3$  and  $b = 1$ , which corresponds to the faster oscillatory waveform depicted in Fig. 12(B). The detailed results are shown in Ref. [1]; we just mention here that the estimated fraction of hubs in this case falls in the range  $F_h = 0.36 - 0.52$ , i.e., a much higher amount than in the previously examined case, where  $F_h \approx 0.05$ .

This comparison suggests that sustaining faster global oscillations requires a relatively higher proportion of hubs to ensure effective synchronization across the network. This observation is consistent with both physical reasoning and physiological plausibility. In the case of slower oscillations, non-hub units—i.e., those that are not intrinsically oscillatory—have more time to respond to network interactions and become synchronized with the hubs through coupling mechanisms. As a result, a smaller fraction of hubs is sufficient to achieve coherent global dynamics. In contrast, faster oscillations provide less time for such entrainment, making synchronization more difficult unless a larger portion of the network is composed of hub units. This contrast is intentionally accentuated in the above comparison by employing markedly different values of  $a$  and  $b$  between the slow and fast wave scenarios. Nonetheless, the authors conclude that it would be valuable for future experimental studies to investigate this trend by comparing the proportion of active pacemaker cells during slow and fast bursting oscillations in  $\beta$ -cell clusters.

Another noteworthy observation is that, for both parameter combinations analyzed, the value of  $\sigma$  at which the diversity-induced resonance reaches its peak exceeds the corresponding threshold  $\varepsilon$  for intrinsic oscillatory behavior. Specifically,  $\varepsilon \approx 0.033$  for  $a = 60$ ,  $b = 1.45$ , and  $\varepsilon \approx 0.279$  for  $a = 3$ ,  $b = 1$ . This suggests that network elements with  $|J| > \varepsilon$ , while not individually oscillatory, can still make a positive contribution to resonance if their  $J_i$  values are not too far from the oscillatory range. Such excitable units can be recruited into collective oscillations via coupling, thereby enhancing the overall synchronization. In contrast, elements located at the extreme tails of the distribution, which lie far from the  $|J| < \varepsilon$  interval, remain unresponsive to coupling and therefore hinder global oscillatory activity. The highest network performance is thus achieved at the diversity-induced resonance maximum, where there is an optimal balance between the number of pacemakers and the number of excitable units that can be more easily driven into an oscillatory behavior, while minimizing the influence of non-responsive elements. Increasing  $\sigma$  beyond this point diminishes performance by simultaneously reducing the fraction of hubs and easily excitable units, while increasing the proportion of inactive, isolated elements.

### 3.3.4 Effect of Heterogeneity on Network Response to Varying Glucose Levels

The authors also analyzed the effect of displacing the mean value  $J_{av}$  of the  $J_i$  distribution relative to the center of the intrinsic oscillatory interval  $|J| < \varepsilon$ , while keeping the standard deviation  $\sigma$  fixed. This analysis provides insight into the network's capacity to sustain global oscillatory behavior when the external stimulus progressively shifts away from the range associated with intrinsic oscillator activity.

The simulations were carried out using  $a = 60$  and  $b = 1.45$ , corresponding to the

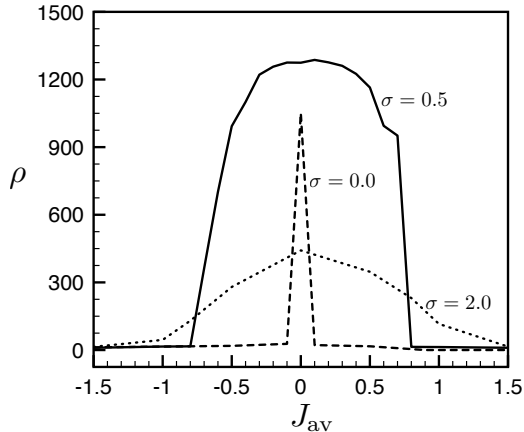


Figure 15: Global oscillatory activity  $\rho$ , defined in Eq. (26), as a function of the average value  $J_{av}$  of the stimulus, for different values of population diversity  $\sigma$  ( $a = 60$ ,  $b = 1.45$ ). Reprinted figure with permission from [S. Scialla, A. Loppini, M. Patriarca, E. Heinsalu. *Phys. Rev. E* **103**, 052211 (2021)]. Copyright 2021 by the American Physical Society. <https://journals.aps.org/pre/abstract/10.1103/PhysRevE.103.052211>

reference waveform described earlier, and were performed for three different values of  $\sigma$  representing distinct levels of heterogeneity:  $\sigma = 0$  (a fully homogeneous population),  $\sigma = 0.5$  (corresponding to the resonance maximum), and  $\sigma = 2.0$  (an example of pronounced diversity).

As shown in Fig. 15, oscillator diversity significantly broadens the range of external stimulus values  $J$  over which the network exhibits efficient global oscillations. In the absence of diversity ( $\sigma = 0$ ), all units are identical, and thus global oscillatory activity is confined strictly to the narrow interval  $|J| < \varepsilon \approx 0.033$ . In contrast, introducing heterogeneity enables the network to respond effectively across a much wider span of  $J$  values. This range increases with growing  $\sigma$ , although the efficiency of global oscillations, as quantified by  $\rho$ , diminishes beyond the resonance optimum. This trade-off is clearly illustrated by the comparison between the  $\rho$  curves for  $\sigma = 0.5$  and  $\sigma = 2.0$ , where the broader range of activity at higher  $\sigma$  is accompanied by a noticeable reduction in amplitude.

Further insight can be gained by examining the temporal evolution of the global signal  $X(t)$ , defined as the sum of the individual  $x_i(t)$  contributions, for various degrees of diversity. For example, at  $J_{av} = 0.5$ , the network exhibits resonant behavior and global oscillations for both  $\sigma = 0.5$  and  $\sigma = 2.0$ . However, a direct comparison of the corresponding  $X(t)$  traces (see Fig. 16) reveals substantial differences in both amplitude and regularity of the oscillations, which are reflected in the respective  $\rho$  values for the two parameter sets.

These differences can be attributed to two main factors: first, the broader  $J_i$  distribution at higher  $\sigma$  results in a larger fraction of units with  $J_i$  values lying well outside the oscillatory regime  $|J| < \varepsilon$ , making them less responsive to coupling. Second, the number of intrinsically oscillatory units (hubs) decreases substantially with increasing  $\sigma$ , further reducing the network's ability to sustain coordinated global activity.

From a physiological perspective, progressing from lower to higher values of  $J$  along the horizontal axis in Fig. 15 can be interpreted as simulating an increase in glucose concentration, ranging from basal to elevated levels, as discussed in Sec. 3.3.1 and illustrated

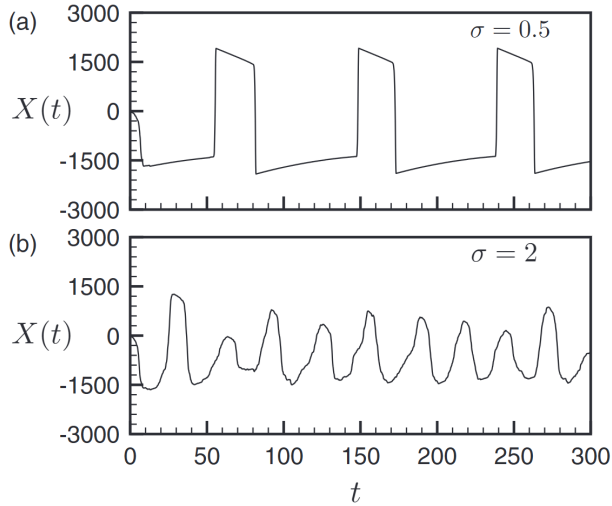


Figure 16: Global network oscillation  $X(t)$  for different values of population diversity  $\sigma$ , at the average value  $J_{av} = 0.5$  of the stimulus ( $a = 60$ ,  $b = 1.45$ ). Reprinted figure with permission from [S. Scialla, A. Loppini, M. Patriarca, E. Heinsalu. *Phys. Rev. E* **103**, 052211 (2021)]. Copyright 2021 by the American Physical Society. <https://journals.aps.org/pre/abstract/10.1103/PhysRevE.103.052211>

in Fig. 13. This observation supports the idea that  $\beta$ -cell heterogeneity may serve as a functional mechanism to enhance the robustness of islet oscillatory responses across a broad spectrum of glucose levels.

Another noteworthy feature in Fig. 15 is the asymmetry in the shape of the  $\rho(J_{av})$  curves for  $\sigma = 0.5$  and  $\sigma = 2.0$ . Specifically, the rise in oscillatory activity on the left-hand side of each curve is more gradual compared to the steeper decline observed on the right-hand side. Nevertheless, the right half of each curve spans a wider range of  $J_{av}$  values. Interpreting this again in physiological terms, one could say that as glucose levels increase, the network gradually enhances its collective oscillatory behavior and sustains a high level of activity for as long as the system remains capable of compensating for the strengthening input. This type of response profile, where global activity ramps up and is then maintained before an eventual decline, is consistent with predictions from more detailed biophysical models [79]. However, the model based on coupled oscillators offers a more transparent framework for understanding the fundamental role of network dynamics and oscillator diversity in shaping such behavior.

## 4 HETEROGENEITY AND NOISE

In the past two-three decades, increasing attention has been devoted to understanding how noise can play a constructive role in a variety of systems across biology, physics, and chemistry. Rather than merely being an undesired perturbation, noise has been shown to enhance or even enable complex dynamical behaviors, under certain conditions. This line of inquiry has become a central theme in the study of complex systems, particularly in exploring mechanisms by which variability contributes to functionality and emergent phenomena. A landmark contribution to this area was the conceptual development of stochastic resonance (SR), introduced in the early 1980s. Originally proposed as a mechanism to account for the periodic recurrence of Earth's ice ages [80], the idea of SR sparked wide interdisciplinary interest. Since then, it has been extensively investigated across numerous fields, from neuroscience [81, 82] and more generally biology to climate science [83], chemical kinetics [15], and electronic circuits [84], demonstrating that noise, when properly tuned, can enhance the detection or transmission of weak signals and lead to optimized system performance.

### 4.1 Stochastic Resonance and Noise-Driven Resonance Phenomena

Stochastic resonance (SR) is a phenomenon that can arise in nonlinear systems subjected simultaneously to a weak periodic input and stochastic fluctuations. Under suitable conditions, the presence of noise does not simply perturb the system but instead facilitates an enhanced response to the external signal. Specifically, when the noise intensity is tuned appropriately, the output of the system becomes synchronized with the periodic input, leading to an effective amplification of the signal, a counterintuitive effect that highlights the constructive role noise can play in nonlinear dynamics [15].

The concept of SR was introduced in a seminal paper by Benzi et al. [85], in which the authors proposed this idea as a mechanism to explain the periodic alternation between glacial and interglacial climate states on Earth. This alternation is more or less consistent with the period of a peak in the intensity of solar radiation, which occurs approximately every  $10^5$  years. However, the height of this peak, corresponding to about 0.1% of the solar constant, is not sufficient to explain a 10 K jump in average global temperatures, which characterizes the alternation between glacial and interglacial climate states. Specifically, it can be calculated that this external forcing alone cannot account for changes larger than about 1 K around a stable climate state. Benzi et al. [80] hypothesized that the alternation may derive from the combination of two factors: a periodic external forcing, with a period of  $10^5$  years, and an internal noise factor, associated with random fluctuations of the Earth's temperature, which are typically caused by large-scale oceanic and atmospheric processes and volcanic eruptions. The latter fluctuations, which can be modeled as random noise, are able in principle to cause transitions with a rate given by the inverse of Kramers time. However, such transitions have a very low probability because the energy associated with typical climatic fluctuations is much smaller than the height of the potential barrier separating stable states. Moreover, these transitions would occur randomly, without any periodicity.

The model they used is based on the following Langevin equation [80]:

$$\frac{dx}{dt} = x(a - x^2) + A \cos \omega t + \eta \xi(t) \quad (28)$$

where  $x(t)$  is the dynamical variable of interest, which in this case is temperature;  $a$  is a control parameter that defines the shape of the double-well potential (see discussion

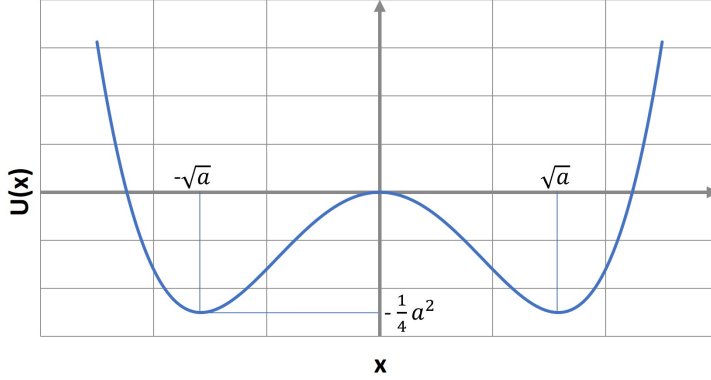


Figure 17: Plot of the symmetric double-well potential defined in Eq. (31), showing the coordinates of the minima and the height of the potential barrier.

below);  $A \cos \omega t$  is a weak periodic forcing; and  $\eta$  is the noise intensity.  $\xi(t)$  is a Gaussian white noise that satisfies the following conditions:

$$\langle \xi(t) \rangle = 0 \quad (29)$$

$$\langle \xi(t) \xi(t') \rangle = \delta(t - t') \quad (30)$$

Eq. (29) expresses the fact that the noise is unbiased, i.e., it fluctuates equally in the positive and negative direction. Eq. (30) states that the noise is uncorrelated in time. The latter condition implies that the noise is *white*, i.e., it has equal power at all frequencies.

In the absence of external forcing ( $A = 0$ ) and noise ( $\eta = 0$ ), the deterministic part of Equation (28) corresponds to motion in a double-well potential:

$$U(x) = -\frac{1}{2}ax^2 + \frac{1}{4}x^4. \quad (31)$$

When  $a > 0$ , this potential has minima at  $x = \pm\sqrt{a}$  and a maximum at  $x = 0$ , forming two stable symmetric wells separated by a barrier of height  $\Delta U = \frac{1}{4}a^2$ , as shown in Fig. 17.

Let us now consider the effect of the external periodic forcing alone,  $A \cos \omega t$ , on a system subjected to this double-well potential in the absence of noise, where  $A$  is chosen to be small enough that the contribution from this term is not capable of causing a transition between the two potential wells. This deterministic system will simply oscillate around the potential minimum in one of two wells.

On the other hand, the addition to this system of white noise alone (without periodic forcing) can cause random transitions between the two potential wells, characterized by absence of periodicity and an average transition rate  $W$  given by [86, 87]:

$$W = 1/\tau_k \approx \frac{\sqrt{|U''(0)U''(\sqrt{a})|}}{2\pi} \exp\left(-\frac{2\Delta U}{\eta}\right), \quad (32)$$

where  $\tau_k$  is Kramers time;  $U''(0)$  and  $U''(\sqrt{a})$  are, respectively, the curvature of  $U(x)$  at the maximum of the potential barrier, occurring at  $x=0$ , and at one of the potential minima, occurring at  $x = \sqrt{a}$ ;  $\Delta U$  is the height of the potential barrier; and  $\eta$  is the noise intensity defined in Eq. (28).

If both the external periodic forcing (with *small*  $A$ ) and the white noise are present together, as in the complete Eq. (28), then there are three possible regimes: a) in the case of *small* noise intensity  $\eta$ , transitions between the two minima occur rarely and irregularly, without periodicity; b) in the case of *large* values of  $\eta$ , the dynamics is dominated by noise and transitions occur very frequently and in a totally random fashion; c) for suitable, *intermediate* values of  $\eta$ , Kramers time becomes about equal to half the period  $T$  of the external forcing oscillations, i.e.,  $\tau_k = T/2$ , with the result that the effects of the external forcing and noise are synchronized. In this case, the system is able to transition from one potential minimum to the other in a periodic fashion and in phase with the external signal. This is the condition corresponding to SR, where the effect of an external forcing or signal is amplified by a synergistic interaction with noise of appropriate intensity.

Table 1: Comparison of different noise-induced resonance phenomena

Resonance Type	Key Mechanism	System Type	Role of Noise	Key References
<b>Stochastic Resonance (SR)</b>	Synchronization of noise-induced transitions with a weak <i>external periodic</i> signal.	Bistable systems (e.g., double-well potential).	Enables transitions over potential barrier; maximal efficiency when Kramers time matches signal period.	Benzi et al., <i>J. of Physics A</i> (1981) [80]; Benzi et al., <i>Tellus</i> (1982) [85].
<b>Autonomous SR</b>	Resonance via synchronization with <i>internal slow modulation</i> ; no external periodicity.	Bistable or excitable systems with internally fluctuating dynamics.	Induces transitions aligned with emergent timescales.	Gang et al., <i>PRL</i> (1993) [88].
<b>Self-Induced Stochastic Resonance (SISR)</b>	Noise-triggered transitions in fast variable synchronized with deterministic slow variable in a multiscale system.	Excitable systems with slow-fast timescale separation.	Weak noise perturbs fast variable; timing is set by slow dynamics.	Muratov et al., <i>Physica D</i> (2005) [89].
<b>Coherence Resonance (CR)</b>	Regularity emerges from noise alone, without any periodic signal or slow modulation.	Excitable systems.	Noise alone induces spikes; regularity is maximized at optimal noise intensity.	Pikovsky and Kurths, <i>PRL</i> (1997) [90].

Beyond its wide range of applications across various disciplines, SR has inspired the discovery of other constructive noise-induced phenomena that exhibit similar behavior. For example, it has been demonstrated that SR can emerge even in the absence of an external periodic signal, arising exclusively from the nonlinear internal dynamics of the system [88]. This phenomenon has been referred to as autonomous SR.

Another interesting example is provided by self-induced stochastic resonance (SISR) [89, 91], which we will describe in detail in the next section. In this case, an excitable system, e.g., a FHN unit, characterized by a strong separation of timescales, exhibits coherent oscillatory behavior due to the interplay between weak noise and the intrinsic slow dynamics of the system. Specifically, the noise perturbs the fast variable (which governs the system's rapid transitions), while the slow variable controls the timing at which the system becomes sensitive to those perturbations. This concerted interaction results in the emergence of a regular temporal structure, even though the system is not subjected to any external modulation.

Another closely related phenomenon is coherence resonance (CR), introduced by Pikovsky and Kurths [90]. Unlike both classical SR and its self-induced version, CR occurs in the complete absence of any internal or external periodic modulation. It arises in excitable systems, where the application of noise alone can induce quasi-periodic spiking behavior. The regularity of these noise-induced spikes reaches a maximum at an optimal noise level, beyond which the system becomes increasingly irregular again. CR is particularly intriguing because it shows that intrinsic system properties, such as excitability and

timescale separation, are sufficient to generate order from the addition of noise, even without any guiding periodic structure.

Together, all of the above mentioned phenomena, i.e., SR, autonomous SR, SISR, and CR, summarized in Table 1, illustrate some of the diverse and often counterintuitive ways in which noise can improve signal processing and temporal regularity in nonlinear systems.

In addition to its impact on individual nonlinear systems, the influence of noise has been widely investigated in the context of its capacity to enhance synchronization within networks of coupled oscillators [92–94]. These studies have considered both scenarios, i.e., where an external periodic driving is present and where it is absent, highlighting the constructive role of noise in facilitating coherent collective phenomena.

## 4.2 Role of Noise in Biological Systems

Biological systems are inherently noisy. At all levels of organization, from signaling pathways used in intercellular communication, to neuronal circuits and physiological rhythms, random fluctuations are an unavoidable consequence of the probabilistic nature of biological interactions and the influence of a fluctuating environment. While noise was historically regarded as a perturbation that impairs the precision and reliability of biological processes, it is now widely recognized that noise can play a constructive and even essential role in the functioning of living systems.

As illustrated in Sec. 4.1, one of the most compelling examples of the beneficial effect of noise is SR. Following its introduction in the context of climate dynamics, SR has since been observed or proposed in a wide range of biological contexts. These include sensory systems, where it can enhance signal detection in mechanoreceptors, electroreceptors, and photoreceptors, as well as in neural dynamics, where it can improve information transmission and temporal precision [81, 95, 96].

Beyond single-cell dynamics, the role of noise has been extensively investigated in networks of coupled biological oscillators, such as neural populations, genetic circuits, and pancreatic  $\beta$ -cells. In such systems, through mechanisms like not only SR but also autonomous SR, SISR and CR, noise has been shown to facilitate synchronization, promote coherence among oscillators, and even induce collective rhythms in the absence of external pacing. These effects may be particularly important in biological systems where external periodic inputs are weak, irregular, or completely absent, and where coherent behavior must emerge from the interplay of internal dynamics and stochastic fluctuations [82, 97–99].

In the case of pancreatic  $\beta$ -cells, which exhibit bursting electrical activity that is crucial for pulsatile insulin release, noise plays a multifaceted role. Experimental and computational studies suggest that stochastic fluctuations can both trigger and modulate bursting patterns in Langerhans islets [17, 100–102]. It has been shown that noise can enhance the robustness of burst generation, help overcome quiescent states, and promote synchronization between otherwise weakly coupled cells. These effects are important for understanding how oscillations in insulin secretion observed at the systemic level emerge from complex intracellular and intercellular dynamics. Moreover, models of coupled excitable or bursting  $\beta$ -cells indicate that noise may support the emergence of collective oscillations even in the absence of strong external stimuli, providing an example of autonomous SR or SC relevant to the endocrine function.

Understanding the role of noise in biological systems is not only of theoretical interest, but also holds practical implications. For example, it can inform the design of bioinspired computing systems as well as neural prostheses, and in therapeutic strategies for correcting pathological heart rhythms. Overall, this challenges the traditional view that biological

function must depend on precise deterministic control, offering instead a picture of biological reliability that is deeply rooted in and enhanced by stochastic processes.

### 4.3 Diversity and Noise in Excitable Cell Networks

At the turn of the 21st century, it was discovered that effects qualitatively similar to those induced by noise could also arise in networks of coupled oscillators due to population heterogeneity, sometimes referred to as *quenched disorder* [12, 13]. This observation led to the formulation of the concept of DIR, described in Sec. 3.2.2, which concerns the enhancement of the collective response of a system to an external input that results specifically from variability among the individual units composing the network [13, 103–111]. Analogously to SR, DIR has been shown to manifest in both externally driven systems and in the absence of any external periodic forcing. In the latter case, the phenomenon is referred to as diversity-induced coherence [112]. These findings highlight a subtle interplay between noise and diversity, which, despite their distinct origins, can lead to comparable dynamical outcomes under certain conditions.

However, it is important to point out [II] that typical noise-induced resonance phenomena, e.g., SR and CR, may arise even in isolated systems consisting of a single nonlinear element, and are therefore not necessarily collective in nature. In contrast, DIR is inherently a collective effect, as it is intrinsically linked to statistical variability across a population of interacting units. Noise can be understood as representing fluctuations over time within the state space (or phase space) of a system, whereas heterogeneity reflects variations across a population in the parameter space of the system. In this sense, noise and heterogeneity act as analogous sources of disorder, but they operate on distinct aspects of the model: noise perturbs the dynamical evolution of individual systems over time, while heterogeneity introduces static differences across members of a population [113]. Another fundamental distinction lies in the reproducibility of system responses: a heterogeneous population tends to exhibit consistent and repeatable dynamics across different trials, owing to the fixed nature of parameter distributions, whereas systems influenced by noise produce outcomes that are only consistent when considered statistically, i.e., in terms of averaged behavior over multiple realizations [113]. Despite these important differences between the two types of disorder, many studies have emphasized the formal similarities between SR and DIR, often portraying them as different manifestations of the same underlying mechanism [13, 114], while other contributions have focused on how tuning the level of heterogeneity can enhance noise-induced resonances or, vice versa, how the presence of noise can amplify resonance effects arising from diversity [115–118].

Instead, relatively few works have addressed the deeper implications of the fundamental difference between the two mechanisms, namely that DIR stems from structural variability in a population, while SR is driven by stochastic perturbations [119, 120]. This conceptual distinction remains an open area of investigation and has not yet been explored in a fully systematic and quantitative manner [II].

### 4.4 Interplay Between Diversity and Noise: A Quantitative Study

#### 4.4.1 The Model

In Ref. [II], the authors attempted to address this gap by studying a prototypical example, represented by a network of coupled FHN units with cubit lattice topology, which was used to model a  $\beta$ -cell cluster, as in Ref. [I]. The key difference versus Ref. [I] is the addition of noise to the dynamical equations of the system, which become:

$$\dot{x}_i = a \left[ x_i - x_i^3/3 + y_i + C \sum_{j \in \Omega_i} (x_j - x_i) + \xi_i(t) \right], \quad (33a)$$

$$\dot{y}_i = -\frac{1}{a} (x_i + by_i - J_i). \quad (33b)$$

The sum over  $j$  in Eq. (33a) is limited to the set  $\Omega_i$  of the  $n = 6$  neighbors coupled to the  $i$ th oscillator. Just like in Eqs. (25) for the corresponding deterministic system, the  $J_i$  parameters in Eqs. (33) are different for each network element and are used to introduce diversity; the  $i$ th element will be in an oscillatory state if  $|J_i| < \varepsilon$  or in an excitable state if  $|J_i| > \varepsilon$ , with  $\varepsilon$  defined by Eq. (23) (see Sec. 3.1). The  $J_i$  values, which are drawn from a Gaussian distribution with standard deviation  $\sigma_d$  and mean value  $J_{av}$ , are randomly assigned to network elements. The standard deviation  $\sigma_d$  is used in the model as a measure of oscillator population diversity, while the mean value  $J_{av}$  expresses the position of the diversity distribution with respect to the oscillatory range  $(-\varepsilon, +\varepsilon)$ .

The term  $\xi_i(t)$  in Eq. (33a) is a Gaussian white noise with zero mean, standard deviation  $\sigma_n$ , and correlation function  $\langle \xi_i(t)\xi_j(t') \rangle = \sigma_n^2 \delta_{ij} \delta(t-t')$ , meaning that  $\xi_i(t)$  and  $\xi_j(t)$  ( $i \neq j$ ) are statistically independent of each other. Similarly to  $\sigma_d$  for diversity, the standard deviation  $\sigma_n$  is used as a measure of the noise applied to each network element. The reason for incorporating the noise term  $\xi_i(t)$  specifically into the first equation (Eq. (33a)), which governs the fast variable, is to ensure that the influence of noise on the system's dynamics is maximized. This choice facilitates the investigation of how stochastic fluctuations interact with the heterogeneity of network units. In contrast, adding the noise term to the second equation, associated with the slower recovery variable, would lead to a significantly reduced or no effect on network synchronization [115], as stochastic perturbations would be averaged out to zero over time.

The authors of Ref. [II] proposed the use of the above model to mimic various excitable biological systems, such as pancreatic  $\beta$ -cell clusters and some types of neurons [12, 115, 121–123]. In their study, they focused on analyzing the combined effect of diversity and noise on the synchronization and efficiency of collective network oscillations. Their goal was to identify potential synergies or antagonistic effects, as well as to better understand differences in the action mechanisms of the two sources of disorder.

#### 4.4.2 Qualitative Mean Field Analysis

The white noise term  $\xi_i(t)$  in Eq. (33a) can be interpreted as modeling a randomly varying external input current. Such fluctuations are able to vertically displace the nullcline associated with the variable  $x_i$ , thereby causing a momentary shift in the position of the equilibrium point of each FHN unit. Depending on the magnitude and direction of this shift, as well as on the specific value of the parameter  $J_i$ , the unit may undergo a change from a stable to an unstable equilibrium, or vice versa, corresponding to a transition in the oscillator state from quiescence to active spiking, or vice versa [II].

To study this mechanism from a collective viewpoint, one can introduce the global variables  $X(t) = N^{-1} \sum_{i=1}^N x_i(t)$  and  $Y(t) = N^{-1} \sum_{i=1}^N y_i(t)$  and use the transformation  $x_i = X + \delta_i$ , assuming that diversity is small [II, III, 13, 124]. Upon substitution in Eqs (33), one

obtains

$$\dot{X} = a \left[ X + \delta_i - \frac{(X + \delta_i)^3}{3} + y_i + C \sum (X + \delta_j - X - \delta_i) + \xi_i(t) \right], \quad (34a)$$

$$\dot{y}_i = -\frac{X + \delta_i + by_i - J_i}{a}, \quad (34b)$$

where the transformation  $y_i = Y + \delta_i$  has not been used, because the  $y_i$  terms are all linear. Also, for simplicity, all-to-all coupling is assumed, therefore the sum in Eq. (34a) runs over all  $i$ 's and  $j$ 's.

Developing the cube of the binomial in Eq. (34a) leads to

$$\dot{X} = a \left[ X + \delta_i - \frac{X^3 + \delta_i^3 + 3X^2\delta_i + 3X\delta_i^2}{3} + y_i + C \sum (X + \delta_j - X - \delta_i) + \xi_G(t) \right]. \quad (35)$$

Under the assumption that the distribution of  $J_i$  values is symmetric and  $\delta_i$ 's are small, corresponding to low diversity, one can make the approximations  $\sum_{i=1}^N \delta_i \cong 0$  and  $\sum_{i=1}^N \delta_i^3 \cong 0$ . Therefore, averaging Eq. (35) and Eq. (34b) over all  $i$ 's leads to

$$\dot{X} = a \left[ X - \frac{X^3}{3} - X \frac{1}{N} \sum_{i=1}^N \delta_i^2 + Y + \xi_G(t) \right], \quad (36a)$$

$$\dot{Y} = -\frac{X + bY - J_{av}}{a}, \quad (36b)$$

which, using the definition  $M \equiv \frac{1}{N} \sum_{i=1}^N \delta_i^2$ , can be rewritten as

$$\dot{X} = a \left[ X(1 - M) - \frac{X^3}{3} + Y + \xi_G(t) \right], \quad (37a)$$

$$\dot{Y} = -\frac{X + bY - J_{av}}{a}. \quad (37b)$$

In Eqs. (37),  $M$  expresses the level of diversity (it increases with increasing diversity and  $M = 0$  for a homogeneous system with  $\sigma_d = 0$ ). Noise effects are represented by a global white noise term  $\xi_G(t) = N^{-1} \sum_i \xi_i(t)$  with zero mean and correlation function  $\langle \xi_G(t) \xi_G(t') \rangle = N^{-1} \sigma_n^2 \delta(t - t')$ .

It is instructive to analyze how diversity and noise influence the nullclines associated with Eqs. (37). Variations in diversity, i.e., in the standard deviation  $\sigma_d$  of the  $J_i$  distribution, result in a change of the parameter  $M$ . This, in turn, alters the shape of the cubic nullcline by modifying the coefficient of the linear term in  $X$ , as illustrated in panels (a) and (b) of Fig. 18. Such deformation of the nullcline geometry demonstrates that diversity has the capacity to exert a substantial influence on the overall dynamics of the network, regardless of whether the mean value  $J_{av}$  lies within or outside the intrinsic oscillatory interval  $(-\varepsilon, +\varepsilon)$ .

By contrast, the effect of the global noise term  $\xi_G(t)$  is restricted to inducing vertical displacements, either upward or downward, of the cubic nullcline. These shifts result from instantaneous stochastic fluctuations and leave the nullcline shape unchanged (see the comparison between dashed and solid curves in Fig. 18). This behavior implies that noise is unlikely to exert a beneficial or resonance-enhancing influence when diversity is already tuned to an optimal value (i.e., under the conditions that characterize DIR) and the mean input  $J_{av}$  is set to zero. Under such circumstances, the network resides in an

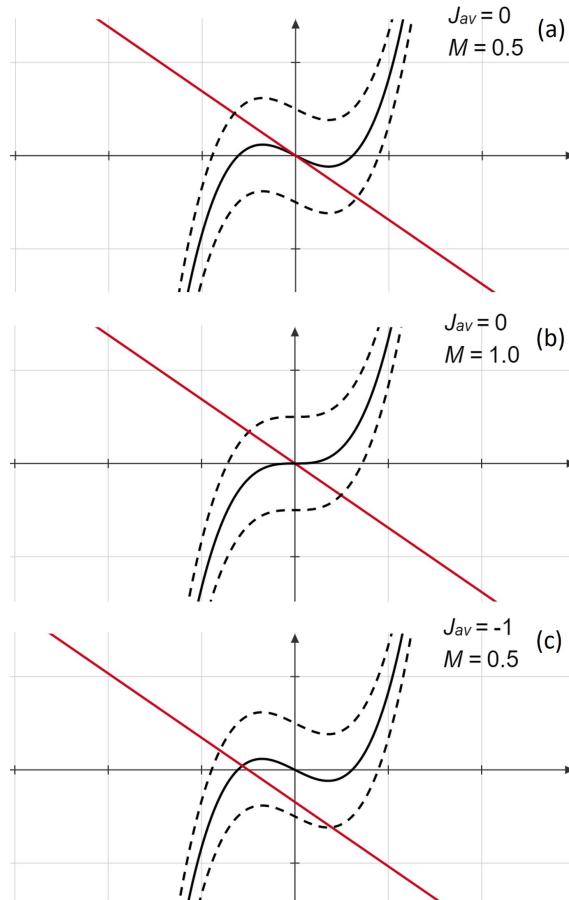


Figure 18: Nullclines of Eqs. (37a) and (37b) for different values of  $J_{av}$  and  $M$ . A comparison between panel (a) and (b) shows the effect of  $M$  on the shape of the cubic nullcline. The area delimited by the dashed curves above and below the cubic nullcline in each panel illustrates the effect of instantaneous shifts caused by noise with an amplitude of up to  $\pm 1$ . Reprinted with permission from [Stefano Scialla, Marco Patriarca, and Els Heinsalu. The interplay between diversity and noise in an excitable cell network model. EPL **137** (2022) 51001.] Copyright © 2022 EPLA. <https://iopscience.iop.org/article/10.1209/0295-5075/ac5cdb>

inherently oscillatory and resonant regime, and the presence of noise would more likely act as a perturbing rather than constructive factor.

The situation changes significantly when the mean input  $J_{av}$  is different from zero, as depicted in panel (c) of Fig. 18. In this case, the nonzero value of  $J_{av}$  introduces a constant term that translates the second nullcline vertically, either upward or downward, depending on the sign of  $J_{av}$ . This shift modifies the location of the equilibrium point of the system and may induce a transition from an oscillatory regime to an excitable one. Under such conditions, noise can constructively interact with diversity by generating rapid vertical shifts of the cubic nullcline that partially offset the displacement caused by  $J_{av}$ , thereby enabling the emergence of collective network oscillations.

It should also be noted that the system under consideration does not include a periodic driving force of the form  $A \sin \Omega t$ . As discussed in the previous sections, such a term is not required for the appearance of either noise- or diversity-induced resonance phenomena. Furthermore, its inclusion would impose an additional constraint by requiring the alignment of two characteristic timescales: the period of the external drive and the intrinsic oscillation period of the FHN units constituting the network.

#### 4.4.3 Key Simulation Results and Discussion

Ref. [II] presents the results of several numerical simulations aimed at quantitatively studying the combined effect of diversity and noise on network synchronization. The network topology and dimensions, the coupling constant, and the parameters  $a$  and  $b$  in the FHN equations were the same as in Ref. [I], in order to produce a model resembling the electrical behavior of pancreatic  $\beta$ -cells. Consequently, the value of  $\varepsilon$  was the same as in Ref. [I], i.e.,  $\varepsilon \approx 0.033$ .

The network synchronization efficiency  $\rho$  was computed using the same definition as in Ref. [I], specifically as given by Eq. 26. For each fixed value of  $J_{av}$ , the quantity  $\rho$  was evaluated over a range of diversity values  $0 \leq \sigma_d \leq 2.5$ , and simultaneously over a range of noise standard deviation values  $0 \leq \sigma_n \leq 5$ . Upon plotting  $\rho$  as a function of both  $\sigma_d$  and  $\sigma_n$  for the following diversity distribution mean values:  $J_{av} = 0, \pm 0.5, \pm 1$ , five three-dimensional surfaces were obtained, showing the effect of the interaction between diversity and noise in different  $J_{av}$  regimes.

In the parameter regime defined by  $J_{av} = 0$  (see Fig. 19), a condition in which a substantial portion, or even the entirety, of the network units fall within the intrinsic oscillatory range, the simulation results indicate that both diversity and noise are individually capable of inducing a resonance phenomenon. When the system is explored along the diversity axis (i.e., setting  $\sigma_n = 0$ , thereby eliminating noise) or along the noise axis (i.e.,  $\sigma_d = 0$ , thereby removing diversity), a clear resonance peak is observed in both cases. In each scenario, the synchronization efficiency  $\rho$  reaches a peak approximately 20–25% higher than its value at the origin of the  $\sigma_d$ - $\sigma_n$  parameter space.

Furthermore, for  $J_{av} = 0$ , the two sources of disorder, diversity and noise, appear to contribute in a mutually independent manner, with no indication of a synergistic enhancement. In fact, the global maximum of the response surface is located precisely at the point corresponding to optimal diversity in the absence of noise, specifically at  $\sigma_d = 0.5$  and  $\sigma_n = 0$ . This maximum, represented by a solid blue dot in Fig. 19, lies directly on the diversity axis.

From this optimal point, any movement toward the interior of the surface, i.e., any increase in noise while maintaining diversity, fails to produce an additional enhancement in global network synchronization. This observation aligns well with the predictions derived from our qualitative mean-field analysis, which suggests that, under conditions of

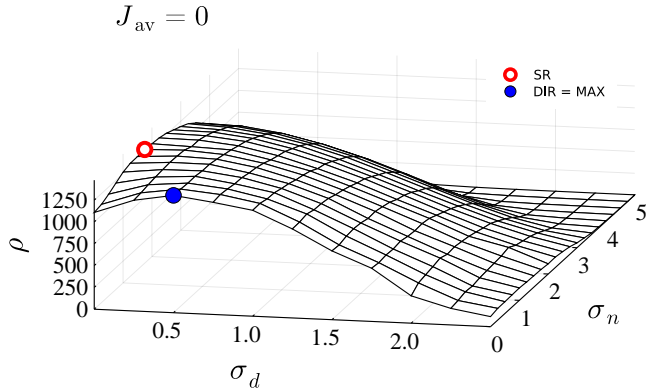


Figure 19: Global oscillatory activity  $\rho$  as a function of diversity ( $\sigma_d$ ) and noise ( $\sigma_n$ ), for  $J_{av} = 0$ . The full blue dot highlights the global surface maximum, which is coincident with the DIR maximum. The empty red dot corresponds to the noise-induced resonance maximum. Reprinted with permission from [Stefano Scialla, Marco Patriarca, and Els Heinsalu. The interplay between diversity and noise in an excitable cell network model. *EPL* **137** (2022) 51001.] Copyright © 2022 EPLA. <https://iopscience.iop.org/article/10.1209/0295-5075/ac5cdb>

optimized diversity and  $J_{av} = 0$ , the addition of noise is unlikely to exert a beneficial or amplifying effect on collective oscillatory behavior.

At the opposite extreme of the  $J_{av}$  spectrum, namely when  $J_{av} = \pm 1$  (see Fig. 20), the behavior of the system differs markedly from the  $J_{av} = 0$  regime. In this case, the majority of the network units lie outside the intrinsic oscillatory interval, either below it when  $J_{av} = -1$ , or above it when  $J_{av} = +1$ . Under such conditions, the incorporation of noise in addition to diversity consistently produces a marked enhancement in the overall level of network oscillatory activity.

This observation aligns with theoretical insights based on the behavior of global system variables. When  $J_{av} = -1$ , most elements of the network are situated in an excitable regime, meaning they are below the threshold required for self-sustained oscillations. However, strong positive fluctuations introduced by the noise term can transiently elevate these elements into the oscillatory regime by effectively injecting a temporary positive current. Conversely, when  $J_{av} = +1$ , the majority of elements reside above the upper bound of the intrinsic oscillatory range, placing them in an excitation-block state. In this scenario, negative noise fluctuations of sufficient amplitude can lower their effective input current, transiently bringing them into the oscillatory range.

In both conditions, the interaction between diversity and noise produces a synergistic effect, leading to a substantial increase in network synchronization. As an illustrative example, consider the case  $J_{av} = +1$ : the synchronization efficiency  $\rho$  increases by nearly 50% when comparing the diversity-induced peak (with  $\rho \approx 515$ , indicated by an empty green dot in Fig. 20, panel (b)) to the global maximum of the response surface (with  $\rho \approx 738$ , shown as a full blue dot in the same panel), which arises from the combined influence of noise and diversity.

Another notable feature emerging from the data is that, in this regime, noise appears to be a more effective driver of resonance than diversity alone. This is evident from the fact that the noise-induced resonance maxima along the noise axis (denoted by empty red dots in panels (a) and (b) of Fig. 20) are consistently higher than their diversity-induced counterparts along the diversity axis (empty green dots in the same panels).

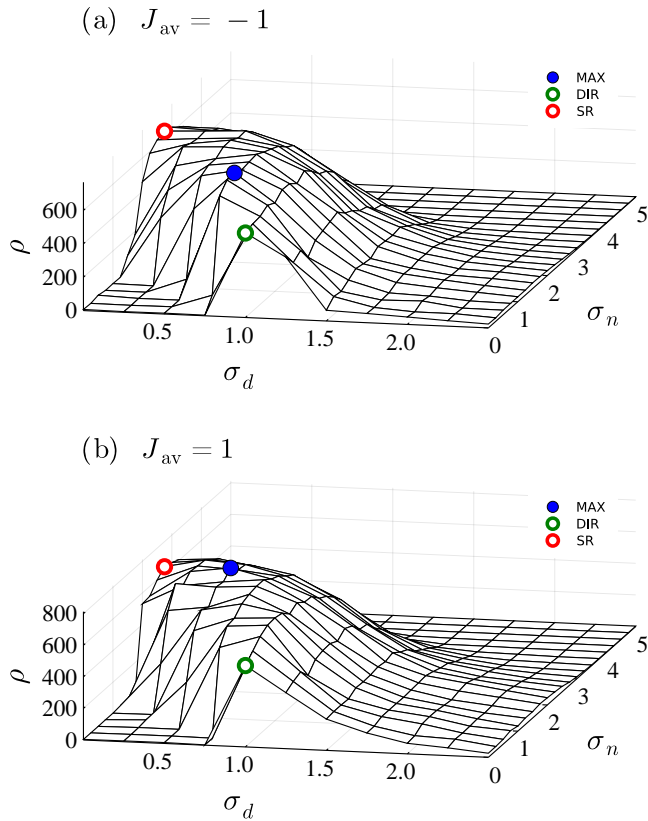


Figure 20: Global oscillatory activity  $\rho$  as a function of diversity ( $\sigma_d$ ) and noise ( $\sigma_n$ ), for  $J_{\text{av}} = -1$  (panel (a)) and  $J_{\text{av}} = +1$  (panel (b)). The full blue and empty green/red dots in each panel highlight the global surface maximum, the DIR maximum and the noise-induced resonance maximum, respectively. Reprinted with permission from [Stefano Scialla, Marco Patriarca, and Els Heinsalu. The interplay between diversity and noise in an excitable cell network model. EPL 137 (2022) 51001.] Copyright © 2022 EPLA. <https://iopscience.iop.org/article/10.1209/0295-5075/ac5cdb>

It is also important to observe that the location of the DIR peak shifts toward higher values of  $\sigma_d$  as  $J_{av}$  increases in magnitude. Specifically, the diversity-induced maximum occurs at  $\sigma_d = 0.5$  when  $J_{av} = 0$ , but shifts to  $\sigma_d = 1.0$  for both  $J_{av} = -1$  and  $J_{av} = +1$  (see empty green dots in Fig. 20, panels (a) and (b)). However, once both noise and diversity are introduced simultaneously, the global maximum of  $\rho$  shifts back toward the same optimal diversity value observed in the  $J_{av} = 0$  regime (see full blue dots in Fig. 20).

The underlying mechanism can be understood as follows: noise introduces random fluctuations that effectively “scatter” network elements across the  $J$  axis, causing them to move toward or into the oscillatory range. The position from which each element is stochastically displaced depends on its  $J_i$  value, which itself is determined by the distribution of diversity. When this process achieves maximum efficiency, corresponding to the global peak of the  $\rho$  surface, the optimal diversity for  $J_{av} = \pm 1$  converges with that found for  $J_{av} = 0$ .

In summary, for  $J_{av} = \pm 1$ , the interplay between diversity and stochasticity leads to a pronounced synergistic effect. This interaction significantly broadens the region of parameter space where resonance phenomena are observed, compared to what is achievable when either source of disorder, noise or diversity, is applied in isolation.

Finally, in the intermediate regime corresponding to  $J_{av} = \pm 0.5$ , an in-between situation can be observed, as described in detail in Ref. [II].

#### 4.4.4 Concluding Remarks

The theoretical and numerical investigations presented in Ref. [II] reveal that, although diversity- and noise-induced synchronization exhibit certain similarities, they differ not only in how they affect the system individually, but also in how they interact with each other. Their combined effect depends critically on the location of the mean value  $J_{av}$  of the diversity distribution relative to the intrinsic oscillatory range of the network elements. When  $J_{av} = 0$ , meaning that the distribution is centered within the oscillatory regime, diversity and noise influence synchronization independently, and no synergistic interaction is observed. In contrast, when  $J_{av} = \pm 1$ , so that most elements are placed outside the oscillatory range, a clear synergy emerges between the two sources of disorder. Under these conditions, their joint action leads to a pronounced enhancement of network synchronization, with noise exerting a more dominant effect than diversity. These observations offer valuable insight into the relative contribution of diversity and noise across different network configurations, highlighting scenarios in which one source of disorder may effectively be disregarded.

A further key result is that, when noise is present, the optimal level of diversity remains consistent across all regimes. That is, the value of  $\sigma_d$  that maximizes synchronization appears to be an intrinsic feature of the network, independent of  $J_{av}$ .

The finding that diversity and noise act through distinct mechanisms, rather than as interchangeable forms of disorder, may carry implications for biological systems. The best balance between heterogeneity and noise could vary across biological networks, as some systems may have evolved to rely more heavily on one form of disorder than the other, or to a similar degree on both, depending on their functional context and required signal processing capabilities.

## 5 INHIBITORY EFFECTS OF DISORDER

In the previous sections of this thesis, we have examined systems in which heterogeneity, noise, or their combination played a constructive role, contributing to an amplified response or enhanced activity of the system, either at the level of individual elements or across an entire network. However, there are also some circumstances in which noise or heterogeneity can play an inhibitory or antagonistic role. Clearly, we are not referring to the trivial case, which has already been described in this thesis, where an excess of noise or heterogeneity causes a disruption of the response, coherence, or synchronization of a system, as this is a general and expected phenomenon. Here we refer to specific situations where the addition of a relatively low, optimal level of noise or heterogeneity results in a major disruption or complete silencing of the activity of a system, i.e., what may be defined as an inverse resonance effect.

### 5.1 Inverse Stochastic Resonance

The possibility that noise may have an inhibitory effect on the activity of neurons was shown both experimentally and theoretically during the first decade of the present century [125]. In their experimental investigation of neuronal pacemaker activity, Paydarfar et al. [126] examined how noise affects excitability in an *in vitro* setup using squid axons. Their results demonstrated that the application of small-amplitude stochastic currents could trigger a switching dynamics, causing the system to alternate between sustained repetitive spiking and periods of quiescent, non-firing behavior. On the theoretical side, Gutkin, Tuckwell, and Jost [127, 128] studied how noise affects rhythmic spiking in Hodgkin–Huxley neurons. Without noise, sustained firing emerges when the input current  $\mu$  exceeds a critical value  $\mu_c$ . Near this threshold (i.e., for  $\mu$  just slightly above  $\mu_c$ ), they found that even weak noise in the input current can markedly suppress firing, with the firing rate exhibiting a pronounced minimum as noise increases, which is the opposite of SR or CR. For this reason, the authors proposed the name inverse stochastic resonance (ISR) for the phenomenon they observed. This effect proved to be robust to random initial conditions and noise onset times. Similar results were obtained with conductance-based noise (instead of current-based noise), suggesting that this behavior may be a general feature of neuronal dynamics.

ISR has also been studied in systems based on the FHN model, both in a single FHN unit and in networks of FHN elements [91, 129]. Taking the simpler example of a single FHN unit, the equations to be considered, derived from Eqs. (13) with the addition of a noise term  $\xi(t)$ , are:

$$\dot{x} = a [x - x^3/3 + y + \xi(t)], \quad (38a)$$

$$\dot{y} = -\frac{1}{a} (x + by - J). \quad (38b)$$

Here  $\xi(t)$  is a Gaussian white noise with zero mean and correlation function  $\langle \xi(t)\xi(t') \rangle = \sigma_n^2 \delta(t - t')$ . As shown in Sec. 3.1, in the absence of noise this system is in a limit cycle (oscillatory) regime for  $|J| < \varepsilon$  and in an excitable state for  $|J| > \varepsilon$ , where  $\varepsilon$  is defined by Eq. (23). For ISR to occur in this context, the conditions that must be satisfied are analogous to the ones required for the Hodgkin–Huxley model, i.e.:

- The value of  $J$  in Eq. (38b) should be such that  $|J| < \varepsilon$  and, at the same time,  $|J| \approx \varepsilon$ , i.e., in the absence of noise the deterministic system should be in an oscillatory regime and in close proximity to the bifurcation point (see Sec. 3.1).

- The additive noise term should have a small to intermediate intensity. This typically corresponds to noise strengths in the range  $D \sim 10^{-3}$  to  $10^{-1}$  (equivalent to  $\sigma_n = \sqrt{2D} \sim 0.04$  to  $0.45$ ), where the perturbations are sufficient to transiently alter the trajectory of the system without overwhelming the intrinsic dynamics. Excessively strong noise can re-initiate spiking or induce irregular, erratic activity.
- There should be a large timescale difference between the fast and slow variables, which can be ensured through a suitable choice of the system parameters. In particular, the condition  $a \gg 1$  determines a pronounced separation of timescales, whereby  $x$  exhibits fast dynamics and  $y$  evolves on a significantly slower timescale.

## 5.2 Diversity Induced Decoherence

We now turn to a system [III] in which an inverse resonance effect is driven by heterogeneity rather than noise. To our knowledge, this is the first documented example of a non-trivial inhibitory or antagonistic role played by heterogeneity in a complex network. The authors of Ref. [III] investigated how small-amplitude noise and parameter heterogeneity influence the dynamics of a network composed of coupled excitable oscillators operating under strong timescale separation. In contrast to earlier studies, which demonstrated that tuning network heterogeneity can improve collective phenomena such as synchronization and coherence, Ref. [III] showed that, if the network satisfies the conditions for SISR to occur, the effect of adding diversity can only be antagonistic, leading to a reduction or suppression of the coherence of collective oscillations.

As mentioned in Sec. 4.1, SISR occurs when an excitable system, e.g., a FHN unit, characterized by a strong separation of timescales, exhibits coherent oscillatory behavior due to the interplay between weak noise and the intrinsic slow dynamics of the system [89, 91]. Specifically, the noise perturbs the fast variable, while the slow variable controls the timing at which the system becomes sensitive to those perturbations. This concerted interaction results in the emergence of a regular temporal structure, even though the system is not subjected to any external modulation. It has been demonstrated that SISR can take place not only in a single isolated FHN unit but also in a network of coupled FHN elements [130].

### 5.2.1 The Model

In order to study the interaction between noise and heterogeneity under the conditions required for the emergence of SISR, following Ref. [III], we use a network of globally coupled FHN units [9–11], represented by the following equations:

$$\frac{dv_i}{dt} = v_i(a_i - v_i)(v_i - 1) - w_i + C \sum_{j=1}^N (v_j - v_i) + \xi_i(t), \quad (39a)$$

$$\frac{dw_i}{dt} = \tilde{\epsilon}(bv_i - cw_i). \quad (39b)$$

In this system, the state variables  $v_i, w_i$  represent the fast membrane potential and the slow recovery current of the  $i$ -th unit, respectively. The index  $i = 1, \dots, N$  identifies the nodes of the network. The parameter  $C > 0$  denotes the coupling strength, while  $\tilde{\epsilon}$ , with  $0 < \tilde{\epsilon} \ll 1$ , characterizes the separation of timescales between the dynamics of  $v_i$  and  $w_i$ . The constants  $b$  and  $c$  are assumed to be positive.

Diversity across the network is introduced by assigning a distinct value of  $a_i$  to each unit, as will be detailed below. Stochastic fluctuations are modeled by the terms  $\xi_i(t)$ ,

which are independent Gaussian white noise processes with zero mean, standard deviation  $\sigma_n$ , and correlation function  $\langle \eta_i(t) \eta_j(t') \rangle = \sigma_n^2 \delta_{ij} \delta(t - t')$ . Therefore, the noise intensity acting on each network unit is measured by  $\sigma_n$ .

It should be noted that in this section we adopt a different version of the FHN model, given in Eqs. (39), which is more suitable for the study of SISR and is consistent with the one used in Ref. [III]. This alternative representation emphasizes the separation of timescales between the fast and slow variables by explicitly including the parameter  $\tilde{\varepsilon}$  as a multiplicative factor in the slow equation (note that  $\tilde{\varepsilon}$  is a different parameter from  $\varepsilon$ , used in other sections of the thesis). This choice is particularly advantageous for SISR analysis, where the presence of a strong timescale disparity is essential for the emergence of noise-induced oscillations. Moreover, in contrast to the previously considered FHN equations, the present version does not include an explicit external current term. This reflects the typical setting of SISR, which arises intrinsically from the interplay between the system's internal dynamics and stochastic fluctuations, rather than being triggered by an external forcing.

To determine the conditions under which the FHN model is in an excitable or oscillatory regime, we perform a linear stability analysis of the fixed point at the origin. We consider the uncoupled, noise-free system corresponding to Eqs. (39), i.e.

$$\dot{v} = v(a - v)(v - 1) - w, \quad (40a)$$

$$\dot{w} = \tilde{\varepsilon}(bv - cw), \quad (40b)$$

with  $\tilde{\varepsilon} \ll 1$ . The origin  $(v, w) = (0, 0)$  is always a fixed point of this system in the absence of external input. To analyze its stability, we compute the Jacobian matrix  $\mathcal{J}$  (see Sec. 3.1) by evaluating the partial derivatives of the right-hand sides of Eqs. (40) at the fixed point. The Jacobian matrix at  $(0, 0)$  is given by

$$\mathcal{J} = \begin{bmatrix} a & -1 \\ b\tilde{\varepsilon} & -c\tilde{\varepsilon} \end{bmatrix},$$

which implies that  $\text{tr}(\mathcal{J}) = a - c\tilde{\varepsilon}$  and  $\det(\mathcal{J}) = -ac\tilde{\varepsilon} + b\tilde{\varepsilon} = \tilde{\varepsilon}(b - ac)$ .

The fixed point is stable when  $\text{tr}(\mathcal{J}) < 0$  and  $\det(\mathcal{J}) > 0$ , and it loses stability via a Hopf bifurcation when the trace changes sign and the determinant remains positive. In the limit  $\tilde{\varepsilon} \rightarrow 0$ , the trace crosses zero at  $a = 0$ , indicating that the bifurcation occurs near this point. Assuming that the determinant is positive, i.e.,  $\tilde{\varepsilon}(b - ac) > 0$ , the system has a stable fixed point for  $a > 0$ , corresponding to an excitable state, and transitions to an oscillatory regime for  $a < 0$ , where the fixed point becomes unstable. This gives us the necessary condition  $a > 0$ , i.e., excitability, to be able to observe SISR.

We also want to require that the fixed point at the origin is unique. The reason is to ensure that the system can be in an excitable state with a stable fixed point, where it stays at rest unless noise (in the case of SISR) triggers a spike. If there are two or more stable fixed points, the system is bistable, not excitable: A small perturbation might move the system from one attractor basin to another, resulting in a switch rather than a spike. The corresponding dynamics in that case is fundamentally different, as there is no refractory return to a single resting state.

To determine the condition under which the origin  $(v, w) = (0, 0)$  is a unique fixed point, we set to zero the right-hand sides of Eqs. (40), as this by definition provides the fixed points (where the two derivatives vanish). This yields the nullclines

$$w = v(a - v)(v - 1), \quad (41a)$$

$$w = \frac{b}{c}v. \quad (41b)$$

Equating the two expressions for  $w$  from Eqs. (41a) and (41b) gives the condition for fixed points:

$$v(a-v)(v-1) = \frac{b}{c}v. \quad (42)$$

Assuming  $v \neq 0$ , we can divide both sides by  $v$ :

$$(a-v)(v-1) = \frac{b}{c}. \quad (43)$$

Expanding the left-hand side and rewriting the equation as a standard quadratic, it becomes

$$-v^2 + (a+1)v - \left(a + \frac{b}{c}\right) = 0. \quad (44)$$

To ensure that the origin is the *only* fixed point, we require that this equation has no real solutions (if this is the case,  $v = 0$  becomes the only solution to Eq. (42)). This occurs when its discriminant  $\Delta$  is negative:

$$\Delta = (a+1)^2 - 4\left(a + \frac{b}{c}\right) = (a-1)^2 - \frac{4b}{c} < 0. \quad (45)$$

Therefore, the condition for the origin to be the only fixed point is

$$(a-1)^2 - \frac{4b}{c} < 0 \quad \Rightarrow \quad \frac{(a-1)^2}{4} < \frac{b}{c}. \quad (46)$$

This inequality defines the interval of  $a$  values for which no additional fixed points arise beyond the origin. It is particularly relevant when analyzing excitable or noise-induced dynamics, as it ensures the global uniqueness of the resting state. It is essential for studying self-induced stochastic resonance, where noise alone causes transitions, without external forcing or intrinsic oscillations [131–133].

Following Ref. [III], we set  $b = 1$  and  $c = 2$ , which transforms Eq. (46) into

$$\frac{(a-1)^2}{4} < \frac{1}{2}. \quad (47)$$

Eq. (47) has the solution  $a \in (1 - \sqrt{2}, 1 + \sqrt{2})$ . Combining this with the condition for excitability, i.e.,  $a > 0$ , we obtain the interval  $a \in (0, 1 + \sqrt{2})$ , which ensures at the same time the uniqueness and stability of the fixed point at the origin. To be able to observe SISR, the  $a_i$  values in Eqs. (39) must be chosen within this interval. Therefore, to incorporate heterogeneity, the parameters  $a_i$  in Eq. (39a) are sampled from a Gaussian distribution truncated within the interval  $a_i \in (0, 1 + \sqrt{2})$ , and then randomly assigned to the individual units in the network. The mean value  $a_m$  determines the distance of the system from the oscillatory regime (which occurs for  $a_i \leq 0$ ), while the standard deviation  $\sigma_d$  quantifies the degree of diversity across the network.

## 5.2.2 Analytic Study of the Effects of Diversity on SISR

### 5.2.2.1 Mean-Field Approximation.

We now study the effects of diversity  $\sigma_d$  on SISR analytically and from a collective viewpoint, adopting a mean-field approximation [3, 13, 124]. This is done through an extension of the approach presented in Ref. [II], which has been discussed in detail in Sec. 4.4.2 of this thesis.

Before performing variable substitutions analogous to those shown in Sec. 4.4.2, we rewrite Eq. (39a) as:

$$\dot{v}_i = a_i(v_i^2 - v_i) - v_i^3 + v_i^2 - w_i + K \sum_j (v_j - v_i) + \xi_i(t). \quad (48)$$

Upon introducing the global variables  $V(t) = N^{-1} \sum_{i=1}^N v_i(t)$  and  $W(t) = N^{-1} \sum_{i=1}^N w_i(t)$ , we set  $v_i = V + \delta_i$  and substitute it into Eq. (48), obtaining:

$$\dot{V} = a_i [(V + \delta_i)^2 - (V + \delta_i)] - (V + \delta_i)^3 + (V + \delta_i)^2 - w_i + K \sum_j (v_j - v_i) + \xi_i(t). \quad (49)$$

Also in this case, like in Sec. 4.4.2, we do not make the transformation  $y_i = Y + \delta_i$  in Eq. (39b), because the  $y_i$  terms are all linear. Eq. (49) must be averaged over all  $i$ 's to obtain the corresponding equation for the global variable  $V$ . Assuming that the diversity  $\sigma_d$  of the distribution of  $a_i$  values is small, we make the approximation:

$$\langle a_i [(V + \delta_i)^2 - (V + \delta_i)] \rangle \approx \langle a_i \rangle \langle (V + \delta_i)^2 - (V + \delta_i) \rangle, \quad (50)$$

where  $\langle \dots \rangle$  designates an average over the  $N$  units constituting the network. Then, by averaging Eqs. (49) and (39b) over all  $i$ 's and again assuming  $\sum_{i=1}^N \delta_i \cong 0$  and  $\sum_{i=1}^N \delta_i^3 \cong 0$  (see Sec. 4.4.2), we arrive at the following dynamical equations for the global variables  $V$  and  $W$ :

$$\dot{V} = V [(A - V)(V - 1) - 3M] + M(A + 1) - W + \xi_G(t), \quad (51a)$$

$$\dot{W} = \tilde{\varepsilon} (bV - cW), \quad (51b)$$

where  $M = N^{-1} \sum_{i=1}^N \delta_i^2$  and  $A = N^{-1} \sum_{i=1}^N a_i$ .  $M$  expresses the level of diversity (greater diversity results in higher values of  $M$  and  $M = 0$  for a homogeneous system with  $\sigma_d = 0$ ), while  $A$  is the mean value of the truncated  $a_i$  distribution. Note that  $A$  is different from  $a_m$ , which is the mean of the full Gaussian distribution of  $a_i$  values, without truncation. Noise effects are represented by a global white noise term  $\xi_G = N^{-1} \sum_{i=1}^N \xi_i$  with zero mean and correlation function  $\langle \xi_G(t), \xi_G(t') \rangle = N^{-1} \sigma_n^2 \delta(t - t')$ .

**5.2.2.2 Analysis of the Mean-Field Equations.** Let us study the dynamics of Eqs. (51) in the absence of noise, that is, setting  $\xi_G(t) = 0$ . In the singular limit  $\tilde{\varepsilon} \rightarrow 0$ , which emphasizes the separation between fast and slow dynamics, the behavior of the system simplifies considerably. For generic initial conditions, the trajectory first undergoes a rapid vertical motion in phase space, relaxing to the nearest attracting branch of the  $V$ -nullcline. Typically, the system is first attracted to the right stable branch, along which it slowly drifts upwards as the slow variable  $W$  evolves. When the trajectory reaches the fold point of the right branch, where stability is lost, it undergoes a fast jump to the left stable branch. From there, it follows a slow descent toward the stable fixed point  $(V_f, W_f)$  located on the left branch. Thus, in the deterministic regime, the dynamics tends to relax in a two-stage process: fast convergence to the right branch, followed by a slow evolution and eventual transition to the left branch [134, 135]. The  $V$  nullcline is defined implicitly by the equation

$$V[(A - V)(V - 1) - 3M] + M(A + 1) - W = 0, \quad (52)$$

which, for fixed  $W$ , admits three real solutions:  $V_L^*(W)$ ,  $V_S^*(W)$ , and  $V_R^*(W)$ . These correspond respectively to the left stable, intermediate unstable, and right stable branches of the nullcline.

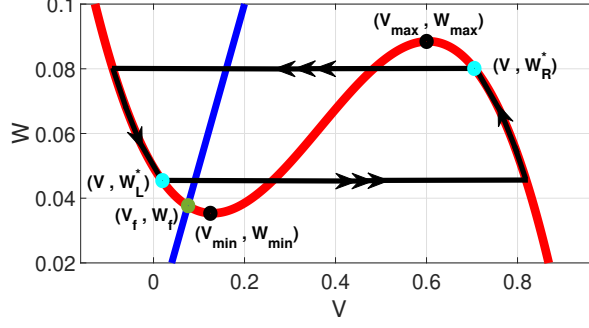


Figure 21:  $W$  nullcline (blue line) and  $V$  nullcline (red curve) of Eqs. (51) intersect at a unique fixed point  $(V_f, W_f)$ . The black loop represents a typical stochastic trajectory induced by SISR, where the horizontal parts with triple arrows indicate the fast escape at points  $V_L^*$  and  $V_R^*$  from the left and right stable branches of the  $V$  nullcline, respectively. The almost vertical parts of the trajectory, with single arrow, represent the slow motion of  $W$  governed by Eqs. (53).  $A = 0.1$ ,  $M = 0.045$ . Reprinted figure with permission from [M.E. Yamakou, E. Heinsalu, M. Patriarca, and S. Scialla. *Phys. Rev. E* **106**, L032401 (2022).] Copyright 2022 by the American Physical Society. <https://journals.aps.org/pre/abstract/10.1103/PhysRevE.106.L032401>

Upon substituting  $V = V_L^*(W)$  and  $V = V_R^*(W)$  into Eq. 51b, we obtain:

$$\frac{dW}{dt} = \tilde{\epsilon} [bV_L^*(W) - cW], \quad (53a)$$

$$\frac{dW}{dt} = \tilde{\epsilon} [bV_R^*(W) - cW]. \quad (53b)$$

These equations govern the slow drift of the system along the respective branches of the  $V$  nullcline in the noise-free case. Specifically, Eq. (53a) refers to the downward drift on the left stable branch, while Eq. (53b) describes the upward drift on the right stable branch.

When a small-amplitude noise is introduced ( $0 < \sigma_n \ll 1$ ), the deterministic structure is perturbed, enabling the system (under certain conditions) to escape from the metastable state associated with the left branch of the nullcline, before the stable fixed point  $(V_f, W_f)$  is reached. When this happens, SISR occurs. For SISR to be possible, the noise must induce a horizontal transition from the left to the right branch of the  $V$  nullcline at a critical point  $W = W_L^* > W_f$ , before the trajectory gets trapped in the basin of attraction of the fixed point  $(V_f, W_f)$ . The process is illustrated in Fig. 21.

To analyze the mechanism of this transition, one can consider that in the limit  $\tilde{\epsilon} \rightarrow 0$ , in which the slow variable  $W$  is effectively constant over the fast dynamics timescale, the system of Eqs. (51) reduces to a one-dimensional Langevin equation for  $V$ :

$$\frac{dV}{dt} = -\frac{\partial U(V, W)}{\partial V} + \xi_G(t), \quad (54)$$

where  $U(V, W)$  is an effective double-well potential of the form

$$U(V, W) = \frac{V^4}{4} - \frac{(1+A)}{3}V^3 + \frac{(3M+A)}{2}V^2 - [W - M(1+A)]V. \quad (55)$$

$U(V, W)$  is obtained from the integral:

$$U(V, W) = -\int F(V, W) dV, \quad (56)$$

where  $F(V, W)$  is the right hand side of Eq. (51a) without the noise term and  $W$  is treated as a constant parameter.

It is worth pointing out that the double-well potential in Eq. (55) depends on the diversity parameter  $M$ . The escape from the left well occurs when noise overcomes the energy barrier separating  $V_L^*(W)$  and  $V_S^*(W)$ , i.e., the previously defined solutions of Eq. (52). The corresponding barrier height is

$$\Delta U_L(W) = U(V_S^*(W), W) - U(V_L^*(W), W), \quad (57)$$

while the barrier for the reverse transition (which occurs independently of noise, as explained above) is

$$\Delta U_R(W) = U(V_S^*(W), W) - U(V_R^*(W), W). \quad (58)$$

SISR requires a specific balance between the noise intensity and the height of the potential barrier. If the noise is too weak, the system remains trapped near  $(V_f, W_f)$ ; if it is too strong, the transitions become irregular and coherence is lost. Hence, there exists an optimal noise interval for the occurrence of SISR,  $(\sigma_n^{\min}, \sigma_n^{\max})$ , with

$$\sigma_n^{\min} = \sqrt{\frac{2\Delta U_L(W_f)}{\ln(\tilde{\epsilon}^{-1})}}, \quad \sigma_n^{\max} = \sqrt{\frac{2\Phi}{\ln(\tilde{\epsilon}^{-1})}}. \quad (59)$$

Here  $\Phi$  is the value of the energy barrier at the point  $W = W_s$ , where the two barrier functions intersect, therefore are equal, i.e.,  $\Delta U_L(W_s) = \Delta U_R(W_s) = \Phi$  [89, 130]. This symmetry point identifies the optimal condition for SISR, where the barrier for escape from the metastable state is minimal (yet still deep enough to preserve the bistable structure of the system) and the interplay between noise and timescale separation leads to highly regular, noise-driven excursions from the metastable state.

The expressions for  $\sigma_n^{\min}$  and  $\sigma_n^{\max}$  in Eq. (59) can be derived as follows [86, 136]. According to Kramers formula, the escape probability decreases exponentially with the ratio  $\Delta U/\sigma_n^2$ . However, the slow evolution of  $W$  imposes a competing timescale  $\sim 1/\tilde{\epsilon}$ , setting a constraint on how long the system remains near a potential minimum before the slow drift alters the barrier landscape. This interplay defines a critical matching condition: escape occurs with high probability when the activation energy satisfies

$$\frac{\sigma_n^2}{2} \ln(\tilde{\epsilon}^{-1}) \in (\Delta U_L(W_f), \Phi), \quad (60)$$

where  $\Delta U_L(W_f)$  is the barrier height from the left stable branch at the fixed point. Solving this inequality for  $\sigma_n$  yields the optimal noise window for SISR, i.e., the values of  $\sigma_n^{\min}$  and  $\sigma_n^{\max}$  in Eq. (59).

Importantly, both  $\Delta U_L(W)$  and  $\Phi$  depend on the diversity parameter  $M$ . As  $M$  increases,  $\Phi$  decreases and the double-well potential becomes shallower and less symmetric [3]. From Eq. (59), we can see that this leads to a shrinkage of the noise interval in which SISR is observed, and for sufficiently large  $M$ , the resonance is completely suppressed. In Ref. [III], this phenomenon was named *diversity-induced decoherence* (DID).

### 5.2.3 Numerical Simulations

To validate the above theoretical analysis and quantitatively assess the interplay of noise and heterogeneity in the dynamics of SISR, numerical simulations of the system defined by Eqs. (39) were carried out in Ref. [III]. Simulations were performed using the fourth-order Runge-Kutta algorithm for stochastic processes [137] and the Box-Muller algorithm [138].

The integration time step was  $dt = 0.01$ , ensuring sufficient temporal resolution for both the fast and slow dynamics of the system, and the total simulation time was  $T = 1.5 \times 10^6$ .

Each simulation involved a network of  $N = 100$  units, where heterogeneity was introduced through a random assignment of the individual parameters  $a_i$ . As explained in Sec. 5.2.1, the  $a_i$  values were drawn from a truncated Gaussian distribution in the interval  $(0, 1 + \sqrt{2})$ , with mean  $a_m$  and standard deviation  $\sigma_d$ . The parameters  $a_m$  and  $\sigma_d$  control, respectively, the mean proximity to the oscillatory regime and the degree of diversity within the network.

To characterize the macroscopic behavior, the average membrane potential across the network,

$$\bar{V}(t) = \frac{1}{N} \sum_{i=1}^N V_i(t), \quad (61)$$

was calculated and the temporal pattern of its excursions was analyzed. The hallmark of SISR is the appearance of quasi-periodic, noise-driven collective excursions of  $\bar{V}(t)$  away from the resting state. These excursions resemble spikes and are separated by stochastic interspike intervals (ISIs).

The regularity of these noise-induced events was quantified using the *coefficient of variation* (CV), defined as the normalized standard deviation of the ISI [90, 139]:

$$\text{CV} = \frac{\sqrt{\langle \tau^2 \rangle - \langle \tau \rangle^2}}{\langle \tau \rangle}, \quad (62)$$

where  $\langle \tau \rangle = N^{-1} \sum_{i=1}^N \langle \tau_i \rangle$  and  $\langle \tau^2 \rangle = N^{-1} \sum_{i=1}^N \langle \tau_i^2 \rangle$ , with  $\langle \tau_i \rangle$  and  $\langle \tau_i^2 \rangle$  representing the mean and mean squared ISI (over time) of unit  $i$ .  $\tau_i = t_i^{\ell+1} - t_i^\ell > 0$  is the time elapsed between spike  $\ell$  and the subsequent spike,  $\ell + 1$ , for unit  $i$ . The more variable the ISIs are, the higher the CV will be. Consequently, a minimum in the CV as a function of the noise amplitude  $\sigma_n$  indicates an optimal level of stochastic coherence, characteristic of the SISR regime.

A first series of simulations were conducted over a range of noise intensities  $\sigma_n$ , while keeping other parameters fixed and in the absence of diversity ( $\sigma_d = 0$ ). For each value of  $\sigma_n$ , the system was allowed to evolve for a sufficiently long duration to collect statistically significant samples of ISIs. As shown in Fig. 22, the resulting CV curves exhibited a well-defined minimum between two critical noise levels,  $\sigma_n^{\min}$  and  $\sigma_n^{\max}$ , which mark the lower and upper bounds of the SISR window. These critical values were consistent with theoretical estimates based on Kramers rate theory, as detailed in Sec. 5.2.2.2.

Subsequently, the effect of diversity combined with noise was investigated by varying the standard deviation  $\sigma_d$  of the  $a_i$  distribution at several different values of  $\sigma_n$ . As expected based on mean-field analysis, it was observed that the loss of coherence begins to manifest as soon as a minimal amount of diversity is introduced into the system and increases rapidly, eventually leading to the complete suppression of the resonant behavior (see Fig. 22). The fundamental cause of this decoherence lies in the fact that heterogeneity progressively eliminates the energy barrier in the effective mean-field potential, as shown in Sec. 5.2.2.2. The double-well structure of this potential is crucial for sustaining the coherent noise-driven spiking that characterizes SISR.

Thus, the numerical simulations confirm that in the system studied in Ref. [III], diversity cannot be fine-tuned to improve coherence; instead, its effect is purely disruptive, leading to DID. This is a particularly significant observation, as numerous previous studies have demonstrated that adjusting the degree of heterogeneity in a network can enhance various forms of collective behavior, including synchronization and coherence [I, II, 12, 13,

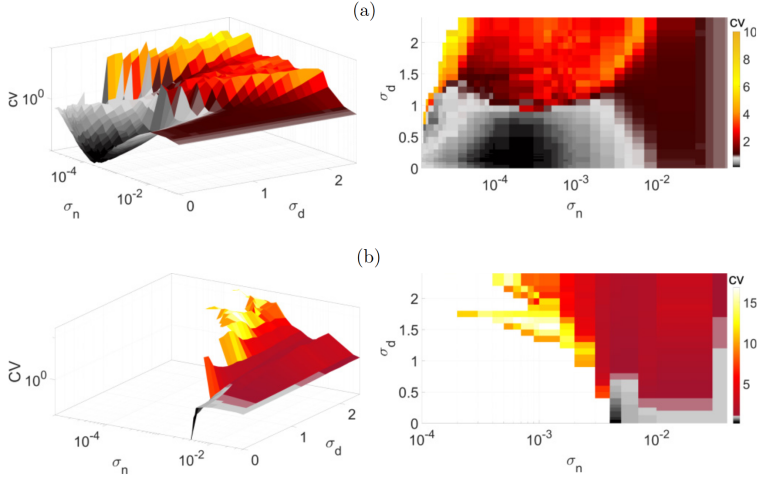


Figure 22: Panel (a): CV versus  $\sigma_n$  and  $\sigma_d$  in 3D with the 2D projection onto  $(\sigma_n, \sigma_d)$ -plane when  $a_m = 0.05$ . Panel (b): CV versus  $\sigma_n$  and  $\sigma_d$  in 3D with the 2D projection onto  $(\sigma_n, \sigma_d)$ -plane when  $a_m = 1.2$ . In both panels, the black and grey colors indicate values of  $CV < 1$ , corresponding to SISr. Larger values of  $\sigma_d$  lead to larger CV values, inhibiting SISr. Reprinted figure with permission from [M.E. Yamakou, E. Heinsalu, M. Patriarca, and S. Scialla. *Phys. Rev. E* **106**, L032401 (2022).] Copyright 2022 by the American Physical Society. <https://journals.aps.org/pre/abstract/10.1103/PhysRevE.106.L032401>

103–112, 114, 140]. The absence of such an optimizing effect here highlights an important and nontrivial departure from a well-established and widespread phenomenon observed in a variety of network architectures and dynamical settings.

### 5.2.4 Biological Relevance

It is important to emphasize that resonance phenomena in biological systems can have not only beneficial but also detrimental effects. Emerging evidence from research on Parkinson’s disease [141], for example, suggests that dopaminergic neurons typically exhibit a substantial degree of heterogeneity, and that disease progression is linked to the selective degeneration of one or more specific neuronal subpopulations. This selective cell loss results in a reduction of neuronal diversity compared to healthy tissue. These findings support the idea that, at least in some circumstances, diversity among neuronal types may have a protective function, acting through compensatory mechanisms to suppress harmful resonant activity. When such diversity is compromised, the absence of this buffering capacity may give rise to pathological dynamics.

Building on their theoretical findings, along with the above-mentioned experimental observations about a potential link between reduction in neuronal diversity and hyperkinetic disorders such as Parkinson’s disease, the authors of Ref. [III] propose that diversity in biological systems may have a broader functional role than previously thought. In addition to its well-known ability to enhance the detection of weak signals, heterogeneity might also act as a regulatory mechanism that suppresses pathological or unwanted resonant responses. This perspective suggests that the modulation of diversity could provide an intrinsic means of controlling excitability and stabilizing activity in complex neural networks.

The ability of cellular heterogeneity to suppress resonance-like behavior might also be

relevant in the context of pancreatic  $\beta$ -cell networks. While synchronization of  $\beta$ -cells is essential for coordinated insulin release, excessive resonance effects could disrupt normal glucose regulation. In this context, heterogeneity in excitability or metabolic responsiveness might serve as a stabilizing factor, preventing pathological oscillations driven by noise-induced collective bursting. This mechanism could play a protective role, ensuring the robustness of insulin secretion dynamics under variable physiological conditions. Conversely, loss of heterogeneity, whether due to selective  $\beta$ -cell loss or dedifferentiation, might compromise this control, potentially contributing to dysfunctional insulin dynamics observed in diabetes.

## 6 UNDERSTANDING THE MECHANISM OF DIR

In Sec. 3, we described various systems characterized by the occurrence of resonance phenomena induced by heterogeneity. In particular, in Sec. 3.2.1 we discussed Ref. [12], which presents a  $\beta$ -cell network model based on coupled FHN units of two distinct types, where heterogeneity is introduced by randomly assigning to each unit one of two parameter values, specifically  $J_i = -v$  or  $J_i = +v$ , in the dynamical equations of the system, Eqs. (25).

Another model (see Sec. 3.2.2), in which oscillations emerge as a result of heterogeneity, involves assigning to each cell a value of the forcing parameter drawn from a continuum Gaussian distribution [13]. This model demonstrated that there exists an optimal degree of diversity, typically quantified by the standard deviation of the Gaussian distribution, at which the network exhibits maximal coherence in its collective response. This phenomenon was named DIR [13] and highlighted the constructive role that a suitable amount of heterogeneity can play in enhancing the overall dynamical behavior of the system.

Both modeling approaches exhibit the emergence of oscillations driven by heterogeneity, as well as a pronounced resonant behavior in synchronization when certain parameters are varied. However, they employ distinct methods for introducing diversity into the oscillator parameters. Whether the dynamical effects resulting from a Gaussian distribution of parameter values and those arising from a binary (two-value) distribution of the bias force are equivalent or fundamentally related remains an unresolved question. Trying to answer this question can help shed light on the fundamental mechanisms behind resonance phenomena caused by diversity and is the main goal of Ref. [IV], which this Section is mainly based on.

We will start by considering the analogy between the simpler of these two systems, i.e., the one with a binary distribution of the bias force, and the diffusion of a dimer on a periodic substrate potential. We will show that the diffusion resonance effect experienced by the dimer when the distance between its constituting monomers has a certain optimal value, is a mechanical analog of the oscillatory resonance shown by a network of FHN units with a binary bias distribution. Following Ref. [IV], we will call this effect dimer-diffusion resonance (DDR). Since DDR can be extended to the case of polymer dynamics, as we will demonstrate, this approach will also provide a mechanical analogy to DIR, observed in the case of oscillator networks with a Gaussian distribution of parameter values. The DDR mechanism, along with its polymer-based extension, is inherently general and is anticipated to operate across a broad class of systems and under a variety of conditions.

### 6.1 Dimer-Diffusion Resonance

Let us begin by considering the minimal case of a single pair of oscillators. For the sake of simplicity, we will first examine a pair of quartic oscillators in place of FHN units. We have already encountered quartic oscillators in Sec. 4.1, where we introduced SR. Assuming a diffusive coupling between the two oscillators, the corresponding dynamical equations are:

$$\begin{aligned}\dot{x}_1 &= -V'(x_1) + f(t) + C(x_2 - x_1) - \bar{a}, \\ \dot{x}_2 &= -V'(x_2) + f(t) - C(x_2 - x_1) + \bar{a},\end{aligned}\tag{63}$$

where  $V(x)$  is a symmetric double-well potential, which after a suitable rescaling takes the form

$$V(x) = -\frac{1}{2}x^2 + \frac{1}{4}x^4, \quad (64)$$

while  $f(t)$  is a periodic forcing, which we assume to be represented by a simple sinusoidal,  $f(t) = b \sin \omega t$ . The amplitude  $b$  is chosen to be small enough that either oscillator taken individually (without coupling) cannot oscillate, i.e., the effective potential  $V(x) - xf(t)$  always keeps two minima at any time  $t$ . Finally, the first oscillator in Eqs. (63) is subjected to a bias  $a = -\bar{a}$ , while the second experiences a bias  $a = +\bar{a}$ . Both the biases and the coupling strength  $C$  are constant.

We now turn to the above-mentioned dimer analogy by rewriting Eqs. (63) as follows:

$$\begin{aligned} \dot{x}_1 &= -V'(x_1) + f(t) + C(x_2 - x_1 - \ell), \\ \dot{x}_2 &= -V'(x_2) + f(t) - C(x_2 - x_1 - \ell), \end{aligned} \quad (65)$$

where  $\ell = \bar{a}/C$ . This highlights that the dynamics of the two-oscillator system described by Eqs. (63) are mathematically equivalent to those of a harmonic dimer with rest length  $\ell$ , formed by two particles located at  $x_1$  and  $x_2$ , which are linearly coupled with strength  $C$  and evolve under the influence of the external potential  $V(x) - xf(t)$ .

Continuing to build on this analogy, we define the center-of-mass coordinate  $X$  of the dimer and the relative coordinate  $y$  as:

$$X = \frac{x_1 + x_2}{2}, \quad y = x_2 - x_1. \quad (66)$$

Transforming Eqs. (65) into these new coordinates yields:

$$\begin{aligned} \dot{X} &= -\frac{1}{2} \left[ V' \left( X - \frac{y}{2} \right) + V' \left( X + \frac{y}{2} \right) \right] + f(t), \\ \dot{y} &= - \left[ V' \left( X + \frac{y}{2} \right) - V' \left( X - \frac{y}{2} \right) \right] - 2C(y - \ell). \end{aligned} \quad (67)$$

Let us assume the substrate potential acting on the dimer is sinusoidal, with amplitude  $V_0$  and spatial period  $\lambda$ :

$$V(x) = V_0 \cos \left( \frac{2\pi x}{\lambda} \right), \quad (68)$$

so that

$$V'(x) = -\frac{2\pi V_0}{\lambda} \sin \left( \frac{2\pi x}{\lambda} \right). \quad (69)$$

Substituting into Eqs. (67) gives:

$$\begin{aligned} \dot{X} &= \frac{\pi V_0}{\lambda} \left[ \sin \left( \frac{2\pi(X - y/2)}{\lambda} \right) + \sin \left( \frac{2\pi(X + y/2)}{\lambda} \right) \right] + f(t), \\ \dot{y} &= \frac{2\pi V_0}{\lambda} \left[ \sin \left( \frac{2\pi(X + y/2)}{\lambda} \right) - \sin \left( \frac{2\pi(X - y/2)}{\lambda} \right) \right] - 2C(y - \ell). \end{aligned} \quad (70)$$

Using the trigonometric identities:

$$\begin{aligned} \sin(A + B) + \sin(A - B) &= 2 \sin A \cos B, \\ \sin(A + B) - \sin(A - B) &= 2 \cos A \sin B, \end{aligned} \quad (71)$$

we obtain:

$$\begin{aligned}\dot{X} &= \frac{2\pi V_0}{\lambda} \sin\left(\frac{2\pi X}{\lambda}\right) \cos\left(\frac{\pi y}{\lambda}\right) + f(t), \\ \dot{y} &= \frac{4\pi V_0}{\lambda} \cos\left(\frac{2\pi X}{\lambda}\right) \sin\left(\frac{\pi y}{\lambda}\right) - 2C(y - \ell).\end{aligned}\tag{72}$$

This shows that the dimer center-of-mass motion is governed by an effective potential of the form:

$$V_{\text{eff}}(X) = -V_0 \cos\left(\frac{2\pi X}{\lambda}\right) \cos\left(\frac{\pi y}{\lambda}\right).\tag{73}$$

When  $y$  relaxes close to  $\ell$ , this becomes:

$$V_{\text{eff}}(X) \approx -V_0 \cos\left(\frac{2\pi X}{\lambda}\right) \cos\left(\frac{\pi \ell}{\lambda}\right).\tag{74}$$

We can see that the amplitude of this effective potential is modulated by  $\cos\left(\frac{\pi \ell}{\lambda}\right)$ . This amplitude vanishes when:

$$\cos\left(\frac{\pi \ell^*}{\lambda}\right) = 0 \quad \Rightarrow \quad \ell^* = \frac{\lambda}{2} + n\lambda, \quad n \in \mathbb{Z}.\tag{75}$$

Hence, when  $\ell = \ell^* = \lambda/2$ , i.e., when the distance between the monomers is half the spatial period of the potential, the effective substrate potential seen by the center of mass disappears, and the dimer can move with minimal resistance, leading to the DDR effect [142–144].

These arguments also apply to the dynamics of a dimer in a double-well potential, with the distinction that, unlike the periodic case, there exists a single resonant rest length  $\ell^*$ , approximately equal to half the separation between the two potential minima, instead of an infinite set of resonant lengths [142]. Recalling the definition  $\ell = \bar{a}/C$ , it becomes clear that DDR, which can be observed when  $\ell \approx \lambda/2$ , is completely analogous to the resonance phenomenon that arises in the equivalent two-oscillator system upon fixing the bias  $\bar{a}$  and tuning the coupling strength  $C$  [IV, 12].

## 6.2 Extension of DDR to a Polymer

### 6.2.1 Networks with Two Types of Oscillators

We now examine the case in which the network is composed of an even number  $N$  of interacting quartic oscillators governed by the equation

$$\dot{x}_i = -V'(x_i) + f(t) + C \sum_{j \in \mathcal{N}(i)} (x_j - x_i) + a_i,\tag{76}$$

where  $i = 1, \dots, N$ . The sum in Eq. (76) represents the interactions between the generic oscillator  $i$  and the other oscillators, where a linear coupling of strength  $C$  is assumed, extending over the set of oscillators  $j \in \mathcal{N}(i)$  that interact with oscillator  $i$ . Like in the previous two-oscillator example, with  $V(x)$  we denote a symmetric double-well potential and  $f(t)$  is an external time-periodic forcing.

Each oscillator is randomly assigned a bias force from a two-value discrete distribution, such that half of the units (set  $I_-$ ) experience  $a = -\bar{a}$ , while the complementary half (set  $I_+$ ) experience  $a = +\bar{a}$ . This configuration yields a zero mean bias,  $\langle a \rangle = 0$ . This distribution is analogous to that used in Ref. [12] in the context of FHN networks. Here, however,

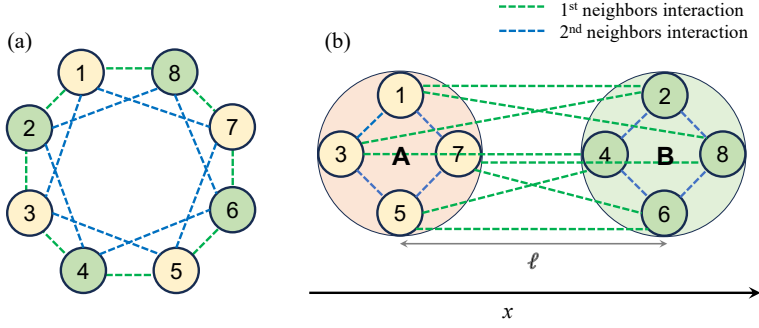


Figure 23: **(a)** Regular network composed of alternating types of oscillators with bias  $a = -\bar{a}$  (yellow nodes) and  $a = +\bar{a}$  (green nodes). Each node is coupled to two nearest neighbors on both sides, so the degree is  $k_0 = 4$ . Blue links represent interactions between two oscillators of the same type, green links between oscillators of different types. **(b)** Polymer mechanical analog in  $x$ -space. The harmonic forces between particles of the same type tend to induce localized clusters, while harmonic interactions between particles of different type induce the formation of two clusters at a distance  $\ell$ . As a result, the system behaves similarly to two interacting monomers A and B that compose a dimer with equilibrium length  $\ell$ . Reprinted from [Marco Patriarca, Stefano Scialla, Els Heinsalu, Marius E. Yamakou, Julyan H. E. Cartwright; Dynamical equivalence between resonant translocation of a polymer chain and diversity-induced resonance. *Chaos* 1 July 2025; **35** (7): 073115. <https://doi.org/10.1063/5.0262633>], with the permission of AIP Publishing.

we consider it first for quartic oscillators, and subsequently in Sec. 6.3 in relation to FHN models.

We separate the system described by Eq. (76) into two coupled subsystems, corresponding to the disjoint sets  $I_{\pm}$ , and denote the respective variables as  $x_i^{\pm}$ . Accordingly, the total interaction term can be decomposed into two partial sums involving intra- and inter-group interactions.

As a representative configuration, we analyze a regular network in which each oscillator is connected to an even number  $k_0$  of neighbors, with a symmetrical distribution of the connections: half of them ( $k_0/2$ ) link to oscillators in the set  $I_+$ , and the remaining half to those in  $I_-$ . An illustration of this structure for  $k_0 = 4$  is provided in Fig. 23(a). To facilitate analysis, we begin by introducing a rescaled coupling parameter  $c$  in Eq. (76), such that  $C = 2c/k_0$ . Using this definition, the associated bias  $a_i$  for each oscillator  $i$  can be expressed as

$$a_i \equiv \frac{2}{k_0} \sum_{j=1}^{k_0/2} a_i. \quad (77)$$

The individual terms  $\frac{2a_i}{k_0}$  can then be incorporated into the linear coupling terms that describe the interaction between oscillator  $i$  and its  $k_0/2$  neighbors belonging to the opposite subset. With this reformulation, Eqs. (63) can be recast as

$$\begin{aligned} \dot{x}_i^- &= -V'(x_i^-) + f(t) + C \sum_{j \in I_-} (x_j^- - x_i^-) + C \sum_{j \in I_+} (x_j^+ - x_i^- - \ell), \\ \dot{x}_i^+ &= -V'(x_i^+) + f(t) + C \sum_{j \in I_+} (x_j^+ - x_i^+) - C \sum_{j \in I_-} (x_i^+ - x_j^- - \ell). \end{aligned} \quad (78)$$

In both equations, the first summations on the right-hand side describe standard harmonic interactions between oscillator  $i$  and those of the same type, while the second

summations correspond to interactions with oscillators of the opposite type, with an equilibrium distance

$$\ell = \frac{2\bar{a}}{k_0 C} \equiv \frac{\bar{a}}{c}. \quad (79)$$

Upon introducing a total potential

$$\begin{aligned} W_Q^{\text{reg}}(x_1, \dots, x_N, t) &= \sum_{i=1}^N [V(x_i) - x_i f(t)] + \frac{C}{2} \sum_{i,j \in I_-} (x_j - x_i)^2 \\ &+ \frac{C}{2} \sum_{i,j \in I_+} (x_j - x_i)^2 + C \sum_{i \in I_-, j \in I_+} (x_j - x_i - \ell)^2, \end{aligned} \quad (80)$$

we can express Eqs. (78) as

$$\begin{aligned} \dot{x}_i^- &= -\frac{\partial}{\partial x_i^-} W_Q^{\text{reg}}(x_1, \dots, x_N, t), \\ \dot{x}_i^+ &= -\frac{\partial}{\partial x_i^+} W_Q^{\text{reg}}(x_1, \dots, x_N, t). \end{aligned} \quad (81)$$

This reformulation of the dynamics in terms of  $N$  interacting overdamped particles evolving in the total potential  $W_Q^{\text{reg}}(x_1, \dots, x_N, t)$  leads to a natural mechanical analogy with a one-dimensional polymer. The polymer consists of two types of monomers, corresponding to the oscillator subsets  $I_-$  and  $I_+$ . Monomers from different subsets interact as in a dimer, with an equilibrium separation  $\ell$  defined by Eq. (79), and therefore tend to maintain a spacing  $\ell$  between them (this corresponds to the final term in Eq. (80)). On the other hand, monomers of the same type experience purely harmonic coupling, favoring minimal distance (represented by the second and third terms in Eq. (80)). As a result, elements within  $I_-$  and within  $I_+$  tend to aggregate into two spatially localized, internally homogeneous clusters. These clusters, labeled A and B, naturally arrange themselves at a distance  $\ell$  from one another, as illustrated in Fig. 23(b). Consequently, the collective response of a network of  $N$  oscillators with a two-value bias distribution under periodic forcing closely mirrors the behavior of a single dimer with rest length  $\ell$ , as discussed in Sec. 6.1. Such structures also appear in physical systems; for instance, an applied electric field acting on charged dipoles produces opposing forces on the constituent charges [143].

The mechanical analogy between a heterogeneous oscillator network and an overdamped polymer chain provides a useful framework to estimate the resonant bias  $a^*$  or the resonant coupling  $c^*$ . As a first approximation, the barrier of the double-well potential can be interpreted as one of the peaks in a spatially periodic potential, such as a sinusoidal potential. The quartic potential  $V(x) = -x^2/2 + x^4/4$  exhibits two minima located at  $x = \pm 1$  with depth  $-1/4$ , implying a separation of  $\lambda = 2$  between adjacent wells. This distance effectively defines the spatial period of a corresponding periodic potential. As explained in Sec. 6.1, maximal transport occurs when the dimer rest length  $\ell$  matches half the period, i.e.,  $\ell = \lambda/2$  [142-144]. Applying this condition to Eq. (79), one obtains the following estimate for the resonance condition in a regular network of degree  $k_0$ :

$$\frac{2\bar{a}}{k_0 C} \equiv \frac{\bar{a}}{c} = \frac{\lambda}{2}. \quad (82)$$

This criterion can be rephrased either in terms of a resonant value of the bias parameter,  $\bar{a} = a^*$ , or a resonant coupling strength,  $c = c^*$ , depending on which variable is controlled.

As an example, let us consider the case of a fully connected network of  $N = 100$  oscillators where the bias follows a two-value discrete distribution (as previously explained)

and  $C = 1$ . The effective connectivity for such a network is  $k_0 = N - 1$ . Substituting into Eq. (82) gives a resonant dimer length  $a^* = 0.5$ , which is in excellent agreement with the numerical results presented in Ref. [IV] (see Fig. 2(a) in the paper).

### 6.2.2 Networks with a Continuous Bias Distribution

In this Section, we demonstrate that DDR also arises in heterogeneous networks with arbitrary bias distributions, and in such cases, it can be related to DIR.

Consider an all-to-all connected network of oscillators with biases assigned from a continuous distribution  $P(a)$ . The oscillators are labeled in order of increasing bias, so that  $a_1 < a_2 < a_3 < \dots < a_N$ . To be able to compare this network with a homogeneous unbiased system, we impose the condition of zero mean bias:  $\langle a \rangle = N^{-1} \sum_{i=1}^N a_i = 0$ . The bias for each oscillator can then be expressed as

$$a_i = a_i - \langle a \rangle \equiv \frac{1}{N} \sum_{j=1}^N (a_i - a_j), \quad (83)$$

and the equations of motion become:

$$\begin{aligned} \dot{x}_i &= -V'(x_i) + f(t) + \frac{c}{N} \sum_{j=1}^N \left( x_j - x_i + \frac{a_i - a_j}{c} \right) \\ &= -V'(x_i) + f(t) - \frac{c}{N} \sum_{j=1}^{i-1} (x_i - x_j - \ell_{ij}) + \frac{c}{N} \sum_{j=i+1}^N (x_j - x_i - \ell_{j,i}). \end{aligned} \quad (84)$$

Here, the sum is split into two parts: one over indices  $j < i$  (with  $a_j < a_i$ ) and one over indices  $j > i$  (with  $a_j > a_i$ ), such that all terms

$$\ell_{m,n} = \frac{a_m - a_n}{c} > 0 \quad \text{if } m > n; \quad m, n = 1, \dots, N, \quad (85)$$

are positive and can be interpreted as equilibrium lengths for harmonic interactions.

This structure suggests a mechanical analog of a heterogeneous oscillator network: a 1D polymer composed of  $N$  monomers located at positions  $x_i$ , where each monomer interacts with all others via harmonic springs. The monomers align in order of increasing bias, forming a well-ordered chain without frustration, since the equilibrium lengths satisfy the consistency condition  $\ell_{ij} = \ell_{ik} + \ell_{kj}$ . For example, the interaction between monomers 1 and 3 is stabilized by the relation  $\ell_{31} = \ell_{21} + \ell_{32}$ , reinforcing the ordered structure—see Fig. 24.

Because interactions scale with  $|a_i - a_j|$ , the system self-organizes into a configuration where monomer positions reflect bias values. With increasing number of interactions, the chain rigidity grows, leading to a well-defined structure with total length

$$\ell_{\text{tot}} = \sum_{i=1}^{N-1} \ell_{i,i+1} = \frac{a_N - a_1}{c}. \quad (86)$$

Rewriting the dynamics in gradient form,

$$\dot{x}_i = -\frac{\partial}{\partial x_i} W_Q^{\text{full}}(x_1, \dots, x_N, t), \quad (87)$$

with total potential

$$W_Q^{\text{full}}(x_1, \dots, x_N, t) = \sum_i [V(x_i) - f(t)x_i] + \frac{C}{2} \sum_{i < j} (x_j - x_i - \ell_{ji})^2, \quad (88)$$

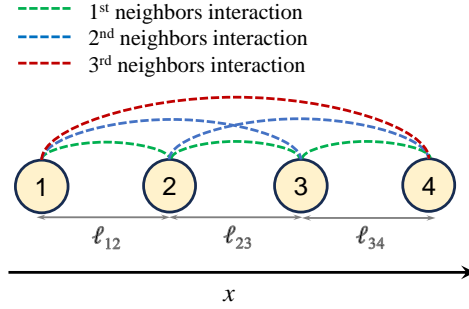


Figure 24: Mechanical analog of a small network of four oscillators. Each oscillator interacts with all others via consistent equilibrium distances, forming a robust 1D chain, as defined in Eq. (85). Reprinted from [Marco Patriarca, Stefano Scialla, Els Heinsalu, Marius E. Yamakou, Julyan H. E. Cartwright; Dynamical equivalence between resonant translocation of a polymer chain and diversity-induced resonance. *Chaos* 1 July 2025; **35** (7): 073115. <https://doi.org/10.1063/5.0262633>], with the permission of AIP Publishing.

shows that the system evolves as an overdamped polymer in a collective potential.

Numerical simulations (see Ref. [IV] for details) confirm that global oscillations correspond to complete *translocations* of the polymer across the potential wells, in which the monomers preserve their order. When network parameters prevent a collective oscillatory state, no polymer translocation or partial translocation occurs so that the entire polymer, or a segment, stays in the same potential well. This supports previous observations [13] that excessive diversity in the bias can hinder collective network dynamics, preventing the emergence of DIR.

### 6.3 DDR and Polymer Translocation in Networks of FHN Units

All considerations made for quartic oscillators also apply to FHN oscillators [9–11]. The equations for a single FHN oscillator can be written as

$$\begin{aligned} \dot{x} &= -V'(x) - y + a, \\ \dot{y} &= \alpha x - \beta y, \end{aligned} \tag{89}$$

where  $V(x)$  is the same quartic potential as in Eq. (53), and  $\alpha, \beta$  are constants defining the slow variable  $y$ . The constant bias  $a$  appears in the fast equation for  $x$ , as opposed to other versions of the FHN equations. This equation form facilitates the comparison with the quartic oscillator case and implies no loss of generality, since different formulations of the FHN equations can be transformed into one another by appropriately rescaling the variables and shifting the  $y$  coordinate.

Next, we consider two coupled FHN units with linear coupling in  $x_1$  and  $x_2$ ,

$$\begin{aligned} \dot{x}_1 &= -V'(x_1) - y_1 + C(x_2 - x_1) + a_1, \\ \dot{x}_2 &= -V'(x_2) - y_2 - C(x_2 - x_1) + a_2, \\ \dot{y}_1 &= \alpha x_1 - \beta y_1, \\ \dot{y}_2 &= \alpha x_2 - \beta y_2. \end{aligned} \tag{90}$$

Setting  $a_1 = -\bar{a}$ ,  $a_2 = +\bar{a}$ , and defining  $\ell = \bar{a}/C$ , the system becomes

$$\begin{aligned} \dot{x}_1 &= -\frac{\partial}{\partial x_1} W_{\text{FHN}}^{\text{dim}}(x_1, x_2) - y_1, \\ \dot{x}_2 &= -\frac{\partial}{\partial x_2} W_{\text{FHN}}^{\text{dim}}(x_1, x_2) - y_2, \\ \dot{y}_1 &= \alpha x_1 - \beta y_1, \\ \dot{y}_2 &= \alpha x_2 - \beta y_2, \end{aligned} \quad (91)$$

with effective potential

$$W_{\text{FHN}}^{\text{dim}}(x_1, x_2) = V(x_1) + V(x_2) + \frac{C}{2} (x_2 - x_1 - \ell)^2. \quad (92)$$

As in the quartic case, the  $x$ -variables describe a dimer of rest length  $\ell$  moving in  $V(x)$ , while the  $y$ -variables provide active modulation. If  $\alpha$ ,  $\beta$  are such that the  $y$ -sector alone cannot push the system across the potential barrier, the dimer remains confined. However, harmonic coupling can enable translocation with a resonance near  $\ell = \lambda/2$ .

This generalizes to a network of  $N$  FHN units with arbitrary zero-mean bias distribution  $P(a)$ , governed by

$$\begin{aligned} \dot{x}_i &= -\frac{\partial}{\partial x_i} W_{\text{FHN}}^{\text{dim}}(x_1, \dots, x_N) - y_i, \\ \dot{y}_i &= \alpha x_i - \beta y_i. \end{aligned} \quad (93)$$

For a regular network with degree  $k_0$ , consisting of two oscillator types with  $a = \pm\bar{a}$ , the potential reads

$$\begin{aligned} W_{\text{FHN}}^{\text{reg}}(x_1, \dots, x_N) &= \sum_{i=1}^N V(x_i) + \frac{C}{2} \sum_{i,j \in I_-} (x_j - x_i)^2 \\ &+ \frac{C}{2} \sum_{i,j \in I_+} (x_j - x_i)^2 + C \sum_{i \in I_-, j \in I_+} (x_j - x_i - \ell)^2, \end{aligned} \quad (94)$$

identical to Eq. (80) but without external forcing. The resonance condition is the same as in Eq. (82).

In the fully connected case with symmetric  $P(a)$ , the total potential is

$$W_{\text{FHN}}^{\text{full}}(x_1, \dots, x_N) = \sum_i V(x_i) + \frac{C}{2} \sum_{i < j} (x_j - x_i - \ell_{ji})^2, \quad (95)$$

matching Eq. (88) apart from the external drive. Simulations for  $N$  all-to-all connected FHN oscillators with bimodal bias  $P(a)$  confirm a DDR response similar to quartic oscillators, as shown in detail in Ref. [IV]. The alignment in response curves and resonant lengths  $\ell^*$  stems from the shared bistable potential  $V(x)$ .

## 6.4 Final Considerations

The study reported in Ref. [IV] demonstrates that DIR can be understood as a general phenomenon arising in systems where heterogeneity allows for optimal collective response. By interpreting the dynamics of heterogeneous oscillator networks as equivalent to a polymer system with nonlocal harmonic interactions, the study provides a mechanical analogy that clarifies how synchronization emerges and how resonance conditions are determined. This framework is validated both in networks of quartic and FHN oscillators.

Importantly, the findings bridge DDR and DIR under a unified perspective, showing that both effects arise from the interaction between distributed biases and coupling in the system. The results may help guide the analysis and design of other complex systems where disorder can play a constructive role in enhancing collective dynamics.

## 7 SYMMETRY OF THE DIVERSITY DISTRIBUTION AS A DETERMINANT OF GLOBAL OSCILLATIONS

In the preceding chapters, we investigated the mechanisms that govern the emergence of global oscillations in heterogeneous networks of excitable units, with particular emphasis on diversity-induced effects. A central theme was the phenomenon of DIR, wherein an optimal degree of heterogeneity among the units can lead to coherent macroscopic oscillations, even when the individual units are not oscillatory in isolation.

A common assumption in previous studies [13, 69, 70] has been that the key determinant for the emergence of global oscillations is the presence of a sufficient fraction of individually oscillatory units that are able to “pull” the remaining, excitable ones through the coupling terms. However, recent findings from Ref. [V] suggest that the *symmetry* of the diversity distribution—rather than the number of oscillatory units per se—may play a fundamental role in determining the dynamical regime of the network.

Therefore, in this chapter, we extend our analysis to systematically examine how the *degree of symmetry* of the diversity distribution influences collective network behavior across three different coupling topologies: all-to-all, cubic lattice, and small-world (Newman-Watts). Based on results from Ref. [V], we show that symmetric distributions promote global oscillations even in the absence of oscillatory units, while asymmetric ones may suppress oscillations even when a significant fraction of the units are individually active. This result generalizes the mechanism of DIR by highlighting a structural property, i.e., symmetry, as a key determinant of emergent behavior in excitable systems.

### 7.1 Model Framework

We consider a network of  $N$  coupled FHN units, governed by the equations:

$$\dot{x}_i = a \left[ x_i - x_i^3/3 + y_i + C \sum_{j \in \mathcal{N}_i} (x_j - x_i) \right], \quad (96a)$$

$$\dot{y}_i = -\frac{1}{a} (x_i + by_i - J_i), \quad (96b)$$

where  $x_i$  and  $y_i$  represent the fast and slow variables, respectively, of the  $i$ -th unit;  $a$  and  $b$  are parameters chosen based on physiological constraints;  $C$  is the uniform coupling strength; and  $J_i$  is a bias term encoding intrinsic heterogeneity.

Unless otherwise specified, all numerical simulations presented in this chapter use the following parameter values:  $a = 60$ ,  $b = 1.45$ , and  $C = 0.15$ . The coupling strength  $C = 0.15$  corresponds to the minimal value required for the onset of collective oscillations and aligns with findings from previous studies [I]. The parameters  $a$  and  $b$  are also taken from earlier work [I-II], where they were calibrated to reproduce key electrophysiological features of pancreatic  $\beta$ -cells. While variations in  $a$  and  $b$  affect the value of  $\varepsilon$  and alter the geometry of the nullclines in Eqs. (96), the qualitative behaviors that will be discussed in the rest of this chapter remain robust with respect to these changes.

The coupling topology in Eqs. (96) is defined by the set  $\mathcal{N}_i$  of neighbors of unit  $i$ , which can vary depending on whether we consider an all-to-all, cubic lattice, or small-world network. It should be noted that Eqs. (96) are identical to Eqs. (25), already shown in Chapter 2, with the only difference that  $\mathcal{N}_i$  can change as a function of the coupling topology.

As established in Chapter 2, the dynamical regime of each unit is determined by the parameter  $J_i$ : the unit is excitable for  $|J_i| > \varepsilon$  and oscillatory otherwise. The threshold  $\varepsilon$

is determined analytically via the linear stability analysis of the fixed point:

$$\varepsilon = \frac{\sqrt{a^2 - b(3a^2 - 2a^2b - b^2)}}{3a^3}. \quad (97)$$

In earlier chapters, we considered heterogeneity by assigning  $J_i$  values drawn from symmetric Gaussian distributions usually centered at  $J_0 = 0$ , with the standard deviation  $\sigma$  controlling the degree of diversity in the network [13, I, II]. Here, following Ref. [V], we extend the analysis by examining how the *shape and symmetry* of the distribution from which the  $J_i$  values are drawn affects the network behavior. To this aim, we consider modified distributions obtained by truncating the normal distribution, either on one or both sides, as well as half-normal distributions. These variants, discussed in detail in Sec. 7.3, allow us to explore the impact of different types and degrees of asymmetry on the network dynamics.

## 7.2 Mean-Field Analysis

Recall from Chapter 3 that a mean-field approximation of the full network dynamics leads to a reduced system for the average variables  $X(t)$  and  $Y(t)$  [II, V]:

$$\dot{X} = a \left[ X(1 - M) - \frac{X^3}{3} + Y \right], \quad (98a)$$

$$\dot{Y} = -\frac{1}{a}(X - bY + \bar{J}), \quad (98b)$$

where  $M$  expresses the level of diversity, larger  $M$  values meaning greater diversity.  $\bar{J}$  is the average of the  $J_i$  values over the  $N$  units constituting the network. As detailed in Chapter 3 and in Ref. [II, V], Eqs. (98) are derived under the assumption that the deviations  $\delta_i$  of individual units from the mean field are small and symmetrically distributed. Specifically, the approximations  $N^{-1} \sum_{i=1}^N \delta_i \cong 0$  and  $N^{-1} \sum_{i=1}^N \delta_i^3 \cong 0$  are used to neglect the first and third moments of the deviation distribution. These conditions are satisfied only when the diversity distribution of the bias parameters  $J_i$  is symmetric (e.g., Gaussian or uniform with zero mean) and narrow enough so that higher-order fluctuations around the mean can be ignored.

If the diversity distribution is asymmetric, the above terms must be retained, as their contribution becomes non-negligible. Their presence leads to a displacement of the equilibrium point of the system along the cubic nullcline (see Fig. 18 in Chapter 4), either toward the ascending or descending branch depending on the sign of the asymmetric terms. As a consequence, increasing diversity under these conditions may shift the system toward an excitable rather than an oscillatory regime. Furthermore, if the asymmetry in the distribution of  $J_i$  values results in a substantial deviation of the mean  $J_{av}$  from its original position, this additional shift can further stabilize the system and suppress collective oscillations.

Although these arguments are qualitative, they highlight the critical role played by the symmetry of the diversity distribution in shaping the global dynamics of the network. In particular, they provide insight into network behaviors that cannot be accounted for by simpler criteria, such as the proportion of oscillatory versus excitable units.

## 7.3 Numerical Simulations

We now present a set of representative examples to illustrate how the symmetry of the diversity distribution influences the emergence of global oscillations in networks of excitable

units. The examples cover a range of diversity distributions and are tested across different network topologies. While numerical results are shown for selected cases, the qualitative outcome—namely, the presence or absence of collective oscillatory activity—was found to be consistent across all three considered configurations: all-to-all coupling, cubic lattice, and cubic lattice with added small-world features. The latter was implemented following the Newman–Watts model, using rewiring probabilities in the range  $0 \leq p \leq 1$  [145].

### 7.3.1 Symmetry Metrics

To quantify the degree of symmetry of the diversity distributions, following Ref. [V], we introduce two metrics: the Normalized Center of Mass (nCOM) and the Symmetry Balance Score (SBS). The nCOM captures the displacement of the overall mass of the  $J_i$  distribution with respect to the center of the oscillatory regime:

$$\text{nCOM} = \frac{|\sum_{i=1}^N (J_i - J_0)|}{N \cdot \varepsilon}. \quad (99)$$

Here,  $J_0$  is the midpoint of the oscillatory interval, which we take as 0 in our case. Values  $\text{nCOM} < 1$  indicate that the distribution is fairly symmetric or centered within the oscillatory interval, while values  $\text{nCOM} \geq 1$  signify that the distribution is predominantly skewed to one side.

Instead, the SBS measures the relative balance of units with positive and negative  $J_i$  values:

$$\text{SBS} = \frac{\min(N_+, N_-)}{\max(N_+, N_-)}, \quad (100)$$

where  $N_+$  and  $N_-$  are the number of units with  $J_i > J_0$  and  $J_i < J_0$ , respectively. SBS ranges from 0 (maximal asymmetry) to 1 (perfect balance).

These two metrics provide complementary characterizations of the diversity distribution. While nCOM reflects mass displacement, SBS captures population balance. Both factors influence the effective dynamics of the network, as shown by the following results.

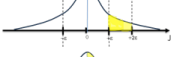
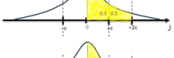
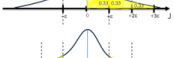
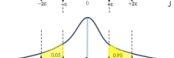
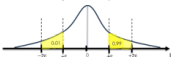
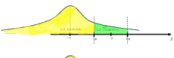
Table 2 reports the values of nCOM and SBS for all diversity distributions analyzed in the following sections, together with the corresponding ratios of oscillatory to non-oscillatory units. The latter ratio has been the principal criterion adopted in previous studies to predict the emergence of global network oscillations. However, this approach is applicable only to a limited class of distributions and suffers from the lack of a well-defined threshold above which collective oscillations are reliably expected. In Table 2, we have adopted a threshold value of approximately 0.3, which correctly anticipates the behavior of the distribution shown in Fig. 32. Nevertheless, prior work has reported cases in which global oscillations occurred even with an oscillator-to-excitable unit ratio as low as 0.25 [69], underscoring the limitations of this criterion.

### 7.3.2 Half-normal Diversity Distributions

We begin by analyzing half-normal diversity distributions and consider as a first example a truncated case with  $J_{av} = 0$  and  $\sigma = 0.5$ , in which  $J_i$  values are drawn exclusively from the interval  $[0, \varepsilon)$ . In this configuration, all units are individually oscillatory, but the distribution is asymmetric, as values are sampled only from the positive semiaxis (Fig. 25).

Numerical simulations based on Eqs. (96) for both cubic lattice (with  $N = 1000$ ) and all-to-all (with  $N = 125$ ) topologies confirm that this network exhibits strong global oscillations. The collective activity is quantified by the parameter  $\rho$ , defined as in Chapter 3

Table 2: Comparison of symmetry metrics and oscillatory behavior for the nine bias distributions corresponding to Figs 2–10. Green indicates correct predictions, while red highlights discrepancies. The criterion for global network oscillations is shown in parentheses in each column heading. [Reprinted from: M. Patriarca, S. Scialla, E. Heinsalu, M. E. Yamakou, and J. H. E. Cartwright, Effect of diversity distribution symmetry on global oscillations of networks of excitable units. *arXiv preprint arXiv:2507.09804* (2025). <https://doi.org/10.48550/arXiv.2507.09804> (Submitted to *Phys. Rev. E*)].

Figure	Distribution	Oscillator/ Nonoscillator Ratio ( $> 0.3$ )	Normalized Center of Mass ( $< 1$ )	Symmetry Balance Score ( $\geq 0$ )	Global Oscillations? ( $> 0.3$ )
2		Inf.	0.50	n.a.	Yes
3		0	1.50	n.a.	No
4		1	0.99	n.a.	Yes
5		0.5	1.52	n.a.	No
6		0	0.00	0.95	Yes
7		0	1.37	0.045	Yes
8		0	1.47	0.015	No
9		0.25	25.15	0.00	No
10		0	24.01	0.26	Yes

and 4 [I, II, V]:

$$\rho \equiv N^{-2} \sqrt{\langle [S(t) - \bar{S}]^2 \rangle}, \quad (101)$$

where  $N$  is the number of units,  $S(t) = \sum_i x_i(t)$ , and  $\bar{S} = \langle S(t) \rangle$  denotes the time average of  $S(t)$ . Values of  $\rho \approx 1$  indicate strong collective oscillations, while  $\rho \approx 0$  corresponds to an incoherent or quiescent network state.

We next consider a similar diversity distribution where  $J_i$  values are still sampled only from the positive semiaxis, but within the interval  $(\varepsilon, 2\varepsilon]$ , so that all units are individually excitable. In this case, the network does not exhibit collective oscillations, as shown in Fig. 26, regardless of the coupling topology.

We then analyze an intermediate case in which half the units are selected from  $[0, \varepsilon)$  (oscillatory) and half from  $(\varepsilon, 2\varepsilon]$  (excitable), forming a truncated half-normal distribution that includes both types (Fig. 27). Despite its asymmetry, this distribution supports strong global oscillations, similar to the fully oscillatory case in Fig. 25. Results are shown for the cubic lattice, but analogous behavior is observed with all-to-all coupling.

This outcome is consistent with previous studies [13, 69, 70], which attributed the emergence of global oscillations to a pull mechanism, whereby the oscillatory units entrain the excitable ones. To test the limits of this mechanism, we consider a case where the fraction of excitable units is increased to two-thirds, yielding a 1:2 oscillatory-to-excitable ratio (Fig. 28). Under these conditions, collective oscillations are suppressed, likely due to both the reduced fraction of oscillatory units and the higher asymmetry of the distribution.

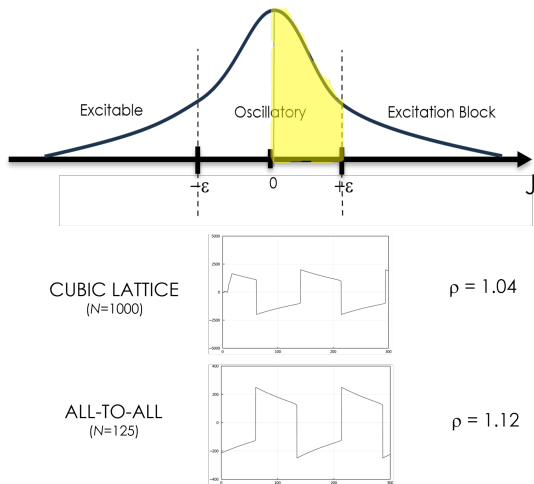


Figure 25: Truncated half-normal diversity distribution comprising oscillatory units only ( $J_{av} = 0$ ,  $\sigma = 0.5$ ). The yellow area highlights the portion of the Gaussian used to sample  $J_i$  values. In this case, the lack of symmetry does not inhibit global network oscillations. The nCOM parameter (nCOM = 0.50, Table 2) correctly predicts the emergence of collective oscillations. [Reprinted from: M. Patriarca, S. Scialla, E. Heinsalu, M. E. Yamakou, and J. H. E. Cartwright, Effect of diversity distribution symmetry on global oscillations of networks of excitable units. *arXiv preprint arXiv:2507.09804* (2025). <https://doi.org/10.48550/arXiv.2507.09804> (Submitted to *Phys. Rev. E*)].

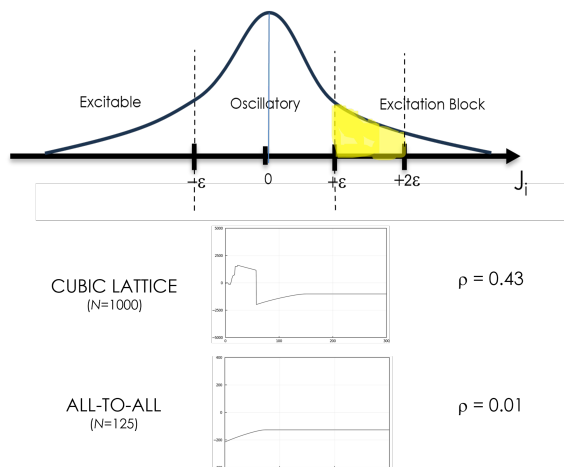


Figure 26: Truncated half-normal diversity distribution comprising excitable units only. The yellow area highlights the portion of the Gaussian used to sample  $J_i$  values. Here, the asymmetry prevents global oscillations. The nCOM value (1.50) correctly predicts this outcome (Table 2). [Reprinted from: M. Patriarca, S. Scialla, E. Heinsalu, M. E. Yamakou, and J. H. E. Cartwright, Effect of diversity distribution symmetry on global oscillations of networks of excitable units. *arXiv preprint arXiv:2507.09804* (2025). <https://doi.org/10.48550/arXiv.2507.09804> (Submitted to *Phys. Rev. E*)].

As summarized in Table 2, the distributions in Fig. 25 and Fig. 27, both with nCOM < 1, support global oscillations, while those in Fig. 26 and Fig. 28, with nCOM > 1, do not. Thus, the nCOM parameter successfully distinguishes between oscillatory and non-oscillatory

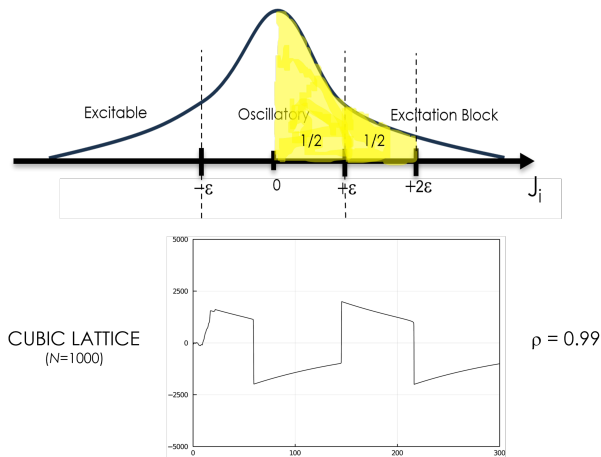


Figure 27: Truncated half-normal diversity distribution comprising equal fractions of oscillatory and excitable units (50/50%). The yellow area highlights the portion of the Gaussian used to sample  $J_i$  values. Global oscillations are maintained despite the asymmetry. The nCOM value (0.99) correctly predicts this result (Table 2). [Reprinted from: M. Patriarca, S. Scialla, E. Heinsalu, M. E. Yamakou, and J. H. E. Cartwright, Effect of diversity distribution symmetry on global oscillations of networks of excitable units. *arXiv preprint arXiv:2507.09804* (2025). <https://doi.org/10.48550/arXiv.2507.09804> (Submitted to *Phys. Rev. E*)].

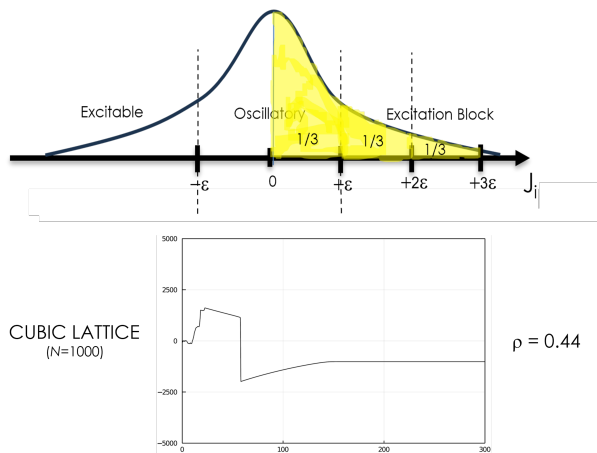


Figure 28: Truncated half-normal diversity distribution comprising one-third oscillatory and two-thirds excitable units. The yellow area highlights the portion of the Gaussian used to sample  $J_i$  values. The increased asymmetry results in the suppression of global oscillations. The nCOM value (1.52) correctly captures this outcome (Table 2). [Reprinted from: M. Patriarca, S. Scialla, E. Heinsalu, M. E. Yamakou, and J. H. E. Cartwright, Effect of diversity distribution symmetry on global oscillations of networks of excitable units. *arXiv preprint arXiv:2507.09804* (2025). <https://doi.org/10.48550/arXiv.2507.09804> (Submitted to *Phys. Rev. E*)].

regimes in all cases examined here. Notably, the oscillator fraction criterion fails to account for the absence of global oscillations in the distribution corresponding to Fig. 28, highlighting the greater relevance of symmetry-based criteria.

### 7.3.3 Normal Diversity Distributions

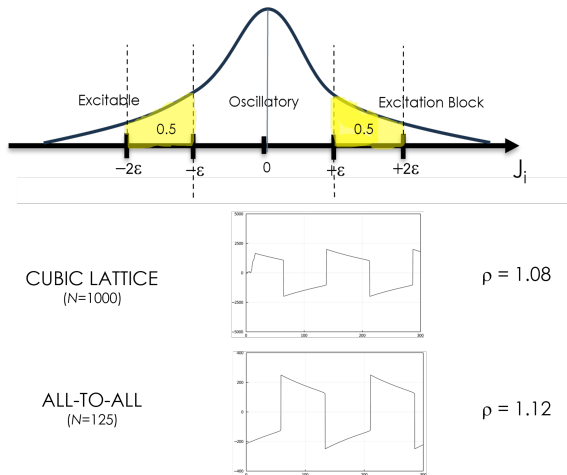


Figure 29: Truncated normal diversity distribution comprising excitable units only. The units are symmetrically distributed on the two sides of the mode in a 1/1 ratio. The yellow area highlights the portion of the Gaussian used to sample  $J_i$  values. This fully symmetric distribution gives rise to global network oscillations. The symmetry measures ( $nCOM = 0$ ,  $SBS = 0.95$ ) correctly predict this behavior, whereas the oscillator fraction criterion fails. [Reprinted from: M. Patriarca, S. Scialla, E. Heinsalu, M. E. Yamakou, and J. H. E. Cartwright, Effect of diversity distribution symmetry on global oscillations of networks of excitable units. arXiv preprint arXiv:2507.09804 (2025). <https://doi.org/10.48550/arXiv.2507.09804> (Submitted to Phys. Rev. E)].

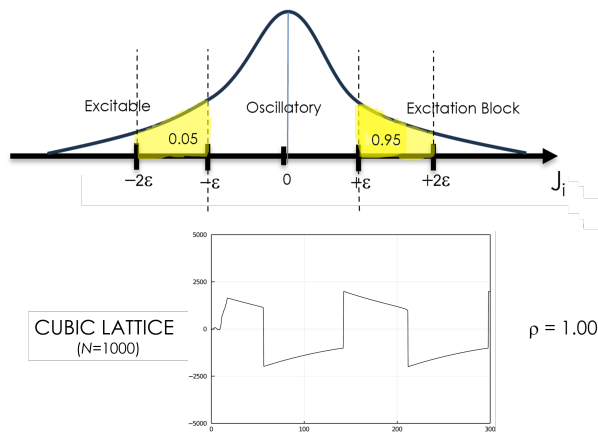


Figure 30: Truncated normal diversity distribution with a 5/95% ratio of units on the two sides of the mode. Despite the asymmetry, the network displays global oscillations. Symmetry metrics correctly rank this case as more likely to oscillate than those in Figs. 26, 28, and 31. [Reprinted from: M. Patriarca, S. Scialla, E. Heinsalu, M. E. Yamakou, and J. H. E. Cartwright, Effect of diversity distribution symmetry on global oscillations of networks of excitable units. arXiv preprint arXiv:2507.09804 (2025). <https://doi.org/10.48550/arXiv.2507.09804> (Submitted to Phys. Rev. E)].

We now consider truncated normal diversity distributions where  $J_i$  values are drawn from both sides of the mode of a Gaussian. In the first example (Fig. 29), the distribution

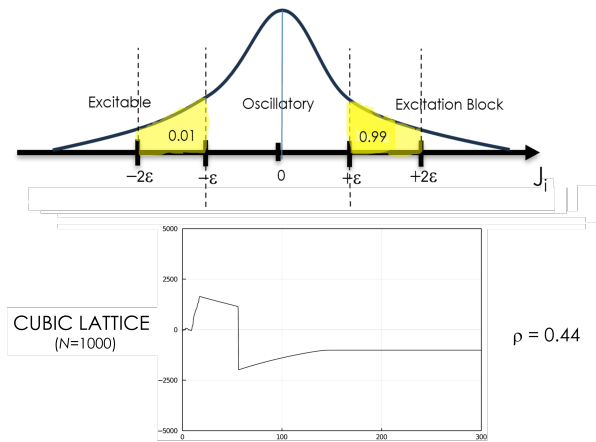


Figure 31: Truncated normal diversity distribution with a 1/99% ratio of units on the two sides of the mode. The asymmetry is sufficient to suppress global oscillations, as confirmed by all metrics in Table 2. [Reprinted from: M. Patriarca, S. Scialla, E. Heinsalu, M. E. Yamakou, and J. H. E. Cartwright, Effect of diversity distribution symmetry on global oscillations of networks of excitable units. arXiv preprint arXiv:2507.09804 (2025). <https://doi.org/10.48550/arXiv.2507.09804> (Submitted to Phys. Rev. E)].

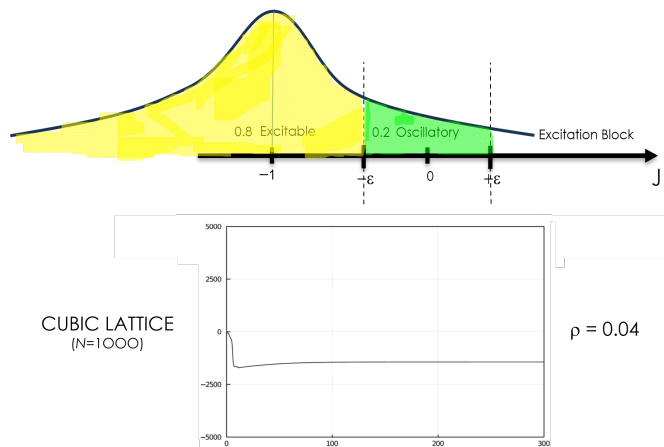


Figure 32: Truncated normal diversity distribution with excitable units drawn from  $(-\infty, -\epsilon)$  and oscillatory units from  $(-\epsilon, +\epsilon)$ . The resulting asymmetry ( $nCOM = 25.15$ ) leads to the absence of global oscillations. [Reprinted from: M. Patriarca, S. Scialla, E. Heinsalu, M. E. Yamakou, and J. H. E. Cartwright, Effect of diversity distribution symmetry on global oscillations of networks of excitable units. arXiv preprint arXiv:2507.09804 (2025). <https://doi.org/10.48550/arXiv.2507.09804> (Submitted to Phys. Rev. E)].

is fully symmetric, with excitable units equally distributed across the two tails. Despite the absence of individually oscillatory units, the network exhibits global oscillations, consistent with the low nCOM and high SBS values. This behavior cannot be explained using the oscillator fraction criterion, which would predict no collective activity.

We then introduce asymmetry by drawing a greater fraction of units from the positive side of the distribution. In Fig. 30, the asymmetry is relatively high (95/5%) but still such

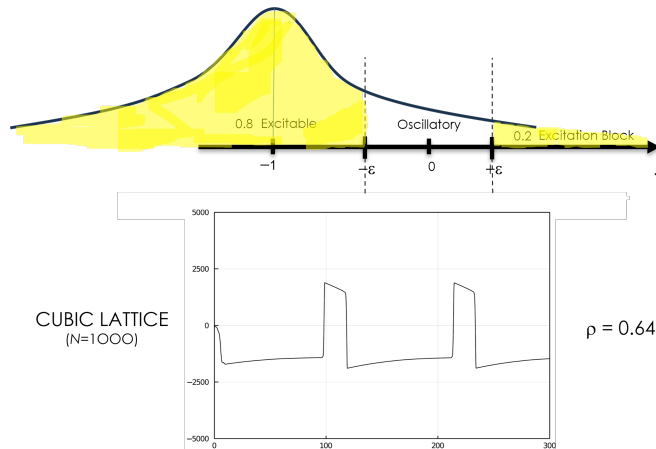


Figure 33: Truncated normal distribution with excitable units only, drawn symmetrically from  $(-\infty, -\varepsilon) \cup (+\varepsilon, +\infty)$ . The relative symmetry results in global oscillations despite the absence of oscillatory units.  $SBS = 0.26$  and  $nCOM = 24.01$ . [Reprinted from: M. Patriarca, S. Scialla, E. Heinsalu, M. E. Yamakou, and J. H. E. Cartwright, Effect of diversity distribution symmetry on global oscillations of networks of excitable units. *arXiv preprint arXiv:2507.09804* (2025). <https://doi.org/10.48550/arXiv.2507.09804> (Submitted to *Phys. Rev. E*)].

that global oscillations can occur, while in Fig. 31, a more pronounced asymmetry (99/1%) leads to their suppression. Although the  $nCOM < 1$  criterion is not satisfied in either case, the  $nCOM$  and  $SBS$  metrics correctly rank the tendency of the two distributions to support global oscillations in the order Fig. 30 > Fig. 31.

As a further example, we examine a case in which the mode of the distribution lies below the oscillatory range (Fig. 32), resulting in a highly asymmetric distribution. In this case, the network does not display global oscillations, which is consistent with the very high  $nCOM$  value and low oscillator fraction. However, a more symmetric distribution composed solely of excitable units (Fig. 33), drawn from both extremes of the Gaussian, does give rise to oscillations. The  $SBS$  values for the two distributions are consistent with simulation results. The  $nCOM$  criterion fails to predict this behavior directly, however, it still correctly ranks the symmetry of Fig. 33 as higher than that of Fig. 32, aligning with the observed dynamics. Instead, the oscillator fraction criterion is unable to explain the behavior of the distribution corresponding to Fig. 33.

Figure 29 shows a symmetric distribution of excitable units, similar to the configuration studied in Ref. [12]. Despite the absence of individually oscillatory units, the network exhibits global oscillations—consistent with its high symmetry and unlike what would be expected from the oscillator fraction criterion.

## 7.4 Two-Unit Reduction and Effective Potential

To gain insight into how collective oscillations can arise in networks where all or most units are individually excitable, we consider a minimal system of two coupled FHN units [IV, V]. While the FHN model is not a gradient system and lacks a true potential, an effective pseudo-potential can be defined for the fast variables by treating the slow variables  $y_i$  as

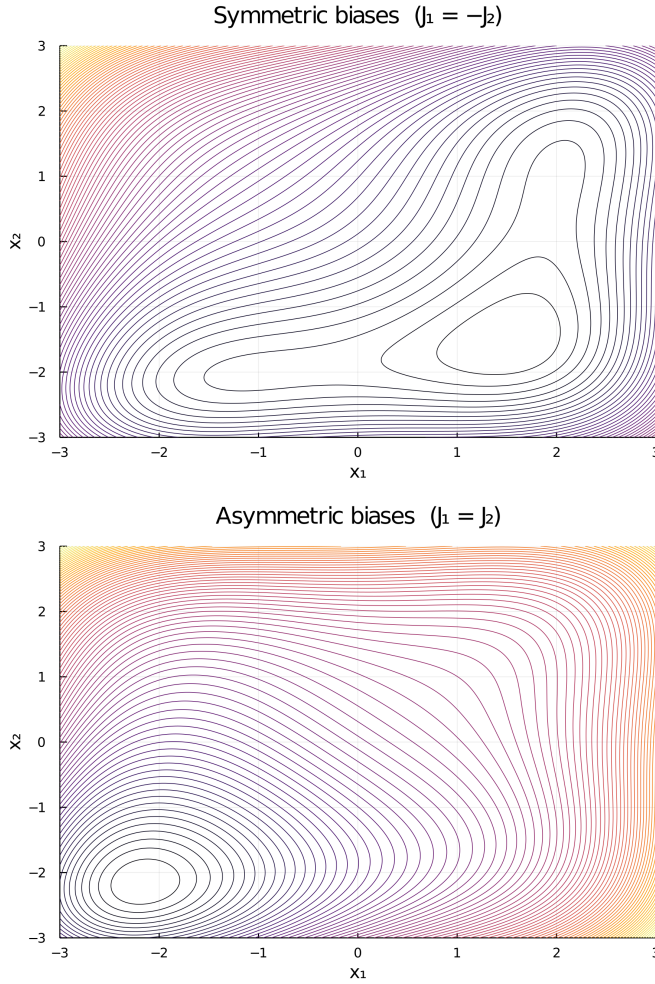


Figure 34: Contour plots of the effective pseudo-potential from Eq. (104). Top: symmetric case with  $J_1 = -1.2$ ,  $J_2 = 1.2$ . Bottom: asymmetric case with  $J_1 = J_2 = 1.2$ . Other parameters:  $C = 0.5$ ,  $\varepsilon = 1.0$ ,  $y_i = J_i$ . A cyclic valley forms only in the symmetric case. [Reprinted from: M. Patriarca, S. Scialla, E. Heinsalu, M. E. Yamakou, and J. H. E. Cartwright, Effect of diversity distribution symmetry on global oscillations of networks of excitable units. arXiv preprint arXiv:2507.09804 (2025). <https://doi.org/10.48550/arXiv.2507.09804> (Submitted to Phys. Rev. E)].

quasi-static [III]. The dynamics for the fast variables reads:

$$\dot{x}_1 = a \left[ x_1 - \frac{x_1^3}{3} + y_1 + C(x_2 - x_1) \right], \quad (102a)$$

$$\dot{x}_2 = a \left[ x_2 - \frac{x_2^3}{3} + y_2 + C(x_1 - x_2) \right], \quad (102b)$$

while the slow variables evolve as in Eq. (96b). Under the approximation  $a \gg 1$ , the associated effective pseudo-potential becomes

$$V_{\text{eff}}(x_1, x_2; y_1, y_2) = V_1(x_1; y_1) + V_2(x_2; y_2) + \frac{C}{2}(x_1 - x_2)^2, \quad (103)$$

with local terms

$$V_i(x_i; y_i) = -\frac{1}{2}x_i^2 + \frac{1}{12}x_i^4 + x_i y_i, \quad (i = 1, 2). \quad (104)$$

Here, the quadratic term promotes synchronization, while the local pseudo-potentials reflect the individual unit dynamics. For uncoupled excitable units, the system relaxes to a fixed point. However, moderate coupling deforms the landscape, possibly forming a cyclic valley that enables a collective oscillatory state.

This mechanism critically depends on symmetry: if the  $J_i$  values of the two units lie on opposite sides of the oscillatory interval center, the pseudo-potentials are tilted in opposite directions, yielding a double-well-like structure that supports a limit cycle (Fig. 34, upper panel). If the  $J_i$  values have the same sign, the landscape collapses into a single minimum (Fig. 34, lower panel), precluding oscillations.

This concept can be generalized to larger systems, by dividing the population into two subgroups based on the sign of  $J_i$  and defining average coordinates  $(x_+, y_+)$  and  $(x_-, y_-)$  for each. The dynamics of these coarse-grained variables can be approximated by a two-unit system with effective pseudo-potential

$$V_{\text{eff}}(x_+, x_-) = V_+(x_+; y_+) + V_-(x_-; y_-) + \frac{C}{2}(x_+ - x_-)^2, \quad (105)$$

where

$$V_{\pm}(x_{\pm}; y_{\pm}) = -\frac{1}{2}x_{\pm}^2 + \frac{1}{12}x_{\pm}^4 + x_{\pm}y_{\pm}. \quad (106)$$

If the subgroup averages  $J_+$  and  $J_-$  are positioned symmetrically with respect to the center of the oscillatory interval, the resulting landscape can support global oscillations, even in populations composed largely or entirely of excitable units. Instead, if both subgroups are biased in the same direction, the system stabilizes at a single minimum, and oscillations do not arise.

## 7.5 Discussion and Implications

This analysis shows that diversity-induced resonance can arise not only from an optimal level of heterogeneity but also from an optimal *structure* of the heterogeneity distribution. Symmetric diversity distributions can generate coherence in excitable media, regardless of whether individually oscillatory units are present. The nCOM and SBS metrics developed here can be used to predict the dynamical regime of a network based on its diversity distribution structure.

From a biological perspective, this mechanism may help explain how collective oscillations in cellular networks are maintained or disrupted under conditions such as disease or aging, which can introduce asymmetries in the distribution of excitability thresholds—for instance, through selective cell loss or uneven degradation of cellular function [146–149].

In conclusion, we have shown that the symmetry of the diversity distribution plays a fundamental role in determining the emergence of global oscillations in networks of excitable units. Through a combination of numerical simulations, mean-field analysis, and minimal models, we provided mechanistic insights showing that symmetric distributions robustly support collective oscillations across different topologies, whereas increasing asymmetry tends to suppress them. These findings substantially extend the current understanding of the principles governing collective dynamics in heterogeneous networks, moving beyond earlier interpretations based solely on the numerical ratio of oscillatory to excitable units. We hope this work will pave the way for future studies exploring how asymmetries in the diversity distribution influence the dynamics of biological and synthetic excitable systems.

## CONCLUSIONS

This thesis investigated the emergent dynamics of excitable cell networks, with a specific focus on how heterogeneity influences synchronization, resonance, and information propagation within systems inspired by pancreatic  $\beta$ -cell clusters. Using mathematical modeling approaches based on networks of coupled nonlinear oscillators, we examined both constructive and inhibitory roles played by diversity, alone or in conjunction with stochastic fluctuations.

The central motivation was grounded in biological observations: in pancreatic islets, collective electrical and calcium oscillations among  $\beta$ -cells are essential for coordinated insulin release and metabolic regulation. Yet, the mechanisms underlying such coordination, particularly in the presence of intercellular variability, remain only partially understood. This work contributed to addressing this gap by developing and analyzing reduced-order, yet physiologically meaningful, models capable of shedding light on how heterogeneous components can give rise to coherent macroscopic behavior.

### Summary of Main Findings

The first part of the thesis (Chapters 1–2) provided a physiological and modeling overview of excitable cells, with an emphasis on  $\beta$ -cells. The electrophysiology of action potentials, the role of membrane ion channels, and the architecture of Langerhans islets were discussed to justify the relevance of simplified mathematical models such as FHN oscillators for capturing essential aspects of  $\beta$ -cell dynamics.

In Chapter 3, we examined networks of FHN oscillators with parameter heterogeneity and showed that diversity can enhance collective synchronization through the phenomenon of DIR. This mechanism was demonstrated in fully connected and three-dimensional networks, where an optimal level of heterogeneity in the excitability parameter led to maximal amplitude and coherence of the collective response. Importantly, this effect was observed in a model specifically tuned to replicate  $\beta$ -cell dynamics, establishing a potential physiological role for heterogeneity within islets and enabling the prediction of the proportion of hub cells in agreement with experimental observations.

Chapter 4 addressed the interplay between heterogeneity and noise, contrasting two fundamentally different sources of disorder. Through a combined numerical and mean-field approach, we showed that noise and diversity can independently or synergistically enhance collective behavior, depending on the operating regime of the network. In particular, when most of the population is outside the intrinsic oscillatory range, noise and heterogeneity can act together to induce collective oscillations; however, when a high percentage of units is near or inside the oscillatory threshold, their effects become independent. These results illustrate that the two forms of disorder are not simply interchangeable but interact in a nonlinear and context-dependent manner.

Chapter 5 explored scenarios in which diversity plays an inhibitory role, contrary to the constructive function emphasized in earlier chapters and in the existing literature. Specifically, we investigated how even a minimal degree of heterogeneity can suppress the phenomenon of self-induced stochastic resonance (SISR), a form of noise-driven synchronization that emerges in excitable systems. This effect, which we named *diversity-induced decoherence* (DID), was characterized both numerically and analytically, providing a counterexample that highlights the dual nature of heterogeneity, capable of both facilitating and impairing collective behavior depending on system conditions.

In Chapter 6, we bridged the gap between the abstract DIR mechanism and a physical system by establishing a formal equivalence between diversity-induced synchronization in

oscillator networks and the resonant translocation of a polymer composed of nonlinear units through a periodic potential. This analogy, based on the concept of dimer diffusion resonance (DDR), elucidated the mechanical principles behind the DIR phenomenon and offered a broader framework in which to interpret it. The mapping to polymer dynamics suggests that DIR may be a generic feature of spatially extended systems with competing length scales and local asymmetries.

Chapter 7 extended the analysis of excitable networks by investigating the role of symmetry in the diversity distribution of excitability parameters. Using networks of FHN oscillators with various truncations of Gaussian distributions and different topologies (all-to-all, cubic lattice, and small-world), the study showed that symmetric distributions robustly support global oscillations, whereas increasing asymmetry tends to suppress them, even when a high fraction of units is individually oscillatory. Standard criteria based on the oscillator-to-non-oscillator ratio proved inadequate to explain the observed dynamics. Instead, the newly introduced symmetry metrics, nCOM and SBS, proved to be more accurate predictors of global oscillations. This suggests that the symmetry of the diversity distribution, rather than its mean or variance alone, plays a decisive role in determining whether coherence emerges or fails in heterogeneous excitable networks.

## Conceptual Contributions

The thesis offers several conceptual insights:

- Reduced-order models such as FHN oscillator networks, when properly tuned, are capable of replicating key features of  $\beta$ -cell network behavior and can be used to test hypotheses about the physiological role of cell variability.
- Heterogeneity and noise, although often lumped together as forms of disorder, act through distinct mechanisms and have different implications for network dynamics.
- Diversity is not inherently beneficial or detrimental: its impact depends on the underlying regime of excitability, coupling strength, and the presence of noise.
- DIR, a resonance mechanism that occurs in heterogeneous oscillator networks such as the ones we used to model  $\beta$ -cell clusters, can also be reproduced in mechanical analogs, highlighting its universal dynamical features.
- The degree of symmetry in the diversity distribution, rather than the fraction of oscillatory units, is a key determinant of global coherence in excitable networks, with potential implications for biological systems affected by aging or disease.

## Implications for Biological Systems

Although this work was grounded in simplified mathematical representations, the findings have implications for understanding physiological and pathophysiological processes in pancreatic islets and other excitable tissues:

- The existence of hub-like  $\beta$ -cells or functional subpopulations may be interpreted as a manifestation of optimal heterogeneity that supports synchronization.
- The degradation of gap junction coupling or increase in heterogeneity due to disease (e.g., in type 2 diabetes) could push the system from a DIR-favorable regime into one where synchronization is impaired.
- Interventions aiming to restore islet function may benefit from understanding the critical levels of diversity that optimize rather than suppress coordination.

## Outlook and Future Directions

Several future research avenues emerge from the present work:

1. **Time-Dependent Parameters:** Incorporating dynamic changes in excitability, due to metabolic feedback or plasticity mechanisms, could reveal richer forms of resonance and adaptation.
2. **Multiscale Modeling:** Bridging the current reduced-order models with more detailed biophysical representations (e.g., including ion channel kinetics or glucose metabolism) could improve physiological representativity.
3. **Heterogeneous Topologies:** Another direction for future research is to study potentially more realistic network structures, such as additional small-world or scale-free networks, reflecting the nonuniform connectivity seen in biological tissues.
4. **Symmetry Effects:** Further investigation of how symmetry in parameter distributions influences collective behavior may reveal new general organizing principles and offer novel control strategies for complex excitable systems.
5. **Control and Modulation:** Understanding how to externally modulate heterogeneity (e.g., through pharmacological means) to steer the system toward beneficial dynamical regimes represents a potential translational application.

In conclusion, this thesis has aimed to establish a coherent theoretical framework for understanding how heterogeneity—alone or in combination with noise—shapes the dynamics of excitable networks. Far from being a mere source of variability, diversity emerges as a fundamental determinant of collective behavior, capable of modulating, enhancing, or suppressing global oscillations. By drawing conceptual links between biological systems and abstract physical models, this work not only advances our understanding of  $\beta$ -cell network function and dysfunction, but also lays the groundwork for extending these insights to a broader class of complex dynamical systems.

## List of Figures

1	Schematic structure of a $\beta$ -cell .....	18
2	Typical profile of bursting oscillations in $\beta$ -cells .....	20
3	Bursting oscillations with intermediate period produced by the Phantom Bursting model .....	24
4	Example of compound bursting .....	25
5	Membrane potential and $\text{Ca}^{2+}$ ion concentration oscillations predicted by the Sherman and Rinzel model .....	27
6	Three-dimensional structures used in multicellular models of pancreatic cells .....	28
7	Residual beta-cell mass versus gap junction conductance .....	29
8	Plots of $x(t)$ (fast variable) produced by the FHN model .....	34
9	Nullclines of the FHN model .....	34
10	Examples of cubic lattice networks .....	35
11	DIR in an ensemble of heterogeneous, globally coupled bistable oscillators with periodic external forcing .....	37
12	Oscillation $x(t)$ of a single FHN element for different values of the equation parameters .....	39
13	Correspondence between $\beta$ -cell activity and FHN oscillator states .....	40
14	Global oscillatory activity $\rho$ and fraction of hubs $F_h$ as a function of popu- lation diversity $\sigma$ .....	41
15	Global oscillatory activity $\rho$ as a function of the average value $J_{av}$ of the stimulus, for different values of population diversity $\sigma$ .....	44
16	Global network oscillation $X(t)$ for different values of population diversity $\sigma$ , at the average value $J_{av} = 0.5$ of the stimulus .....	45
17	Plot of a symmetric double-well potential .....	47
18	Nullclines of mean-field FHN equations for different values of the stimulus $J_{av}$ and diversity parameter $M$ .....	53
19	Global oscillatory activity $\rho$ as a function of diversity ( $\sigma_d$ ) and noise ( $\sigma_n$ ), for $J_{av} = 0$ .....	55
20	Global oscillatory activity $\rho$ as a function of diversity ( $\sigma_d$ ) and noise ( $\sigma_n$ ), for $J_{av} = -1$ and $J_{av} = +1$ .....	56
21	Typical stochastic trajectory induced by SISR .....	63
22	Inhibition of SISR caused by different degrees of heterogeneity .....	66
23	Polymer mechanical analogs .....	71
24	Mechanical analog of a small network of four oscillators .....	74
25	Truncated half-normal diversity distribution comprising oscillatory units only	81
26	Truncated half-normal diversity distribution comprising excitable units only	81
27	Truncated half-normal diversity distribution comprising equal fractions of oscillatory and excitable units .....	82
28	Truncated half-normal diversity distribution comprising one-third oscilla- tory and two-thirds excitable units .....	82
29	Truncated normal diversity distribution comprising excitable units only .....	83
30	Truncated normal diversity distribution with a 5/95% ratio of units on the two sides of the mode .....	83
31	Truncated normal diversity distribution with a 1/99% ratio of units on the two sides of the mode .....	84
32	Truncated normal diversity distribution with excitable units drawn from $(-\infty, -\varepsilon)$ and oscillatory units from $(-\varepsilon, +\varepsilon)$ .....	84

33	Truncated normal distribution with excitable units only, drawn symmetrically from $(-\infty, -\varepsilon) \cup (+\varepsilon, +\infty)$ .....	85
34	Contour plots of the effective pseudo-potential from Eq. (104) .....	86

## List of Tables

1	Comparison of different noise-induced resonance phenomena .....	48
2	Comparison of symmetry metrics and oscillatory behavior for the nine bias distributions shown in Chapter 7 .....	80

## References

- [1] S. Scialla, A. Loppini, M. Patriarca, and E. Heinsalu, "Hubs, diversity, and synchronization in FitzHugh-Nagumo oscillator networks: Resonance effects and biophysical implications," *Phys. Rev. E*, vol. 103, p. 052211, 2021.
- [2] S. Scialla, M. Patriarca, and E. Heinsalu, "The interplay between diversity and noise in an excitable cell network model," *EPL*, vol. 137, p. 51001, 2022.
- [3] M. E. Yamakou, E. Heinsalu, M. Patriarca, and S. Scialla, "Diversity-induced decoherence," *Phys. Rev. E*, vol. 106, p. L032401, 2022.
- [4] M. Patriarca, S. Scialla, E. Heinsalu, M. E. Yamakou, and J. H. E. Cartwright, "Dynamical equivalence between resonant translocation of a polymer chain and diversity-induced resonance," *Chaos*, vol. 35, p. 073115, 2025.
- [5] S. Scialla, M. Patriarca, E. Heinsalu, M. E. Yamakou, and J. H. E. Cartwright, "Effect of diversity distribution symmetry on global oscillations of networks of excitable units," *Phys. Rev. E*, vol. 112, p. 054201, 2025.
- [6] J. P. Keener and J. Sneyd, *Mathematical Physiology*, vol. 8 of *Interdisciplinary Applied Mathematics*. Springer, 1998.
- [7] E. M. Izhikevich, *Dynamical Systems in Neuroscience: The Geometry of Excitability and Bursting*. MIT Press, 2007.
- [8] J. Rinzel and B. Ermentrout, "Analysis of neural excitability and oscillations," *Methods in Neuronal Modeling*, pp. 251–291, 1989.
- [9] R. Fitzhugh, "Thresholds and plateaus in the hodgkin-huxley nerve equations," *Journal of General Physiology*, vol. 43, pp. 867–896, may 1960.
- [10] R. FitzHugh, "Impulses and physiological states in theoretical models of nerve membrane," *Biophysical Journal*, vol. 1, pp. 445–466, jul 1961.
- [11] J. Nagumo, S. Arimoto, and S. Yoshizawa, "An active pulse transmission line simulating nerve axon," *Proceedings of the IRE*, vol. 50, pp. 2061–2070, oct 1962.
- [12] J. H. E. Cartwright, "Emergent global oscillations in heterogeneous excitable media: The example of pancreatic  $\beta$  cells," *Physical Review E*, vol. 62, pp. 1149–1154, July 2000.
- [13] C. J. Tessone, C. R. Mirasso, R. Toral, and J. D. Gunton, "Diversity-induced resonance," *Phys. Rev. Lett.*, vol. 97, p. 194101, Nov 2006.
- [14] A. S. Pikovsky and J. Kurths, "Coherence resonance in a noise-driven excitable system," *Physical Review Letters*, vol. 78, no. 5, pp. 775–778, 1997.
- [15] L. Gammaitoni, P. Hänggi, P. Jung, and F. Marchesoni, "Stochastic resonance," *Reviews of Modern Physics*, vol. 70, no. 1, pp. 223–287, 1998.
- [16] B. Lindner, J. García-Ojalvo, A. Neiman, and L. Schimansky-Geier, "Effects of noise in excitable systems," *Physics Reports*, vol. 392, no. 6, pp. 321–424, 2004.
- [17] R. Bertram, L. Satin, M. Zhang, P. Smolen, and A. Sherman, "Calcium and glycolysis mediate multiple bursting modes in pancreatic islets," *Biophysical Journal*, vol. 87, pp. 3074–3087, Nov. 2004.

- [18] G. J. Félix-Martínez and J. R. Godínez-Fernández, "Mathematical models of electrical activity of the pancreatic  $\beta$ -cell: A physiological review," *Islets*, vol. 6, p. e949195, May 2014.
- [19] R. K. P. Benninger and D. W. Piston, "Cellular communication and heterogeneity in pancreatic islet insulin secretion dynamics," *Trends in Endocrinology & Metabolism*, vol. 25, no. 8, pp. 399–406, 2014.
- [20] I. J. Stamper, E. Jackson, and X. Wang, "Phase transitions in pancreatic islet cellular networks and implications for type-1 diabetes.," *Physical review. E, Statistical, nonlinear, and soft matter physics*, vol. 89, p. 012719, Jan. 2014.
- [21] N. R. Johnston, R. K. Mitchell, E. Haythorne, M. P. Pessoa, F. Semplici, J. Ferrer, L. Piemonti, P. Marchetti, M. Bugliani, D. Bosco, E. Berishvili, P. Duncanson, M. Watkinson, J. Broichhagen, D. Trauner, G. A. Rutter, and D. J. Hodson, "Beta cell hubs dictate pancreatic islet responses to glucose," *Cell Metab.*, vol. 24, pp. 389–401, Sept. 2016.
- [22] L. Sörnmo and P. Laguna, "Chapter 1 - introduction," in *Bioelectrical Signal Processing in Cardiac and Neurological Applications* (L. Sörnmo and P. Laguna, eds.), Biomedical Engineering, pp. 1–24, Burlington: Academic Press, [nachdr.] ed., 2005.
- [23] B. Hille, *Ion Channels of Excitable Membranes*. Sinauer Associates, 3rd ed., 2001.
- [24] B. P. Bean, "The action potential in mammalian central neurons," *Nature Reviews Neuroscience*, vol. 8, pp. 451–465, 2007.
- [25] R. Bertram, L. S. Satin, M. G. Pedersen, D. S. Luciani, and A. Sherman, "Interaction of glycolysis and mitochondrial respiration in metabolic oscillations of pancreatic islets," *Biophysical Journal*, vol. 92, pp. 1544–1555, Mar. 2007.
- [26] R. K. P. Benninger and D. W. Piston, "Cellular communication and heterogeneity in pancreatic islet insulin secretion dynamics," *Trends in Endocrinology & Metabolism*, vol. 25, no. 8, pp. 399–406, 2014.
- [27] G. A. Rutter and D. J. Hodson, "Beta cell connectivity in pancreatic islets: a type 2 diabetes target?," *Cellular and Molecular Life Sciences*, vol. 77, no. 1, pp. 27–38, 2020.
- [28] M. Pérez-Armendariz, C. Roy, D. C. Spray, and M. V. Bennett, "Biophysical properties of gap junctions between freshly dispersed pairs of mouse pancreatic beta cells," *Biophysical Journal*, vol. 59, pp. 76–92, Jan. 1991.
- [29] R. Lupi, F. Dotta, L. Marselli, and et al., "Prolonged exposure to free fatty acids has cytostatic and pro-apoptotic effects on human pancreatic islets: evidence that  $\beta$ -cell death is caspase mediated, partially dependent on ceramide pathway, and bcl-2 regulated," *Diabetes*, vol. 51, no. 5, pp. 1437–1442, 2007.
- [30] M. Zhang, P. Goforth, R. Bertram, A. Sherman, and L. Satin, "The  $ca_{2+}$  dynamics of isolated mouse  $\beta$ -cells and islets: Implications for mathematical models," *Biophysical Journal*, vol. 84, pp. 2852–2870, May 2003.
- [31] S. A. Daghlas and S. S. Mohiuddin, *Biochemistry, Glycogen*. StatPearls Publishing, Treasure Island (FL), 2023.

- [32] G. J. Félix-Martínez and J. R. Godínez-Fernández, "A primer on modelling pancreatic islets: from models of coupled  $\beta$ -cells to multicellular islet models," *Islets*, vol. 15, July 2023.
- [33] E. P. Liao, B. Brass, Z. Abelev, and L. Poretsky, "Endocrine pancreas," in *Principles of Diabetes Mellitus* (L. Poretsky, ed.), pp. 43–55, Cham: Springer International Publishing, 2017.
- [34] M. Feldman, L. S. Friedman, and L. J. Brandt, *Sleisenger and Fordtran's gastrointestinal and liver disease E-book: pathophysiology, diagnosis, management*. Elsevier health sciences, 2020.
- [35] A. M. Navale and A. N. Paranjape, "Glucose transporters: physiological and pathological roles," *Biophysical Reviews*, vol. 8, pp. 5–9, Jan. 2016.
- [36] P. Detimary, S. Dejonghe, Z. Ling, D. Pipeleers, F. Schuit, and J.-C. Henquin, "The changes in adenine nucleotides measured in glucose-stimulated rodent islets occur in  $\beta$  cells but not in  $\alpha$  cells and are also observed in human islets\*," *Journal of Biological Chemistry*, vol. 273, no. 51, pp. 33905–33908, 1998.
- [37] I. R. Sweet, D. L. Cook, E. DeJulio, A. R. Wallen, G. Khalil, J. Callis, and J. Reems, "Regulation of atp/adp in pancreatic islets," *Diabetes*, vol. 53, pp. 401–409, 02 2004.
- [38] Z. Fu, E. R. Gilbert, and D. Liu, "Regulation of insulin synthesis and secretion and pancreatic beta-cell dysfunction in diabetes," *Current Diabetes Reviews*, vol. 9, pp. 25–53, Nov. 2012.
- [39] V. Serre-Beinier, D. Bosco, L. Zulianello, A. Charollais, D. Caille, E. Charpantier, B. R. Gauthier, G. R. Diaferia, B. N. Giepmans, R. Lupi, P. Marchetti, S. Deng, L. Buhler, T. Berney, V. Cirulli, and P. Meda, "Cx36 makes channels coupling human pancreatic  $\beta$ -cells, and correlates with insulin expression," *Human Molecular Genetics*, vol. 18, pp. 428–439, 11 2008.
- [40] R. K. P. Benninger, W. S. Head, M. Zhang, L. S. Satin, and D. W. Piston, "Gap junctions and other mechanisms of cell–cell communication regulate basal insulin secretion in the pancreatic islet," *The Journal of Physiology*, vol. 589, pp. 5453–5466, Nov. 2011.
- [41] B. E. Peercy and D. J. Hodson, "Insulin release: Synchronizing beta cells in the pancreas," *eLife*, vol. 13, p. e95103, jan 2024.
- [42] T. A. Wynn and K. M. Vannella, "Macrophages in tissue repair, regeneration, and fibrosis," *Immunity*, vol. 44, no. 3, pp. 450–462, 2016.
- [43] F. Ginhoux and S. Jung, "Monocytes and macrophages: developmental pathways and functional diversification," *Nature Reviews Immunology*, vol. 14, no. 6, pp. 392–404, 2014.
- [44] J. DeFelipe, "From the connectome to the synaptome: an epic love story," *Science*, vol. 330, no. 6008, pp. 1198–1201, 2010.
- [45] R. J. Zatorre, R. D. Fields, and H. Johansen-Berg, "Plasticity in gray and white: neuroimaging changes in brain structure during learning," *Nature Neuroscience*, vol. 15, no. 4, pp. 528–536, 2012.

- [46] K. B. Halpern, R. Shenhav, and E. E. Massasa, "Single-cell spatial reconstruction reveals global division of labour in the mammalian liver," *Nature*, vol. 542, pp. 352–356, 2017.
- [47] R. Gebhardt and M. Matz-Soja, "Liver zonation: novel aspects of its regulation and its impact on homeostasis," *World Journal of Gastroenterology*, vol. 20, no. 26, pp. 8491–8504, 2014.
- [48] M. Biton, A. Haber, and N. e. a. Rogel, "Tissue specialization and homeostasis achieved by the cooperative gene regulation of stem cells," *Cell*, vol. 175, no. 4, pp. 934–947.e15, 2018.
- [49] P. W. Tetteh, H. F. Farin, and H. Clevers, "Stem cell dynamics in homeostasis and injury of the intestinal epithelium," *Nature Reviews Gastroenterology & Hepatology*, vol. 12, no. 7, pp. 383–391, 2016.
- [50] R. Satija, J. A. Farrell, D. Gennert, A. F. Schier, and A. Regev, "Spatial reconstruction of single-cell gene expression data," *Nature Biotechnology*, vol. 33, no. 5, pp. 495–502, 2015.
- [51] L. Zhang, S. Zhang, and Y. e. a. Ma, "Cell-type-specific spatial transcriptome mapping reveals subpopulations in the mouse brain," *Nature Neuroscience*, vol. 24, no. 10, pp. 1484–1494, 2021.
- [52] D. G. Pipeleers, "Heterogeneity in pancreatic beta-cell population," *Diabetes*, vol. 41, no. 7, pp. 777–781, 1992.
- [53] G. Dominguez Gutierrez, J. Gromada, and L. Sussel, "Heterogeneity of the pancreatic beta cell," *Frontiers in Genetics*, vol. 8, p. 22, 2017.
- [54] D. Nasteska and D. J. Hodson, "The role of beta cell heterogeneity in islet function and insulin release," *Journal of Molecular Endocrinology*, vol. 61, no. 1, pp. R43–R60, 2018.
- [55] R. K. Benninger and D. J. Hodson, "New understanding of  $\beta$ -cell heterogeneity and in situ islet function," *Diabetes*, vol. 67, no. 4, pp. 537–547, 2018.
- [56] R. T. Scarl, K. L. Corbin, N. W. Vann, H. M. Smith, L. S. Satin, A. Sherman, and C. S. Nunemaker, "Intact pancreatic islets and dispersed beta-cells both generate intracellular calcium oscillations but differ in their responsiveness to glucose," *Cell Calcium*, vol. 83, p. 102081, 2019.
- [57] C.-L. Lei, J. A. Kellard, M. Hara, J. D. Johnson, B. Rodriguez, and L. J. Briant, "Beta-cell hubs maintain  $\text{Ca}^{2+}$  oscillations in human and mouse islet simulations," *Islets*, vol. 10, no. 4, pp. 151–167, 2018. PMID: 30142036.
- [58] B. E. Peercy and A. S. Sherman, "Do oscillations in pancreatic islets require pacemaker cells?," *Journal of Biosciences*, vol. 47, Feb. 2022.
- [59] N. Aldous, A. S. M. Moin, and E. M. Abdelalim, "Pancreatic  $\beta$ -cell heterogeneity in adult human islets and stem cell-derived islets," *Cellular and Molecular Life Sciences*, vol. 80, no. 1, p. 176, 2023.
- [60] T. R. Chay and J. Keizer, "Minimal model for membrane oscillations in the pancreatic beta-cell," *Biophysical Journal*, vol. 42, no. 2, pp. 181–189, 1983.

- [61] M. Valdeolmillos, R. M. Santos, D. Contreras, B. Soria, and L. M. Rosario, "Glucose-induced oscillations of intracellular  $Ca^{2+}$  concentration resembling bursting electrical activity in single mouse islets of langerhans," *FEBS Letters*, vol. 259, pp. 19–23, Dec. 1989.
- [62] R. M. Santos, L. M. Rosario, A. Nadal, J. Garcia-Sancho, B. Soria, and M. Valdeolmillos, "Widespread synchronous  $[Ca^{2+}]_i$  oscillations due to bursting electrical activity in single pancreatic islets," *Pflugers Archiv European Journal of Physiology*, vol. 418, pp. 417–422, May 1991.
- [63] R. Bertram, J. Previte, A. Sherman, T. A. Kinard, and L. S. Satin, "The phantom burster model for pancreatic  $\beta$ -cells," *Biophysical Journal*, vol. 79, pp. 2880–2892, Dec. 2000.
- [64] R. Bertram, A. Sherman, and L. S. Satin, "Metabolic and electrical oscillations: partners in controlling pulsatile insulin secretion," *American Journal of Physiology-Endocrinology and Metabolism*, vol. 293, pp. E890–E900, Oct. 2007.
- [65] A. Sherman and J. Rinzel, "Model for synchronization of pancreatic beta-cells by gap junction coupling," *Biophysical Journal*, vol. 59, pp. 547–559, Mar. 1991.
- [66] M. Saadati and Y. Jamali, "The effects of beta-cell mass and function, intercellular coupling, and islet synchrony on  $Ca^{2+}$  dynamics," *Scientific Reports*, vol. 11, May 2021.
- [67] D. Cebrián-Lacasa, P. Parra-Rivas, D. Ruiz-Reynés, and L. Gelens, "Six decades of the fitzhugh–nagumo model: A guide through its spatio-temporal dynamics and influence across disciplines," *Physics Reports*, vol. 1096, pp. 1–39, Dec. 2024.
- [68] E. M. Izhikevich and R. FitzHugh, "FitzHugh-Nagumo model," *Scholarpedia*, vol. 1, no. 9, p. 1349, 2006. revision #123664.
- [69] D. Pazó and E. Montbrío, "Universal behavior in populations composed of excitable and self-oscillatory elements," *Phys. Rev. E*, vol. 73, p. 055202, May 2006.
- [70] S. Chuan-Sheng, C. Han-Shuang, and Z. Ji-Qian, "Amplified signal response by neuronal diversity on complex networks," *Chinese Physics Letters*, vol. 25, p. 1591, may 2008.
- [71] S. J. Persaud, A. C. Hauge-Evans, and P. M. Jones, "Chapter 15 - Insulin-Secreting Cell Lines: Potential for Research and Diabetes Therapy," in *Cellular Endocrinology in Health and Disease* (A. Ulloa-Aguirre and P. M. Conn, eds.), pp. 239–256, Boston: Academic Press, 2014.
- [72] D. Nasteska and D. J. Hodson, "The role of beta cell heterogeneity in islet function and insulin release," *J. Mol. Endocrinol.*, vol. 61, pp. R43–R60, July 2018.
- [73] T. Aizawa, T. Kaneko, K. Yamauchi, H. Yajima, T. Nishizawa, T. Yada, H. Matsukawa, M. Nagai, S. Yamada, Y. Sato, M. Komatsu, N. Itoh, H. Hidaka, Y. Kajimoto, and K. Hashizume, "Size-related and size-unrelated functional heterogeneity among pancreatic islets," *Life Sci.*, vol. 69, pp. 2627–2639, Oct. 2001.
- [74] M. Karaca, "In vivo functional heterogeneity among  $\beta$ -cells," *Islets*, vol. 2, pp. 124–126, Mar. 2010.

- [75] M. Riz, M. Braun, and M. G. Pedersen, "Mathematical modeling of heterogeneous electrophysiological responses in human  $\beta$ -cells.," *PLoS Comput. Biol.*, vol. 10, p. e1003389, Jan. 2014.
- [76] J. Kolic and J. Johnson, "Specialized hub beta cells trade maximal insulin production for perfect timing," *Cell Metab.*, vol. 24, pp. 371–373, Sept. 2016.
- [77] M. J. Westacott, N. W. F. Ludin, and R. K. P. Benninger, "Spatially organized  $\beta$ -cell subpopulations control electrical dynamics across islets of Langerhans," *Biophys. J.*, vol. 113, pp. 1093–1108, Sept. 2017.
- [78] V. Salem, L. D. Silva, K. Suba, E. Georgiadou, S. N. M. Gharavy, N. Akhtar, A. Martin-Alonso, D. C. A. Gaboriau, S. M. Rothery, T. Stylianides, G. Carrat, T. J. Pullen, S. P. Singh, D. J. Hodson, I. Leclerc, A. M. J. Shapiro, P. Marchetti, L. J. B. Briant, W. Distaso, N. Ninov, and G. A. Rutter, "Leader  $\beta$ -cells coordinate  $\text{Ca}^{2+}$  dynamics across pancreatic islets in vivo," *Nature Metabolism*, vol. 1, pp. 615–629, June 2019.
- [79] I. J. Stamper and X. Wang, "Integrated multiscale mathematical modeling of insulin secretion reveals the role of islet network integrity for proper oscillatory glucose-dose response," *J. Theor. Biol.*, vol. 475, pp. 1–24, Aug. 2019.
- [80] R. Benzi, A. Sutera, and A. Vulpiani, "The mechanism of stochastic resonance," *Journal of Physics A: Mathematical and General*, vol. 14, no. 11, pp. L453–L457, 1981.
- [81] F. Moss, D. Pierson, and D. O’Gorman, "Stochastic resonance: Tutorial and update," *International Journal of Bifurcation and Chaos*, vol. 4, no. 6, pp. 1383–1397, 1994.
- [82] M. D. McDonnell and D. Abbott, "What is stochastic resonance? definitions, misconceptions, debates, and its relevance to biology," *PLoS Computational Biology*, vol. 5, no. 5, p. e1000348, 2009.
- [83] C. Nicolis, "Stochastic aspects of climatic transitions—responses to periodic forcing," *Tellus*, vol. 34, no. 1, pp. 1–9, 1982.
- [84] S. Fauve and F. Heslot, "Stochastic resonance in a bistable system," *Physics Letters A*, vol. 97, no. 1-2, pp. 5–7, 1983.
- [85] R. Benzi, G. Parisi, A. Sutera, and A. Vulpiani, "Stochastic resonance in climatic change," *Tellus*, vol. 34, no. 1, pp. 10–16, 1982.
- [86] H. Kramers, "Brownian motion in a field of force and the diffusion model of chemical reactions," *Physica*, vol. 7, pp. 284–304, Apr. 1940.
- [87] T. Wellens, V. Shatokhin, and A. Buchleitner, "Stochastic resonance," *Reports on Progress in Physics*, vol. 67, p. 45, dec 2003.
- [88] H. Gang, T. Ditzinger, C. Z. Ning, and H. Haken, "Stochastic resonance without external periodic force," *Physical Review Letters*, vol. 71, no. 6, pp. 807–810, 1993.
- [89] C. B. Muratov, E. Vanden-Eijnden, and W. E. "Self-induced stochastic resonance in excitable systems," *Physica D: Nonlinear Phenomena*, vol. 210, pp. 227–240, 2005.
- [90] A. S. Pikovsky and J. Kurths, "Coherence resonance in a noise-driven excitable system," *Physical Review Letters*, vol. 78, no. 5, pp. 775–778, 1997.

- [91] M. E. Yamakou and J. Jost, "A simple parameter can switch between different weak-noise-induced phenomena in a simple neuron model," *Europhysics Letters*, vol. 120, p. 18002, 2017.
- [92] P. Jung and G. Mayer-Kress, "Spatiotemporal stochastic resonance in excitable media," *Phys. Rev. Lett.*, vol. 74, pp. 2130–2133, mar 1995.
- [93] H. Busch and F. Kaiser, "Influence of spatiotemporally correlated noise on structure formation in excitable media," *Phys. Rev. E*, vol. 67, apr 2003.
- [94] F. Liu and W. Wang, "Stochastic resonance in a globally coupled neuronal network," *J. Phys. Soc. Jpn.*, vol. 68, pp. 3456–3461, oct 1999.
- [95] J. K. Douglass, L. Wilkens, E. Pantazelou, and F. Moss, "Noise enhancement of information transfer in crayfish mechanoreceptors by stochastic resonance," *Nature*, vol. 365, pp. 337–340, 1993.
- [96] A. Longtin, "Autonomous stochastic resonance in bursting neurons," *Phys. Rev. E*, vol. 55, pp. 868–876, Jan 1997.
- [97] P. Hänggi, "Stochastic resonance in biology. how noise can enhance detection of weak signals and help improve biological information processing," *ChemPhysChem*, vol. 3, no. 3, pp. 285–290, 2002.
- [98] T. Mori and S. Kai, "Noise-induced entrainment and stochastic resonance in human brain waves," *Phys. Rev. Lett.*, vol. 88, may 2002.
- [99] C. V. Rao, D. M. Wolf, and A. P. Arkin, "Control, exploitation and tolerance of intracellular noise," *Nature*, vol. 420, pp. 231–237, nov 2002.
- [100] T. R. Chay and H. S. Kang, "Role of single-channel stochastic noise on bursting clusters of pancreatic beta-cells," *Biophysical Journal*, vol. 54, no. 3, pp. 427–435, 1988.
- [101] P. Smolen, "A model for glycolytic oscillations based on skeletal muscle phosphofructokinase kinetics," *Journal of Theoretical Biology*, vol. 174, no. 2, pp. 137–148, 1995.
- [102] M. G. Pedersen, "Phantom bursting is highly sensitive to noise and unlikely to account for slow bursting in beta-cells: considerations in favor of metabolically driven oscillations," *Journal of Theoretical Biology*, vol. 248, no. 2, pp. 391–400, 2007.
- [103] R. Toral, E. Hernandez-Garcia, and J. D. Gunton, "Diversity-induced resonance in a system of globally coupled linear oscillators," *Int. J. Bifurcation Chaos*, vol. 19, p. 3499–3508, Oct. 2009.
- [104] H. Chen, Z. Hou, and H. Xin, "Threshold-diversity-induced resonance," *Physica A Statistical Mechanics and its Applications*, vol. 388, p. 2299–2305, June 2009.
- [105] L. Wu, S. Zhu, and X. Luo, "Diversity-induced resonance on weighted scale-free networks," *Chaos: An Interdisciplinary Journal of Nonlinear Science*, vol. 20, p. 033113, Sept. 2010.
- [106] L. Wu, S. Zhu, X. Luo, and D. Wu, "Effects of clustering on diversity-induced resonance in hidden metric spaces," *Phys. Rev. E*, vol. 81, p. 061118, June 2010.

- [107] M. Patriarca, S. Postnova, H. A. Braun, E. Hernández-García, and R. Toral, "Diversity and noise effects in a model of homeostatic regulation of the sleep-wake cycle," *PLoS Comput. Biol.*, vol. 8, p. e1002650, Aug. 2012.
- [108] C. J. Tessone, A. Sánchez, and F. Schweitzer, "Diversity-induced resonance in the response to social norms," *Phys. Rev. E*, vol. 87, p. 022803, Feb. 2013.
- [109] M. Patriarca, E. Hernández-García, and R. Toral, "Constructive effects of diversity in a multi-neuron model of the homeostatic regulation of the sleep-wake cycle," *Chaos, Solitons & Fractals*, vol. 81, p. 567–574, Dec. 2015.
- [110] M. Grace and M.-T. Hütt, "Pattern competition as a driver of diversity-induced resonance," *Eur. Phys. J. B*, vol. 87, p. 29, Feb. 2014.
- [111] X. Liang, X. Zhang, and L. Zhao, "Diversity-induced resonance for optimally suprathreshold signals," *Chaos: An Interdisciplinary Journal of Nonlinear Science*, vol. 30, p. 103101, Oct. 2020.
- [112] N. K. Kamal and S. Sinha, "Dynamic random links enhance diversity-induced coherence in strongly coupled neuronal systems," *Pramana – J. Phys.*, vol. 84, pp. 249–256, Jan. 2015.
- [113] E. Hunsberger, M. Scott, and C. Eliasmith, "The competing benefits of noise and heterogeneity in neural coding," *Neural Comput.*, vol. 26, p. 1600–1623, Aug. 2014.
- [114] C. J. Tessone, A. Scirè, R. Toral, and P. Colet, "Theory of collective firing induced by noise or diversity in excitable media," *Phys. Rev. E*, vol. 75, p. 016203, Jan. 2007.
- [115] C. Degli Esposti Boschi, E. Louis, and G. Ortega, "Triggering synchronized oscillations through arbitrarily weak diversity in close-to-threshold excitable media," *Phys. Rev. E*, vol. 65, p. 012901, Dec. 2001.
- [116] Y.-Y. Li, B. Jia, H.-G. Gu, and S.-C. An, "Parameter diversity induced multiple spatial coherence resonances and spiral waves in neuronal network with and without noise," *Commun. Theor. Phys.*, vol. 57, pp. 817–824, May 2012.
- [117] Y.-Y. Li and X.-L. Ding, "Multiple spatial coherence resonances and spatial patterns in a noise-driven heterogeneous neuronal network," *Commun. Theor. Phys.*, vol. 62, pp. 917–926, Dec. 2014.
- [118] M. Gassel, E. Glatt, and F. Kaiser, "Doubly diversity-induced resonance," *Phys. Rev. E*, vol. 76, p. 016203, Jul. 2007.
- [119] C. Zhou, J. Kurths, and B. Hu, "Array-enhanced coherence resonance: Nontrivial effects of heterogeneity and spatial independence of noise," *Phys. Rev. Lett.*, vol. 87, p. 098101, Aug. 2001.
- [120] E. Glatt, M. Gassel, and F. Kaiser, "Noise-induced synchronisation in heterogeneous nets of neural elements," *Europhys. Lett.*, vol. 81, p. 40004, Jan. 2008.
- [121] R. Poznanski and O. Umino, "Syncytial integration by a network of coupled bipolar cells in the retina," *Progress in Neurobiology*, vol. 53, pp. 273–291, Oct. 1997.
- [122] E. Andreu, E. Fernández, E. Louis, G. Ortega, and J. V. Sánchez-Andrés, "Role of architecture in determining passive electrical properties in gap junction-connected cells," *Eur. J. Physiol.*, vol. 439, no. 6, p. 789, 2000.

- [123] I. Vragović, E. Louis, C. Degli Esposti Boschi, and G. Ortega, “Diversity-induced synchronized oscillations in close-to-threshold excitable elements arranged on regular networks: Effects of network topology,” *Physica D: Nonlinear Phenomena*, vol. 219, no. 2, pp. 111–119, 2006.
- [124] R. C. Desai and R. Zwanzig, “Statistical mechanics of a nonlinear stochastic model,” *J. Stat. Phys.*, vol. 19, p. 1, jan 1978.
- [125] M. Uzuntarla, J. R. Cressman, M. Ozer, and E. Barreto, “Dynamical structure underlying inverse stochastic resonance and its implications,” *Phys. Rev. E*, vol. 88, p. 042712, Oct 2013.
- [126] D. Paydarfar, D. B. Forger, and J. R. Clay, “Noisy inputs and the induction of on-off switching behavior in a neuronal pacemaker,” *Journal of Neurophysiology*, vol. 96, no. 6, pp. 3338–3348, 2006. PMID: 16956993.
- [127] B. S. Gutkin, J. Jost, and H. C. Tuckwell, “Inhibition of rhythmic neural spiking by noise: the occurrence of a minimum in activity with increasing noise,” *Naturwissenschaften*, vol. 96, pp. 1091–1097, Sept. 2009.
- [128] H. C. Tuckwell, J. Jost, and B. S. Gutkin, “Inhibition and modulation of rhythmic neuronal spiking by noise,” *Phys. Rev. E*, vol. 80, p. 031907, Sep 2009.
- [129] M. E. Yamakou, J. Zhu, and E. A. Martens, “Inverse stochastic resonance in adaptive small-world neural networks,” *Chaos: An Interdisciplinary Journal of Nonlinear Science*, vol. 34, p. 113119, 11 2024.
- [130] M. E. Yamakou and J. Jost, “Control of coherence resonance by self-induced stochastic resonance in a multiplex neural network,” *Phys. Rev. E*, vol. 100, p. 022313, Aug 2019.
- [131] R. E. L. DeVille and E. Vanden-Eijnden, “Self-induced stochastic resonance for brownian ratchets under load,” *Communications in Mathematical Sciences*, vol. 5, no. 2, pp. 431–446, 2007.
- [132] M. E. Yamakou and J. Jost, “Coherent neural oscillations induced by weak synaptic noise,” *Nonlinear Dynamics*, vol. 93, no. 4, pp. 2121–2144, 2018.
- [133] M. E. Yamakou, P. G. Hjorth, and E. A. Martens, “Optimal self-induced stochastic resonance in multiplex neural networks: Electrical vs. chemical synapses,” *Frontiers in Computational Neuroscience*, vol. 14, p. 62, 2020.
- [134] C. Kuehn, *Multiple Time Scale Dynamics*, vol. 191 of *Applied Mathematical Sciences*. Springer, 2015.
- [135] N. Fenichel, “Geometric singular perturbation theory for ordinary differential equations,” *Journal of Differential Equations*, vol. 31, pp. 53–98, 1979.
- [136] M. FREIDLIN, “On stochastic perturbations of dynamical systems with fast and slow components,” *Stochastics and Dynamics*, vol. 01, no. 02, pp. 261–281, 2001.
- [137] N. J. Kasdin, “Runge-kutta algorithm for the numerical integration of stochastic differential equations,” *Journal of Guidance, Control, and Dynamics*, vol. 18, no. 1, pp. 114–120, 1995.

- [138] D. E. Knuth, "The art of computer programming, vol. 2, addison-wesley," *Reading, MA*, p. 51, 1973.
- [139] M. Masoliver, N. Malik, E. Schöll, and A. Zakharova, "Coherence resonance in a network of fitzhugh-nagumo systems: Interplay of noise, time-delay, and topology," *Chaos: An Interdisciplinary Journal of Nonlinear Science*, vol. 27, p. 101102, 10 2017.
- [140] T. Shibata and K. Kaneko, "Heterogeneity-induced order in globally coupled chaotic systems," *EPL (Europhysics Letters)*, vol. 38, no. 6, p. 417, 1997.
- [141] D. M. Vogt Weisenhorn, F. Giesert, and W. Wurst, "Diversity matters – heterogeneity of dopaminergic neurons in the ventral mesencephalon and its relation to parkinson's disease," *Journal of Neurochemistry*, vol. 139, no. S1, pp. 8–26, 2016.
- [142] E. Heinsalu, M. Patriarca, and F. Marchesoni, "Dimer diffusion in a washboard potential," *Phys. Rev. E*, vol. 77, p. 021129, 2008.
- [143] E. Heinsalu, M. Patriarca, and F. Marchesoni, "Stochastic resonance in a surface dipole," *Chem. Phys.*, vol. 375, no. 2, pp. 410–415, 2010.
- [144] M. Patriarca, P. Szelestey, and E. Heinsalu, "Brownian model of dissociated dislocations," *Acta Phys. Pol. B*, vol. 36, p. 1745, 2005.
- [145] M. Newman and D. Watts, "Renormalization group analysis of the small-world network model," *Phys. Lett. A*, vol. 263, no. 4, pp. 341–346, 1999.
- [146] D. M. Vogt Weisenhorn, F. Giesert, and W. Wurst, "Diversity matters–heterogeneity of dopaminergic neurons in the ventral mesencephalon and its relation to parkinson's disease," *J. Neurochem.*, vol. 139, pp. 8–26, 2016.
- [147] S. Efrat, "Beta-cell dedifferentiation in type 2 diabetes: Concise review," *Stem Cells*, vol. 37, no. 10, pp. 1267–1272, 2019.
- [148] F. Leenders, E. J. P. de Koning, and F. Carlotti, "Pancreatic  $\beta$ -cell identity change through the lens of single-cell omics research," *Int. J. Mol. Sci.*, vol. 25, no. 9, p. 4720, 2024.
- [149] J. U. Wagner and S. Dimmeler, "Cellular cross-talks in the diseased and aging heart," *J. Mol. Cell. Cardiol.*, vol. 138, pp. 136–146, 2020.
- [150] M. V. Tamm, E. Heinsalu, S. Scialla, and M. Patriarca, "Learning thresholds lead to stable language coexistence," *Phys. Rev. E*, vol. 111, no. 2, p. 024304, 2025.
- [151] L. Marcotullio, P. Gröb, S. Scialla, and P. Saveyn, "Understanding perfume deposition mechanisms on different textile substrates in a realistic laundering process," *Journal of Surfactants and Detergents*, vol. 28, no. 4, pp. 731–745, 2025.
- [152] X. Han, S. Scialla, E. Limiti, E. T. Davis, M. Trombetta, A. Rainer, S. W. Jones, E. Mauri, and Z. J. Zhang, "Nanosopic gel particle for intra-articular injection formulation," *Biomaterials Advances*, vol. 163, p. 213956, 2024.
- [153] S. Scialla, J. K. Liivand, M. Patriarca, and E. Heinsalu, "A three-state language competition model including language learning and attrition," *Frontiers in Complex Systems*, vol. 1, 2023.

- [154] E. Mauri and S. Scialla, "Nanogels based on hyaluronic acid as potential active carriers for dermatological and cosmetic applications," *Cosmetics*, vol. 10, no. 4, p. 113, 2023.
- [155] S. M. Giannitelli, E. Limiti, P. Mozetic, F. Pinelli, X. Han, F. Abbruzzese, F. Basoli, D. D. Rio, S. Scialla, F. Rossi, M. Trombetta, L. Rosanò, G. Gigli, Z. J. Zhang, E. Mauri, and A. Rainer, "Droplet-based microfluidic synthesis of nanogels for controlled drug delivery: tailoring nanomaterial properties via pneumatically actuated flow-focusing junction," *Nanoscale*, vol. 14, no. 31, pp. 11415–11428, 2022.
- [156] E. Limiti, P. Mozetic, S. M. Giannitelli, F. Pinelli, X. Han, D. D. Rio, F. Abbruzzese, F. Basoli, L. Rosanò, S. Scialla, M. Trombetta, G. Gigli, Z. J. Zhang, E. Mauri, and A. Rainer, "Hyaluronic acid–polyethyleneimine nanogels for controlled drug delivery in cancer treatment," *ACS Applied Nano Materials*, vol. 5, no. 4, pp. 5544–5557, 2022.
- [157] K. A. Berrington, V. M. Burke, P. G. Burke, and S. Scialla, "Electron impact excitation of  $n=3$  states of C III: an application of a new R-matrix package," *Journal of Physics B: Atomic, Molecular and Optical Physics*, vol. 22, no. 4, pp. 665–676, 1989.
- [158] F. A. Gianturco, L. C. Pantano, and S. Scialla, "Low-energy structure in electron-silane scattering," *Phys. Rev. A*, vol. 36, no. 2, pp. 557–563, 1987.
- [159] F. A. Gianturco and S. Scialla, "Low-energy electron scattering from water molecules: A study of angular distributions," *The Journal of Chemical Physics*, vol. 87, no. 11, pp. 6468–6473, 1987.
- [160] F. A. Gianturco and S. Scialla, "Local approximations of exchange interaction in electron-molecule collisions: the methane molecule," *Journal of Physics B: Atomic and Molecular Physics*, vol. 20, no. 13, pp. 3171–3189, 1987.
- [161] P. Morganti and S. Scialla, "Nanoparticles, nanofibrils, and tissues as novel carriers in cosmetic dermatology," in *Soft Particles*, pp. 257–287, Elsevier, 2023.
- [162] S. Scialla and O. Todini, "Liquid bleach formulations," in *Handbook of Detergents, Part D*, pp. 179–206, CRC Press, 2005.
- [163] S. Scialla, "The formulation of liquid household cleaners," in *Handbook of Detergents, Part D*, pp. 153–177, CRC Press, 2005.
- [164] F. A. Gianturco and S. Scialla, "A parameter-free theoretical model for low-energy electron scattering from polyatomic molecules," in *Nonequilibrium Processes in Partially Ionized Gases*, pp. 323–332, Springer US, 1990.
- [165] F. A. Gianturco and S. Scialla, "Electron scattering by polyatomic molecules: Recent advances in theory and calculations," in *Electron-Molecule Scattering and Photoionization*, pp. 169–186, Springer US, 1988.

## Acknowledgements

First and foremost, I would like to express my deepest gratitude to my wife for her unwavering support and patience throughout the long journey that led to this thesis. Her understanding during the countless hours I spent engaged in research and writing has been a source of strength and reassurance. Without her encouragement and quiet endurance, this work would not have been possible.

I am profoundly thankful to my PhD supervisors and lifelong friends, Dr. Marco Patriarca and Dr. Els Heinsalu, for their invaluable guidance, insightful feedback, and continuous encouragement. Their willingness to support and mentor me as I embarked on a PhD program at this stage in life — beyond the age of 60 — was both very generous and inspiring. Their confidence in my ability to contribute meaningfully to the scientific community has been a major motivation throughout this endeavor.

Importantly, this journey was enabled by the Open University program at Tallinn University of Technology and the research activities carried out at the National Institute of Chemical Physics and Biophysics. I also gratefully acknowledge the financial support provided by the Estonian Research Council through grant PRG1059.

Finally, to all those who have supported me directly or indirectly — colleagues, friends, and family — thank you. Your encouragement and belief in the value of lifelong learning have helped make this remarkable achievement possible.

## Abstract

# The Role of Heterogeneity in the Dynamics of Excitable Cell Networks

Excitable cells such as neurons, cardiomyocytes, and pancreatic  $\beta$ -cells exhibit dynamic behaviors that are fundamental to biological function, including signal transmission, muscle contraction, and hormone secretion. In the case of pancreatic  $\beta$ -cells, electrical and calcium oscillations across cellular networks regulate insulin release and thus play a crucial role in glucose homeostasis. Recent studies have highlighted that the functional performance of such networks is critically shaped by the presence of intrinsic heterogeneity. This thesis investigates the interplay of heterogeneity, coupling topology, and stochastic fluctuations in excitable cell networks, with an emphasis on identifying conditions under which these factors either promote or suppress collective behavior such as synchronization and resonance.

A primary goal of the thesis is to gain a better understanding of the influence of heterogeneity on the collective behavior of excitable cell networks, focusing on pancreatic  $\beta$ -cell clusters as a representative biological example. While individual  $\beta$ -cells often exhibit irregular or absent oscillatory activity, their synchronization within clusters enables robust and pulsatile insulin secretion. However, the mechanisms by which heterogeneity among cells contributes to or detracts from this coordinated behavior remain not fully understood. Notably, while a multitude of previous studies have shown that stochastic noise can enhance responsiveness in nonlinear systems (e.g., stochastic resonance), the concept that *diversity* among network elements may similarly play a constructive dynamical role, referred to as *diversity-induced resonance* (DIR), is comparatively recent and less studied.

This thesis addresses the open questions: a) Under what conditions does cellular heterogeneity enhance or suppress collective oscillations in excitable networks, and how does its influence compare with or complement that of intrinsic noise? b) What are the underlying dynamical mechanisms? c) What is the biological relevance of these effects, particularly for  $\beta$ -cell networks?

To address these questions, the thesis develops and analyzes a series of mathematical models. The FitzHugh–Nagumo (FHN) oscillator is employed as a prototypical model of excitable cell dynamics, due to its balance between simplicity and ability to reproduce fundamental features of action potentials. Networks of diffusively coupled FHN units are constructed to mimic  $\beta$ -cell clusters and investigated under different regimes of parameter heterogeneity and noise intensity.

The methodology combines numerical simulations with analytical techniques such as bifurcation analysis and mean-field approximations. Heterogeneity is introduced either as a discrete bimodal distribution or as a continuous (e.g., Gaussian) distribution of excitability parameters. Noise is modeled as additive stochastic perturbations. The response of the system is quantified via synchronization measures, oscillation amplitude, coherence, and response curves.

The thesis yields several novel insights:

- **Modeling  $\beta$ -Cell Network Dynamics with FHN Oscillators:** A Langerhans islet model based on a 3D network of heterogeneous FHN oscillators with parameter heterogeneity exhibits a resonance-like peak in collective oscillatory activity, analogous to stochastic resonance. Thanks to the choice of model parameters, which are representative of  $\beta$ -cell electrical activity in a realistic cluster, it illustrates how physiological diversity among  $\beta$ -cells can enhance synchronized bursts resulting in more

efficient insulin secretion.

- **Hubs and Network Structure:** The above model also suggests that the presence in Langerhans islets of a specific subset of highly active  $\beta$ -cells (hub cells) can be regarded as an emergent property of the network. The percentage of such hubs corresponding to the DIR peak (estimated by the model) aligns with recent experimental findings.
- **Interplay Between Noise and Diversity:** The combination of noise and heterogeneity leads to regimes of both synergy and competition. When most of the network population is outside the intrinsic oscillatory range, noise and diversity tend to cooperate, enhancing synchronization. Instead, when a high percentage of units is near the oscillatory threshold, diversity and noise influence synchronization independently, and no synergistic interaction is observed. In contrast to previous studies, this highlights that heterogeneity and noise represent fundamentally distinct sources of disorder which, although capable of producing analogous effects under certain conditions, generally influence the dynamics of complex systems in different ways.
- **Inhibitory Role of Diversity:** While it is known from previous studies that diversity is capable of enhancing global network oscillations and amplifying signals, this thesis identifies a specific regime in which small levels of diversity are shown, for the first time, to *suppress* synchronization, inhibiting self-induced stochastic resonance (SISR). This result illustrates that heterogeneity can also have a destabilizing effect, depending on the dynamical regime.
- **Mechanical Analogy with Polymer Translocation:** A dynamical equivalence is demonstrated between DIR in oscillator networks and the resonant translocation of a polymer across a periodic potential. This analogy offers mechanistic insight into the underlying physical principles of DIR and supports its interpretation as a generalizable phenomenon.
- **Symmetry of Diversity Distribution:** The degree of symmetry in the diversity distribution—rather than the mere fraction of intrinsically oscillatory units—is a key determinant of global coherence in excitable networks. Networks with symmetric or moderately asymmetric distributions exhibit robust synchronization, while strongly asymmetric ones fail to sustain collective oscillations, even when a significant fraction of units is oscillatory. This suggests that structural features of variability, such as distributional symmetry, play a central role in shaping emergent dynamics and may be critical for understanding dysfunction in biological systems affected by aging or disease.

In conclusion, this work advances the understanding of how heterogeneity shapes collective dynamics in excitable cell networks, particularly in biologically relevant systems such as pancreatic  $\beta$ -cell clusters. While diversity is often viewed as a mere source of disorder, the results presented here demonstrate its dual role as both a potential enhancer and inhibitor of coordinated activity, depending on system parameters. Furthermore, the development of an abstract polymer model reinforces the universality of the DIR mechanism across different physical systems.

By bridging simplified dynamical models with biological phenomena, the thesis offers a theoretical foundation that complements experimental efforts in  $\beta$ -cell physiology. These

insights may ultimately inform the design of therapeutic strategies in type 2 diabetes, where restoring or preserving functional  $\beta$ -cell heterogeneity could improve Langerhans islet performance.

## Kokkuvõte

### Heterogeensuse roll ergastatavate rakuvõrgustike dünaamikas

Ergastatavad rakud, nagu neuronid, kardiomüotsüüdid ja pankrease  $\beta$ -rakud, omavad dünaamilist käitumist, mis on fundamentaalne erinevate bioloogiliste protsesside toimimiseks; näiteks signaaliülekanne, lihaskontraktsioon ja hormoonide sekretsioon. Pankrease  $\beta$ -rakkude puhul reguleerivad rakuvõrgustikes aset leidvad elektrilised ja kaltsiumi taseme ostsillatsioonid insuliini vabanemist ning omavad seega kesket rolli glükoosi homöostaasis. Hiljutised uuringud on näidanud, et säärase võrgustike funktsionaalne toimimine on oluliselt seotud nende heterogeensusega. Käesolev väitekirj uurib heterogeensuse, interaktsiooni ja stohhastiliste fluktuatsioonide vastastikmõjusid ergastatavates rakuvõrgustikes, eesmärgiga teha kindlaks, milliste tingimuste korral toimub kollektiivse käitumise, nagu näiteks süsteemis ilmneva sünkronisatsiooni või resonantsi, soodustamine või pärssimine.

Väitekirja üheks peamiseks eesmärgiks on, keskendudes pankrease  $\beta$ -rakkude klastrite näitele, paremini mõista, kuidas heterogeensus mõjutab ergastatavates rakuvõrgustikes ilmnevat kollektiivset dünaamikat. Kuigi  $\beta$ -rakud üksikult ostsilleerivad enamasti kas ebaregulaarset või üldse mitte, siis klastrites toimub nende sünkronisatsioon, mis tagab tõhusa ja pulseeruva insuliini sekretsiooni. Kuidas rakkude heterogeensus seda koordineeritud käitumist soodustab või takistab, pole kaugeltki veel selge. Mitmed varasemad uuringud on näidanud, et stohhastiline müra võib tugevdada mittelineaarsete süsteemide tundlikkust (nt stohhastiline resonants), kuid hiljuti on näidatud ning hakatud suuremat tähelepanu pöörama sellele, et ka võrgustiku elementide *mitmekesisus* võib omada konstruktiivset dünaamilist rolli; seda nähtust nimetatakse *mitmekesisuse poolt indutseeritud resonantsiks* (MIR).

Väitekirj käsitleb järgmisi küsimusi: a) Millistel tingimustel tugevdab või pärsib rakkude heterogeensus kollektiivseid ostsillatsioone ergastatavates võrgustikes ning milline on säärane heterogeensuse mõju võrreldes süsteemi sisemise müraga? b) Millised on aset leidvate nähtuste aluseks olevad dünaamilised mehhanismid? c) Milline on nende nähtuste olulisus bioloogiliste süsteemide, eeskätt  $\beta$ -rakkude võrgustike, jaoks?

Nende küsimuste uurimiseks pakutakse väitekirjas välja ja analüüsitakse mitmeid matemaatilisi mudeleid. Ergastatavate rakkude dünaamika prototüüpilise mudelina on kasutatud FitzHugh-Nagumo (FHN) ostsillaatorit, kuna see on ühtaegu lihtne, kuid võimaldab samas siiski reprodutseerida aktsioonipotentsiaalide põhiomadusi. Kirjeldamiseks  $\beta$ -rakkude klastreid, on konstrueeritud difuusselt seotud FHN-ostsillaatorite võrgustikud, mille käitumist on uuritud erinevate heterogeensuse ning müra intensiivsuse režiimides.

Uurimistöö käigus on kasutatud erinevaid numbrilisi ja analüütilisi meetodeid, nagu bifurkatsiooni analüüs ja keskmise välja lähendus. Heterogeensus on toodud sisse sisse kas parameetrite diskreetse bimodaalse jaotuse või pideva (nt Gaussi) jaotuse kaudu. Müra on modelleeritud additiivsete stohhastiliste perturbatsioonidena. Süsteemi reageeringut on mõõdetud sünkronisatsiooni iseloomustavate suuruste, ostsillatsioonide amplituudi, koherentsuse ja vastus kõverate abil.

Töö käigus on jõutud mitmete uute teadmiseni:

- **$\beta$ -rakkude võrgustike dünaamika modelleerimine FHN-ostsillaatorite abil:** Langerhansi saare mudel, mille aluseks on 3D võrgustik, mis koosneb heterogeensetest FHN-ostsillaatoritest, näitab, et kollektiivsete ostsillatsioonide aktiivsus omab resonantsile omast maksimumi. Tänu mudelis kasutatavatele parameetrite realistlikele väärtustele, mis vastavad  $\beta$ -rakkude elektrilisele aktiivsusele reaalses klastrites, demonstreerib see tulemus, kuidas  $\beta$ -rakkude füsioloogiline mitmekesisus võib või-

mendada sünkroniseeritud käitumist ja parandada insuliini sekretsiooni tõhusust.

- **Sõlmpunktid ja võrgustiku struktuur:** Ülalkirjeldatud mudel viitab, et Langerhansi saartes leidub kindel hulk väga aktiivseid  $\beta$ -rakke (sõlmrakke), mida võib pidada võrgustikule iseloomulikuks omaduseks. Selliste rakkude mudeli poolt hinnatud osakaal, mis vastab MIR maksimumile, on heas kooskõlas ka hiljutiste eksperimentaalsete tulemustega.
- **Müra ja mitmekesisuse vastasmõju:** Müra ja heterogeensuse koostoime tulemuseks võib olla nii sünergia kui ka konkurents. Kui suurem osa võrgustiku elementidest on väljaspool sisemiste ostsillatsioonide režiimi, toimivad müra ja mitmekesisus üksteist toetavalt ja suurendavad sünkronisatsiooni. Kui suur osa elementidest on aga ostsillatsioonide ilmnemise piiril, mõjutavad müra ja mitmekesisus sünkronisatsiooni eraldi ning sünergia puudub. See viib uudsele ja veidi ootamatule järeltulele, et heterogeensus ja müra on oma olemuselt fundamentaalselt erinevad korrapärase allikad, mis võivad teatud tingimuste juures viia sarnaste efektide ilmnemisele, kuid mis üldiselt mõjutavad kompleksete süsteemide dünaamikat erinevalt.
- **Mitmekesisuse pärssiv mõju:** Varasematest uuringutest on teada, et mitmekesisus võib võimendada signaale ja võrgustikus aset leidvaid globaalseid võnkumisi. Käesolev väitekirjeldus näitab, et teatud režiimides võib väike mitmekesisus sünkronisatsiooni hoopis pärssida ja takistada iseenesliku stohhastilise resonantsi (ISR) tekkimist. See-ga võib heterogeensus, sõltuvalt dünaamilisest režiimist, omada ja destabiliseerivat mõju.
- **Mehaaniline analoogia polümeeri translokatsiooniga:** On näidatud, et ostsillaatorite võrgustikus ilmnev MIR ja polümeeri resonantne translokatsioon perioodilisel potentsiaalil on dünaamiliselt ekvivalentsed. See analoogia aitab mõista MIR-i aluseks olevaid füüsikalisi mehhanisme ja üldist ilmingut.
- **Mitmekesisuse jaotuse sümmeetria:** Ergastatavates võrgustikes ilmnev globaalne koherentsus on määratud mitmekesisuse jaotuse sümmeetria poolt, mitte iseeneslikult ostsillatsioonide ühikute osakaalu poolt. Võrgustikes, kus mitmekesisuse jaotus on sümmeetriline või veidi asümmeetriline, leiab aset tugev sünkronisatsioon, samas kui tugev asümmeetria pärssib kollektiivseid võnkumisi, isegi kui suur osa üksustest on ostsillatavas olekus. See viitab, et varieeruvuse struktuursed omadused, nagu näiteks parameetrite jaotuse sümmeetria, omavad olulist rolli süsteemi dünaamika jaoks ja võivad olla määrava tähtsusega bioloogiliste süsteemide talitlushäirete mõistmiseks, näiteks vananemise või haiguste korral.

Kokkuvõttes aitab käesolev töö paremini mõista, kuidas heterogeensus mõjutab kollektiivset dünaamikat ergastatavates rakuvõrgustikes, eriti bioloogiliselt olulistest süsteemides, nagu pankrease  $\beta$ -rakkude klastrid. Kuigi mitmekesisust peetakse sageli pelgalt korrapärase allikaks, näitavad käesolevas väitekirjas esitatud tulemused, et sõltuvalt süsteemi parameetritest, võib mitmekesisus koordineeritud toimimist nii soodustada kui ka pärssida. Lisaks toetab abstraktne polümeeri mudel MIR-mehhanismi üldistatavust erinevate füüsikaliste süsteemide jaoks.

Ühendades endas lihtsustatud dünaamilisi mudeleid ja bioloogilisi nähtusi, pakub väitekirjeldus teoreetilist alust, mis täiendab  $\beta$ -rakkude füsioloogia eksperimentaalset uurimist. Saadud teadmised võivad aidata kaasa töötamiseks välja 2. tüüpi diabeedi ravi strateegiaid, eesmärgiga taastada või säilitada  $\beta$ -rakkude funktsiooni.

## Appendix 1

### I

S. Scialla, A. Loppini, M. Patriarca, and E. Heinsalu, "Hubs, diversity, and synchronization in FitzHugh-Nagumo oscillator networks: Resonance effects and biophysical implications," *Phys. Rev. E*, vol. 103, p. 052211, 2021



## Hubs, diversity, and synchronization in FitzHugh-Nagumo oscillator networks: Resonance effects and biophysical implications

Stefano Scialla<sup>⊗\*</sup> and Alessandro Loppini<sup>†</sup>

*Department of Engineering, Università Campus Bio-Medico di Roma, Via Á. del Portillo 21, 00128 Rome, Italy*

Marco Patriarca<sup>⊗‡</sup> and Els Heinsalu<sup>§</sup>

*National Institute of Chemical Physics and Biophysics, Rāvala 10, Tallinn 15042, Estonia*



(Received 25 January 2021; accepted 3 May 2021; published 17 May 2021)

Using the FitzHugh-Nagumo equations to represent the oscillatory electrical behavior of  $\beta$ -cells, we develop a coupled oscillator network model with cubic lattice topology, showing that the emergence of pacemakers or hubs in the system can be viewed as a natural consequence of oscillator population diversity. The optimal hub to nonhub ratio is determined by the position of the diversity-induced resonance maximum for a given set of FitzHugh-Nagumo equation parameters and is predicted by the model to be in a range that is fully consistent with experimental observations. The model also suggests that hubs in a  $\beta$ -cell network should have the ability to “switch on” and “off” their pacemaker function. As a consequence, their relative amount in the population can vary in order to ensure an optimal oscillatory performance of the network in response to environmental changes, such as variations of an external stimulus.

DOI: [10.1103/PhysRevE.103.052211](https://doi.org/10.1103/PhysRevE.103.052211)

### I. INTRODUCTION

Pancreatic  $\beta$ -cells in Langerhans islets are characterized by a remarkable coordination of their periodic electrochemical activity, which is linked to their ability to secrete insulin in a pulsatile manner [1–4]. Pulsatile release is thought to be essential for the efficacy of insulin on its target organs and is disrupted in type 2 diabetes [5–8]. This justifies the vast amount of literature aimed at understanding the mechanism of  $\beta$ -cell electrical oscillations and their synchronization in Langerhans islets, both from the standpoint of cell biology and in terms of biophysical models describing  $\beta$ -cell clusters as networks of coupled oscillators [9–22].

In recent years an increasing number of studies have focused on elucidating the behavior and function of pacemaker cells, also named “hubs” or “leaders,” i.e., subpopulations of  $\beta$ -cells showing higher oscillatory activity [17,23–28]. Due to their ability to respond earlier to changes in glucose concentration in the blood stream, hubs would play a crucial role in determining the dynamics of electrical activity of  $\beta$ -cell clusters, by initiating and synchronizing coordinated electrical oscillations across an islet. While the presence of pacemaker cells in Langerhans islets has been hypothesized several times [29–34], the confirmation of their existence via direct observation has become feasible only in recent years, by leveraging new imaging techniques based on optogenetics and recombinant fluorescent probes [23–26].

In spite of this exciting progress and improved understanding, some key questions remain unanswered, specifically: (a) Are hubs a permanently distinct subpopulation of  $\beta$ -cells, or can different  $\beta$ -cell subsets turn into hubs or nonhubs as a function of time and external factors, such as glucose concentration? and (b) What are the mechanisms that drive the overall frequency of bursting events, i.e., the global oscillatory behavior of an islet as a whole? While we do not aim to find a definitive solution to these problems, we will show that studying the fundamental dynamical properties of a 3D system of coupled oscillators, mimicking some key features of the electrical behavior of  $\beta$ -cells, can provide useful insights to understand the collective cell network behavior and to guide future research.

Individual  $\beta$ -cells that have been isolated from an islet exhibit a heterogeneous electrical activity, ranging from a quiescent state, where their membrane potential stays constantly polarized, to continuous spiking (repeated action potential firings) or bursting events that occur irregularly as a function of time (discrete groups of repeated firings, followed by a period of quiescence) [35–37]. In contrast, when the same cells are part of an islet, they show strikingly coordinated and regular bursting oscillations, characterized by a period typically ranging from 2 to 5 minutes [38,39]. Such membrane potential oscillations are coherent with cytosolic  $\text{Ca}^{2+}$  ion level fluctuations and correspond to a pulsatile insulin secretion from  $\beta$ -cells, which is so important for glucose homeostasis and progressively gets lost in type 2 diabetes [7,40–42].

From a dynamical standpoint, bursting activity can be conceived as periodic oscillations of an excitable dynamical system, triggered by an external force that is strong enough to overcome the excitability threshold. In the case of  $\beta$ -cell islets, this force originates from a series of metabolic

\*stefano.scialla@unicampus.it

†a.loppini@unicampus.it

‡marco.patriarca@kbfi.ee

§els.heinsalu@kbfi.ee

processes triggered by glucose in the blood stream, therefore it is a function of glucose concentration.

Because of the above mentioned heterogeneity,  $\beta$ -cells have been a source of inspiration for modeling studies about the effects of diversity on the synchronization of oscillator networks [43,44], which has then become a key research topic in complex systems dynamics. Numerous studies have documented the emergence of resonance effects, i.e., the amplification of global network oscillations due to diversity, for both bistable and excitable oscillator networks [45–54]. This effect has been named diversity-induced resonance [45] and constitutes an important phenomenon in the context of the present work, where it will be studied by choosing network configurations, topology, and coupling relevant to realistic  $\beta$ -cell clusters.

Indeed, previous studies about diversity-induced resonance focused on  $\beta$ -cells have not considered the role of pacemakers or hubs, also due to the fact that their existence in Langerhans islets has been confirmed only relatively recently. The goal of the present work is to investigate whether the existence and key biophysical properties of hubs can be predicted from the general dynamical properties of a network of coupled oscillators mimicking  $\beta$ -cell electrical behavior.

The paper is organized as follows. In Sec. II A we summarize the FitzHugh-Nagumo model. In Sec. II B we build a coupled oscillator network model that incorporates heterogeneity and cubic lattice topology. In Sec. III A we define a metric for estimating the global network oscillation activity and show the emergence of diversity-induced resonance from our model, upon varying oscillator population heterogeneity. In Sec. III B we demonstrate that the presence of pacemakers or hubs in the network can be viewed as a natural consequence of oscillator diversity optimization. We also use the model to estimate the percentage of hubs in a network with topological and oscillatory features similar to those of  $\beta$ -cell clusters in Langerhans islets. In Sec. III C we show that, with respect to the homogeneous system, diversity allows the network to exhibit a more efficient oscillatory response to a range of external stimulus values. Finally, in Sec. IV we discuss the relevance of our results to the understanding of the collective behavior of  $\beta$ -cells in Langerhans islets, as well as potential correlations with physiological mechanisms underlying pathological conditions, such as type 2 diabetes. We also provide perspective on future extensions of this work, such as its comparison to biophysical models and possible applications to other biological systems.

## II. MODEL

### A. FitzHugh-Nagumo model

Since our aim is to focus mainly on trends and understanding fundamental mechanisms, we will describe individual oscillators by the FitzHugh-Nagumo model, defined by the following dimensionless equations [44,55–57]:

$$\dot{x} = a(x - x^3/3 + y), \quad (1a)$$

$$\dot{y} = -(x + by - J)/a. \quad (1b)$$

Here  $x(t)$  is proportional to the membrane potential and  $y(t)$  is a recovery variable. The quantity  $J$  plays the role of

an external stimulus, and in physiological terms it is related to the glucose level  $G$  in the blood stream through some function,  $J = f(G)$ . Parameters  $a$  and  $b$  are proportional, respectively, to the ratio between inductance and capacitance and to the electrical resistance of the  $\beta$ -cell membrane [44]. As will be shown later, they also determine oscillation period and shape.

The above equations are characterized by an equilibrium point, whose stability is determined by the threshold value  $\varepsilon$  of the external stimulus  $J$ :

$$\varepsilon = \frac{3a^2 - 2a^2b - b^2}{3a^3} \sqrt{a^2 - b}. \quad (2)$$

The equilibrium point is stable when  $|J| > \varepsilon$  and unstable when  $|J| < \varepsilon$ . This means that, when  $|J| < \varepsilon$ , the system oscillates, while for  $|J| > \varepsilon$ , it is either in an excitable state ( $J < -\varepsilon$ ), corresponding to a constant negative value of  $x(t)$ , or in an “excitation block” state ( $J > \varepsilon$ ), corresponding to a constant positive value of  $x(t)$  [44,56]. From the standpoint of the electrical behavior of  $\beta$ -cells, we assume that the interval  $|J| < \varepsilon$  corresponds to bursting oscillations, while  $J < -\varepsilon$  represents a quiescent polarized state and  $J > \varepsilon$  a continuous firing state [44] (see Fig. 1).

It may seem strange that we correlate  $J$ , which can assume both positive and negative values, to glucose level, which is a positive quantity. However, we are not interested in a quantitative correlation between  $J$  and glucose level, but want to study trends and mechanisms. Therefore, we just need to keep in mind that  $J$  can vary from negative values below  $-\varepsilon$ , corresponding to a *low* glucose level; to negative, zero, or positive values in the range  $-\varepsilon < J < \varepsilon$ , corresponding to *intermediate* glucose levels; and up to positive values above  $\varepsilon$ , which are representative of *high* glucose levels; see Fig. 1. Notice that all the values  $J > -\varepsilon$  correspond to glucose levels  $G_0 \geq G_{th} > 0$ , where  $G_{th}$  denotes the activation threshold to induce electrical oscillations in  $\beta$ -cells.

It is also worth pointing out that  $J$  is a constant term in our model equations. This is consistent with most mathematical models on  $\beta$ -cell electrical activity and is justified by the timescale of bursting, which is much faster than the time required to promote significant glucose variations due to peripheral tissue absorption and hepatic feedback.

The values of parameters  $a$  and  $b$  in Eqs. (1a)–(1b) determine, besides the width of the  $|J| < \varepsilon$  interval, the shape of  $x(t)$  oscillations. Specifically, the oscillation period  $T$  is proportional to parameter  $a$  (higher values of  $a$  correspond to longer oscillation periods), whereas the main effect of parameter  $b$  is to modulate the ratio between the time spent by the system at elevated versus lower  $x(t)$ . This is illustrated in Fig. 2, showing a comparison between slower [Fig. 2(a)] and faster [Fig. 2(b)] oscillations, corresponding to different combinations of  $a$  and  $b$  values. We will use the combination  $a = 60$ ,  $b = 1.45$  [Fig. 2(a)] in most of the calculations presented in this work. If time is expressed in seconds, this combination of values generates a wave with period  $T \approx 150$  s and a slightly longer duration of low versus high  $x(t)$  phases, which matches the typical profile of bursting oscillations in  $\beta$ -cell clusters [39].

It is worth noting that  $\beta$ -cells have complex dynamical features that are not captured in our approach, i.e., faster action potential spikes superimposed on the slower bursting

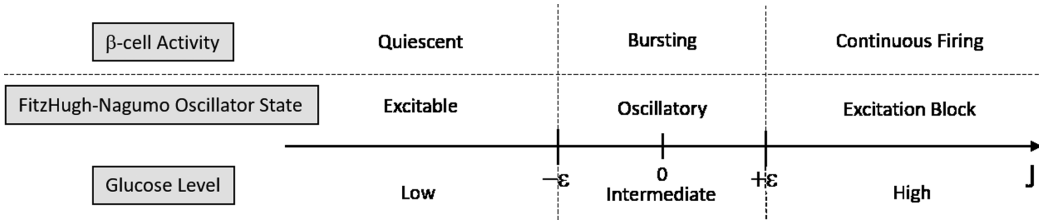


FIG. 1. Correspondence between  $\beta$ -cell activity and FitzHugh-Nagumo oscillator states.

oscillations, which we reproduce by a FitzHugh-Nagumo description. However, our focus is on the collective dynamics and synchronization of oscillator networks representative of  $\beta$ -cell clusters, and the role of heterogeneity. In this context, the slower bursting oscillations are more relevant than the action potential spikes, also due to their correlation with pulsatile insulin release, which is critically important from a physiological standpoint.

**B. Heterogeneous model**

In order to describe a  $\beta$ -cell cluster mimicking a Langerhans islet, we need to build a 3D network of FitzHugh-Nagumo oscillators, which are coupled to their neighbors via coupling factors  $C_{ij}(x_j - x_i)$ , where  $i$  and  $j$  are indexes that identify an oscillator  $i$  and one of its coupled nearest neighbors  $j$ . We make the simplified assumption that the value of the coupling constant is the same for each oscillator in the network, i.e., it is independent of  $i$  and  $j$ ,  $C_{ij} \equiv C$ , and that each oscillator is connected to the same number  $n$  of neighbors. Then the corresponding FitzHugh-Nagumo equations for the  $i$ th oscillator in the network become [44]

$$\dot{x}_i = a \left[ x_i - x_i^3/3 + y_i + C \sum_{j \in \{n\}_i} (x_j - x_i) \right], \tag{3a}$$

$$\dot{y}_i = -(x_i + by_i - J_i)/a, \tag{3b}$$

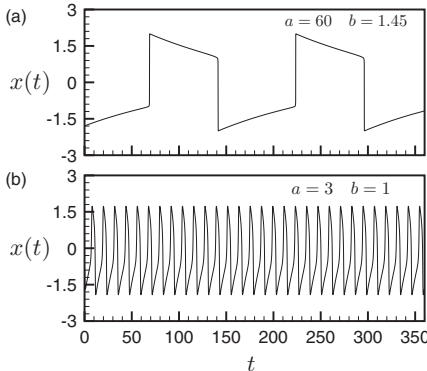


FIG. 2. Oscillation  $x(t)$  of a single FitzHugh-Nagumo element for different values of parameters  $a, b$  and an external stimulus  $J < |\epsilon|$  [see Eq. (2)], corresponding to the oscillatory regime.

where the sum over  $j$  in Eq. (3a) is limited to the set  $\{n\}_i$  of the  $n$  neighbors coupled to the  $i$ th oscillator.

In order to introduce diversity in our coupled oscillator network [45], we have assumed in Eq. (3b) that each oscillator has a different sensitivity to the external stimulus, which is equivalent to associating a different  $J_i$  value to each oscillator  $i$ . In physiological terms, this can be interpreted as attributing to each  $\beta$ -cell in an islet a different sensitivity to glucose level, which is a realistic assumption based on available experimental evidence of  $\beta$ -cell heterogeneity [58–61].

We draw the  $J_i$  values from a Gaussian distribution with mean  $J_{av}$  and standard deviation  $\sigma$ , which measures the diversity of the oscillator population [45]. As discussed previously, the mean value of the external stimulus,  $J_{av}$ , is related to glucose level in blood and can therefore be varied in a relatively broad range. For simplicity, we initially study the case  $J_{av} = 0$ , corresponding to a distribution with a certain number of oscillators, depending on the value of  $\sigma$ , in the oscillatory regime ( $|J_i| < \epsilon$ ), and equal numbers of oscillators in the excitable state ( $J_i < -\epsilon$ ) and in the excitation block state ( $J_i > +\epsilon$ ).

Using this  $J_i$  distribution, we numerically solve the FitzHugh-Nagumo equations for a network of  $10^3$  oscillators with cubic lattice topology, where each element is coupled to its six nearest neighbors. The  $J_i$  values from the Gaussian distribution are randomly assigned to network oscillators throughout the  $10 \times 10 \times 10$  cube geometry. While the cubic geometry is a simplification, both the total number of oscillators and the number of nearest neighbors per oscillator are consistent with what is known about the structure of Langerhans islets, where each  $\beta$ -cell is electrically coupled via gap junctions to six or seven neighbor cells on average [62,63].

We set the coupling constant  $C = 0.15$  because this value provides an optimal coupling efficiency (lower values cause a steep decrease of global network oscillations, while going higher does not result in a significant increase). This is illustrated in more detail in the next section and is a reasonable choice to ensure effective but not unrealistically strong coupling, considering that our goal is to mimic a biological system.

**III. RESULTS**

**A. Diversity-induced resonance**

After solving the FitzHugh-Nagumo equations (3a)–(3b), corresponding to the above described topology, we compute

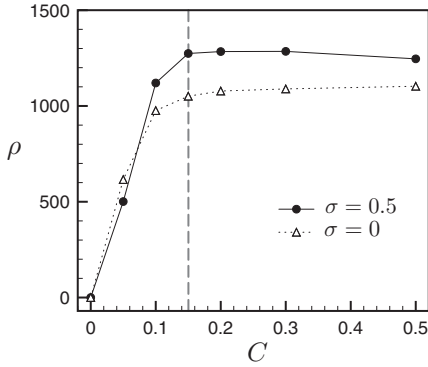


FIG. 3. Global oscillatory activity  $\rho$  as a function of coupling strength  $C$ , for different values of population diversity  $\sigma$ . The vertical dashed line at  $C = 0.15$  corresponds to the coupling strength used in the simulations.

the global oscillatory activity of the network [44],

$$\rho = \frac{1}{N} \sqrt{\frac{1}{t_f} \int_0^{t_f} dt [X(t) - \bar{X}]^2}. \quad (4)$$

Here  $N = 10^3$  is the total number of oscillators,  $X(t)$  is the sum over all  $i$  of the individual  $x_i(t)$  functions, and  $\bar{X}$  is the mean of  $X(t)$  in the time interval  $[0, t_f]$ . By its very definition,  $\rho$  is the root mean square amplitude over time of the global network oscillation  $X(t)$ , which has a periodic character. As a consequence,  $\rho$  is substantially independent of  $t_f$ , if  $t_f$  is sufficiently large. We verified that by setting  $t_f = 300$  time units, this condition is satisfied in our calculations.

We simulate numerically the oscillator network for a range of population diversity values  $\sigma$ , while keeping other parameters constant, i.e.,  $a = 60$ ,  $b = 1.45$ , and  $C = 0.15$ . As mentioned in Sec. II B, this choice of  $C$  corresponds to an optimal coupling efficiency, i.e., to the beginning of a plateau when plotting  $\rho$  against  $C$ , as shown in Fig. 3 for  $\sigma = 0$  and  $\sigma = 0.5$ .

Using the above parameters, the results for the global oscillatory activity  $\rho$  are plotted versus  $\sigma$  in Fig. 4(a) and show a clear diversity-induced resonance maximum at  $\sigma = 0.5$ . This value of  $\sigma$  represents the degree of population diversity resulting in the most efficient global network oscillations, due to the interaction between network elements that are individually in an oscillatory regime, i.e., elements for which  $|J| < \varepsilon$ , and elements that would be, individually, in a nonoscillatory regime, due to either quiescence or excitation block state ( $|J| > \varepsilon$ ), but are in fact oscillating due to network coupling and resonance effects. Notably, the  $\rho$  value corresponding to the diversity-induced resonance maximum is significantly higher than the one achieved with a homogeneous population ( $\sigma = 0$ ) where every element of the network is in the same oscillatory state.

### B. Emergence of hubs from diversity optimization

After introducing oscillator diversity via a Gaussian distribution of  $J_i$  values and observing the results in terms of global network oscillations, it becomes quite natural to identify

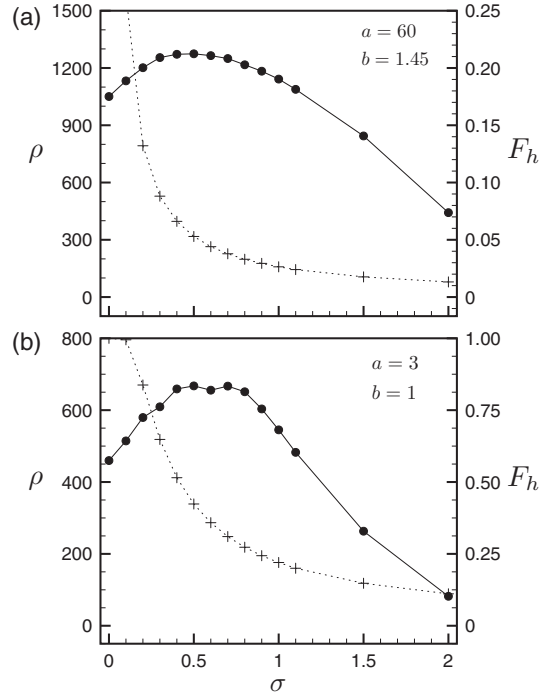


FIG. 4. Global oscillatory activity  $\rho$  (dots, solid curve, left axis) defined in Eq. (4) and fraction of hubs  $F_h$  (crosses, dotted curve, right axis) defined in Eq. (5) as a function of population diversity  $\sigma$ , for different values of  $a$  and  $b$ ;  $J_{av} = 0$ .

network elements corresponding to the interval  $|J| < \varepsilon$ , which are intrinsically in an oscillatory regime, as pacemakers or “hubs” of the system. Instead, elements outside the  $|J| < \varepsilon$  range are nonhubs, which can become active as a consequence of their network interactions and depending on how far their individual values  $J_i$  are from the  $|J| < \varepsilon$  range.

The hub to nonhub ratio corresponding to the diversity-induced resonance maximum represents the most efficient network configuration, because it maximizes global network oscillations. We can estimate this ratio by computing the following normalized Gaussian integral,

$$F_h = \frac{1}{\sqrt{2\pi}\sigma} \int_{-\varepsilon}^{\varepsilon} dJ \exp \left[ -\frac{(J - J_{av})^2}{2\sigma^2} \right], \quad (5)$$

which by definition expresses the fraction of oscillators with  $J_i$  values inside the  $|J| < \varepsilon$  range, i.e., the fraction of hubs in the population.

The dependence of  $F_h$  on  $\sigma$  for  $a = 60$  and  $b = 1.45$  is shown in Fig. 4(a). The optimal fraction of hubs corresponding to the diversity-induced resonance maximum ( $\sigma = 0.5$ ) is  $F_h = 0.053$ . This means a percentage of hubs in the total network population of about 5%, in good agreement with experimental observations of pacemaker  $\beta$ -cells in Langerhans islets based on optogenetic methods [23–26], which report this fraction to be 1%–10%. This prediction of our model is dependent on a specific choice of  $a$ ,  $b$  values in Eqs. (3a)–(3b),

by which we have empirically matched the oscillation period of individual FitzHugh-Nagumo elements with that experimentally observed for  $\beta$ -cells, as explained in Sec. II A.

The above results show that *in vivo*  $\beta$ -cell behavior in Langerhans islets, from the standpoint of collective dynamics and network configuration, is consistent with the intrinsic properties of a FitzHugh-Nagumo oscillator network with optimal diversity. From Fig. 4(a) one can also see that moving towards higher  $\sigma$  values beyond the diversity resonance maximum at  $\sigma = 0.5$ , the slope of  $\rho$  becomes progressively more negative, and, for  $\sigma = 2$ , where  $\rho$  is almost one third of its maximum value, the fraction of hubs,  $F_h$ , drops to about 1%. This illustrates the correlation between percentage of hubs and global oscillatory efficiency of the network and helps understanding what may happen in Langerhans islets, when the optimal hub to nonhub ratio is altered by a pathological condition.

For comparison, we repeat the calculations using the values  $a = 3$  and  $b = 1$  that correspond to the faster wave in Fig. 2(b). As shown in Fig. 4(b), for these values of  $a$  and  $b$  the global oscillatory activity  $\rho(\sigma)$  exhibits a more complex resonance pattern with two maxima, one at  $\sigma \approx 0.4$  and the other at  $\sigma \approx 0.6$ . The corresponding  $F_h$  values are  $F_h = 0.52$  and  $F_h = 0.36$ , respectively.

The above comparison indicates that faster global oscillations require a higher relative number of hubs to maintain a good coordination of the oscillator network, which makes sense from both a physical and a physiological standpoint. In the case of a slower wave, network elements that are not initially or individually in an oscillatory state have more time to become active and synchronize with hubs via coupling effects, and therefore a lower number of hubs is required to obtain efficient global oscillations. With a faster wave, synchronization is more challenging and can be achieved only with a sufficiently high percentage of hubs in the network. This difference is deliberately exaggerated in our faster wave example, by choosing very different values of  $a$  and  $b$  versus the slower wave example used in our calculations. However, it would be interesting to look for a confirmation of this trend in future experimental work, by comparing the number of detectable hubs in slow versus fast bursting oscillations of  $\beta$ -cell clusters.

It is also worth noting that in both combinations of  $a, b$  parameters we studied, the  $\sigma$  value where the diversity-induced resonance maximum occurs is larger than the corresponding  $\epsilon$  ( $\epsilon \approx 0.033$  for  $a = 60, b = 1.45$  and  $\epsilon \approx 0.279$  for  $a = 3, b = 1$ ). This may be due to a positive contribution to network resonance from elements that are outside the intrinsic oscillatory range  $|J| < \epsilon$ , but not too far away from it. These excitable elements can easily start oscillating and contribute to resonance thanks to coupling. Instead, elements that are far away from the oscillatory range, i.e., at the tails of the distribution, remain quiescent regardless of coupling, therefore are detrimental to global oscillatory efficiency. The best network oscillatory performance is achieved at the diversity-induced resonance maximum, due to an optimal balance of these opposite effects. When  $\sigma$  is increased beyond the resonance maximum, the network loses efficiency, because not only the amount of pacemakers and more easily excitable elements decreases but also, at the same

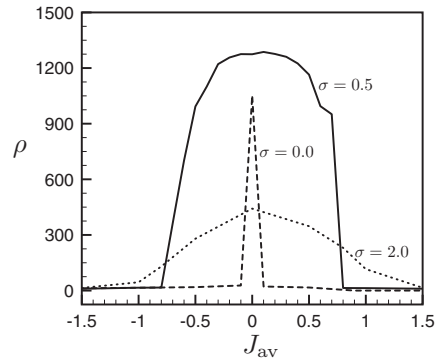


FIG. 5. Global oscillatory activity  $\rho$ , defined in Eq. (4), as a function of the average value  $J_{av}$  of the stimulus, for different values of population diversity  $\sigma$  ( $a = 60, b = 1.45$ ).

time, the amount of the most distant, quiescent elements increases.

### C. The optimal hub to nonhub ratio maximizes the dynamic range of response to glucose level

We now study what happens when we shift the position of the mean value  $J_{av}$  of the  $J_i$  distribution with respect to the midpoint of the  $|J| < \epsilon$  interval, keeping  $\sigma$  constant. This will give us information about the ability of the oscillator population to cope with a stimulus corresponding to  $J$  values that are increasingly distant from the range corresponding to the intrinsic oscillatory regime.

We perform the calculations with  $a = 60$  and  $b = 1.45$ , corresponding to the reference wave, for three different degrees of diversity:  $\sigma = 0$  (homogeneous system),  $\sigma = 0.5$  (the diversity-induced resonance maximum), and  $\sigma = 2.0$  (as an example of large diversity).

The results reported in Fig. 5 show that oscillator diversity is able to considerably increase the range of the external stimulus  $J$ , where the network exhibits efficient global oscillations. If all network elements were identical ( $\sigma = 0$ ), their global oscillatory activity would be limited to the narrow interval  $|J| < \epsilon \approx 0.033$ . Instead, oscillator diversity and coupling allow the network to respond effectively to a much broader range of  $J$ . This range gets broader and broader as  $\sigma$  is increased; however, at the same time, increasing  $\sigma$  causes a progressively weaker response in terms of global oscillatory efficiency, as shown by the comparison between  $\rho$  curves for  $\sigma = 0.5$  and  $\sigma = 2.0$ .

It is also helpful to look at the behavior of  $X(t)$  [the sum of the individual  $x_i(t)$ ] for different values of  $\sigma$ . For instance, for  $J_{av} = 0.5$ , the network is in a resonant state and presents global oscillations for both  $\sigma = 0.5$  and  $\sigma = 2.0$ . However, a comparison between the corresponding  $X(t)$  curves shows a large difference in terms of oscillation amplitude and regularity (Fig. 6), which then reflects into very different  $\rho$  values for the two parameter sets. This large difference is a consequence both of a broader  $J_i$  distribution, which causes more network elements to have  $J_i$  values that are increasingly far away from

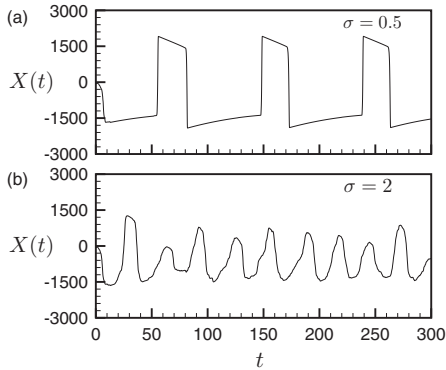


FIG. 6. Global network oscillation  $X(t)$  for different values of population diversity  $\sigma$ , at the average value  $J_{av} = 0.5$  of the stimulus ( $a = 60$ ,  $b = 1.45$ ).

the oscillatory range  $|J| < \varepsilon$ , and of a significantly lower number of hubs.

In physiological terms, moving from lower to higher values of  $J$  in Fig. 5 can be considered equivalent to increasing glucose concentration from basal up to elevated levels, as explained in Sec. II A. This illustrates that  $\beta$ -cell diversity can be a mechanism to achieve a much more robust oscillatory behavior of islets in response to varying glucose levels.

It is also interesting to observe that the increase of oscillatory activity from left to right of the  $\sigma = 0.5$  and  $\sigma = 2.0$  curves in Fig. 5 is less steep than the drop on the right side; however, at the same time, the right half of the curve is more extended. Again, reading this in physiological terms, we could say that as glucose concentration is gradually increased, the network responds by progressively increasing its oscillatory activity, which is then kept as high as possible for as long as the system is able to cope with the increasing external signal strength. A similar response profile has been predicted also by more complex biophysical models [64]; however our approach and analysis helps to clarify and understand the underlying network dynamics.

#### IV. CONCLUSIONS

Using the FitzHugh-Nagumo equations to represent the electrical behavior of  $\beta$ -cells, we developed a coupled oscillator network model with cubic lattice topology and showed that the optimization of diversity results in the emergence of pacemakers or hubs, which play a key role in determining the global oscillatory behavior of the network. The optimal hub to nonhub ratio predicted by the model is defined by the position of the diversity-induced resonance maximum and depends on oscillation period and shape, which are determined by the FitzHugh-Nagumo equation parameters. If we select these parameters in order to match the experimentally measured period of bursting oscillations in  $\beta$ -cell clusters, we find that the corresponding hub percentage predicted by the model (about 5%) is in very good agreement with observations of

pacemaker  $\beta$ -cells in Langerhans islets based on optogenetic methods, i.e., *in vivo*  $\beta$ -cell behavior in islets is in this respect consistent with the intrinsic oscillatory properties of a heterogeneous, coupled FitzHugh-Nagumo oscillator network embedded in a cubic lattice.

The model also gives an approximate indication of the hub percentage threshold below which the oscillatory performance of a network gets significantly worse, i.e., around 3%, which may be indicative of the level of  $\beta$ -cell population alteration corresponding to a pathological condition, such as type 2 diabetes. Furthermore, the results obtained suggest the trend that higher bursting oscillation frequencies should correspond to larger hub to nonhub ratios, which would be interesting to verify in future experimental work.

We also showed that diversity is a key mechanism to significantly broaden the dynamic range and robustness of the network response to an external stimulus, i.e., glucose concentration in the case of  $\beta$ -cells. This is relevant from a physiological viewpoint, and, again, an altered network configuration with suboptimal diversity and hub to nonhub ratio will reflect into a compromised oscillatory performance, which in the case of  $\beta$ -cells translates into an insulin secretion profile that may be insufficient or does not have the required pulsatile characteristics.

Looking back at a key question we asked in the introduction, i.e., whether hubs are a permanently distinct subpopulation of  $\beta$ -cells, our model suggests that the relative number of hubs in a network can change as a consequence of the external stimulus strength. Therefore, network elements that are nonhubs can turn into hubs and vice versa, as the network reconfigures itself in response to an environmental change. Whether hubs are a permanently distinct subpopulation is irrelevant from the standpoint of the dynamical behavior of the oscillator network; however, the model suggests that hubs should have the ability to “turn on” and “off” their pacemaker function in order to ensure optimal network performance in different conditions.

Topics for future extensions of this work include a comparison of the insights from our approach to biophysical modeling predictions, as well as an in-depth investigation of the combined effects on resonance phenomena of heterogeneity, stochasticity, and connectivity, which have been so far partially studied [65]. In addition, we will consider the opportunity to apply our approach or its adaptations to other biological systems beyond  $\beta$ -cells, e.g., cardiomyocytes and neurons.

#### ACKNOWLEDGMENTS

A.L. acknowledges the support of Gruppo Nazionale per la Fisica Matematica (GNFM-INdAM). E.H. and M.P. acknowledge support from the Estonian Ministry of Education and Research through Institutional Research Funding IUT39-1, the Estonian Research Council through Grants PUT1356 and PRG1059, and the ERDF (European Development Research Fund) CoE (Center of Excellence) program through Grant TK133.

- [1] J. Keizer, *Math. Biosci.* **90**, 127 (1988).
- [2] R. M. Santos, L. M. Rosario, A. Nadal, J. Garcia-Sancho, B. Soria, and M. Valdeolmillos, *Pflügers Arch.* **418**, 417 (1991).
- [3] R. K. P. Benninger, M. Zhang, W. S. Head, L. S. Satin, and D. W. Piston, *Biophys. J.* **95**, 5048 (2008).
- [4] P. Rorsman and F. M. Ashcroft, *Physiol. Rev.* **98**, 117 (2018).
- [5] P. Bergsten, *Diabetes Metab. Res. Rev.* **16**, 179 (2000).
- [6] L. S. Satin, P. C. Butler, J. Ha, and A. S. Sherman, *Mol. Aspects Med.* **42**, 61 (2015).
- [7] O. Idevall-Hagren and A. Tengholm, *Semin. Cell Dev. Biol.* **103**, 20 (2020).
- [8] M. C. Laurenti, C. D. Man, R. T. Varghese, J. C. Andrews, R. A. Rizza, A. Matveyenko, G. D. Nicolao, C. Cobelli, and A. Vella, *JCI Insight* **5**, e136136 (2020).
- [9] R. Bertram, A. Sherman, and L. S. Satin, *Am. J. Physiol.-Endocrinol. Metab.* **293**, E890 (2007).
- [10] M. G. Pedersen, *J. Diabetes Sci. Technol.* **3**, 12 (2009).
- [11] Y. H. Chew, Y. L. Shia, C. T. Lee, F. A. A. Majid, L. S. Chua, M. R. Sarmidi, and R. A. Aziz, *Mol. Cell. Endocrinol.* **307**, 57 (2009).
- [12] P. Goel and A. Sherman, *SIAM J. Appl. Dyn. Syst.* **8**, 1664 (2009).
- [13] R. Bertram, A. Sherman, and L. S. Satin, in *Advances in Experimental Medicine and Biology* (Springer Netherlands, Amsterdam, 2010), pp. 261–279.
- [14] M. Meyer-Hermann and R. K. P. Benninger, *HFSP J.* **4**, 61 (2010).
- [15] A. Stožer, M. Gosak, J. Dolenšek, M. Perc, M. Marhl, M. S. Rupnik, and D. Korošak, *PLoS Comput. Biol.* **9**, e1002923 (2013).
- [16] G. J. Félix-Martínez and J. R. Godínez-Fernández, *Islets* **6**, e949195 (2014).
- [17] A. Loppini, M. Braun, S. Filippi, and M. G. Pedersen, *Phys. Biol.* **12**, 066002 (2015).
- [18] C. Cherubini, S. Filippi, A. Gizzi, and A. Loppini, *Phys. Rev. E* **92**, 042702 (2015).
- [19] R. Markovič, A. Stožer, M. Gosak, J. Dolenšek, M. Marhl, and M. S. Rupnik, *Sci. Rep.* **5**, 7845 (2015).
- [20] J. P. McKenna, R. Dhumpa, N. Mukhitov, M. G. Roper, and R. Bertram, *PLoS Comput. Biol.* **12**, e1005143 (2016).
- [21] A. Loppini, M. G. Pedersen, M. Braun, and S. Filippi, *Phys. Rev. E* **96**, 032403 (2017).
- [22] A. Loppini and M. G. Pedersen, *Chaos* **28**, 063111 (2018).
- [23] J. Kolic and J. Johnson, *Cell Metab.* **24**, 371 (2016).
- [24] N. R. Johnston, R. K. Mitchell, E. Haythorne, M. P. Pessoa, F. Semplici, J. Ferrer, L. Piemonti, P. Marchetti, M. Bugliani, D. Bosco *et al.*, *Cell Metab.* **24**, 389 (2016).
- [25] M. J. Westacott, N. W. F. Ludin, and R. K. P. Benninger, *Biophys. J.* **113**, 1093 (2017).
- [26] V. Salem, L. D. Silva, K. Suba, E. Georgiadou, S. N. M. Gharavy, N. Akhtar, A. Martin-Alonso, D. C. A. Gaboriau, S. M. Rothery, T. Stylianides *et al.*, *Nat. Metab.* **1**, 615 (2019).
- [27] C.-L. Lei, J. A. Kellard, M. Hara, J. D. Johnson, B. Rodriguez, and L. J. B. Briant, *Islets* **10**, 151 (2018).
- [28] A. Loppini, C. Cherubini, and S. Filippi, *Chaos, Solitons Fractals* **109**, 269 (2018).
- [29] E. Gylfe, E. Grapengiesser, and B. Hellman, *Cell Calcium* **12**, 229 (1991).
- [30] C. Ämmälä, O. Larsson, P.-O. Berggren, K. Bokvist, L. Juntti-Berggren, H. Kindmark, and P. Rorsman, *Nature (London)* **353**, 849 (1991).
- [31] Y. Palti, G. B. David, E. Lachov, Y. H. Mika, G. Omri, and R. Schatzberger, *Diabetes* **45**, 595 (1996).
- [32] P. E. Squires, S. J. Persaud, A. C. Hauge-Evans, E. Gray, H. Ratcliff, and P. M. Jones, *Cell Calcium* **31**, 209 (2002).
- [33] J. V. Rocheleau, G. M. Walker, W. S. Head, O. P. McGuinness, and D. W. Piston, *Proc. Natl. Acad. Sci. USA* **101**, 12899 (2004).
- [34] R. K. P. Benninger, T. Hutchens, W. S. Head, M. J. McCaughey, M. Zhang, S. J. L. Marchand, L. S. Satin, and D. W. Piston, *Biophys. J.* **107**, 2723 (2014).
- [35] A. Sherman, J. Rinzel, and J. Keizer, *Biophys. J.* **54**, 411 (1988).
- [36] P. Rorsman and G. Trube, *J. Physiol.* **374**, 531 (1986).
- [37] F. C. Jonkers, J.-C. Jonas, P. Gilon, and J.-C. Henquin, *J. Physiol.* **520**, 839 (1999).
- [38] P. Smolen, J. Rinzel, and A. Sherman, *Biophys. J.* **64**, 1668 (1993).
- [39] M. Zhang, P. Goforth, R. Bertram, A. Sherman, and L. Satin, *Biophys. J.* **84**, 2852 (2003).
- [40] A. Goldbeter, G. Dupont, and M. J. Berridge, *Proc. Natl. Acad. Sci. USA* **87**, 1461 (1990).
- [41] M. Düfer, D. Haspel, P. Krippeit-Drews, L. Aguilar-Bryan, J. Bryan, and G. Drews, *Diabetologia* **47**, 488 (2004).
- [42] L. E. Fridlyand, N. Tamarina, and L. H. Philipson, *Am. J. Physiol.-Endocrinol. Metab.* **299**, E517 (2010).
- [43] A. Sherman, *Bull. Math. Biol.* **56**, 811 (1994).
- [44] J. H. E. Cartwright, *Phys. Rev. E* **62**, 1149 (2000).
- [45] C. J. Tessone, C. R. Mirasso, R. Toral, and J. D. Gunton, *Phys. Rev. Lett.* **97**, 194101 (2006).
- [46] R. Toral, E. Hernandez-García, and J. D. Gunton, *Int. J. Bifurcation Chaos* **19**, 3499 (2009).
- [47] H. Chen, Z. Hou, and H. Xin, *Physica A* **388**, 2299 (2009).
- [48] L. Wu, S. Zhu, X. Luo, and D. Wu, *Phys. Rev. E* **81**, 061118 (2010).
- [49] L. Wu, S. Zhu, and X. Luo, *Chaos* **20**, 033113 (2010).
- [50] M. Patriarca, S. Postnova, H. A. Braun, E. Hernández-García, and R. Toral, *PLoS Comput. Biol.* **8**, e1002650 (2012).
- [51] C. J. Tessone, A. Sánchez, and F. Schweitzer, *Phys. Rev. E* **87**, 022803 (2013).
- [52] M. Grace and M.-T. Hütt, *Eur. Phys. J. B* **87**, 29 (2014).
- [53] M. Patriarca, E. Hernández-García, and R. Toral, *Chaos Solitons Fractals* **81**, 567 (2015).
- [54] X. Liang, X. Zhang, and L. Zhao, *Chaos* **30**, 103101 (2020).
- [55] R. FitzHugh, *J. Gen. Physiol.* **43**, 867 (1960).
- [56] R. FitzHugh, *Biophys. J.* **1**, 445 (1961).
- [57] J. Nagumo, S. Arimoto, and S. Yoshizawa, *Proc. IRE* **50**, 2061 (1962).
- [58] T. Aizawa, T. Kaneko, K. Yamauchi, H. Yajima, T. Nishizawa, T. Yada, H. Matsukawa, M. Nagai, S. Yamada, Y. Sato *et al.*, *Life Sci.* **69**, 2627 (2001).
- [59] M. Karaca, *Islets* **2**, 124 (2010).
- [60] M. Riz, M. Braun, and M. G. Pedersen, *PLoS Comput. Biol.* **10**, e1003389 (2014).
- [61] G. D. Gutierrez, J. Gromada, and L. Sussel, *Front. Genet.* **8**, 22 (2017).

- [62] S. J. Persaud, A. C. Hauge-Evans, and P. M. Jones, in *Cellular Endocrinology in Health and Disease*, edited by A. Ulloa-Aguirre and P. M. Conn (Academic Press, Boston, 2014), pp. 239–256.
- [63] D. Nasteska and D. J. Hodson, *J. Mol. Endocrinol.* **61**, R43 (2018).
- [64] I. J. Stamper and X. Wang, *J. Theor. Biol.* **475**, 1 (2019).
- [65] M. Gosak, M. Perc, and S. Kralj, *Eur. Phys. J. B* **80**, 519 (2011).

## Appendix 2

### II

S. Scialla, M. Patriarca, and E. Heinsalu, "The interplay between diversity and noise in an excitable cell network model," *EPL*, vol. 137, p. 51001, 2022



# The interplay between diversity and noise in an excitable cell network model

STEFANO SCIALLA<sup>1,2(a)</sup> , MARCO PATRIARCA<sup>1(b)</sup> and ELS HEINSALU<sup>1(c)</sup>

<sup>1</sup> National Institute of Chemical Physics and Biophysics - Akadeemia tee 23, 12618 Tallinn, Estonia

<sup>2</sup> Department of Engineering, Università Campus Bio-Medico di Roma - Via Á. del Portillo 21, 00128 Rome, Italy

received 18 November 2021; accepted in final form 11 March 2022

published online 9 May 2022

**Abstract** – We study the effects of the interplay between diversity and noise in a 3D network of FitzHugh-Nagumo elements, with topology and dimensions chosen to model a pancreatic  $\beta$ -cell cluster, as an example of an excitable cell network. Our results show that diversity and noise are non-equivalent sources of disorder that have different effects on the network dynamics: their synchronization mechanisms may act independently of one another or synergistically, depending on the mean value of the diversity distribution compared to the intrinsic oscillatory range of the network elements.

Copyright © 2022 EPLA

**Introduction.** – The study of the beneficial role of disorder in a broad range of biological, physical, and chemical phenomena has become a fundamental research topic in complex systems dynamics. A seminal work in the field was the introduction of stochastic resonance (SR) in the early eighties, initially proposed to explain the occurrence of Earth ice ages [1] and later on studied by numerous authors across various disciplines [2–11]. SR can happen when a nonlinear system is driven simultaneously by a periodic external forcing and noise, resulting in an amplification of the system response to the external signal [12].

Some of the subsequent studies showed that significant noise-driven effects, analogous to SR, can be observed also without periodicity of the external signal [13], and even in the absence of any external signal, as in self-induced stochastic resonance [14,15] and coherence resonance [16]. Coherence resonance (CR) is an ordered response of a nonlinear excitable system to an optimal noise amplitude, resulting in regular pulses. Beyond its effects on a single nonlinear unit, the role of noise was also extensively studied from the standpoint of its ability to improve synchronization in coupled oscillator networks, again both in the absence and in the presence of an external forcing [17–19]. Broadly speaking, one may say that the first twenty years of research in this field focused, to a large degree, on the effects of noise in bistable or excitable systems [20,21], comprising either several or just one element.

At the beginning of the new century, it was found that somewhat analogous effects to those of noise can be produced in networks of coupled oscillators through the heterogeneity of the oscillator population [22,23]. This led to the introduction of diversity-induced resonance (DIR), which denotes the amplification of a network response to an external signal, driven by the heterogeneity of network elements [23–32]. Just like SR, also DIR can occur both in the presence and in the absence of an external forcing. In the latter case it has been named diversity-induced coherence [33]. This provides an example of the non-trivial analogies and differences between the effects that noise and diversity can have on a given system.

It is clear from the above that SR and CR can occur even in systems made of a single element, therefore they are not intrinsically collective phenomena, whereas, by definition, DIR represents a collective disorder effect driven by population heterogeneity.

Most of the previous literature has emphasized either the analogies between SR and DIR [23,34], considering them as two faces of the same medal, or the possibility to enhance resonance induced by noise thanks to diversity optimization (or vice versa) [35–38].

Relatively little work [39,40] has been devoted to the implications of the above-mentioned intrinsic difference between the two phenomena, which has not yet been fully analyzed. In general, it is not straightforward to distinguish between the effects of a purely external noise and those of chaotic fluctuations associated to a set of degrees of freedom. Such a distinction is difficult to achieve

<sup>(a)</sup>E-mail: [stefano.scialla@kbfi.ee](mailto:stefano.scialla@kbfi.ee) (corresponding author)

<sup>(b)</sup>E-mail: [marco.patriarca@kbfi.ee](mailto:marco.patriarca@kbfi.ee)

<sup>(c)</sup>E-mail: [els.heinsalu@kbfi.ee](mailto:els.heinsalu@kbfi.ee)

and represents a currently open problem of statistical mechanics [41,42]. Numerical methods aimed at extracting information on the inner dynamics of a system, by analyzing the corresponding time series, encounter subtle difficulties that prevent a simple distinction between the effects due to noise and those due to the couplings with other degrees of freedom (see, *e.g.*, ref. [43]). However, in some cases, in which a set of relevant degrees of freedom is known and can be effectively separated from the rest of the system, as for the heterogeneous noisy oscillator network considered here, it is possible to infer the separate effects of noise and disorder by studying the system response to different levels of fluctuations and diversity.

In this paper, by systematically investigating the prototypical model of a heterogeneous network of pancreatic  $\beta$ -cells [22,44] with the addition of noise, we provide insights into the different mechanisms by which diversity and noise can have markedly distinct effects on the network dynamics. Langerhans islets, located in the pancreas, host approximately one thousand  $\beta$ -cells clustered together and electrically connected via resistive gap junctions. The main function of  $\beta$ -cells is the production of insulin, which happens in response to the glucose level in the blood stream. During insulin production, the electrical potentials of  $\beta$ -cells cycle synchronously in slow oscillations (bursts). Various models of pancreatic  $\beta$ -cells have been proposed, in order to explain the origin of such synchronized oscillations. The beneficial effects of the heterogeneity of individual  $\beta$ -cells on global oscillations had been recognized in refs. [45,46]. In ref. [22], using a simplified FitzHugh-Nagumo model of the  $\beta$ -cell network, Cartwright recognized the general constructive role of heterogeneity from a complex systems perspective; and, in particular, the fact that diversity can explain the emergence of synchronization in Langerhans islets, without the need to assume the presence of pacemakers, analogous to the myocardial pacemaker cells. Similar synchronization mechanisms have been shown also in other biological systems [47,48]. Later on, besides the constructive role of noise [49], also the beneficial role of diversity was recognized in the framework of more detailed models of  $\beta$ -cell networks [50].

**Model.** – As a paradigmatic example of a system of coupled nonlinear units, we investigate an excitable network of FitzHugh-Nagumo elements.

Individual elements of such network are described by the dimensionless FitzHugh-Nagumo equations [22,44,51–53]:

$$\dot{x} = a(x - x^3/3 + y), \quad (1)$$

$$\dot{y} = -(x + by - J)/a. \quad (2)$$

When modelling the behavior of a  $\beta$ -cell, the variable  $x(t)$  represents the fast relaxing membrane potential, while  $y(t)$  is a recovery variable mimicking the slow potassium channel gating. Depending on the value of  $J$ , the unit will be in an oscillatory state if  $|J| < \varepsilon$  or in an excitable state if

$|J| > \varepsilon$ , where

$$\varepsilon = \frac{3a^2 - 2a^2b - b^2}{3a^3} \sqrt{a^2 - b}. \quad (3)$$

In addition to determining the width of the oscillatory interval  $(-\varepsilon, +\varepsilon)$ , parameters  $a$  and  $b$  define the oscillation waveform and period.

Moving from the description of a single element to that of a heterogeneous 3D network of  $N$  FitzHugh-Nagumo units, we assume a cubic lattice topology. This implies that each element is coupled to its six nearest neighbors via a coupling term  $C_{ij}(x_j - x_i)$ , where  $i$  and  $j$  are indexes that identify an element  $i$  and one of its coupled neighbors  $j$ , and  $C_{ij}$  is the interaction strength. Notice that the choice of a cubic lattice topology is consistent with what is known about the architecture of  $\beta$ -cell clusters, where each cell is surrounded on average by 6-7 neighbor cells [54, 55]. We make the simplifying assumption that the value of the coupling constants is the same for each network element,  $C_{ij} \equiv C$  for any  $i, j$ . Since we want to study the interplay between diversity and noise, we also add a noise term  $\xi_i(t)$  to the first equation. Then the corresponding FitzHugh-Nagumo equations for the  $i$ -th element of the network are [22,44]:

$$\dot{x}_i = a \left[ x_i - \frac{x_i^3}{3} + y_i + C \sum_{j \in \{n\}_i} (x_j - x_i) + \xi_i(t) \right], \quad (4)$$

$$\dot{y}_i = -(x_i + by_i - J_i)/a. \quad (5)$$

The sum over  $j$  in eq. (4) is limited to the set  $\{n\}_i$  of the  $n = 6$  neighbors coupled to the  $i$ -th oscillator.

The  $J_i$  parameters in eq. (5) are different for each network element and are used to introduce diversity; the  $i$ -th element will be in an oscillatory state if  $|J_i| < \varepsilon$  or in an excitable state if  $|J_i| > \varepsilon$ . The  $J_i$  values are drawn from a Gaussian distribution with standard deviation  $\sigma_d$ , mean value  $J_{av}$ , and are randomly assigned to network elements. The standard deviation  $\sigma_d$  will be used in what follows as a measure of oscillator population diversity, while the mean value  $J_{av}$  expresses how far the whole population is from the oscillatory range  $(-\varepsilon, +\varepsilon)$ .

The term  $\xi_i(t)$  in eq. (4) is a Gaussian noise with zero mean, standard deviation  $\sigma_n$ , and correlation function  $\langle \xi_i(t) \xi_j(t') \rangle = \sigma_n^2 \delta_{ij} \delta(t - t')$ , meaning that  $\xi_i(t)$  and  $\xi_j(t)$  ( $i \neq j$ ) are statistically independent of each other. The standard deviation  $\sigma_n$  will be used in this work as a measure of noise applied to each network element.

The reason why we add  $\xi_i(t)$  to the first equation for the fast variable is that this maximizes the effects of noise, making it easier to study its combination with diversity. Introducing  $\xi_i(t)$  into the second equation would result in a minimal impact of noise on network synchronization [35], due to the slower dynamics of the refractory variable. Noise effects would be mostly averaged out to zero by time integration and coupling, as we will show below with some numerical simulations.

The above model, which to our knowledge is studied here for the first time in the version we propose, can be used to mimic various excitable biological systems, such as pancreatic  $\beta$ -cell clusters and some types of neurons [22,35,44,56–58]. In what follows we use the model to analyze the combined effect of diversity and noise, acting together on the same network. In particular, we are interested in potential synergies or antagonisms, as well as in a possible hierarchy between the two sources of disorder, which in spite of some analogies have fundamentally different synchronization mechanisms.

**Qualitative theoretical analysis.** – The white noise  $\xi_i(t)$  in eq. (4) can represent a randomly fluctuating external current, which is able to shift the nullcline of the  $x$  variable up or down and, therefore, to instantaneously change the position of the equilibrium point of each oscillator. Depending on the extent of the shift and on the value of  $J_i$ , this may result in a switch from a stable to an unstable equilibrium (or vice versa), corresponding to a transition from a resting to a spiking state of the oscillator (or vice versa).

This mechanism can be further illustrated, following ref. [23], by introducing the global variables  $X(t) = N^{-1} \sum_{i=1}^N x_i(t)$  and  $Y(t) = N^{-1} \sum_{i=1}^N y_i(t)$ . We then define  $\delta_i$  as the difference between  $x_i$  and  $X$ , *i.e.*,  $x_i \equiv X + \delta_i$ , and introduce  $M = N^{-1} \sum_{i=1}^N \delta_i^2$  [23,59]. Therefore,  $M$  will increase when diversity increases. By averaging eqs. (4) and (5) over all  $N$  network elements, we obtain the equations for the global variables  $X, Y$ :

$$\dot{X} = a [X(1 - M) - X^3/3 + Y + \xi_G(t)], \quad (6)$$

$$\dot{Y} = -(X + bY - J_{av})/a. \quad (7)$$

Here noise effects are represented by a global white noise term  $\xi_G(t) = N^{-1} \sum_i \xi_i(t)$  with zero mean and correlation function  $\langle \xi_G(t) \xi_G(t') \rangle = N^{-1} \sigma_n^2 \delta(t - t')$ .

It is instructive to observe the different impact of diversity and noise on the nullclines of eqs. (6) and (7). A change in diversity, *i.e.*, in the standard deviation of the  $J_i$  distribution, causes a change in  $M$ , which affects the shape of the cubic nullcline by changing the coefficient of the linear term  $X$  (see fig. 1, panels (a) and (b)). This indicates that diversity can have a significant effect on overall network dynamics, independently of whether the mean value  $J_{av}$  is inside or outside the intrinsic oscillatory range  $(-\varepsilon, +\varepsilon)$ . On the other hand, the global noise term  $\xi_G(t)$  can only cause rigid shifts, positive or negative, of the cubic nullcline along the vertical axis, as a consequence of its instantaneous fluctuations (compare the dashed and solid lines in fig. 1). This suggests that noise is unlikely to play a constructive role when diversity is optimized (*i.e.*, in the conditions corresponding to a DIR) and  $J_{av} = 0$ . In this situation, noise will likely act as a perturbation of the system, which is already in an intrinsically oscillatory and resonant state.

Let us now consider what happens when  $J_{av} \neq 0$  (see fig. 1(c)). In this case, the constant term  $J_{av}$  determines a

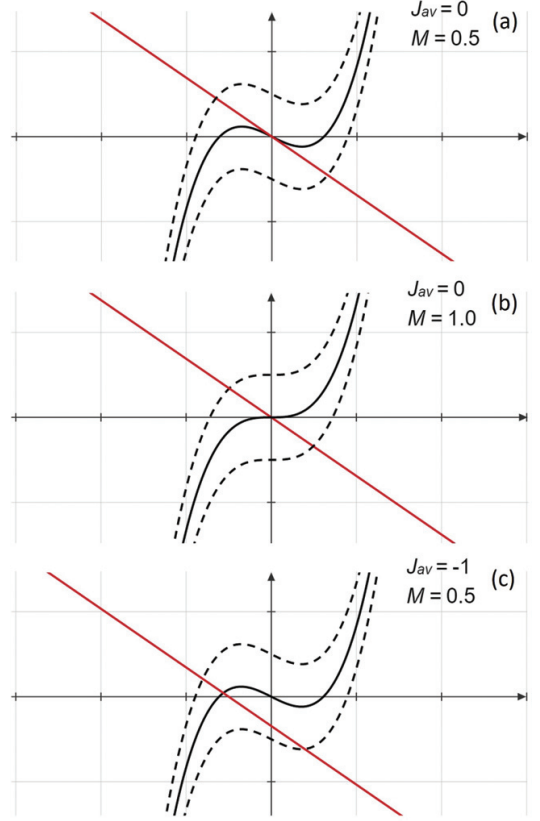


Fig. 1: Nullclines of eqs. (6) and (7) for different values of  $J_{av}$  and  $M$ . A comparison between panel (a) and (b) shows the effect of  $M$  on the shape of the cubic nullcline. The area delimited by the dashed curves above and below the cubic nullcline in each panel illustrates the effect of instantaneous shifts caused by noise with an amplitude of up to  $\pm 1$ .

rigid shift, upwards or downwards, of the second nullcline. This can significantly change the position of the equilibrium point of the system dynamics, turning the network from oscillatory into excitable. In these conditions, noise can play a synergistic role with diversity, by causing instantaneous rigid shifts of the cubic nullcline that counterbalance the effect of  $J_{av}$ , thus triggering global network oscillations.

It should be noted that we did not add a periodic driving force to our system equations, of the type  $A \sin(\Omega t)$ . As mentioned in the introduction, this term is not necessary to observe either stochastic or diversity-induced resonance effects and its presence would introduce the additional constraint of matching two time scales, *i.e.*, the driving force period and the oscillation period of the FitzHugh-Nagumo elements constituting the network.

**Numerical results and discussion.** – In order to quantitatively study the combined effect of diversity and

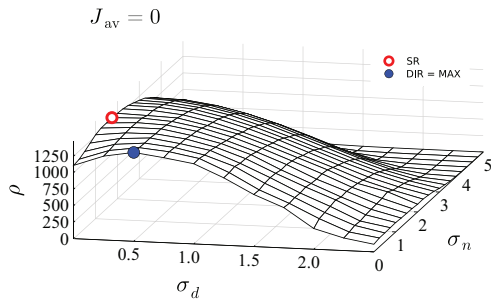


Fig. 2: Global oscillatory activity  $\rho$ , defined in eq. (8), as a function of diversity ( $\sigma_d$ ) and noise ( $\sigma_n$ ), for  $J_{av} = 0$ . The full blue dot highlights the global surface maximum, which is coincident with the DIR maximum. The empty red dot corresponds to the noise-induced resonance maximum.

noise, we numerically solve the FitzHugh-Nagumo equations (4) and (5) for a network of  $10^3$  elements with the above-mentioned topology and the following system parameters:  $a = 60$ ,  $b = 1.45$ ,  $C = 0.15$ . The selected values of  $a$  and  $b$  generate a waveform and period similar to those of bursting oscillations of pancreatic  $\beta$ -cells [44] and, according to eq. (3),  $\varepsilon \approx 0.033$ . We set the coupling constant  $C = 0.15$ , since, as we verified in an earlier work [44], the oscillatory response of the system is substantially unchanged by further increasing  $C$  beyond  $C = 0.15$ .

We run simulations for a range of diversity values  $\sigma_d$  (from  $\sigma_d = 0$  to  $\sigma_d = 2.5$ ) and, at the same time, for a range of white noise standard deviation values  $\sigma_n$  (from  $\sigma_n = 0$  to  $\sigma_n = 5.0$ ). We repeat this for each of the following diversity distribution mean values:  $J_{av} = 0, \pm 0.5, \pm 1$ .

For each simulation, corresponding to a set of  $\sigma_d$ ,  $\sigma_n$ , and  $J_{av}$  values, we quantify the network synchronization efficiency by computing the global oscillatory activity  $\rho$  [22,44],

$$\rho = N^{-1} \sqrt{\langle [S(t) - \bar{S}]^2 \rangle}, \quad (8)$$

where  $N = 10^3$  is the total number of oscillators,  $S(t) = \sum_i x_i(t)$ , and  $\bar{S} = \langle S(t) \rangle$ , with  $\langle \dots \rangle$  denoting a time average. The results for the global oscillatory activity  $\rho$  are plotted *vs.*  $\sigma_d$  and  $\sigma_n$ , generating five three-dimensional surfaces corresponding to each of the above-listed  $J_{av}$  values.

In the  $J_{av} = 0$  regime (fig. 2), where a relatively high fraction or all of the network elements are inside the intrinsic oscillatory range, simulation results show that both diversity and noise are able to generate a resonance on their own. If we move along the diversity axis ( $\sigma_n = 0$ , no noise) or along the noise axis ( $\sigma_d = 0$ , no diversity), we observe in both cases a resonance maximum that is about 20–25% higher than the  $\rho$  value corresponding to the origin. In addition, the two sources of noise seem to act independently of one another, showing no evidence of a synergy. As a matter of fact, the global maximum of the surface coincides with the diversity-induced resonance

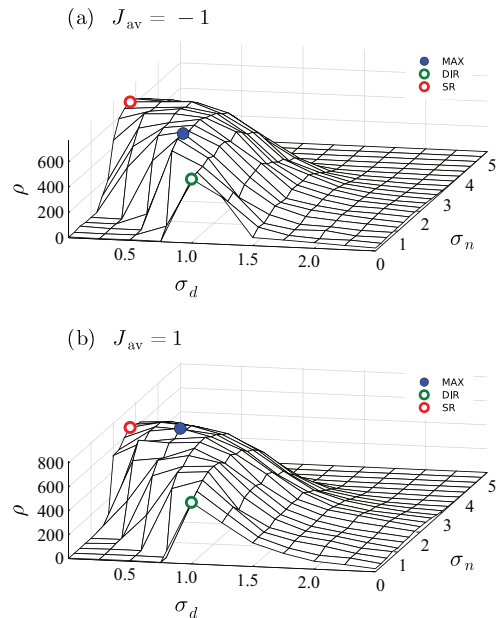


Fig. 3: Global oscillatory activity  $\rho$ , defined in eq. (8), as a function of diversity ( $\sigma_d$ ) and noise ( $\sigma_n$ ), for  $J_{av} = -1$  (panel (a)) and  $J_{av} = +1$  (panel (b)). The full blue and empty green/red dots in each panel highlight the global surface maximum, the DIR maximum and the noise-induced resonance maximum, respectively.

maximum, therefore it occurs on the diversity axis, *i.e.*, at  $\sigma_d = 0.5$ ,  $\sigma_n = 0$ . If, from this global maximum (shown as a full blue dot in fig. 2), we move in any direction towards the middle of the surface, *i.e.*, if we add noise, there is no gain in terms of collective oscillatory activity. This is consistent with the predictions of our qualitative theoretical analysis, indicating that noise is unlikely to play a constructive role for  $J_{av} = 0$ , when diversity is optimized.

Moving to the opposite end of the  $J_{av}$  range, *i.e.*,  $J_{av} = \pm 1$  (fig. 3), we observe a very different situation. In this regime most network elements are outside the intrinsic oscillatory range, either below ( $J_{av} = -1$ ) or above it ( $J_{av} = +1$ ). Here the addition of noise to diversity always results in a significant increase of the network oscillatory activity. In line with the theoretical analysis based on global system variables, this can be explained by considering that, in the case of  $J_{av} = -1$ , most network elements are below the excitation threshold, *i.e.*, in an excitable state, and can be pushed up into the oscillatory range by an instantaneous injection of positive external current, deriving from sufficiently large noise fluctuations with positive sign. Vice versa, in the case of  $J_{av} = +1$ , most elements are above the upper limit of the intrinsic oscillatory range, *i.e.*, in an excitation block state, and can be pushed down into the oscillatory range by an instantaneous injection of negative external current, deriving from negative

noise fluctuations with sufficiently large modulus. In both cases, the addition of noise on top of diversity causes a synergistic effect and a remarkable network synchronization improvement: for instance, the network oscillatory activity for  $J_{av} = +1$  raises by almost 50%, if we compare the DIR maximum ( $\rho \approx 515$ , empty green dot in fig. 3, panel (b)), to the global maximum of the  $\rho$  surface ( $\rho \approx 738$ , full blue dot in fig. 3, panel (b)) resulting from the combination of diversity and noise effects. It is also apparent from the data that, in this regime, noise is more efficient than diversity, as shown by the significantly higher noise-induced resonance maxima along the noise axis (empty red dots in fig. 3, panel (a) and (b)), compared to their equivalents along the diversity axis (empty green dots in fig. 3, panel (a) and (b)).

It is worth noting that the position of the DIR gets shifted towards higher values of  $\sigma_d$  going from  $J_{av} = 0$  to  $J_{av} = \pm 1$ . The DIR maximum is at  $\sigma_d = 0.5$  for  $J_{av} = 0$ , *vs.*  $\sigma_d = 1$  for both  $J_{av} = -1$  and  $J_{av} = +1$  (empty green dots in fig. 3, panels (a) and (b)). However, when we combine together noise and diversity, the position of the global maximum goes back to the same optimal diversity value found for  $J_{av} = 0$  (full blue dots in fig. 3, panels (a) and (b)). The mechanism of this effect is that noise stochastically “throws” network elements towards the oscillatory range, and it does so with respect to an average position on the  $J$ -axis that is determined, for each element, by its  $J_i$  coefficient, deriving from the diversity distribution. When this mechanism reaches the highest efficiency, *i.e.*, at the global maximum of the surface, the optimal diversity for  $J_{av} = \pm 1$  tends to be equal to that for  $J_{av} = 0$ . We may conclude that, in the  $J_{av} = \pm 1$  regime, there is a strong synergy between diversity and stochastic effects, which significantly broadens the range of resonant states of the network *vs.* what can be observed when either source of disorder is applied individually.

Finally, in the intermediate regime corresponding to  $J_{av} = \pm 0.5$  (fig. 4), we observe an in-between situation, with various regions of the  $\rho$  surface where the combination of diversity and noise produces a synergy and an extension of the resonant range of the network. For example, at  $J_{av} = -0.5$  (and  $\sigma_n = 0$ ), there are no network oscillations for diversity values  $\sigma_d = 0.0$  and  $\sigma_d = 0.25$ , whereas, with the addition of noise, resonant states are observed in both cases, starting from  $\sigma_n = 1$  and  $\sigma_n = 0.5$ , respectively. We point out that, also in this regime, the global maximum of the  $\rho$  surface due the combined diversity- and noise-induced resonance occurs, for  $J_{av} = -0.5$ , at  $\sigma_d = 0.5$  (full blue dot in fig. 4, panel (a)) and is shifted to smaller values with respect to the DIR maximum in the absence of noise ( $\sigma_d = 0.75$ , empty green dot in fig. 4, panel (a)). Therefore, the mechanism described in the previous paragraph, regarding the tendency of the optimal diversity value to be equal to that for  $J_{av} = 0$ , is at play here as well.

In order to confirm the rationale for our choice of adding the noise term  $\xi_i(t)$  into the first FitzHugh-Nagumo

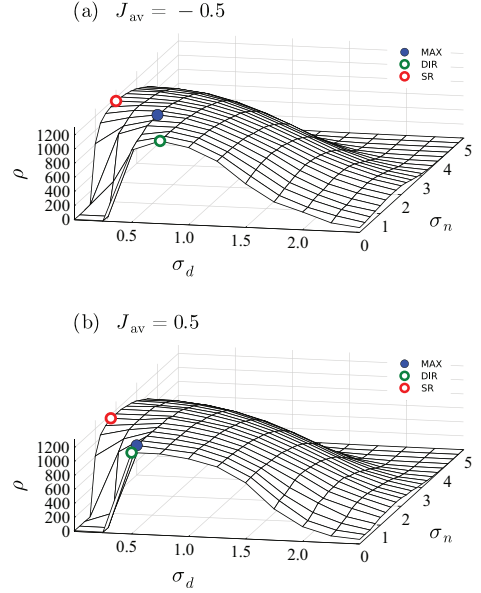


Fig. 4: Global oscillatory activity  $\rho$ , defined in eq. (8), as a function of diversity ( $\sigma_d$ ) and noise ( $\sigma_n$ ), for  $J_{av} = -0.5$  (panel (a)) and  $J_{av} = +0.5$  (panel (b)). The full blue and empty green/red dots in each panel highlight the global surface maximum, the DIR maximum and the noise-induced resonance maximum, respectively.

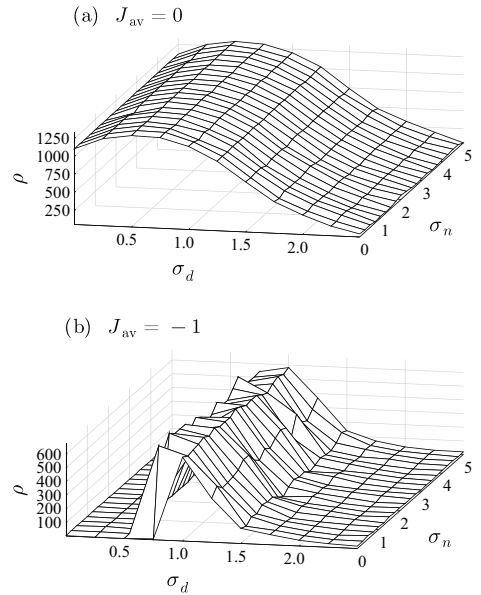


Fig. 5: Global oscillatory activity  $\rho$ , defined in eq. (8), as a function of diversity ( $\sigma_d$ ) and noise ( $\sigma_n$ ), for  $J_{av} = 0$  (panel (a)) and  $J_{av} = -1$  (panel (b)), when noise is added into the second equation, eq. (5).

equation, eq. (4), we also performed some simulations where  $\xi_i(t)$  was added instead into the second equation, eq. (5). We did this for  $J_{av} = 0$  and  $J_{av} = -1$ . As expected, the results reported in fig. 5 show that in this case the effect of noise is negligible and the network dynamics is entirely determined by diversity [35].

**Conclusions.** – Our theoretical and numerical analysis shows that, while there are some analogies between diversity- and noise-induced network synchronization, the two effects are substantially different and interact with each other differently, depending on the distance of the mean value of the diversity distribution from the intrinsic oscillatory range of the network elements. Specifically, when the diversity distribution is centered around the intrinsic oscillatory range ( $J_{av} = 0$ ), diversity and noise act independently of one another and there is no indication of a synergy. On the other hand, when the mean value of the diversity distribution is far away from the intrinsic oscillatory range ( $J_{av} = \pm 1$ ), then there is a clear synergy between the two sources of disorder, which determines a major improvement of network synchronization. In addition, in this regime, noise can improve network synchronization more effectively than diversity. This provides useful indications on the relative importance of the two effects in different network configurations, and on the possibility to neglect one or the other as a consequence.

Another important finding is that the optimal diversity value of the network is the same in all regimes, if noise is taken into account. In other words, when noise effects are added, the amount of diversity that maximizes collective oscillatory efficiency seems to be an intrinsic property of the network, independent of  $J_{av}$ .

The fact that diversity and noise are not equivalent sources of disorder, but have distinct effects on the network dynamics, may have implications for biological systems. Our results suggest that different network configurations can lead to a hierarchy between the two sources of disorder. This may have driven the exploitation of diversity and noise to a different degree in different biological systems during their evolution, depending on their specific nature and on the types of signals that trigger their activity.

As a potential future extension of this work, we plan to study and map out the oscillatory activity of individual network units, again as a function of diversity and noise, in order to further understand the underlying synchronization phenomena at a microscopic level.

\*\*\*

The authors acknowledge support from the Estonian Research Council through Grant PRG1059 and the ERDF (European Development Research Fund) CoE (Center of Excellence) program through Grant TK133. The authors would like to thank ALESSANDRO LOPPINI for helpful discussions.

*Data availability statement:* The data that support the findings of this study are available upon reasonable request from the authors.

## REFERENCES

- [1] BENZI R., SUTERA A. and VULPIANI A., *J. Phys. A*, **14** (1981) L453.
- [2] NICOLIS C., *Sol. Phys.*, **74** (1981) 473.
- [3] NICOLIS C., *Tellus*, **34** (1982) 1.
- [4] BENZI R., PARISI G., SUTERA A. and VULPIANI A., *SIAM J. Appl. Math.*, **43** (1983) 565.
- [5] MCNAMARA B., WIESENFELD K. and ROY R., *Phys. Rev. Lett.*, **60** (1988) 2626.
- [6] GAMMAITONI L., MENICHELLA-SAETTA E., SANTUCCI S., MARCHESONI F. and PRESILLA C., *Phys. Rev. A*, **40** (1989) 2114.
- [7] MATTEUCCI G., *Clim. Dyn.*, **3** (1989) 179.
- [8] JUNG P. and HÄNGGI P., *Phys. Rev. A*, **44** (1991) 8032.
- [9] GAMMAITONI L., MARTINELLI M., PARDI L. and SANTUCCI S., *Phys. Rev. Lett.*, **67** (1991) 1799.
- [10] MORI T. and KAI S., *Phys. Rev. Lett.*, **88** (2002) 218101.
- [11] RAO C. V., WOLF D. M. and ARKIN A. P., *Nature*, **420** (2002) 231.
- [12] HEINSALU E., PATRIARCA M. and MARCHESONI F., *Eur. Phys. J. B*, **69** (2009) 19.
- [13] GANG H., DITZINGER T., NING C. Z. and HAKEN H., *Phys. Rev. Lett.*, **71** (1993) 807.
- [14] MURATOV C. B., VANDEN-ELJNDEN E. and E. W., *Phys. D: Nonlinear Phenom.*, **210** (2005) 227.
- [15] YAMAKOU M. E. and JOST J., *EPL*, **120** (2017) 18002.
- [16] PIKOVSKY A. S. and KÜRTHS J., *Phys. Rev. Lett.*, **78** (1997) 775.
- [17] JUNG P. and MAYER-KRESS G., *Phys. Rev. Lett.*, **74** (1995) 2130.
- [18] LIU F. and WANG W., *J. Phys. Soc. Jpn.*, **68** (1999) 3456.
- [19] BUSCH H. and KAISER F., *Phys. Rev. E*, **67** (2003) 041105.
- [20] GAMMAITONI L., HÄNGGI P., JUNG P. and MARCHESONI F., *Rev. Mod. Phys.*, **70** (1998) 223.
- [21] McDONNELL M. D. and ABBOTT D., *PLoS Comput. Biol.*, **5** (2009) e1000348.
- [22] CARTWRIGHT J. H. E., *Phys. Rev. E*, **62** (2000) 1149.
- [23] TESSONE C. J., MIRASSO C. R., TORAL R. and GUNTON J. D., *Phys. Rev. Lett.*, **97** (2006) 194101.
- [24] TORAL R., HERNANDEZ-GARCIA E. and GUNTON J. D., *Int. J. Bifurc. Chaos*, **19** (2009) 3499.
- [25] CHEN H., HOU S. and XIN H., *Phys. A: Stat. Mech. Appl.*, **388** (2009) 2299.
- [26] WU L., ZHU S. and LUO X., *Chaos*, **20** (2010) 033113.
- [27] WU L., ZHU S., LUO X. and WU D., *Phys. Rev. E*, **81** (2010) 061118.
- [28] PATRIARCA M., POSTNOVA S., BRAUN H. A., HERNÁNDEZ-GARCÍA E. and TORAL R., *PLoS Comput. Biol.*, **8** (2012) e1002650.
- [29] TESSONE C. J., SÁNCHEZ A. and SCHWEITZER F., *Phys. Rev. E*, **87** (2013) 022803.
- [30] GRACE M. and HÜTT M.-T., *Eur. Phys. J. B*, **87** (2014) 29.

- [31] PATRIARCA M., HERNÁNDEZ-GARCÍA E. and TORAL R., *Chaos, Solitons & Fractals*, **81** (2015) 567.
- [32] LIANG X., ZHANG X. and ZHAO L., *Chaos*, **30** (2020) 103101.
- [33] KAMAL N. K. and SINHA S., *Pramana J. Phys.*, **84** (2015) 249.
- [34] TESSONE C. J., SCIRÈ A., TORAL R. and COLET P., *Phys. Rev. E*, **75** (2007) 016203.
- [35] DEGLI ESPOSTI BOSCHI C., LOUIS E. and ORTEGA G., *Phys. Rev. E*, **65** (2001) 012901.
- [36] LI Y.-Y., JIA B., GU H.-G. and AN S.-C., *Commun. Theor. Phys.*, **57** (2012) 817.
- [37] LI Y.-Y. and DING X.-L., *Commun. Theor. Phys.*, **62** (2014) 917.
- [38] GASSEL M., GLATT E. and KAISER F., *Phys. Rev. E*, **76** (2007) 016203.
- [39] ZHOU C., KURTHS J. and HU B., *Phys. Rev. Lett.*, **87** (2001) 098101.
- [40] GLATT E., GASSEL M. and KAISER F., *EPL*, **81** (2008) 40004.
- [41] CENCINI M., FALCIONI M., OLBRICH E., KANTZ H. and VULPIANI A., *Phys. Rev. E*, **62** (2000) 427.
- [42] BALDOVIN M., CECCONI F. and VULPIANI A., *Phys. Rev. Res.*, **2** (2020) 043436.
- [43] MORI F. and KORI H., *Proc. Natl. Acad. Sci. U.S.A.*, **119** (2022) e2113620119.
- [44] SCIALLA S., LOPPINI A., PATRIARCA M. and HEINSALU E., *Phys. Rev. E*, **103** (2021) 052211.
- [45] SMOLEN P., RINZEL J. and SHERMAN A., *Biophys. J.*, **64** (1993) 1668.
- [46] SHERMAN A., *Bull. Math. Biol.*, **56** (1994) 811.
- [47] SINGH R., XU J., GARNIER N. G., PUMIR A. and SINHA S., *Phys. Rev. Lett.*, **108** (2012) 068102.
- [48] JEDYNAK M., PONS A. J. and GARCIA-OJALVO J., *Phys. Rev. E*, **97** (2018) 012204.
- [49] DE VRIES G. and SHERMAN A., *J. Theor. Biol.*, **207** (2000) 513.
- [50] PEDERSEN M., *J. Theor. Biol.*, **235** (2005) 1.
- [51] FITZHUGH R., *J. Gen. Physiol.*, **43** (1960) 867.
- [52] FITZHUGH R., *Biophys. J.*, **1** (1961) 445.
- [53] NAGUMO J., ARIMOTO S. and YOSHIZAWA S., *Proc. IRE*, **50** (1962) 2061.
- [54] PERSAUD S. J., HAUGE-EVANS A. C. and JONES P. M., *Chapter 15 - Insulin-Secreting Cell Lines: Potential for Research and Diabetes Therapy*, in *Cellular Endocrinology in Health and Disease*, edited by ULLOA-AGUIRRE A. and CONN P. M. (Academic Press, Boston) 2014, pp. 239–256.
- [55] NASTESKA D. and HODSON D. J., *J. Mol. Endocrinol.*, **61** (2018) R43.
- [56] POZNANSKI R. R. and UMINO O., *Prog. Neurobiol.*, **412** (1997) 273.
- [57] ANDREU E., FERNÁNDEZ E., LOUIS E., ORTEGA G. and SÁNCHEZ-ANDRÁS J. V., *Eur. J. Physiol.*, **439** (2000) 789.
- [58] VRAGOVIĆ I., LOUIS E., DEGLI ESPOSTI BOSCHI C. and ORTEGA G., *Phys. D: Nonlinear Phenom.*, **219** (2006) 111.
- [59] DESAI R. C. and ZWANZIG R., *J. Stat. Phys.*, **19** (1978) 1.



## Appendix 3

### III

M. E. Yamakou, E. Heinsalu, M. Patriarca, and S. Scialla, "Diversity-induced decoherence," *Phys. Rev. E*, vol. 106, p. L032401, 2022



## Diversity-induced decoherence

Marius E. Yamakou<sup>1,\*</sup>, Els Heinsalu<sup>2,†</sup>, Marco Patriarca<sup>2,‡</sup> and Stefano Scialla<sup>2,3,§</sup>

<sup>1</sup>*Department of Data Science, Friedrich-Alexander-Universität Erlangen-Nürnberg, Cauerstr. 11, 91058 Erlangen, Germany*

<sup>2</sup>*National Institute of Chemical Physics and Biophysics - Akadeemia tee 23, 12618 Tallinn, Estonia*

<sup>3</sup>*Department of Engineering, Università Campus Bio-Medico di Roma - Via A. del Portillo 21, 00128 Rome, Italy*



(Received 17 June 2022; accepted 15 August 2022; published 1 September 2022)

We analyze the effect of small-amplitude noise and heterogeneity in a network of coupled excitable oscillators with strong timescale separation. Using mean-field analysis, we uncover the mechanism of a nontrivial effect—*diversity-induced decoherence* (DIDC)—in which heterogeneity modulates the mechanism of self-induced stochastic resonance to inhibit the coherence of oscillations. We argue that DIDC may offer one possible mechanism via which, in excitable neural systems, generic heterogeneity and background noise can synergistically prevent unwanted resonances that may be related to hyperkinetic movement disorders.

DOI: [10.1103/PhysRevE.106.L032401](https://doi.org/10.1103/PhysRevE.106.L032401)

The role of disorder in the dynamics of complex networks has been extensively studied in terms of noise and diversity (i.e., heterogeneity) effects [1–6]. For example, Shibata and Kaneko showed that heterogeneity enhances regularity in the collective dynamics of coupled map lattices, even if each element has chaotic dynamics [7]. Later, Cartwright observed the emergence of collective network oscillations in a cubic lattice of locally coupled and diverse FitzHugh-Nagumo (FHN) units, none of which were individually in an oscillatory state [8]. Tessone *et al.* demonstrated an amplification of the response of a coupled oscillator network to an external signal, driven by an optimal level of heterogeneity of its elements, and named this effect diversity-induced resonance (DIR) [9–18]. Other authors showed that DIR can occur even in the absence of an external forcing [19,20]. Some of these studies concluded that stochastic resonance and DIR are substantially analogous phenomena [9,21] to the point that diversity may be viewed as a form of quenched noise.

Diversity in complex networks dynamics has also been studied in terms of its interaction with noise by introducing both types of disorder in a system. Most of this research highlighted the possibility to amplify resonance effects caused by noise thanks to diversity optimization, and vice versa [22–25]. Recently, Scialla *et al.* [26] showed that the impact of diversity on network dynamics can be significantly different from that of noise and may result in an antagonistic effect, depending on the specific network configuration. At the same time, however, various regions of synergy between the two types of disorder, giving rise to strong resonance effects, were observed. Also, it has been shown that diversity in a network of FHN neurons can enhance coherence resonance (CR) [27], which is a regular response (i.e., a limit cycle behavior) to an optimal noise

amplitude [28], occurring when the system is bounded near the bifurcation thresholds [29,30].

Another form of noise-induced resonance is self-induced stochastic resonance (SISR), which has a different mechanism from CR for the emergence of regular oscillations [31,32]. SISR occurs when a small-amplitude noise perturbing the fast variable of an excitable system with a strong timescale separation results in the onset of coherent oscillations [32,33]. Due to the peculiarity of operating at relatively weak noise, SISR represents a particularly interesting case to study the effects of the interplay between noise and diversity. This is relevant to the potential role of SISR as a signal amplification mechanism in biological systems, given that diversity is inherent to networks of neurons or other cells.

In this Letter, we demonstrate that in contrast to previous literature, showing that network diversity can be optimized to enhance collective behaviors such as synchronization or coherence [7–21,26,27], the effect of diversity on SISR, instead, can only be antagonistic. This indicates that the enhancement or deterioration of a noise-induced resonance phenomenon by diversity strongly depends on the underlying mechanism.

We point out that not only constructive but also destructive resonance effects may have significant biological consequences. For instance, an increasing number of studies on Parkinson's disease [34] indicate that dopaminergic neurons are characterized by a relatively high degree of heterogeneity and disease progression is associated with the death of only one or a few specific dopaminergic neuron subpopulations, leading to a loss of neuron diversity with respect to healthy brain tissues. Thus, the role of diversity in biological systems might be also to inhibit unwanted resonances through compensatory mechanisms between different neuron subtypes, which can result in pathological conditions, if missing.

There is still a very limited understanding of the named phenomena from a complex systems modeling viewpoint, as previous works have focused mostly on systems and conditions that favor constructive resonance effects. In this paper, we uncover a *diversity-induced decoherence* (DIDC)

\*marius.yamakou@fau.de

†els.heinsalu@kbfi.ee

‡marco.patriarca@kbfi.ee

§stefano.scialla@kbfi.ee

mechanism, where, in contrast to its effect on CR, diversity deteriorates the coherence of oscillations due to SISR.

As a paradigmatic model with well-known biological relevance, we study the effects of diversity in a network of globally coupled FHN units [35–37]:

$$\begin{cases} \frac{dv_i}{dt} = v_i(a_i - v_i)(v_i - 1) - w_i \\ \quad + K \sum_{j=1}^N (v_j - v_i) + \eta_i(t) \\ \frac{dw_i}{dt} = \varepsilon(bv_i - cw_i). \end{cases} \quad (1)$$

Here  $(v_i, w_i) \in \mathbb{R}^2$  represent the fast membrane potential and slow recovery current variables of the elements, respectively; the index  $i = 1, \dots, N$  stands for nodes;  $K > 0$  is the synaptic coupling strength;  $0 < \varepsilon \ll 1$  is the timescale separation between  $v_i$  and  $w_i$ ; and  $b, c > 0$  are constant parameters. Diversity is introduced by assigning to each network element  $i$  a different value of  $a_i$ , as specified below. The terms  $\eta_i$  ( $i = 1, \dots, N$ ) are independent Gaussian noises with zero mean, standard deviation  $\sigma_n$ , and correlation function  $\langle \eta_i(t), \eta_j(t') \rangle = \sigma_n^2 \delta_{ij} \delta(t - t')$ . The noise intensity applied to each neuron will be measured by  $\sigma_n$ .

The excitable regime where the network defined by Eq. (1) has a *unique* and *stable* fixed point is the required deterministic state for the occurrence of SISR [38–40]. When  $\eta_i = 0$ , the point  $(v, w) = (0, 0)$  becomes a fixed point of Eq. (1) and is unique if and only if

$$\frac{(a_i - 1)^2}{4} < \frac{b}{c}. \quad (2)$$

For the fixed point  $(v_f, w_f) = (0, 0)$  to be stable, we must have  $\text{tr}J_{ij} < 0$  and  $\det J_{ij} > 0$ , where  $J_{ij}$  is the Jacobian matrix of the linearized Eq. (1). Since  $\varepsilon, c > 0$ , we have  $\text{tr}J_{ij} < 0$  and  $\det J_{ij} > 0$  only if

$$-3v_f^2 + 2(a_i + 1)v_f - a_i < 0. \quad (3)$$

To ensure that the network defined by Eq. (1) lies in the excitable regime required for SISR, in the following we set  $b = 1$  and  $c = 2$ . We also set  $\varepsilon = 0.001$ ,  $K = 0.1$ , and  $N = 100$ . To introduce diversity, the values of  $a_i$  are drawn from a truncated Gaussian distribution in the interval  $a_i \in (0, 1 + \sqrt{2})$ , and are randomly assigned to network elements. The standard deviation  $\sigma_d$  and mean  $a_m$  of the distribution measure diversity and how far the network is from the oscillatory regime (corresponding to  $a_i \leq 0$ ), respectively.

To study the effects of diversity  $\sigma_d$  on SISR analytically, we apply the mean-field approach, introducing the global variables  $V(t) = N^{-1} \sum_{i=1}^N v_i(t)$  and  $W(t) = N^{-1} \sum_{i=1}^N w_i(t)$ . Adapting the method used in Refs. [9,26,41], we set  $v_i = V + \delta_i$  in Eq. (1), alongside the assumptions that  $\sum_{i=1}^N \delta_i \approx 0$ ,  $\sum_{i=1}^N \delta_i^3 \approx 0$ .

We further assume that the standard deviation  $\sigma_d$  of the  $a_i$  distribution is small, allowing the approximation

$$\langle a_i[(V + \delta_i)^2 - (V + \delta_i)] \rangle \approx \langle a_i \rangle \langle (V + \delta_i)^2 - (V + \delta_i) \rangle, \quad (4)$$

where  $\langle \dots \rangle$  denotes an average over the  $N$  neurons. We note that the Gaussian distribution of  $a_i \sim \mathcal{N}(a_m, \sigma_d)$  in the range  $(0, 1 + \sqrt{2})$  is always truncated whenever a given value of  $a_m$

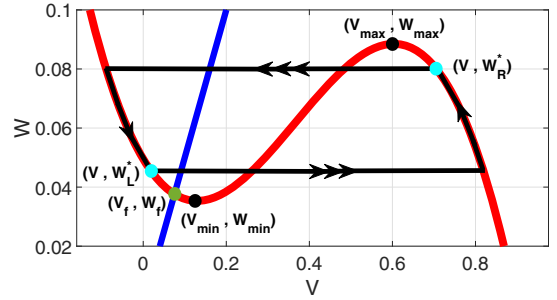


FIG. 1.  $W$  nullcline (blue line) and  $V$  nullcline (red curve) of Eq. (5) intersect at a unique fixed point  $(V_f, W_f)$ . Note that if  $V_f < V_{\min}$ , then  $(V_f, W_f)$  is stable and, in addition, if  $W \in [W_{\min}, W_{\max}]$ , then  $W_f^*, W_f \in [W_{\min}, W_{\max}]$ . The black loop represents a typical stochastic trajectory induced by SISR, where the horizontal parts with triple arrows indicate the fast escape at points  $W_L^*$  and  $W_R^*$  from the left and right stable branches of the  $V$  nullcline, respectively. The almost vertical parts of the trajectory, with single arrow, represent the slow motion of  $W$  governed by Eqs. (6). Note that  $W_L^* > W_f$ .  $A = 0.1$ ,  $M = 0.045$ .

and/or  $\sigma_d$  pushes  $a_i$  out of bounds, especially when  $a_m$  is very close to the boundaries of  $(0, 1 + \sqrt{2})$ .

Using these assumptions and averaging Eq. (1) over the  $N$  neurons, we obtain the following dynamical equations for the global variables  $V$  and  $W$ :

$$\begin{cases} \frac{dV}{dt} = V[(A - V)(V - 1) - 3M] \\ \quad + M(A + 1) - W + \eta_G(t) \\ \frac{dW}{dt} = \varepsilon(bV - cW), \end{cases} \quad (5)$$

where  $M = N^{-1} \sum_{i=1}^N \delta_i^2$  and  $A = N^{-1} \sum_{i=1}^N a_i$ .  $M$  can be considered as a diversity parameter in that it increases with diversity in the network and  $M = 0$  for a homogeneous system ( $\sigma_d = 0$ ). Noise effects are represented by a global white noise term  $\eta_G = N^{-1} \sum_{i=1}^N \eta_i$  with zero mean and correlation function  $\langle \eta_G(t), \eta_G(t') \rangle = N^{-1} \sigma_n^2 \delta(t - t')$ .

When there is no noise in the first equation of Eq. (5),  $\eta_G(t) = 0$ , then in the adiabatic limit  $\varepsilon \rightarrow 0$ , for any initial condition of Eq. (5) the system relaxes to  $V = V_R^*(W)$  and then to  $V = V_L^*(W)$ , where  $V_R^*(W)$  and  $V_L^*(W)$  are the right and left stable branches of the  $V$  nullcline, respectively. Solving  $V[(A - V)(V - 1) - 3M] + M(A + 1) - W = 0$  for  $V$ , we get three real and ordered solutions, namely,  $V_L^*(W) \leq V_S^*(W) \leq V_R^*(W)$ , which are all functions of  $W$ .

Inserting  $V = V_L^*(W)$  and  $V = V_R^*(W)$  in the equation for  $W$  in Eq. (5) gives

$$\begin{cases} \frac{dW}{dt} = \varepsilon[bV_L^*(W) - cW] \\ \frac{dW}{dt} = \varepsilon[bV_R^*(W) - cW]. \end{cases} \quad (6)$$

The first (second) equation of Eq. (6) together with the expression of  $V_L^*(W)$  [ $V_R^*(W)$ ] governs the slow motion of  $W$  down (up) the left (right) stable branch of the  $V$  nullcline (see

Fig. 1) to the leading order arising on the  $O(\varepsilon^{-1})$  timescale when  $\varepsilon \rightarrow 0$ .

Now, if we switch on the noise, i.e.,  $\eta_c(t) \neq 0$  with a small amplitude,  $0 < \sigma_n \ll 1$ , the first equation of Eq. (6) is not valid all the way down to the stable fixed point  $(V_f, W_f)$  [in fact, for SISR to occur, the point  $(V_f, W_f)$  should never be reached, otherwise, the trajectory would be trapped in the basin of attraction of the stable fixed point for a long time, thereby invoking a Poissonian spike train, leading to the nonoccurrence of SISR], which is located on the left stable branch of the  $V$  nullcline, i.e.,  $V_f < V_{\min}$  (see Fig. 1). But the first equation of Eq. (6) still governs the slow motion of  $W$  until the well-defined point  $W_L^* > W_f$ , where a horizontal escape (invoked by noise) of a trajectory from the left stable branch of the  $V$  nullcline occurs.

The same dynamics occur for the second equation of Eq. (6) except that the horizontal escape from the right stable branch of the  $V$  nullcline certainly occurs with or without noise. This is because the right (unlike the left) stable branch of the  $V$  nullcline has no fixed point to trap the trajectories and destroy the regularity of spikes. Thus, our analysis focuses only on the stochastic dynamics of the trajectories on the left stable branch.

To understand the escape mechanism of a trajectory from the left stable branch of the  $V$  nullcline at point  $W_L^*$ , we consider the limit  $\varepsilon \rightarrow 0$ , where the timescale separation between  $V$  and  $W$  becomes very large and Eq. (5) reduces to the 1D Langevin equation:

$$\frac{dV}{dt} = -\frac{\partial U(V, W)}{\partial V} + \eta_c(t). \quad (7)$$

In this limit,  $W$  which comes from the solution of the first equation of Eq. (6) is practically frozen and can be considered as a fixed parameter, its time variation providing only a  $O(\varepsilon)$  contribution to the dynamics governed by Eq. (7). The function  $U(V, W)$  in Eq. (7) is an effective double-well potential parametrically dependent on  $M$ :

$$U(V, W) = \frac{V^4}{4} - \frac{(1+A)}{3}V^3 + \frac{(3M+A)}{2}V^2 - [W - M(1+A)]V. \quad (8)$$

Based on large deviations theory [42,43] and Kramers' law [44], we write for Eq. (5) the generic conditions for the occurrence of SISR in slow-fast dynamical systems in the standard form [45,46] as follows [33,39,47]:

$$\begin{cases} V_f < V_{\min} \\ \lim_{(\sigma_n, \varepsilon) \rightarrow (0,0)} \left[ \frac{\sigma_n^2}{2} \ln(\varepsilon^{-1}) \right] \in (\Delta U^L(W_L^*), \Phi) \\ W_L^* > W_f \\ \Delta U^L(W), \Delta U^R(W) \nearrow W \in [W_{\min}, W_{\max}]. \end{cases} \quad (9)$$

Here,  $(V_{\min}, W_{\min})$  and  $(V_{\max}, W_{\max})$  are, respectively, the minimum and maximum points of the  $V$  nullcline,  $(V_f, W_f)$  is the unique (and stable) fixed point of Eq. (5), and  $W_L^*$  is the value of  $W$  that satisfies the first equation of Eq. (6) and at which the trajectories escape almost surely from the left stable branch of the  $V$  nullcline. The left ( $\Delta U^L(W) \geq 0$ ) and right

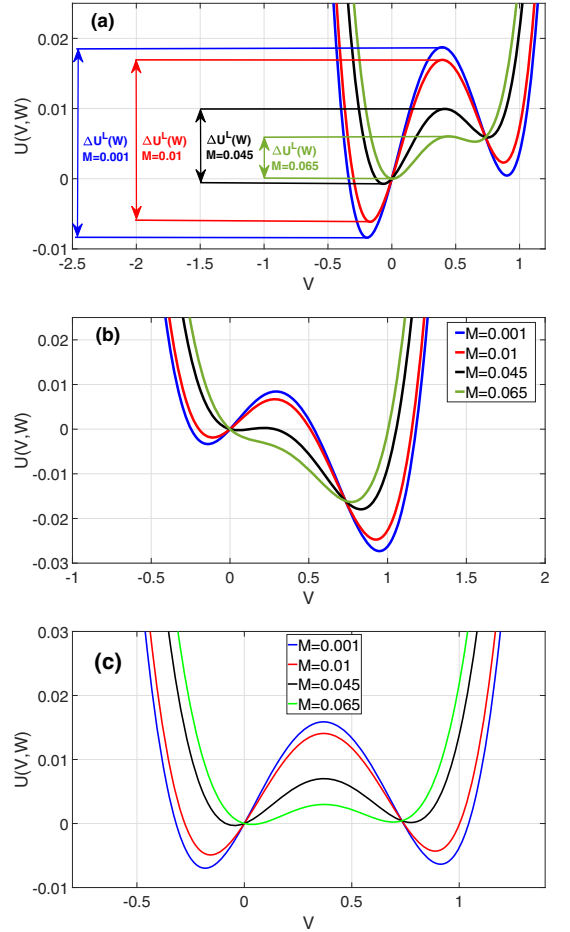


FIG. 2. Landscape of  $U(V, W)$  and energy barriers  $\Delta U^{L,R}(W)$  for different values of  $M$ . (a)  $U(V, W)$  is asymmetric [ $\Delta U^L(W) > \Delta U^R(W)$ ] when  $W (= 0.07) > W_s$ . (b)  $U(V, W)$  is asymmetric [ $\Delta U^L(W) < \Delta U^R(W)$ ] when  $W (= 0.04) < W_s$ . (c)  $U(V, W)$  is symmetric [ $\Delta U^L(W) = \Delta U^R(W)$ ] at  $W_s = 0.0621 > W_f = 0.0376$ .  $A = 0.1$ .

( $\Delta U^R(W) \geq 0$ ) energy barriers of  $U(V, W)$  are

$$\begin{cases} \Delta U^L(W) = U(V_S^*(W), W) - U(V_L^*(W), W) \\ \Delta U^R(W) = U(V_S^*(W), W) - U(V_R^*(W), W), \end{cases} \quad (10)$$

which are both non-negative and monotonic functions of  $W$ , see Fig. 3(a). Figure 2 shows the landscape of  $U(V, W)$  and how  $\Delta U^{L,R}(W)$  varies with  $M$ . We note that the asymmetry of  $U(V, W)$  is governed by  $W$  and the double-well tends to disappear upon increasing  $M$ , resulting in a loss of the bistability required for SISR occurrence.  $\Phi$  represents the intersection point of  $\Delta U^L(W)$  and  $\Delta U^R(W)$  at  $W_s$ , a point at which the two energy barriers are equal to each other. This

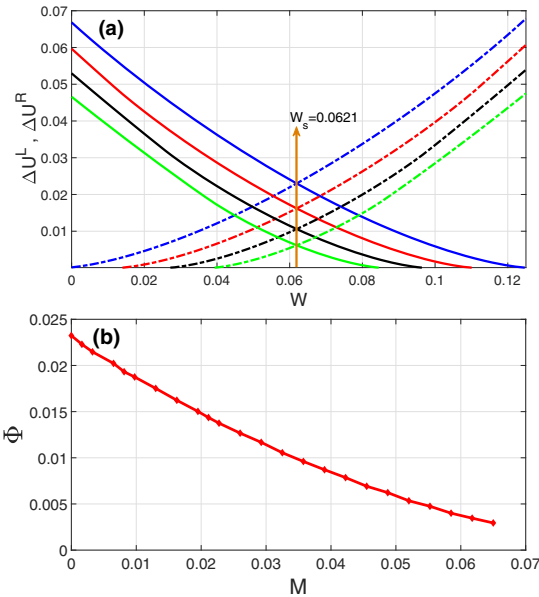


FIG. 3. (a) Variation of  $\Delta U^L$  (dashed lines) and  $\Delta U^R$  (solid lines) versus  $W$  intersecting at  $W = W_s = 0.0621$  for values of  $M = \{0.001, 0.01, 0.045, 0.065\}$  shown in Fig. 2. (b) Variation of  $\Phi$  versus  $M$ .  $A = 0.1$ .

happens when  $U(V, W_s)$  is symmetric at  $W_s > W_f$ , i.e.,

$$\Phi := \{\Delta U^L(W_s) : \Delta U^L(W_s) = \Delta U^R(W_s), W_s > W_f\}. \quad (11)$$

At point  $W_s$ , the escape of a trajectory  $V$  from the left stable branch and from the right stable branch of the  $V$  nullcline are both equally less probable.

In Eq. (9), the first condition ensures that the fixed point is unique and stable; the second condition ensures that a trajectory can escape (almost surely) from the left stable branch of the  $V$  nullcline at the escape point  $W = W_L^*$ ; the third condition ensures that the trajectory escapes before it reaches the stable fixed point, so it does not get trapped into the basin of attraction of this fixed point for too long; and in the fourth condition, the monotonicity of  $\Delta U^L(W)$  and  $\Delta U^R(W)$  in the interval  $[W_{\min}, W_{\max}]$  ensures that the escape points  $W_L^*$  and  $W_R^*$  on the left and right stable branches of the  $V$  nullcline are unique, which would in turn ensure the periodicity of the trajectory leading to coherent spiking.

Since  $W_f$  is the lowest attainable point of a trajectory on the left stable branch of the  $V$  nullcline and the interval  $(\Delta U^L(W_f), \Phi)$  in the second condition in Eq. (9) is open, SISR deteriorates (i.e., the spiking becomes less coherent) and eventually disappears, moving away from the center of the interval. Thus, for a given  $\varepsilon \ll 1$ , we use the boundaries of this interval to calculate the minimum ( $\sigma_n^{\min}$ ) and maximum ( $\sigma_n^{\max}$ ) noise intensity between which the highest degree of SISR can be achieved:

$$\sigma_n^{\min} = \sqrt{\frac{2\Delta U^L(W_f)}{\ln(\varepsilon^{-1})}}, \quad \sigma_n^{\max} = \sqrt{\frac{2\Phi}{\ln(\varepsilon^{-1})}}. \quad (12)$$

The quantities  $\sigma_n^{\min}$  and  $\sigma_n^{\max}$  have a dependence on the diversity parameter  $M$  through  $U(V, W)$  and  $V_{L,S,R}^*(W)$ . Thus, the length of the interval  $(\sigma_n^{\min}, \sigma_n^{\max})$  can be controlled by  $M$ . It is worth noting that when  $\sigma_n = 0$ , diversity alone cannot induce SISR. This is because no single neuron in the network can spike as long as the excitability parameter (which is also the heterogeneity parameter)  $a_i \sim \mathcal{N}(a_m, \sigma_d)$  lies in  $(0, 1 + \sqrt{2})$ , i.e., the excitable regime.

The occurrence of SISR depends on whether the parameter values of the system, including  $M$ , satisfy the four conditions Eq. (9) in the double limit  $(\sigma_n, \varepsilon) \rightarrow (0, 0)$ . Hence, it suffices to study the variation of  $\Phi$  versus  $M$  to uncover the effect of diversity on the degree of SISR. This is done in Fig. 3, showing that  $\Phi$  decreases upon increasing  $M$ . Thus, DDC occurs when diversity in the network increases, leading to a deterioration and eventually destruction of the coherence of the spike train due to SISR, by shrinking the length of the interval  $(\sigma_n^{\min}, \sigma_n^{\max})$  toward zero.

We corroborate the theoretical analysis via numerical simulations. We numerically integrate Eq. (1) for  $N = 100$  neurons using the fourth-order Runge-Kutta algorithm for stochastic processes [48] and the Box-Muller algorithm [49]. The integration time step is  $dt = 0.01$  and the total simulation time is  $T = 1.5 \times 10^6$ . For each realization, we choose for the  $i$ th neuron random initial conditions  $[v_i(0), w_i(0)]$ , with uniform probability in the ranges  $v_i(0) \in (-1, 1)$  and  $w_i(0) \in (0.2, 1)$ . After an initial transient time  $T_0 = 2.5 \times 10^5$ , we start recording the neuron spiking times  $t_i^\ell$  ( $\ell \in \mathbb{N}$  counts the spiking times). Averages are taken over 15 realizations, which warrant appropriate statistical accuracy.

We illustrate the effect of diversity, synaptic noise, and distance of the excitable network from the oscillatory regime, measured by  $\sigma_d$ ,  $\sigma_n$ , and  $a_m$ , respectively, on the degree of coherence of the spikes induced by SISR. We use the coefficient of variation (cv) given by the normalized standard deviation of the mean interspike interval (ISI) [28]. For  $N$  coupled neurons, the cv is given by [50]

$$\text{cv} = \frac{\sqrt{\langle \tau^2 \rangle - \langle \tau \rangle^2}}{\langle \tau \rangle}, \quad (13)$$

where  $\langle \tau \rangle = N^{-1} \sum_{i=1}^N \langle \tau_i \rangle$  and  $\langle \tau^2 \rangle = N^{-1} \sum_{i=1}^N \langle \tau_i^2 \rangle$ , with  $\langle \tau_i \rangle$  and  $\langle \tau_i^2 \rangle$  representing the mean and mean squared ISI (over time),  $\tau_i = t_i^{\ell+1} - t_i^\ell > 0$ , of neuron  $i$ .

We determine the spike occurrence times from the instant the membrane potential variable  $v_i$  crosses the threshold  $v_{\text{th}} = 0.3$ . The cv will be higher the more variable the mean ISIs are. Thus, since Poisson spike train events are independent and all have a normalized standard deviation of unity (i.e.,  $\text{cv} = 1$ ), they can be used as reference for the average variability of spike trains of the network [51]. When  $\text{cv} > 1$ , the average variability of spike trains of the network is higher than a Poisson process. When  $\text{cv} < 1$ , the average spiking activity of the network becomes more coherent, with  $\text{cv} = 0$  corresponding to perfectly periodic spike trains. The degree of coherence is illustrated in Fig. 4, which depicts cv against the synaptic noise  $\sigma_n$  and diversity parameter  $\sigma_d$  at two different values of  $a_m$ .

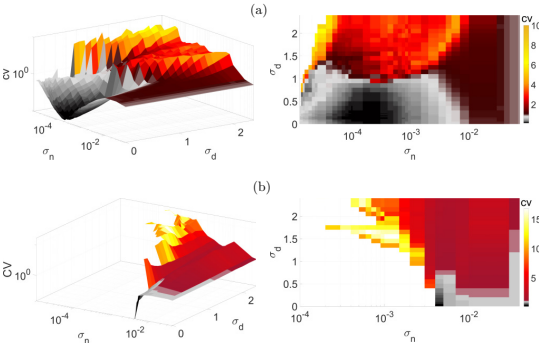


FIG. 4. (a)  $cv$  versus  $\sigma_n$  and  $\sigma_d$  in 3D with the 2D projection onto  $(\sigma_n, \sigma_d)$  plane when  $a_m = 0.05$ . (b)  $cv$  versus  $\sigma_n$  and  $\sigma_d$  in 3D with the 2D projection onto  $(\sigma_n, \sigma_d)$  plane when  $a_m = 1.2$ . In both panels, the black and grey colors indicate values of  $cv < 1$ . Larger values of  $\sigma_d$  inhibit SISR leading to larger  $cv$  values.

In Fig. 4(a), the mean value  $a_m = 0.05$  is close to the lower bound of the interval  $(0, 1 + \sqrt{2})$ , i.e., close to the oscillatory regime. It can be observed that when  $\sigma_n \in [10^{-4}, 10^{-3}]$  and  $\sigma_d \in [0.0001, 0.7]$ , we have a low  $cv \in [0.107, 0.207]$ , indicating a high degree of coherence due to SISR. For  $\sigma_d > 0.7$ , the  $\sigma_n$  interval in which  $cv < 0.207$  has shrunk to zero, i.e.,  $cv \geq 0.276$  for all  $\sigma_n$  values, indicating a significant deterioration and eventual destruction of the coherence as  $\sigma_d$  increases.

In Fig. 4(b), the mean of the diversity distribution is fixed at a higher value  $a_m = 1.2$ . In this case, the unique fixed point  $(v_f, w_f) = (0, 0)$  becomes even more stable than in Fig. 4(a). Small diversities  $\sigma_d \in [0.0001, 0.3]$  and weak synaptic noise intensities  $\sigma_n < 6 \times 10^{-3}$  are not strong enough to induce spiking; thus the network remains inactive and the value of  $cv$  is undefined.

For  $\sigma_n < 9 \times 10^{-4}$  and  $\sigma_d > 2$ , neurons respond differently to the synaptic noise due to the diverse strengths of the excitable regimes. Due to the all-to-all coupling in the network, the large diversity boosts the weak synaptic noise, leading to the production of spikes. However, because the diversity is large, the conditions required for SISR are violated and the spikes produced are incoherent—see in Fig. 4(b) the yellow region bounded by  $\sigma_n < 9 \times 10^{-4}$  and  $\sigma_d \in [1.7, 2.4]$ ,

where  $cv > 1.5$ . At a relatively stronger synaptic noise intensity, i.e.,  $\sigma_n = 4 \times 10^{-3}$  and a very small diversity of  $\sigma_d = 0.001$ , the degree of coherence due to SISR is best and  $cv = 0.14$ . As  $\sigma_d$  increases while the synaptic noise is fixed at  $\sigma_n = 4 \times 10^{-3}$ , the degree of SISR deteriorates and  $cv > 1$ .

The results in Fig. 4 were obtained for a specific value of the time scale parameter ( $\varepsilon = 0.001$ ), which is a crucial parameter for SISR. Moreover, additional simulations performed for other values of  $\varepsilon \ll 1$  and  $K \in (0.025, 1.0)$  (not shown) lead to qualitatively similar results.

In conclusion, we have provided evidence that there are complex network configurations and parameter regimes where diversity can only cause a deterioration of well-known resonance phenomena, such as SISR. This is predicted by our mean field analysis and confirmed by numerical simulations.

The decoherence effect appears as soon as there is a minimal degree of diversity in the system and rapidly grows up to a complete resonance muting as diversity increases. The basic mechanism of this effect is that diversity causes a partial or complete disappearance of the energy barrier in the mean field double-well potential, responsible for the coherent spiking corresponding to SISR. The fact that in this system diversity cannot be optimized to enhance coherence, but can only disrupt it, is a nontrivial result. This is because the possibility to adjust diversity to amplify collective network behaviors has been previously demonstrated across a broad range of network types, configurations, and conditions and is, therefore, a very general phenomenon [7–21,26].

We have illustrated the effect of DIDC in a prototypical excitable model network, which suggests that the effect may be common to other physical, chemical, and biological systems. Based on our analysis and on experimental evidence that a neuron diversity loss can be associated to hyperkinetic disorders characterized by involuntary movements, we hypothesize that diversity may be used in biological systems not only to amplify weak signals, as suggested by previous literature, but also as an efficient control mechanism to prevent undesired resonances.

M.E.Y acknowledges support from the Deutsche Forschungsgemeinschaft (DFG, German Research Foundation) – Project No. 456989199. E.H., M.P. and S.S. acknowledge support from the Estonian Research Council through Grant No. PRG1059.

- [1] P. Jung and G. Mayer-Kress, *Phys. Rev. Lett.* **74**, 2130 (1995).
- [2] F. Liu and W. Wang, *J. Phys. Soc. Jpn.* **68**, 3456 (1999).
- [3] H. Busch and F. Kaiser, *Phys. Rev. E* **67**, 041105 (2003).
- [4] L. Gammaitoni, P. Hänggi, P. Jung, and F. Marchesoni, *Rev. Mod. Phys.* **70**, 223 (1998).
- [5] M. D. McDonnell and D. Abbott, *PLoS Comput. Biol.* **5**, e1000348 (2009).
- [6] T. Pérez, C. R. Mirasso, R. Toral, and J. D. Gunton, *Philos. Trans. R. Soc. A* **368**, 5619 (2010).
- [7] T. Shibata and K. Kaneko, *Europhys. Lett.* **38**, 417 (1997).
- [8] J. H. E. Cartwright, *Phys. Rev. E* **62**, 1149 (2000).
- [9] C. J. Tessone, C. R. Mirasso, R. Toral, and J. D. Gunton, *Phys. Rev. Lett.* **97**, 194101 (2006).
- [10] R. Toral, E. Hernandez-García, and J. D. Gunton, *Int. J. Bifurcation Chaos* **19**, 3499 (2009).
- [11] H. Chen, Z. Hou, and H. Xin, *Physica A* **388**, 2299 (2009).
- [12] L. Wu, S. Zhu, and X. Luo, *Chaos* **20**, 033113 (2010).
- [13] L. Wu, S. Zhu, X. Luo, and D. Wu, *Phys. Rev. E* **81**, 061118 (2010).
- [14] M. Patriarca, S. Postnova, H. A. Braun, E. Hernández-García, and R. Toral, *PLoS Comput. Biol.* **8**, e1002650 (2012).

- [15] C. J. Tessone, A. Sánchez, and F. Schweitzer, *Phys. Rev. E* **87**, 022803 (2013).
- [16] M. Grace and M.-T. Hütt, *Eur. Phys. J. B* **87**, 29 (2014).
- [17] M. Patriarca, E. Hernández-García, and R. Toral, *Chaos, Solitons & Fractals* **81**, 567 (2015).
- [18] X. Liang, X. Zhang, and L. Zhao, *Chaos* **30**, 103101 (2020).
- [19] N. K. Kamal and S. Sinha, *Pramana* **84**, 249 (2015).
- [20] S. Scialla, A. Loppini, M. Patriarca, and E. Heinsalu, *Phys. Rev. E* **103**, 052211 (2021).
- [21] C. J. Tessone, A. Scire, R. Toral, and P. Colet, *Phys. Rev. E* **75**, 016203 (2007).
- [22] C. D. E. Boschi, E. Louis, and G. Ortega, *Phys. Rev. E* **65**, 012901 (2001).
- [23] Y.-Y. Li, B. Jia, H.-G. Gu, and S.-C. An, *Commun. Theor. Phys.* **57**, 817 (2012).
- [24] Y.-Y. Li and X.-L. Ding, *Commun. Theor. Phys.* **62**, 917 (2014).
- [25] M. Gassel, E. Glatt, and F. Kaiser, *Phys. Rev. E* **76**, 016203 (2007).
- [26] S. Scialla, M. Patriarca, and E. Heinsalu, *Europhys. Lett.* **137**, 51001 (2022).
- [27] C. Zhou, J. Kurths, and B. Hu, *Phys. Rev. Lett.* **87**, 098101 (2001).
- [28] A. S. Pikovsky and J. Kurths, *Phys. Rev. Lett.* **78**, 775 (1997).
- [29] A. Neiman, P. I. Saporin, and L. Stone, *Phys. Rev. E* **56**, 270 (1997).
- [30] Z.-Q. Liu, H.-M. Zhang, Y.-Y. Li, C.-C. Hua, H.-G. Gu, and W. Ren, *Physica A* **389**, 2642 (2010).
- [31] R. E. Lee DeVilleville, E. Vanden-Eijnden, and C. B. Muratov, *Phys. Rev. E* **72**, 031105 (2005).
- [32] M. E. Yamakou and J. Jost, *Phys. Rev. E* **100**, 022313 (2019).
- [33] C. B. Muratov, E. Vanden-Eijnden, and E. Weinan, *Physica D* **210**, 227 (2005).
- [34] D. M. Vogt Weisenhorn, F. Giesert, and W. Wurst, *J. Neurochem.* **139**, 8 (2016).
- [35] R. Fitzhugh, *J. Gen. Physiol.* **43**, 867 (1960).
- [36] R. FitzHugh, *Biophys. J.* **1**, 445 (1961).
- [37] J. Nagumo, S. Arimoto, and S. Yoshizawa, *Proc. IRE* **50**, 2061 (1962).
- [38] R. L. DeVilleville and E. Vanden-Eijnden, *Commun. Math. Sci.* **5**, 431 (2007).
- [39] M. E. Yamakou and J. Jost, *Nonlinear Dynamics* **93**, 2121 (2018).
- [40] M. E. Yamakou, P. G. Hjorth, and E. A. Martens, *Front. Comput. Neurosci.* **14**, 62 (2020).
- [41] R. C. Desai and R. Zwanzig, *J. Stat. Phys.* **19**, 1 (1978).
- [42] M. I. Freidlin, *J. Stat. Phys.* **103**, 283 (2001).
- [43] M. Freidlin, *Stochastics and Dynamics* **01**, 261 (2001).
- [44] H. A. Kramers, *Physica* **7**, 284 (1940).
- [45] M. E. Yamakou, Weak-noise-induced phenomena in a slow-fast dynamical system, Ph.D. thesis, Max Planck Institute for Mathematics in the Sciences, Max Planck Society, 2018.
- [46] C. Kuehn, *Multiple Time Scale Dynamics* (Springer, Berlin, 2015), Vol. 191.
- [47] R. DeVilleville and E. Vanden-Eijnden, *J. Stat. Phys.* **126**, 75 (2007).
- [48] N. J. Kasdin, *J. Guid. Control. Dyn.* **18**, 114 (1995).
- [49] D. E. Knuth, *The Art of Computer Programming*, Fundamental Algorithms, Vol. 1, 3rd ed. (Addison-Wesley, Boston, MA, 1997).
- [50] M. Masoliver, N. Malik, E. Schöll, and A. Zakharova, *Chaos* **27**, 101102 (2017).
- [51] F. Gabbiani and C. Koch, Principles of spike train analysis, in *Methods in Neuronal Modeling From Ions to Networks*, edited by C. Koch and I. Segev (The MIT Press, Cambridge, MA, 1998), p.313.

## Appendix 4

### IV

M. Patriarca, S. Scialla, E. Heinsalu, M. E. Yamakou, and J. H. E. Cartwright, "Dynamical equivalence between resonant translocation of a polymer chain and diversity-induced resonance," *Chaos*, vol. 35, p. 073115, 2025



# Dynamical equivalence between resonant translocation of a polymer chain and diversity-induced resonance

Cite as: *Chaos* 35, 073115 (2025); doi: 10.1063/5.0262633

Submitted: 2 February 2025 · Accepted: 13 June 2025 ·

Published Online: 7 July 2025



Marco Patriarca,<sup>1,2,a)</sup> Stefano Scialla,<sup>1,3</sup> Els Heinsalu,<sup>1</sup> Marius E. Yamakou,<sup>4</sup> and Julyan H. E. Cartwright<sup>5,6</sup>

## AFFILIATIONS

<sup>1</sup>National Institute of Chemical Physics and Biophysics, Akadeemia Tee 23, 12618 Tallinn, Estonia

<sup>2</sup>Department of Cybernetics, Tallinn University of Technology, Ehitajate Tee 5, 19086 Tallinn, Estonia

<sup>3</sup>Department of Science and Technology for Sustainable Development and One Health, Università Campus Bio-Medico di Roma, Via Á. del Portillo 21, 00128 Rome, Italy

<sup>4</sup>Department of Data Science, Friedrich-Alexander-Universität Erlangen-Nürnberg, Cauerstr. 11, 91058 Erlangen, Germany

<sup>5</sup>Instituto Andaluz de Ciencias de la Tierra, CSIC, 18100 Armilla, Spain

<sup>6</sup>Instituto Carlos I de Física Teórica y Computacional, Universidad de Granada, 18071 Granada, Spain

<sup>a)</sup> Author to whom correspondence should be addressed: [marco.patriarca@gmail.com](mailto:marco.patriarca@gmail.com)

## ABSTRACT

Networks of heterogeneous oscillators are often seen to display collective synchronized oscillations, even when single elements of the network do not oscillate in isolation. It has been found that it is the diversity of the individual elements that drives the phenomenon, possibly leading to the appearance of a resonance in the response. Here, we study the way in which heterogeneity acts in producing an oscillatory regime in a network and show that the resonance response is based on the same physics underlying the resonant translocation regime observed in models of polymer diffusion on a substrate potential. Such a mechanical analog provides an alternative viewpoint that is useful to interpret and understand the nature of collective oscillations in heterogeneous networks.

Published under an exclusive license by AIP Publishing. <https://doi.org/10.1063/5.0262633>

Many networks of cells in the human body, including neurons,<sup>1</sup>  $\beta$ -cells in the pancreatic islets of Langerhans,<sup>2</sup> and the cardiomyocytes of the heart muscle,<sup>3</sup> present synchronized electrical oscillations. Likewise, other collectives of bio-oscillators show synchronized oscillations, populations of fireflies being a prominent example.<sup>4</sup> In the case of  $\beta$ -cells in the pancreas, responsible for the pulsatile release of the hormone insulin, isolated cells do not oscillate or present irregular oscillation patterns,<sup>5</sup> a fact that points to some collective effect at the origin of the observed coherent oscillations. Collective effects are known to be fundamental for the concerted working of neurons as well,<sup>6</sup> and also in the case of heart cells, the role of non-oscillating cells has been recently revisited.<sup>3</sup> Building on related previous work motivated by the applications to  $\beta$ -cell networks,<sup>7–9</sup> the goal of the present article is to revisit some simple models of heterogeneous networks of nonlinear oscillators, such as FitzHugh–Nagumo (FN) and quartic oscillators, and show their dynamical equivalence to a problem from a very different area of science, the dynamics of a polymer on

a one-dimensional substrate. This equivalence provides an intuitive interpretation of the mechanisms and a simple formulation of the conditions for the appearance of collective oscillations.

## I. INTRODUCTION

Understanding the mechanisms underlying synchronization in networks of nonlinear oscillators is an active field of research with numerous applications.<sup>10,11</sup> In particular, networks of oscillators have a crucial role in modeling many biological systems. The human body, for example, contains multiple different networks of cells, including neurons,<sup>1</sup>  $\beta$ -cells in the pancreatic islets of Langerhans,<sup>2</sup> and the cardiomyocytes of the heart muscle,<sup>3</sup> all of which present synchronized electrical oscillations.

The origin of the oscillations in  $\beta$ -cell networks<sup>2</sup> is a longstanding question still without a complete answer. Various theoretical works have suggested that the heterogeneity of  $\beta$ -cells in the

islets of Langerhans has a key role in producing coherent oscillations. The complexity of the problem is enhanced by the fact that the consequences of heterogeneity can be very different, ranging from the appearance of synchronization to the inhibition of the coherence of oscillations.<sup>12</sup> The possible effects of heterogeneity on initiating oscillations were pointed out in Ref. 13, where it was shown that diversifying the parameters of a Chay–Keizer model of  $\beta$ -cell dynamics<sup>14</sup> can lead to synchronized oscillations, whereas the corresponding homogeneous model does not present oscillations. However, the general meaning of this fact in relation to complex and dynamical systems remained unexplored.

The heterogeneous  $\beta$ -cell network model introduced in Ref. 7 is based on coupled FitzHugh–Nagumo (FN) oscillators of two different types, characterized by a fixed forcing parameter  $f$  that can assume one of the two possible values, either  $f_1$  or  $f_2$ . In this minimal model, synchronization can appear when some diversity is introduced in the system, as an emergent process induced by the interactions between these two different types of cells for suitable values of the coupling constant—whereas the corresponding homogeneous system made up of identical cells would remain in a non-oscillatory state—as observed experimentally;<sup>5</sup> synchronization shows a sharp resonance around a specific strength of coupling between the oscillators.

Another model presenting the appearance of heterogeneity-induced oscillations assigns cells a set of values of the forcing parameter distributed according to a continuum Gaussian distribution.<sup>15</sup> This model revealed the existence of an optimal level of diversity, quantified, e.g., by the standard deviation of the Gaussian distribution, at which the network presents the highest coherent response, a phenomenon named diversity-induced resonance (DIR). Both models present heterogeneity-induced oscillations and a clear resonant behavior of synchronization as some parameters are varied but using different prescriptions for diversifying the parameters of the oscillators. Whether the effects induced by a Gaussian distribution<sup>15</sup> and a two-value distribution of the bias forces<sup>7</sup> are equivalent or related to each other is still an open problem.

Considering the question from a general dynamical perspective, the first approach to the diversification of the parameters, using a continuum distribution, emphasizes the analogy between DIR and stochastic resonance,<sup>15,16</sup> while the second approach, using a two-value distribution, points to some simple underlying process. We show that such a process exists and coincides with the resonance effect of a dimer diffusing on a periodic substrate potential: The dimer attains an optimal diffusion rate at a suitable equilibrium rest length (distance between monomers).<sup>17–19</sup> We propose to call such an effect dimer-diffusion resonance (DDR). As we will discuss, DDR can be generalized straightforwardly to the case of a polymer, and in that case, it represents the basis of a simple mechanical analog of the appearance of DIR in an oscillator network. The DDR mechanism and its extension to polymers are general in nature and are expected to act in a wide category of systems and under different conditions.

## II. QUARTIC OSCILLATORS

In this section, we study the synchronization of a heterogeneous network of quartic oscillators. The results obtained can be

directly reapplied also to the case of FN oscillators, considered in Sec. III D.

### A. Dynamical equations

Consider a network of  $N$  linearly coupled quartic oscillators evolving according to the equation

$$\dot{x}_i = -V'(x_i) + f(t) + C \sum_{j \in \mathcal{N}(i)} (x_j - x_i) + a_i, \quad (1)$$

where  $i = 1, \dots, N$ . The sum in Eq. (1) represents the interactions between the generic oscillator  $i$  and the other oscillators, where a linear coupling of strength  $C$  is assumed, extending over the set of oscillators  $j \in \mathcal{N}(i)$  that interact with oscillator  $i$ . With  $V(x)$ , we denote a symmetric double-well potential and  $f(t)$  is an external time-periodic forcing. In addition,  $a_i$  stands for a diversified constant bias force acting on the  $i$ th oscillator.

Equation (1) has the same form as the equations that describe  $N$  overdamped coupled particles with coordinates  $x_i$ , moving in an oscillating potential  $V(x) - f(t)x$ , and subject to constant diversified biases  $a_i$ . Assuming a suitable rescaling of the space and time coordinates, the potential  $V(x)$  in the present case has the following symmetric form:

$$V(x) = -\frac{1}{2}x^2 + \frac{1}{4}x^4, \quad (2)$$

with a maximum  $V(x=0) = 0$  and two minima  $V(x = \pm 1) = -1/4$ .

In contrast to excitable oscillators, e.g., FitzHugh–Nagumo (FN) oscillators, quartic oscillators do not exhibit spontaneous oscillations. In order to produce an oscillatory regime, a periodic forcing  $f(t)$  is added, with a simple sinusoidal form, an amplitude  $b$ , and a time period  $\tau = 2\pi/\omega$ ,

$$f(t) = b \sin(\omega t). \quad (3)$$

In the following, we keep the amplitude  $b$  constant and small enough that an isolated oscillator cannot oscillate, i.e., the effective potential  $[V(x) - xf(t)]$  maintains two minima at any time  $t$ . We are interested in determining under which conditions a coupling between the oscillators together with a level of diversification in the set of bias forces  $a_i$  induces the appearance of global oscillations in an otherwise silent network. To make comparisons consistent with the case of isolated oscillators, for any choice of biases  $\{a_i\}$ , we assume a zero-mean bias  $\langle a \rangle = \sum_i a_i/N \equiv 0$ .

### B. Effects of diversification on a fully connected network

As discussed in the Introduction, two possible means of diversification that can induce an oscillatory regime are as follows: (a) The zero-mean Gaussian distribution  $P_1(a)$  with standard deviation  $\sigma = \sigma_a$  (used in the study of DIR<sup>15</sup>),

$$P_1(a) = \frac{1}{\sqrt{2\pi}\sigma_a} \exp\left(-\frac{a^2}{2\sigma_a^2}\right), \quad (4)$$

(b) the two-value zero-mean distribution  $P_2(a)$ , with standard deviation  $\sigma = \bar{a}$ , that assigns to the oscillators either a bias  $a = -\bar{a}$  or

$a = +\bar{a}$  (used in Ref. 7),

$$P_2(a) = \frac{1}{2} [\delta(a + \bar{a}) + \delta(a - \bar{a})], \quad (5)$$

where  $\delta(\cdot)$  is the Dirac delta function.

In the following, we explore the response of an all-to-all connected network of  $N$  quartic oscillators to a bimodal distribution of bias forces  $a_i$ . The distribution is assumed to be the superposition of two Gaussian distributions  $P_{\pm}(a)$  with mean values  $\pm\bar{a}$  and with the same standard deviation  $\sigma_a$ ,

$$P(a) = \frac{1}{2}[P_-(a) + P_+(a)] \\ \equiv \frac{1}{2\sqrt{2\pi\sigma_a^2}} \left\{ \exp\left[-\frac{(a + \bar{a})^2}{2\sigma_a^2}\right] + \exp\left[-\frac{(a - \bar{a})^2}{2\sigma_a^2}\right] \right\}. \quad (6)$$

The distribution  $P(a)$  is symmetric with respect to  $a = 0$  and has the mean value  $\langle a \rangle = 0$ . For generic values  $\bar{a}, \sigma_a > 0$ , the distribution  $P(a)$  represents a hybrid diversification strategy that is intermediate between  $P_1(a)$  and  $P_2(a)$ . For  $\bar{a} \rightarrow 0$ , the distribution  $P(a)$  reduces to the zero-mean normal distribution  $P_1(a)$  given by Eq. (4), while for  $\sigma_a \rightarrow 0$ , it becomes the two-point distribution  $P_2(a)$  given by Eq. (5). An example of the distribution  $P(a)$  can be seen in Fig. 1. The standard deviation of this bimodal distribution is  $\sigma = \sqrt{\bar{a}^2 + \sigma_a^2}$ ; for  $\bar{a} \rightarrow 0$ , it reduces to  $\sigma = \sigma_a$  of the Gaussian distribution, while for  $\sigma_a \rightarrow 0$ , it reduces to  $\sigma = \bar{a}$  of the bimodal distribution (thus, the parameter  $\bar{a}$  represents both the absolute value of the modes and the standard deviation of the bimodal distribution).

We consider as a working example the all-to-all connected network topology that allows a clear comparison with the results obtained in Ref. 15 for DIR; we study its response to the bimodal

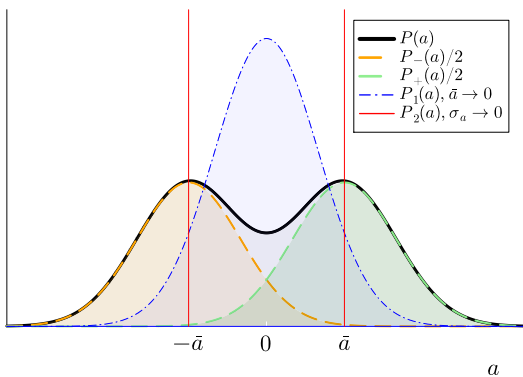


**FIG. 1.** Example of bimodal bias distribution function  $P(a)$  (black curve) for  $\sigma_a/\bar{a} = 2/3$ , resulting from the superposition of the partial bias distribution functions  $\frac{1}{2}P_{\pm}(a)$  of the two different types of oscillators (orange and green dashed curves)—these distributions are defined in Eq. (6). For comparison, we draw also the limiting Gaussian distribution function  $P_1(a)$  (blue dotted-dashed curve), given by Eq. (4), obtained for  $\bar{a} \rightarrow 0$  keeping the standard deviation  $\sigma_a$  constant, and the two-value  $\delta$ -distribution function  $P_2(a)$  (visualized as two red vertical lines), given by Eq. (5), obtained for  $\sigma_a \rightarrow 0$  keeping  $\bar{a}$  constant.

bias distribution  $P(a)$  in the  $\bar{a}$ - $\sigma_a$  plane of the standard deviations of the two limiting distributions given by Eq. (4), used for inducing DIR,<sup>15</sup> and the two-value distribution (5), used in Ref. 7 to induce collective oscillations in an excitable medium. In this way, we can address the question, how different ways to diversify the constant bias forces  $a_i$  affect the synchronization properties of the oscillator network and provide clues about the origin of the oscillatory regime.

We explore a fully connected network of  $N = 100$  quartic oscillators assuming the following parameter values: Rescaled coupling  $C = c/N = 0.01$ , when choosing  $c = 1$ ; tilting amplitude  $b = 0.2$  and tilting period  $2\pi/\omega = 200.0$ ; average bias  $\langle a \rangle = \sum_i a_i/N = 0$ .

We measure the global response of the system through the quantity  $\langle \delta X(t)^2 \rangle$ , representing a mean square deviation of the oscillator coordinates averaged in time and over the system oscillators,

$$\langle \delta X(t)^2 \rangle = \frac{1}{t} \int_0^t ds [X(s) - \langle X(s) \rangle]^2, \quad (7)$$

where

$$X(t) = \frac{1}{N} \sum_i x_i(t), \quad \langle X(t) \rangle = \frac{1}{t} \int_0^t ds X(s). \quad (8)$$

In the case of quartic oscillators and for FN oscillators discussed in Sec. III D,  $\langle X(t) \rangle$  converges to zero in the long time limit.

The behavior of  $\langle \delta X(t)^2 \rangle$  in the  $(\bar{a}, \sigma_a)$ -plane is shown in Fig. 2(a). The DIR response of the system is obtained in the limit  $\bar{a} \rightarrow 0$  and corresponds to the (blue) tick isoline at  $\bar{a} = 0$ . Instead, in the limit  $\sigma_a = 0$ , the corresponding tick (red) isoline represents the response of the oscillator network to the two-point distribution of the bias  $a$ .

A relevant feature of the responses depicted in Fig. 2(a) is that the isolines obtained in the limiting cases  $\bar{a} \rightarrow 0$  and  $\sigma_a \rightarrow 0$  are qualitatively similar to each other. Their direct comparison in Fig. 2(c) shows that both the curves present a (resonance) peak at the common value  $\sigma_a = \bar{a} \approx 1/2$ . Considering that the two curves were obtained using different diversification procedures and are defined using different variables, their similarity suggests a common underlying origin of the respective resonances. At the same time, there are some important differences, namely, the red isoline at  $\sigma_a \approx 0$  is sharper, suggesting the existence of a well-defined resonant condition, while the tail of the blue isoline at  $\bar{a} = 0$  is broader, a fact that is discussed below.

### III. OSCILLATOR NETWORK AS A POLYMER

#### A. Dimer-diffusion resonance

In general, the phenomenon of DIR is based on assigning a (Gaussian) distribution of parameters to the single oscillators, and, thus, it is not obvious how to define it for small  $N$ . However, it is possible to diversify the constant bias forces even in a small system by assigning to each pair of oscillators  $i$  and  $j$  opposite biases  $a_i = -\bar{a}$  and  $a_j = +\bar{a}$ . This remains valid even in the minimal case of a single pair of oscillators ( $N = 2$ ) described by the equations

$$\dot{x}_1 = -V(x_1) + f(t) + C(x_2 - x_1) - \bar{a}, \\ \dot{x}_2 = -V(x_2) + f(t) - C(x_2 - x_1) + \bar{a}, \quad (9)$$

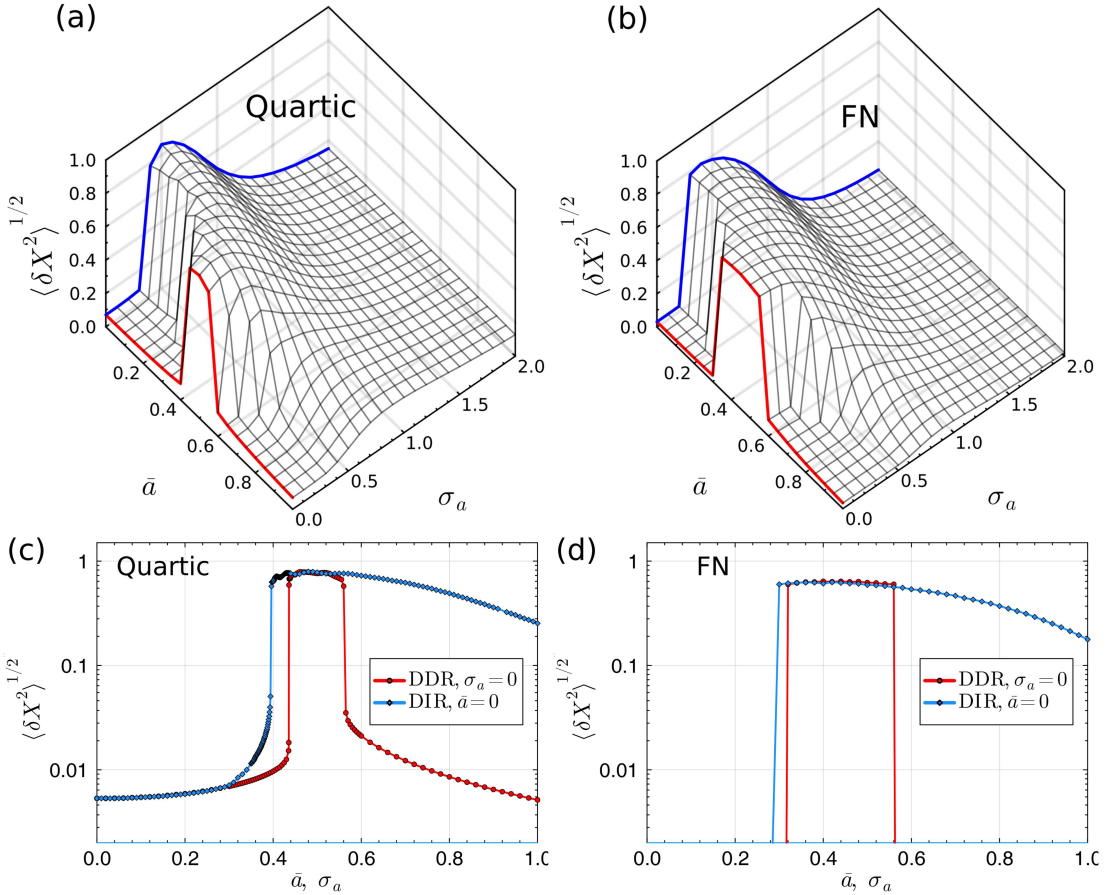


**FIG. 2.** (a) Asymptotic global oscillatory activity  $\sqrt{\langle \delta X^2 \rangle}$ , defined in Eqs. (7) and (8), in the plane  $\bar{a}$ - $\sigma_a$  of a heterogeneous network of quartic oscillators subject to a periodic forcing.  $\bar{a}$  represents the standard deviation for the two-value distribution (5), just as  $\sigma_a$  for the Gaussian distribution (4), so that both quantities measure the diversity of the system. (b) As in (a), but for FN oscillators. In both cases, the blue curves represent the limits for  $\bar{a} \rightarrow 0$  and reproduce the results of DIR,<sup>15</sup> while the red curves correspond to the limit  $\sigma_a \rightarrow 0$  for a network with a two-value bias distribution as in Ref. 7. (c) and (d) A direct comparison between the blue and the red curves reveals a common resonance peak around a standard deviation  $\bar{a}, \sigma_a \approx 0.5$ , when the same potential  $V(x)$  (2) is used. The resonances appear suddenly at some threshold of diversity; however, the resonance disappears equally fast at some threshold value of  $\bar{a}$  in the case of the two-value bias distribution, while it decreases slowly as  $\sigma_a$  increases for the Gaussian bias distribution. For both systems, the total number of oscillators is  $N = 100$ , the coupling constant  $c = 1$ , and the final simulation time  $t = 2000$ . The oscillating force acting on the quartic oscillators, defined in Eq. (3), has period  $\tau = 200$  and amplitude  $b = 0.2$ . The constants in the FN oscillator, Eq. (37), are  $\alpha = 0.02$  and  $\beta = 0.04$ .

where the first oscillator is subject to a bias  $a = -\bar{a}$  and the second one to a bias  $a = +\bar{a}$ . Numerical simulations of this simple two-oscillator system present features analogous to those of the complex network with the two-value bias distribution of Eq. (5), discussed in Sec. II B, suggesting that even in the minimal case of the two-particle system described by Eq. (9) the same mechanism, underlying the global oscillations observed in larger networks, is in action.

It is possible to rewrite Eq. (9) in the form

$$\begin{aligned} \dot{x}_1 &= -V'(x_1) + f(t) + C(x_2 - x_1 - \ell), \\ \dot{x}_2 &= -V'(x_2) + f(t) - C(x_2 - x_1 - \ell), \end{aligned} \tag{10}$$

where  $\ell = \bar{a}/C$ , which shows the equivalence of the two-oscillator problem (9) with that of the motion of a harmonic dimer of rest

length  $\ell$ , composed of two monomers with coordinates  $x_1$  and  $x_2$  linearly coupled with a strength  $C$ , moving in the potential  $V(x) - xf(t)$ . The dynamical equation (10) for a dimer corresponding to two coupled quartic oscillators can be derived from an effective potential  $W_Q^{\text{dim}}(x_1, x_2, t)$ ,

$$\dot{x}_1 = -\frac{\partial}{\partial x_1} W_Q^{\text{dim}}(x_1, x_2, t), \quad \dot{x}_2 = -\frac{\partial}{\partial x_2} W_Q^{\text{dim}}(x_1, x_2, t), \quad (11)$$

where

$$W_Q^{\text{dim}}(x_1, x_2, t) = V(x_1) + V(x_2) - (x_1 + x_2)f(t) + \frac{C}{2} (x_2 - x_1 - \ell)^2. \quad (12)$$

Here, the last term describes the monomer–monomer interaction within the dimer with equilibrium length  $\ell$ .

In Refs. 17–19, it was shown that in a spatially periodic potential, a dimer exhibits a resonant behavior for an optimal value  $\ell^*$  of the rest length  $\ell$  close to half spatial period, at which diffusion and drift under an external force are highest. We identify this type of resonance, referred to in the introduction as DDR, as the mechanism responsible for the resonant bias observed in Ref. 7 and revealed by the red isolate at  $\sigma_a \rightarrow 0$  in Fig. 2(a).

A simple mechanical explanation of DDR lies in the fact that, for a suitable value  $\ell = \ell^*$  of the equilibrium dimer length, the forces acting on the first and second monomer cancel each other, and, therefore, the action of the substrate potential on the dimer is minimized.<sup>17–19</sup> In the particular case of a sinusoidal potential,  $V(x) = V_0 \cos(2\pi x/\lambda)$ , where  $V_0$  and  $\lambda$  are the amplitude and spatial period, respectively, and the effective amplitude of the periodic potential felt by the center of mass of the dimer is reduced from  $V_0$  to  $V_0 \cos(\pi(x_2 - x_1)/\lambda)$ , which implies that when the distance between the monomers is half the spatial period of the potential,  $x_2 - x_1 = \ell^* = \lambda/2$ , the substrate potential disappears—see Refs. 17–19 for details.

These considerations remain valid when applied to the motion of a dimer in a double-well potential, with the difference that there will be only one resonant rest length  $\ell^*$ , given approximately by half the distance between the potential minima, while in the case of a periodic potential, there are infinite resonant lengths  $\ell_n^* = \ell^* + n\lambda$  differing by an integer multiple  $n$  of the spatial period  $\lambda$ .<sup>18</sup>

The optimal rest length  $\ell^* = \bar{a}/c$  depends on the ratio between the bias force and the coupling constant so that one can equally well study the emergence of an optimal rest length  $\ell^*$  fixing the bias  $\bar{a}$  and varying the coupling  $c$ , as done in Ref. 7, or vice versa, fixing  $c$  and varying  $\bar{a}$ , as we do here.

Thus, the two-value distribution (5) represents a “pure DDR” diversification strategy for the bias forces acting on the oscillators, so that the surface plots and the curves in Fig. 2 represent direct comparisons between a diversity-induced and a dimer-diffusion resonant response that provides information on their analogies and differences.

Above, we discussed the dimer analog emerging from the DDR mechanism when  $N = 2$ ; however, the DDR mechanism also acts in networks of oscillators with  $N > 2$ , leading to the analogy with a polymer composed of  $N$  monomers. Before discussing the case of a network composed of an even number  $N > 2$  of interacting oscillators (Sec. III B), let us discuss the example of a small system with an

odd number of heterogeneous oscillators,  $N = 3$ . We assume first-neighbor coupling and a symmetrical zero-mean bias distribution corresponding to the biases  $a_1 = -\bar{a}$ ,  $a_2 = 0$ , and  $a_3 = +\bar{a}$ . Then, the system is described by the equations

$$\begin{aligned} \dot{x}_1 &= -V'(x_1) + f(t) + C(x_2 - x_1) - \bar{a}, \\ \dot{x}_2 &= -V'(x_2) + f(t) - C(x_2 - x_1) + C(x_3 - x_2), \\ \dot{x}_3 &= -V'(x_3) + f(t) - C(x_3 - x_2) + \bar{a}. \end{aligned} \quad (13)$$

These equations can be recast in the form of the equations of a trimer with equilibrium distance  $\ell = \bar{a}/C$  between monomers,

$$\begin{aligned} \dot{x}_1 &= -V'(x_1) + f(t) + C(x_2 - x_1 - \ell), \\ \dot{x}_2 &= -V'(x_2) + f(t) - C(x_2 - x_1 - \ell) + C(x_3 - x_2 - \ell), \\ \dot{x}_3 &= -V'(x_3) + f(t) - C(x_3 - x_2 - \ell). \end{aligned} \quad (14)$$

Like for the dimer, also in this case, the equilibrium distance  $\ell$  between consecutive monomers determines the mobility properties of the trimer through the DDR mechanisms, and a resonance in the mobility is to be expected when  $\ell$  is close to half the distance between the potential minima.

Similarly to the case  $N = 3$ , for general odd values of  $N$ , the biases have to assume at least three different values if the constraint  $\langle a \rangle = 0$  is to be fulfilled, for example, the values  $a = -\bar{a}$  for  $(N - 1)/2$  oscillators,  $a = +\bar{a}$  for another  $(N - 1)/2$  oscillators, and  $a = 0$  for one oscillator.

In general, for any network with  $N > 2$ , the topology of the networks is crucial for the dynamics, each different topology defining a different polymer analog. In particular, the behaviors of two networks with even and odd numbers of oscillators but otherwise equivalent to each other can differ significantly. For some systems, however, the contribution of a single oscillator becomes negligible in the limit of large  $N$ , for example, in large fully connected networks since it scales as  $1/N$ . In this case, the dynamics of a network composed of an even number  $N$  of oscillators with a two-value bias distribution ( $a = \pm\bar{a}$ ) is practically equivalent to that of a network with an odd number of oscillators  $N + 1$  obtained by adding an oscillator with bias  $a = 0$ .

Furthermore, as previously mentioned, certain minimal models exhibit synchronization due to interactions between different cell types for specific coupling strengths, displaying a sharp resonance at a critical coupling strength.<sup>7</sup> This effect is also present in our model [Fig. 2(a)]. The question now is: How sensitive is this resonance to variations in coupling strength? To address this question, a phase diagram or bifurcation analysis could precisely characterize the non-oscillatory-to-oscillatory transition. Notably, both the center and width of the coupling strength window supporting oscillations can be derived analytically—without additional numerics—using an effective-barrier argument, phase-diagram boundaries, the full width at half maximum (FWHM) estimate, and bifurcation criteria.

To see this, we begin with the dimer diffusion, which shows that a synchronized network effectively moves in a one-dimensional potential whose barrier height depends on the coupling  $c$ . The effective barrier is

$$V_{\text{eff}}(c) = V_0 |\cos(\pi \bar{a}/c)|. \quad (15)$$

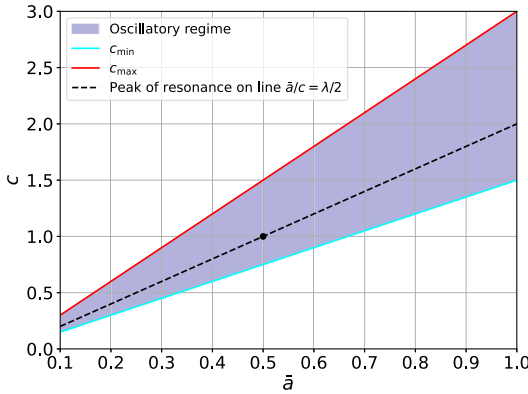


**FIG. 3.** A two-parameter space ( $\bar{a} - c$ ) bifurcation diagram with the curve  $c_{\min}(\bar{a})$  and  $c_{\max}(\bar{a})$  obtained implicitly from  $\cos(\pi \bar{a}/c) = V_{\text{crit}}/V_0$ . A shaded band between them indicates the oscillatory regime, with the outside region being non-oscillatory. The resonance peak is marked at the dashed line  $\bar{a}/c = \lambda/2$ . Parameter values used:  $\lambda = 1.0$ ,  $V_0 = 1.0$ .

A linear stability analysis of the synchronized fixed point  $\{x_i = X^*\}$  shows that it loses stability when this barrier reaches the critical value  $V_{\text{crit}}$ . Hence, the bifurcation condition is

$$V_{\text{eff}}(c) = V_{\text{crit}} \iff V_0 |\cos(\pi \bar{a}/c)| = V_{\text{crit}}. \quad (16)$$

Solving  $\cos(\pi \bar{a}/c) = V_{\text{crit}}/V_0$  gives two boundary curves,

$$\pi \frac{\bar{a}}{c_{\min}} = \arccos\left(\frac{V_{\text{crit}}}{V_0}\right), \quad \pi \frac{\bar{a}}{c_{\max}} = \pi - \arccos\left(\frac{V_{\text{crit}}}{V_0}\right), \quad (17)$$

which separate the non-oscillatory region ( $c < c_{\min}$  or  $c > c_{\max}$ ) from the oscillatory band  $c_{\min} < c < c_{\max}$  (see Fig. 3).

To compute the full width at half maximum (FWHM) of the resonance peak, note that the amplitude of oscillation is maximal where  $V_{\text{eff}}(c)$  is minimal (zero at the optimum  $c^* = 2\bar{a}$ ). By definition, the half-maximum points are those values of  $c$  at which the barrier has risen to half its peak-lowering effect. Since the peak lowering is measured from  $V_{\text{eff}}(c^*) = 0$  up to its maximum value  $V_0$ , half of that is  $V_0/2$ . Hence, we set

$$V_{\text{eff}}(c) = \frac{V_0}{2} \iff |\cos(\pi \bar{a}/c)| = \frac{1}{2}. \quad (18)$$

Solving

$$|\cos(\pi \bar{a}/c)| = \frac{1}{2} \implies \pi \frac{\bar{a}}{c} = \frac{\pi}{3} \quad \text{or} \quad \frac{2\pi}{3} \quad (19)$$

yields the two half-maximum couplings

$$c_{\max} = 3\bar{a}, \quad c_{\min} = \frac{3}{2}\bar{a} \quad (20)$$

so that the FWHM is

$$\text{FWHM} = c_{\max} - c_{\min} = \frac{3}{2}\bar{a}. \quad (21)$$

For  $\bar{a} = 0.5$ , we get  $\text{FWHM} = 0.75$ , consistent with the sharp peak of the red isoline in Fig. 2(a). This illustrates that the resonance is narrow (relatively sharp) and sensitive to variation in the coupling strength  $c$ , especially when  $\bar{a}$  becomes smaller, as indicated in the bifurcation diagram in Fig. 3.

### B. Networks with two types of oscillators

Next, we consider a network composed of an even number  $N$  of interacting quartic oscillators, described by Eq. (1), characterized by the two-value bias distribution of Eq. (5), in which a subset  $I_-$  of  $(N/2)$  oscillators is subject to the bias force  $a = -\bar{a}$  and the complementary subset  $I_+$  with the remaining  $(N/2)$  oscillators to the opposite bias  $a = +\bar{a}$ . The mean bias in the system is, therefore,  $\langle a \rangle = 0$ . Such a distribution of the bias forces is analogous to that employed in Ref. 7 for the study of a network of FN oscillators; here, it is considered in the framework of quartic oscillators and in Sec. III D in relation to a network of FN oscillators, in order to study when and how it can induce global oscillations.

We divide the system of Eq. (1) into two subsystems corresponding to the oscillator sets  $I_{\pm}$  and indicate the respective coordinates with  $x_i^{\pm}$ . Correspondingly, also the sum in Eq. (1) can be divided into two partial sums.

As an example, we consider the case of a regular network where each oscillator has an even number  $k_0$  of links equally shared between  $(k_0/2)$  oscillators of the set  $I_+$  and  $(k_0/2)$  oscillators of the set  $I_-$ ; the system is illustrated in Fig. 4(a) for  $k_0 = 4$ . We start by introducing a rescaled coupling  $c$  in Eq. (1),

$$C = 2c/k_0.$$

Then, for each oscillator  $i$ , we can rewrite the corresponding bias  $a_i$  as  $a_i \equiv (2/k_0) \sum_{j=1}^{k_0/2} a_j$ . The various terms  $(2a_i/k_0)$  can then be absorbed into the linear expressions describing the interaction between oscillator  $i$  and the oscillators  $j$  of the other type. In this way, Eq. (9) can be rewritten as

$$\begin{aligned} \dot{x}_i^- &= -V'(x_i^-) + f(t) + C \sum_{j \in I_-} (x_j^- - x_i^-) + C \sum_{j \in I_+} (x_j^+ - x_i^- - \ell), \\ \dot{x}_i^+ &= -V'(x_i^+) + f(t) + C \sum_{j \in I_+} (x_j^+ - x_i^+) - C \sum_{j \in I_-} (x_j^- - x_i^+ - \ell). \end{aligned} \quad (22)$$

Here, the first sums on the right-hand side represent simple harmonic interactions of oscillator  $i$  with oscillators of the same type and the second sums interactions with oscillators of the other type, characterized by an equilibrium distance,

$$\ell = \frac{2\bar{a}}{k_0 C} \equiv \frac{\bar{a}}{c}. \quad (23)$$

The dynamical equations can be rewritten with the help of the total potential  $W_Q^{\text{reg}}(x_1, \dots, x_N, t)$  as

$$\dot{x}_i^- = -\frac{\partial}{\partial x_i^-} W_Q^{\text{reg}}(x_1, \dots, x_N, t), \quad (24)$$

$$\dot{x}_i^+ = -\frac{\partial}{\partial x_i^+} W_Q^{\text{reg}}(x_1, \dots, x_N, t), \quad (25)$$

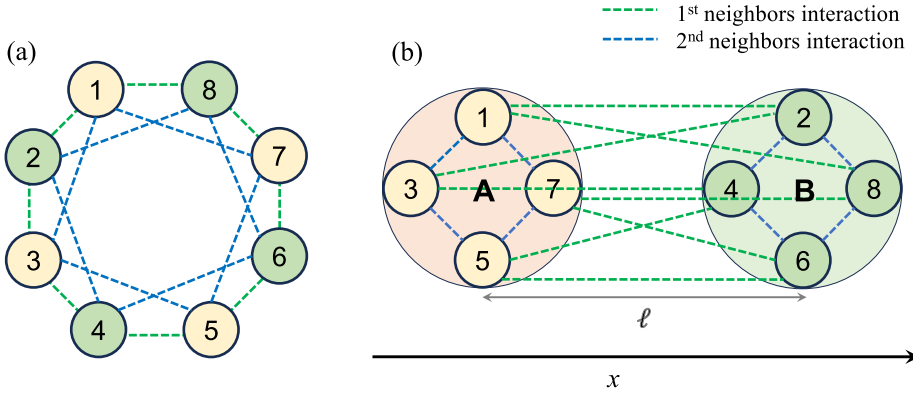


**FIG. 4.** (a) Regular network composed of alternating types of oscillators with bias  $a = -\bar{a}$  (yellow nodes) and  $a = +\bar{a}$  (green nodes). Each node is coupled to two nearest neighbors on both sides, so the degree is  $k_0 = 4$ . Blue links represent interactions between two oscillators of the same type; green links between oscillators of different types. (b) Polymer mechanical analog in  $x$ -space. The harmonic forces between particles of the same type tend to induce localized clusters, while harmonic interactions between particles of different types induce the formation of two clusters at a distance  $\ell$ . As a result, the system behaves similarly to two interacting monomers A and B that compose a dimer with equilibrium length  $\ell$ .

where

$$W_Q^{reg}(x_1, \dots, x_N, t) = \sum_{i=1}^N [V(x_i) - x_i f(t)] + \frac{C}{2} \sum_{ij \in I_-} (x_j - x_i)^2 + \frac{C}{2} \sum_{ij \in I_+} (x_j - x_i)^2 + C \sum_{i \in I_-, j \in I_+} (x_j - x_i - \ell)^2. \tag{26}$$

This reformulation of the problem as that of  $N$  interacting overdamped particles moving in the total potential  $W_Q^{reg}(x_1, \dots, x_N, t)$  suggests a simple mechanical analog of the  $N$ -oscillator network, namely, a polymer moving in a 1D  $x$ -space, composed of two types of particles, belonging to the sets  $I_-$  and  $I_+$ . Pairs of particles of different types interact with each other as monomers of a dimer with an equilibrium length  $\ell$  given by Eq. (23) and, therefore, tend to be at a distance  $\ell$  from each other [corresponding to the last sum in the total potential in Eq. (26)]; instead, pairs of particles of the same type interact through simple harmonic forces and tend to remain as close as possible [second and third sums in Eq. (26)]. As a result, particles of the same type belonging either to  $I_-$  or  $I_+$  will form distinct homogeneous localized clusters: cluster A made up of the particles in  $I_-$  and another B composed of the particles in  $I_+$ , which will tend to be at a distance  $\ell$  from each other [see Fig. 4(b)]. Therefore, the global response of a  $N$ -oscillator (regular) network with two-value bias distribution to an external periodic forcing is expected to be similar to that of a single dimer with equilibrium length  $\ell$ , discussed in Sec. III A—see also Refs. 17–19. Systems of this type occur naturally, for example, the action of an applied electric field on charged dipoles generates opposite forces on the charged monomers.<sup>19</sup>

The dynamical analogy between a network of oscillators and an overdamped polymer can be used to estimate the resonant value

$a^*$  of the red isoline at  $\sigma_a = 0$  in Fig. 2(a). In a first approximation, we can assimilate the barrier of the bistable potential to one of the barriers of a periodic potential, e.g., a sinusoidal potential. Since the potential  $V(x) = -x^2/2 + x^4/4$  has two minima  $V(x = \pm 1) = -1/4$ , their separation  $\lambda = 2$  would represent the period of the hypothetical periodic potential, in which it is known that the dimer will exhibit a resonant response when its rest length  $\ell$  is equal to half the spatial period  $\lambda$ .<sup>17–19</sup> Using Eq. (23), we obtain the following approximate resonance condition for a regular network of degree  $k_0$ :

$$\frac{2\bar{a}}{k_0 C} \equiv \frac{\bar{a}}{c} = \frac{\lambda}{2}. \tag{27}$$

The condition is determined by the ratio  $\bar{a}/c$  so that the resonance can be characterized in terms of a resonant bias  $\bar{a} = a^*$  or resonant coupling  $c = c^*$ .

In the example of the all-to-all connected network of oscillators studied above, with bias distribution given by Eq. (5), discussed in Sec. II B, we have  $c = 1$  and  $N = 100$ . Thus, since a fully connected network is a particular case of a regular network with degree  $k_0 = N - 1$ , from Eq. (27), we obtain a resonant dimer length  $a^* = 0.5$ , which coincides with the resonant bias value observed in the simulations—see the red curve in Fig. 2(a) obtained in the limit  $\sigma_a \rightarrow 0$ .

As an example of dynamics of an oscillator network with bimodal distribution, Figs. 5(a) and 5(b) show the time evolution of the coordinates  $x_i(t)$  of a small system with  $N = 20$  heterogeneous quartic oscillators, with a bimodal bias distribution with  $\bar{a} = 0.5$ . The blow-up at small times in Fig. 5(a) shows the fast relaxation of the system toward the polymer-like configuration in which the monomers order themselves according to the respective value of

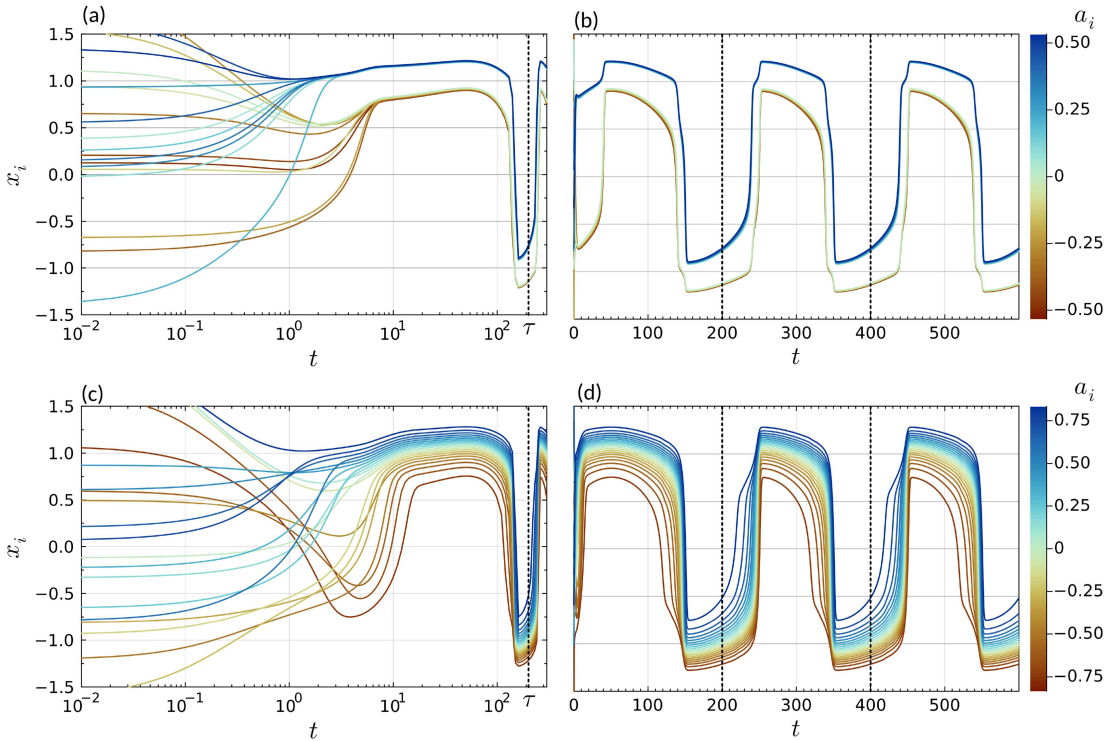


**FIG. 5.** Time evolution of the coordinates  $x_i(t)$ ,  $i = 1, \dots, N$ , of  $N = 20$  heterogeneous quartic oscillators in a fully connected network with coupling  $c = 1$ , subject to a periodic forcing with amplitude  $b = 0.2$  and period  $\tau = 200$ . (a) Short-time evolution (logarithmic time scale) for a two-value bias distribution similar to that of Ref. 7 with  $\bar{a} = 0.5$  (a small standard deviation  $\sigma_a = 0.025$  has been used for a better visualization), showing that, starting from random initial positions, the oscillators reach the periodic regime already within the first period  $\tau$ . (b) Same system as in (a) but showing the time evolution over a time interval equal to  $3\tau$ . (c) and (d) As in (a) and (b), respectively, but for a Gaussian bias distribution with zero-mean value and standard deviation,  $\sigma_a = 0.5$ . The dotted lines mark the times  $t_n = n\tau$  that are multiples of the period of external forcing.

the bias—see also the translocation process in Fig. 8 (Multimedia available online).

In resonance conditions, such a process takes place fast, in a way basically independent of the number of oscillators  $N$ . The relaxation to the polymer configuration, which coincides with the onset of the oscillatory regime, is visualized in Fig. 6 for a network of quartic oscillators through the corresponding global oscillatory activity  $\sqrt{\langle \delta X^2 \rangle}$  defined by Eqs. (7) and (8). For both cases, of a network in the DDR and DIR regimes, the curves show that the onset of oscillations takes place within the time interval  $(0, \tau)$ , independently of the system size  $N$ .

Furthermore, the numerical value of the oscillatory activity reached is the same asymptotic value reported in Fig. 7, even though the time average is computed over a much shorter time interval. The system approaches a stable oscillatory regime that remains as such at all times. The different values of the oscillatory activity shown in

Fig. 2 are due only to the different numbers of monomers involved in the oscillations. In the mechanical analogy of a polymer translocation, the maximal oscillatory activity corresponds to a complete translocation, while smaller values of the oscillatory activity correspond to a partial translocation, in which only a fraction of the monomers moves periodically to the other side of the potential barrier, while a certain number of monomers remain stuck in one of the two potential wells.

### C. Network with general bias distribution: Diversity-induced resonance

In this section, we show that DDR takes place in heterogeneous networks with an arbitrary bias distribution, and in this case, it can be put into correspondence with DIR.

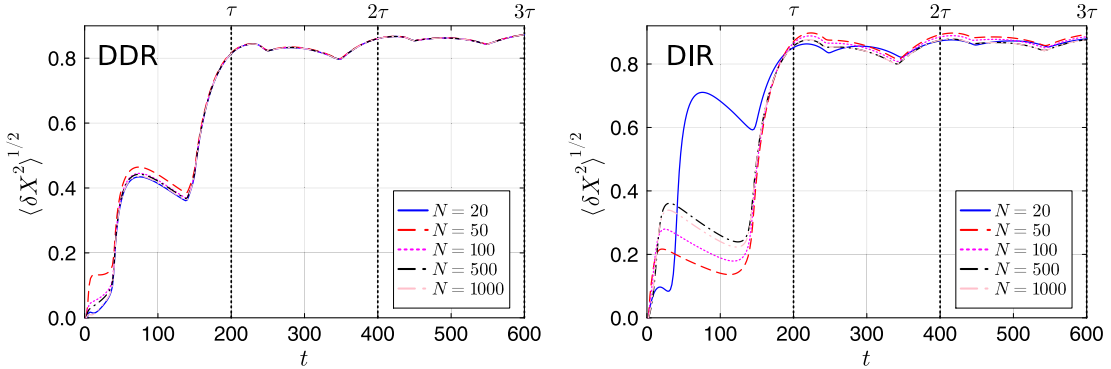


**FIG. 6.** Time evolution of the asymptotic global oscillatory activity  $\sqrt{\langle \delta X^2 \rangle}$  defined in Eqs. (7) and (8) in a network of quartic oscillators in the resonant regime for different numbers of oscillators  $N$  in the legend. Left (DDR): Network with the two-value bias distribution Eq. (5) with  $\bar{a} = 0.5$  in the DDR regime. Right (DIR): Network with the Gaussian bias distribution Eq. (4) with  $\sigma_a = 0.5$  in the DIR regime.

Let us consider the case of an all-to-all connected network, in which the bias values are assigned to the  $N$  oscillators according to some continuous distribution  $P(a)$ , labeling the oscillators in order of increasing bias, i.e.,  $a_1 < a_2 < \dots < a_N$ . In order to compare the effects of diversity with respect to a homogeneous network of unbiased oscillators, the only constraint on the distributions is that the mean value is zero,  $\langle a \rangle = N^{-1} \sum_{i=1}^N a_i = 0$ . Then, we can rewrite the bias of the  $i$ th oscillator as

$$a_i = a_i - \langle a \rangle \equiv \frac{1}{N} \sum_{j=1}^N (a_i - a_j), \tag{28}$$

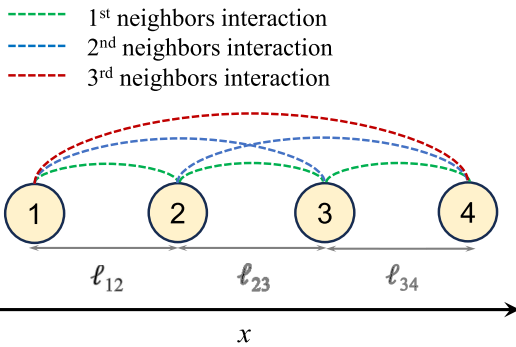


**FIG. 7.** Mechanical analog of a small network of four oscillators. Each oscillator interacts with all other oscillators, but the equilibrium distances of all different interactions are consistent with each other according to Eq. (30) and produce a robust 1D chain structure.

and Eq. (1) becomes

$$\begin{aligned} \dot{x}_i &= -V'(x_i) + f(t) + \frac{c}{N} \sum_{j=1}^N \left( x_j - x_i + \frac{a_i - a_j}{c} \right) \\ &= -V'(x_i) + f(t) - \frac{c}{N} \sum_{j=1}^{i-1} (x_i - x_j - \ell_{ij}) + \frac{c}{N} \sum_{j=i+1}^N (x_j - x_i - \ell_{ji}). \end{aligned} \tag{29}$$

Here, we have split the sum into two contributions: A sum over oscillators with  $j < i$  (therefore, with  $a_j < a_i$ ) and another sum over oscillators with  $j > i$  (with  $a_j > a_i$ ), changing the sign of the first contribution. In this way, all the quantities  $\ell_{mn}$  in the interaction terms in Eq. (29) are positive,

$$\ell_{mn} = \frac{a_m - a_n}{c} > 0 \quad \text{if } m > n; \quad m, n = 1, \dots, N, \tag{30}$$

and can be interpreted as the equilibrium lengths of the corresponding harmonic interaction between the generic  $m$ th and  $n$ th oscillators.

The form of the equations above suggests that a polymer represents a mechanical analog of a heterogeneous network, where by *polymer* we mean a 1D chain of  $N$  mutually interacting monomers with coordinates  $\{x_i\}$ . The interactions between monomers are non-local, i.e., each monomer  $i$  interacts with all the other  $(N - 1)$  monomers in the system due to the all-to-all multiple harmonic interactions of the network. In this 1D polymer model, monomers will order themselves so that  $x_1 < x_2 < \dots < x_{N-1} < x_N$ , i.e., in order of increasing bias. Despite the arbitrariness of the set of bias values  $\{a_i\}$ , the resulting system is not frustrated because the various interactions contribute in a consistent way to maintain the same mutual equilibrium distances between monomers and reinforce the global ordered equilibrium structure of the polymer. This follows directly from the fact that by definition  $\ell_{ij} \equiv \ell_{ik} + \ell_{kj}$  for any  $i, j, k$

[see Eq. (30)]. For example, the interaction between monomers 1 and 2 has an equilibrium length  $\ell_{21}$  and that between monomers 2 and 3 an equilibrium length  $\ell_{32}$ ; but monomer 1 also interacts harmonically with monomer 3, with an equilibrium length given by definition by the right value  $\ell_{31} \equiv \ell_{21} + \ell_{32}$  for stabilizing also the 1–2 and 1–3 interactions—see scheme in Fig. 7. This is valid for each of the  $N(N - 1)/2$  interactions inside the system since, in general, the interaction between monomer  $i$  and monomer  $j$  has an equilibrium length proportional to  $|a_i - a_j|$ . Thus, the order of the monomers within the polymer is determined in a unique way by the  $N$  values of the bias: From the monomer with the smallest  $x$  coordinate, corresponding to the oscillator with the minimum value of the bias, to monomers associated with larger and larger values of bias, until the monomer with the largest coordinate, corresponding to the oscillator with the largest bias. The larger the number of mutual interactions, the more rigid the structure of the polymer will be, and, eventually, a well-defined configuration of the 1D chain will emerge, with equilibrium distances between two generic monomers  $i$  and  $j$  given by  $\ell_{ij} = |a_i - a_j|/c$ . The total equilibrium length of the polymer is  $\ell_{\text{tot}} = \sum_{i=1}^{N-1} \ell_{i,i+1} = (a_N - a_1)/c$ .

The mechanical analog is apparent by rewriting the equations of motion Eq. (29) as

$$\dot{x}_i = -\frac{\partial}{\partial x_i} W_Q^{\text{full}}(x_1, \dots, x_N, t), \tag{31}$$

where the effective total potential is simply given by

$$W_Q^{\text{full}}(x_1, \dots, x_N, t) = \sum_i [V(x_i) - f(t)x_i] + \frac{C}{2} \sum_{i<j} (x_j - x_i - \ell_{ij})^2, \tag{32}$$

and the sums are extended over all the oscillators.

Numerical simulations show that the collective oscillations of the network correspond to (complete) periodic translocations of the polymer across the potential barrier, from one potential well to the other. During the translocation, all the monomers maintain their order in the polymer. An example of translocation is shown in Fig. 8 (Multimedia available online). When the network does not manage to reach a collective oscillatory state, depending on the parameter values, the translocation can be partial, i.e., a part of the polymer remains in the same potential well, or it can not take place at all and the polymer remains entirely bound on one side of the potential barrier. These results confirm the picture that, in DIR scenarios with high levels of diversity, oscillators subject to a bias that is too large in modulus may prevent the whole system from undergoing collective oscillations.<sup>15</sup>

Figure 8 also shows that the oscillators perform their oscillations consecutively, one after another, with a finite delay depending on the bias distribution. In other words, the oscillators, even if oscillating with the same frequency, cannot be in phase. In this respect,

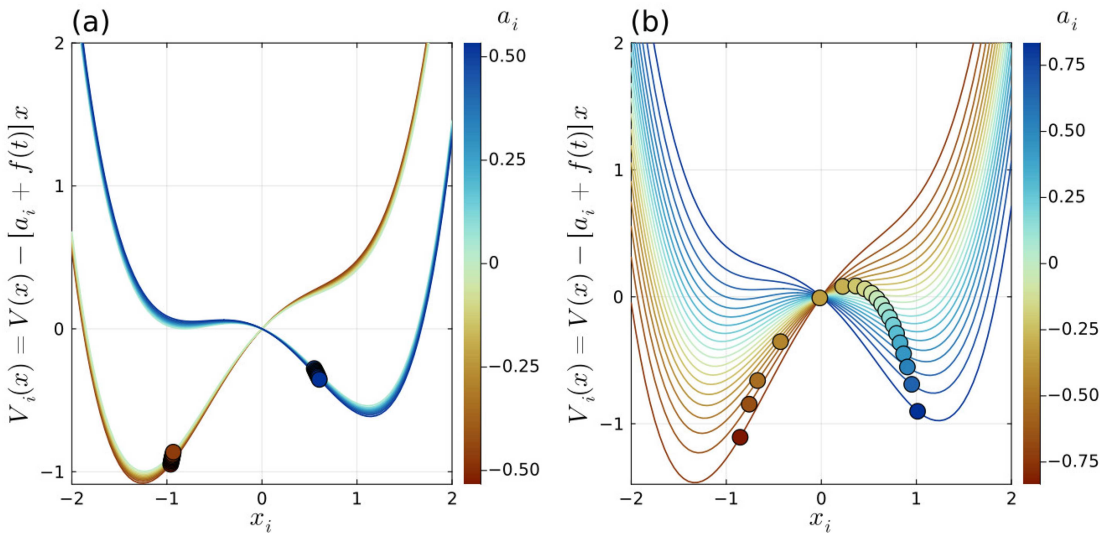


**FIG. 8.** Translocation of the effective polymer corresponding to a fully connected network of  $N = 20$  heterogeneous quartic oscillators with coupling  $c = 1$ , subject to the time-periodic forcing defined in Eq. (3) with amplitude  $b = 0.2$  and period  $\tau = 200$ . (a) Network with bias values extracted from the two-value distribution (5) with  $\bar{a} = 0.5$ ; for reasons of visualization, the distribution used is actually a bimodal distribution (6) with a small  $\sigma_a = 0.02$ . Multimedia available online. (b) Network with bias values extracted from the zero-mean Gaussian distribution (4) with  $\sigma_a = 0.5$ . Multimedia available online. Monomers and corresponding trajectories are color-coded according to the respective values of the external biases  $a_i$ . During each oscillation of the network, corresponding to a double (back and forth) translocation of the polymer, monomers move in a file maintaining the same order based on the bias value, the leftmost (rightmost) monomer having the smallest (largest) bias.

a single collective oscillation resembles the propagation of a pulse along an excitable medium.

The response of an all-to-all connected oscillator network in the DIR regime is represented by the blue curve in Fig. 2. The DIR peak is located at the same numerical value of the optimal distance,  $\sigma_a \approx a^* = 0.5$ , because as  $\sigma_a$  increases starting from  $\sigma_a = 0$ , the system will begin to include an appreciable fraction of oscillators characterized by the resonant equilibrium length  $a = a^*$  only when the value  $\sigma_a \approx a^*$  is reached. The DIR response (blue curve) decreases slower than the red curve, a fact that can be expected because, also at  $\sigma_a > a^*$ , the distribution  $P_1(a)$  will include a fraction of values of  $a$  around  $a = a^*$ . On the contrary, a two-value distribution  $P_2(a)$  with a value of  $\bar{a}$  appreciably different from  $a^*$  will not contain oscillators with equilibrium lengths around the optimal value.

#### D. FitzHugh–Nagumo oscillators

All the considerations made above for quartic oscillators also apply to the case of FitzHugh–Nagumo oscillators.<sup>20–22</sup> We start from the equations of a single FN oscillator, written in the form

$$\begin{aligned} \dot{x} &= -V'(x) - y + a, \\ \dot{y} &= \alpha x - \beta y, \end{aligned} \tag{33}$$

where  $V(x)$  is assumed as the same quartic potential equation (2) considered above,  $\alpha$  and  $\beta$  are constants defining the dynamics of the slow degree of freedom  $y$ , and the constant bias term  $a$  appears in the equation for the fast coordinate  $x$  instead of the equation of  $y$ , as in other formulations of the FN dynamics (one can switch between the various formulations through suitable rescaling of the variables and a shift of the  $y$  variable). In this form, it is easier to compare how the DDR mechanism acts within the FN dynamics with respect to the case of quartic oscillators.

Let us consider first the equations of two coupled FN oscillators, linearly coupled in the variables  $x_1$  and  $x_2$ ,

$$\begin{aligned} \dot{x}_1 &= -V'(x_1) - y_1 + C(x_2 - x_1) + a_1, \\ \dot{x}_2 &= -V'(x_2) - y_2 - C(x_2 - x_1) + a_2, \\ \dot{y}_1 &= \alpha x_1 - \beta y_1, \\ \dot{y}_2 &= \alpha x_2 - \beta y_2. \end{aligned} \tag{34}$$

Setting the bias forces of the two oscillators equal in modulus and opposite in sign, i.e.,  $a_1 = -\bar{a}$  and  $a_2 = +\bar{a}$ , and introducing the length  $\ell = \bar{a}/C$ , we can rewrite Eq. (34) as

$$\begin{aligned} \dot{x}_1 &= -\frac{\partial}{\partial x_1} W_{\text{FN}}^{\text{dim}}(x_1, x_2) - y_1, \\ \dot{x}_2 &= -\frac{\partial}{\partial x_2} W_{\text{FN}}^{\text{dim}}(x_1, x_2) - y_2, \\ \dot{y}_1 &= \alpha x_1 - \beta y_1, \\ \dot{y}_2 &= \alpha x_2 - \beta y_2, \end{aligned} \tag{35}$$

where the potential  $W_{\text{FN}}^{\text{dim}}(x_1, x_2)$  is similar to the potential of the quartic oscillators defined in Eq. (12), apart from the fact that there

is no external oscillating force,

$$W_{\text{FN}}^{\text{dim}}(x_1, x_2) = V(x_1) + V(x_2) + \frac{C}{2} (x_2 - x_1 - \ell)^2. \tag{36}$$

In fact, also in this case, the  $x$ -sector (the equations for  $x_1$  and  $x_2$ ) describes the translational motion in the  $x$ -space of a dimer of rest length  $\ell = \bar{a}/C$ , composed of two monomers with coordinates  $x_1$  and  $x_2$ . In addition, the  $y$ -sector can be interpreted as describing the internal dynamics of the dimer through the additional coordinates  $y_1$  and  $y_2$ , which produce an alternating tilting force acting on the  $x$ -degrees of freedom. In other words, Eq. (35) can be interpreted as describing an active dimer moving on the substrate potential  $V(x)$ . If the values of the parameters  $\alpha$  and  $\beta$  are such that the  $y$  degree of freedom does not manage to produce a force that pushes the dimer onto the other side of the potential barrier, the system will remain in a silent state. However, the harmonic coupling between the two monomers can drastically change the situation and translocation can take place, with a resonance at a rest length  $\ell$  approximately equal to half the distance between the two potential minima.

The above considerations can be generalized to the case of  $N$  coupled FN oscillators subject to diversified bias forces  $a_i$  ( $i = 1, \dots, N$ ) extracted from an arbitrary distribution  $P(a)$  with  $\langle a \rangle = 0$ , described by the equations

$$\begin{aligned} \dot{x}_i &= -\frac{\partial}{\partial x_i} W_{\text{FN}}(x_1, \dots, x_N) - y_i, \\ \dot{y}_i &= \alpha x_i - \beta y_i. \end{aligned} \tag{37}$$

For a regular network with degree  $k_0$ , composed of two types of FN oscillators subject to a bias  $a = \pm \bar{a}$ , analogous to that depicted in Fig. 4, the corresponding potential  $W_{\text{FN}} = W_{\text{FN}}^{\text{reg}}$  is similar to the quartic oscillators potential of the analogous regular network given by Eq. (26), with the difference that there is no external time-periodic force,

$$\begin{aligned} W_{\text{FN}}^{\text{reg}}(x_1, \dots, x_N) &= \sum_{i=1}^N V(x_i) + \frac{C}{2} \sum_{i \in L_-} (x_j - x_i)^2 \\ &+ \frac{C}{2} \sum_{i \in L_+} (x_j - x_i)^2 + C \sum_{i \in L_- - j \in L_+} (x_j - x_i - \ell)^2. \end{aligned} \tag{38}$$

Also the corresponding resonance condition is unchanged with respect to Eq. (27).

Finally, in the case of a fully connected network of FN oscillators, with diversified bias forces  $a_i$  extracted from a general symmetrical bias distribution  $P(a)$ , the effective potential  $W_{\text{FN}} = W_{\text{FN}}^{\text{full}}$  is similar to the potential defined in Eq. (32) of a network of quartic oscillators (apart from the time-periodic force),

$$W_{\text{FN}}^{\text{full}}(x_1, \dots, x_N) = \sum_i V(x_i) + \frac{C}{2} \sum_{i < j} (x_j - x_i - \ell_{ji})^2. \tag{39}$$

For the latter case, we performed numerical simulations of an all-to-all connected network of  $N$  FN oscillators with bias forces  $a_i$  diversified according to the bimodal distribution Eq. (6). The response of

the system in the  $\bar{a}$ - $\sigma_a$  parameter plane, measured through its oscillatory activity, is shown in Fig. 2(b). One can note the close similarity with the response of a system of quartic oscillators, Fig. 2(a), which best illustrates the common DDR underlying action. Also, the DDR limit (blue curve) and the DIR limit (red curve) compare with each other similarly to the case of quartic oscillators. The similarity of the responses and the resonant equilibrium lengths  $\ell^*$  are due to the fact that DDR mainly depends on the form of the bistable potential  $V(x)$ , which has been assumed to be the same in the various oscillator networks considered above.

#### IV. CONCLUSION

In this paper, we have shown that DDR and DIR are related to each other and have provided evidence that DDR can explain DIR in simple terms.

First, we have shown that a harmonic dimer moving in an external periodic potential is a mechanical equivalent of a system of two coupled bistable oscillators and that the existence of a specific rest length at which the harmonic dimer does not feel the external potential and moves as a free particle is analogous to the resonant oscillatory behavior of the bistable system, observed for a specific value of the modulus of the bias forces acting on the two oscillators.

Then, moving from simpler two-element systems, of more intuitive interpretation, to systems made of  $N$  units, we have provided evidence of a connection between a network of bistable or excitable (FN) units and a “polymer,” i.e., a chain of interacting particles moving on a one-dimensional substrate, which allows one to predict the existence of DIR and to derive analytically the conditions for synchronization. Notably, these predictions are fully consistent with the results of numerical simulations presented here and in previous studies by various authors.

The polymer mechanical analogy allowed us to predict that, also in the case of coupled FN units, one must expect a resonant, oscillatory behavior of the network if the condition Eq. (27) is verified, even when the value of  $\bar{a}$  is such that each network element is, individually, in an excitable, i.e., non-oscillatory state. This is consistent with the numerical results presented in Ref. 7.

The dynamical analogy between nonlinear oscillator networks and 1D polymers offers a general way to study and predict the synchronization properties of other nonlinear systems, with a wide range of possible applications, from oscillating biological networks to technological networks. A regular network characterized by a general distribution  $f(a)$  of bias forces has a mechanical analogy in the dynamics of a polymer in the case of both DIR of forced systems, where diversity reproduces effects similar to the noise-induced effects of stochastic resonance, and excitable systems where diversity can induce a diversity-induced coherence resonance. The same dynamical analogy can explain other collective phenomena, such as the diversity-enhanced stability introduced in Ref. 23.

There are various directions to be explored that are open to further research. The present paper focuses on regular, and, in particular, fully connected networks, but the effects of heterogeneity in networks with a general topology represent a relevant side of the problem. Also, although our analysis is based on the assumption that the distribution of bias forces acting on the bistable or excitable units that constitute the network is symmetric and with a zero-mean bias

value, the same approach can be extended to distributions that are asymmetric and with non-zero-mean bias, a topic that we will deal with in the future.

Even if the types of oscillators considered here are usually studied for historical reasons in the regime of slow oscillations (slow forcing in the case of the quartic oscillators) or a clear slow/fast separation of time scales (in the case of FN oscillators), an interesting question to be explored in future work concerns the conditions of resonance in regimes that have no such time-scale constraints.

Finally, the theoretical ideas discussed in this paper can find an interesting and challenging field of application when compared with the experimental knowledge on biological cells—in particular,  $\beta$ -cell networks<sup>24</sup>—developed in recent years.

#### ACKNOWLEDGMENTS

M.P., E.H., and S.S. acknowledge support from the Estonian Research Council through Grant No. PRG1059. M.E.Y. acknowledges support from the Deutsche Forschungsgemeinschaft (DFG, German Research Foundation) via Project No. 456989199.

#### AUTHOR DECLARATIONS

##### Conflict of Interest

The authors have no conflicts to disclose.

#### Author Contributions

**Marco Patriarca:** Conceptualization (equal); Data curation (equal); Formal analysis (equal); Funding acquisition (equal); Investigation (equal); Methodology (equal); Project administration (equal); Software (equal); Supervision (equal); Visualization (equal); Writing – original draft (equal); Writing – review & editing (equal). **Stefano Scialla:** Conceptualization (equal); Data curation (equal); Formal analysis (equal); Investigation (equal); Methodology (equal); Software (equal); Visualization (equal); Writing – original draft (equal); Writing – review & editing (equal). **Els Heinsalu:** Conceptualization (equal); Funding acquisition (equal); Investigation (equal); Methodology (equal); Project administration (equal); Supervision (equal); Visualization (equal); Writing – original draft (equal); Writing – review & editing (equal). **Marius E. Yamakou:** Conceptualization (equal); Investigation (equal); Methodology (equal); Writing – original draft (equal); Writing – review & editing (equal). **Julyan H. E. Cartwright:** Conceptualization (equal); Investigation (equal); Methodology (equal); Writing – original draft (equal); Writing – review & editing (equal).

#### DATA AVAILABILITY

The data that support the findings of this study are available from the corresponding author upon reasonable request.

#### REFERENCES

- J. Soriano, “Neuronal cultures: Exploring biophysics, complex systems, and medicine in a dish,” *Biophysics* 3(1), 181–202 (2023).
- B. E. Peercy and A. S. Sherman, “Do oscillations in pancreatic islets require pacemaker cells? *J. Biosci.* 47, 14 (2022).

- <sup>3</sup>V. A. Maltsev and M. D. Stern, "The paradigm shift: Heatbeat initiation without 'the pacemaker cell'," *Front. Physiol.* **13**, 1090162 (2022).
- <sup>4</sup>J. Buck and E. Buck, "Biology of synchronous flashing of fireflies," *Nature* **211**, 562–564 (1966).
- <sup>5</sup>M. Pérez-Armendariz, C. Roy, D. C. Spray, and M. V. Bennett, "Biophysical properties of gap junctions between freshly dispersed pairs of mouse pancreatic beta cells," *Biophys. J.* **59**(1), 76–92 (1991).
- <sup>6</sup>Y. Penn, M. Segal, and E. Moses, "Network synchronization in hippocampal neurons," *Proc. Natl. Acad. Sci. U.S.A.* **113**(12), 3341–3346 (2016).
- <sup>7</sup>J. H. E. Cartwright, "Emergent global oscillations in heterogeneous excitable media: The example of pancreatic  $\beta$  cells," *Phys. Rev. E* **62**, 1149–1154 (2000).
- <sup>8</sup>S. Scialla, A. Loppini, M. Patriarca, and E. Heinsalu, "Hubs, diversity, and synchronization in FitzHugh-Nagumo oscillator networks: Resonance effects and biophysical implications," *Phys. Rev. E* **103**(5), 052211 (2021).
- <sup>9</sup>S. Scialla, M. Patriarca, and E. Heinsalu, "The interplay between diversity and noise in an excitable cell network model," *Europhys. Lett.* **137**(5), 51001 (2022).
- <sup>10</sup>A. Arenas, A. Díaz-Guilera, J. Kurths, Y. Moreno, and C. Zhou, "Synchronization in complex networks," *Phys. Rep.* **469**(3), 93–153 (2008).
- <sup>11</sup>A. Pikovsky and M. Rosenblum, "Dynamics of globally coupled oscillators: Progress and perspectives," *Chaos* **25**(9), 097616 (2015).
- <sup>12</sup>M. E. Yamakou, E. Heinsalu, M. Patriarca, and S. Scialla, "Diversity-induced decoherence," *Phys. Rev. E* **106**(3), L032401 (2022).
- <sup>13</sup>P. Smolen, J. Rinzel, and A. Sherman, "Why pancreatic islets burst but single beta cells do not. The heterogeneity hypothesis," *Biophys. J.* **64**, 1668 (1993).
- <sup>14</sup>T. R. Chay and J. Keizer, "Minimal model for membrane oscillations in the pancreatic beta-cell," *Biophys. J.* **42**(2), 181–189 (1983).
- <sup>15</sup>C. J. Tessone, C. R. Mirasso, R. Toral, and J. D. Gunton, "Diversity-induced resonance," *Phys. Rev. Lett.* **97**, 194101 (2006).
- <sup>16</sup>C. J. Tessone, A. Sciré, R. Toral, and P. Colet, "Theory of collective firing induced by noise or diversity in excitable media," *Phys. Rev. E* **75**, 016203 (2007).
- <sup>17</sup>M. Patriarca, P. Szelestey, and E. Heinsalu, "Brownian model of dissociated dislocations," *Acta Phys. Pol. B* **36**, 1745 (2005).
- <sup>18</sup>E. Heinsalu, M. Patriarca, and F. Marchesoni, "Dimer diffusion in a washboard potential," *Phys. Rev. E* **77**, 021129 (2008).
- <sup>19</sup>E. Heinsalu, M. Patriarca, and F. Marchesoni, "Stochastic resonance in a surface dipole," *Chem. Phys.* **375**(2–3), 410–415 (2010).
- <sup>20</sup>R. Fitzhugh, "Thresholds and plateaus in the Hodgkin-Huxley nerve equations," *J. Gen. Physiol.* **43**(5), 867–896 (1960).
- <sup>21</sup>R. Fitzhugh, "Impulses and physiological states in theoretical models of nerve membrane," *Biophys. J.* **1**(6), 445–466 (1961).
- <sup>22</sup>J. Nagumo, S. Arimoto, and S. Yoshizawa, "An active pulse transmission line simulating nerve axon," *Proc. IRE* **50**(10), 2061–2070 (1962).
- <sup>23</sup>F. T. Ndjomatchoua, C. L. Gninzanlong, T. L. M. M. Djomo, M. F. Kepnang Pebeu, and C. Tchawoua, "Diversity-enhanced stability," *Phys. Rev. E* **108**, 024206 (2023).
- <sup>24</sup>D. Korošak, S. Postić, A. Stožer, B. Podobnik, and M. Slak Rupnik, "Critical transitions in pancreatic islets," *Phys. Rev. E* **111**, 034405 (2025).



## Appendix 5

### V

S. Scialla, M. Patriarca, E. Heinsalu, M. E. Yamakou, and J. H. E. Cartwright, "Effect of diversity distribution symmetry on global oscillations of networks of excitable units," *Phys. Rev. E*, vol. 112, p. 054201, 2025



## Effect of diversity distribution symmetry on global oscillations of networks of excitable units

Stefano Scialla <sup>1,2</sup> Marco Patriarca <sup>1,3</sup> Els Heinsalu,<sup>1</sup> Marius E. Yamakou <sup>4</sup> and Julyan H. E. Cartwright <sup>5,6</sup>

<sup>1</sup>*National Institute of Chemical Physics and Biophysics—Rävala 10, Tallinn 15042, Estonia*

<sup>2</sup>*Department of Science and Technology for Sustainable Development and One Health, Università Campus Bio-Medico di Roma—Via Á. del Portillo 21, 00128 Rome, Italy*

<sup>3</sup>*Department of Cybernetics, Tallinn University of Technology, 19086 Tallinn, Estonia*

<sup>4</sup>*Department of Data Science, Friedrich-Alexander-Universität Erlangen-Nürnberg, Cauerstrasse 11, 91058 Erlangen, Germany*

<sup>5</sup>*Instituto Andaluz de Ciencias de la Tierra, CSIC, 18100 Armilla, Spain*

<sup>6</sup>*Instituto Carlos I de Física Teórica y Computacional, Universidad de Granada, 18071 Granada, Spain*



(Received 15 July 2025; accepted 9 October 2025; published 3 November 2025)

We show that the degree of symmetry of the diversity distribution is the key determinant of global oscillations in coupled networks of FitzHugh-Nagumo units, used as prototypical examples of excitable systems. In these ensembles, symmetric diversity reliably yields resonant collective oscillations—even when all units are individually excitable—whereas asymmetric diversity suppresses them. Two symmetry-based metrics predict the presence or absence of global oscillations from the distribution alone. A simple mean-field mechanism, corroborated by a minimal two-unit analysis, explains how symmetry creates a landscape that supports limit cycles. These results identify diversity distribution symmetry as a key mechanism for emergent synchronization in excitable media.

DOI: [10.1103/1vb3-dc11](https://doi.org/10.1103/1vb3-dc11)

### I. INTRODUCTION

The impact of diversity, or heterogeneity, on the global oscillations of a network of coupled excitable units has been the subject of many studies [1–17]. Beyond its intrinsic relevance to dynamical systems theory, interest in these excitable media also stems from their use as models for complex and important biological oscillators, such as cardiac tissue [18–21] and excitable endocrine cells of the pancreas [22,23]. A fundamental question related to the understanding of these systems concerns the mechanisms leading to collective oscillations or quiescence of a network of diverse units, some of which are individually in an excitable (nonoscillatory) state, while others are individually oscillatory.

Previous studies emphasized the ratio of oscillatory to excitable units as a key determinant of global network oscillations. In FitzHugh-Nagumo (FHN) networks with linear all-to-all coupling, Tessone *et al.* showed that diversity and external forcing can shift a fraction of units above threshold, turning them from excitable to oscillatory. The resulting oscillatory units then “pull” the remaining excitable ones via coupling, producing collective oscillatory behavior, *i.e.*, diversity-induced resonance (DIR) [2]. The pull effect between oscillatory and excitable units was observed to be the main mechanism driving global network oscillations also by Pazó and Montbrió [24], where a diverse population of Morris-Lecar units subjected to all-to-all coupling was studied. Analogous conclusions were drawn by Shen *et al.* [25], who examined a nearest-neighbor coupled, one-dimensional chain of heterogeneous FHN elements, to which they added random long-range connections.

Importantly, global network oscillations can be observed even in heterogeneous systems that do not have any oscillatory units at all. Cartwright showed that a medium comprising

diverse FHN units, which individually were all in an excitable, nonoscillatory state, was capable of spontaneously giving rise to collective network oscillations [1].

A closely related line of work considers network aging, where the fractions of active and inactive units determine global activity and one seeks the critical inactive fraction beyond which function is lost [26–35]. In biological tissues, however, aging and disease rarely affect all subpopulations uniformly, leading to unequal loss of functional cell mass and thus skewed (asymmetric) diversity distributions [36–39], which provides a biological motivation for our focus on diversity distribution symmetry. To our knowledge, the role of this factor in driving network-level synchronization has not yet been explicitly addressed.

In the present work, we argue that the symmetry of the diversity distribution is a primary determinant of global network oscillations in heterogeneous FHN ensembles. In particular, we show, across different network topologies, that symmetric distributions robustly generate resonant collective oscillations, whereas asymmetric (skewed) distributions suppress them. We also develop a mean-field analysis that retains the third central moment and explains how skewness biases the effective drive and shifts the nullcline intersections. A minimal two-unit reduction with an effective pseudopotential visualizes how symmetry carves a cyclic valley that supports limit cycles, while asymmetry collapses the dynamics to a single equilibrium.

In terms of paper structure, we first introduce the model and the mean-field analysis (Secs. II and III). Then, in Sec. IV, we present numerical results showing symmetry-driven oscillations across topologies, followed by the description of a minimal two-unit pseudopotential mechanism in Sec. V. We also provide perspective on the relevance of our symmetry-based analysis beyond FHN unit networks (Sec. VI). In

the Conclusions (Sec. VII), after summarizing the implications of this work for emergent synchronization in excitable media, we connect our analysis to realistic networks, discuss its limitations relative to biological heterogeneity, and outline directions for future work.

## II. MODEL

As a paradigmatic example of excitable systems, we study networks of FHN units with different topologies, i.e., cubic lattice, all-to-all coupling, and small-world (Newman-Watts).

An individual FHN unit can be described by the following dimensionless equations [1,40–43]:

$$\dot{x} = a(x - x^3/3 + y), \quad (1a)$$

$$\dot{y} = -(x + by - J)/a, \quad (1b)$$

where  $x$  is the fast activator variable,  $y$  is the slow inhibitor variable, and  $a$  and  $b$  are parameters related to the electrical properties of the unit [1]. The value of parameter  $J$  determines whether the unit is in the oscillatory regime, which occurs for  $|J| < \varepsilon$ , or in the excitable one, corresponding to  $|J| > \varepsilon$ , with  $\varepsilon$  defined as

$$\varepsilon = \frac{3a^2 - 2a^2b - b^2}{3a^3} \sqrt{a^2 - b}. \quad (2)$$

We now build a network of heterogeneous and coupled FHN units, assuming for simplicity that the coupling constant  $C$  is the same for all units. The FHN equations for the  $i$ th oscillator in the network then become [1]:

$$\dot{x}_i = a \left[ x_i - x_i^3/3 + y_i + C \sum_j (x_j - x_i) \right], \quad (3a)$$

$$\dot{y}_i = -(x_i + by_i - J_i)/a, \quad (3b)$$

where the sum over  $j$  in the coupling term in Eq. (3a), in the three topologies we will examine, is: (a) limited to the six nearest neighbors of the  $i$ th unit, in the case of cubic lattice topology; (b) running over all network elements, in the case of global coupling; and (c) limited to the units that are linked to the  $i$ th element, in the case of Newman-Watts networks. Unless otherwise indicated, in all numerical simulation examples presented in this paper, the parameter values in the FHN equations (3) are set as follows:  $a = 60$ ,  $b = 1.45$ , and  $C = 0.15$ . The value of the coupling constant  $C = 0.15$  is the minimum required to observe collective network oscillations and is consistent with results from previous studies [43]. The values of parameters  $a$  and  $b$  derive from previous work by some of the authors of this paper, aimed at modeling the electrical behavior of  $\beta$ -cells in the pancreas [43]. Of course, changing  $a$  and  $b$  affects not only the value of  $\varepsilon$  but also the shape and position of the nullclines of Eqs. (3). However, the overall qualitative trends described in Sec. III and exemplified in Sec. IV do not depend substantially on  $a$  and  $b$ .

Heterogeneity or diversity is introduced into Eqs. (3) by randomly assigning a different  $J_i$  value to each unit  $i$ . In the case of symmetric diversity distributions, we draw  $J_i$  values from a Gaussian with mean  $J_{av}$  and standard deviation  $\sigma$ . Therefore, the latter will determine the degree of diversity of the units constituting the network [2,43,44]. To represent

asymmetry and study its effects, as shown in more detail in Sec. IV, we introduce truncations in the normal distribution of  $J_i$  values and will also consider half-normal distributions. We examine different cases where truncations are introduced both on the sides and in the middle of the above distributions.

## III. MEAN-FIELD ANALYSIS

Before presenting numerical results, let us analyze the dynamics of some of the above-mentioned systems through a mean-field approach [2,44], focusing on the differences between symmetric and asymmetric diversity distributions.

Let us introduce the global variables  $X(t) = N^{-1} \sum_{i=1}^N x_i(t)$  and  $Y(t) = N^{-1} \sum_{i=1}^N y_i(t)$ . We then use the transformation  $x_i = X + \delta_i$  [2,44–46]. Upon substitution in the FHN Eqs. (3) we obtain [2]

$$\begin{aligned} \dot{X} = & a \left[ X + \delta_i - \frac{(X + \delta_i)^3}{3} + y_i \right. \\ & \left. + C \sum_j (X + \delta_j - X - \delta_j) \right], \end{aligned} \quad (4a)$$

$$\dot{y}_i = -\frac{X + \delta_i + by_i - J_i}{a}. \quad (4b)$$

We have not used the transformation  $y_i = Y + \delta_j$ , because the  $y_i$  terms are all linear. Also, for simplicity, we only consider the case of all-to-all coupling, therefore the sum in Eq. (4a) runs over all  $i$ 's and  $j$ 's. Using  $\langle \delta_i \rangle = 0$  (by definition) and the identity  $\langle (X + \delta_i)^3 \rangle = X^3 + 3X \langle \delta_i^2 \rangle + \langle \delta_i^3 \rangle$ , and noting that for all-to-all coupling  $(1/N) \sum_i \sum_j (x_j - x_i) = \sum_j \delta_j - \sum_i \delta_i = 0$ , averaging Eqs. (4) over  $i$  gives the exact mean-field equations

$$\dot{X} = a \left( X - \frac{X^3}{3} - XM + Y - \frac{\mu_3}{3} \right), \quad (5a)$$

$$\dot{Y} = -\frac{X + bY - J_{av}}{a}, \quad (5b)$$

where  $M \equiv \langle \delta_i^2 \rangle$  and  $\mu_3 \equiv \langle \delta_i^3 \rangle$ .

If the  $J_i$  distribution is symmetric about its mean and we work in a small-diversity regime in which  $|\mu_3| \ll M$  (in fact,  $M = \mathcal{O}(\sigma^2)$  and  $\mu_3 = \mathcal{O}(\sigma^4)$ ), then the skewness term is sub-leading and we can set  $\mu_3 \approx 0$ . The mean field then reduces to

$$\dot{X} = a \left[ X(1 - M) - \frac{X^3}{3} + Y \right], \quad (6a)$$

$$\dot{Y} = -\frac{X + bY - J_{av}}{a}. \quad (6b)$$

In Eqs. (6),  $M$  expresses the level of diversity, larger  $M$  values meaning greater diversity.

In Fig. 1 we plot the nullclines of Eqs. (6) for different levels of diversity. It can be observed that, upon increasing  $M$ , the equilibrium points of the system tend to approach each other on the middle branch of the cubic nullcline, as shown by the comparison between  $M = 0$  and  $M = 0.3$ . Eventually, as shown for  $M = 0.6$ , the equilibrium points merge, via a sub-critical saddle-node bifurcation of fixed points, into a unique unstable equilibrium point, resulting in enhanced global oscillatory activity of the network. As  $M$  is further increased

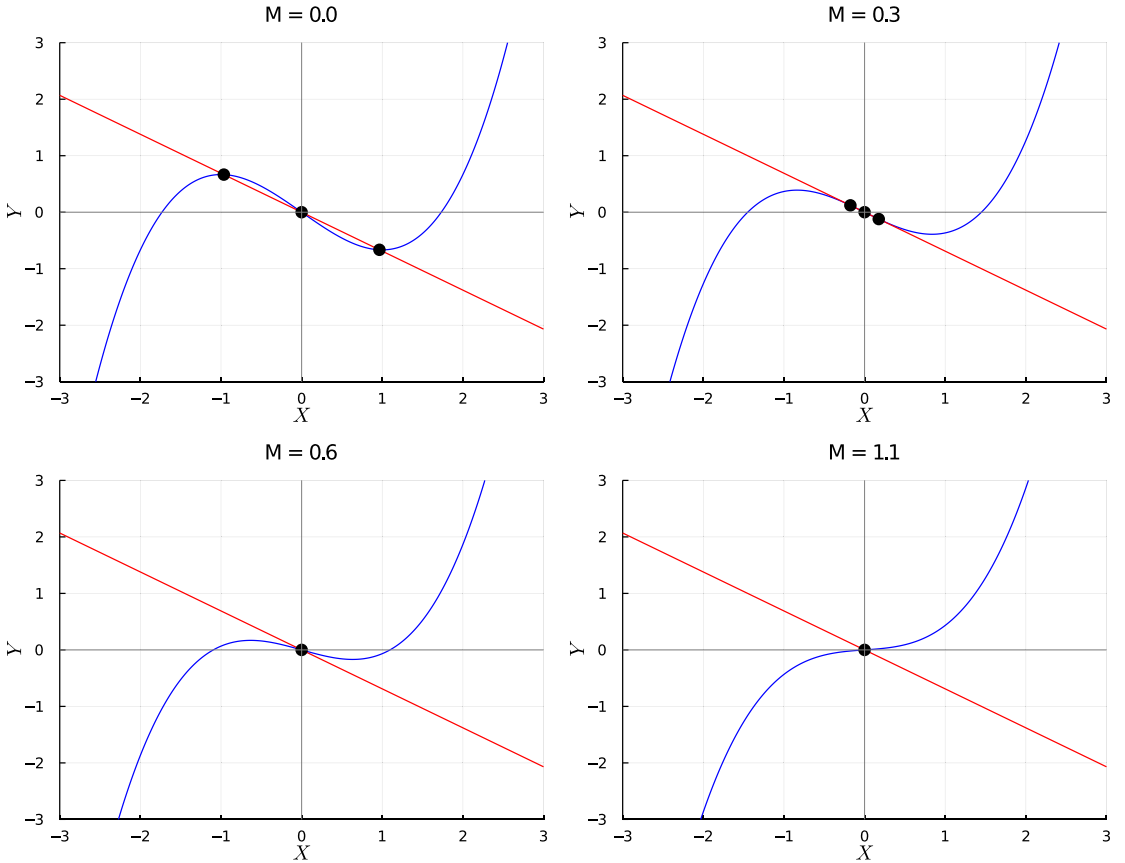


FIG. 1. Nullclines of Eqs. (6) for different values of diversity  $M$ . System parameters are:  $a = 60$ ,  $b = 1.45$ ,  $J_{av} = 0$ .

to  $M = 1.1$ , the middle branch disappears—the cubic nullcline now becomes monotonic—so that the unique remaining equilibrium point becomes stable via a subcritical Hopf bifurcation, resulting in an excitable, nonoscillatory medium. Therefore, the mean-field analysis predicts that, upon increasing  $M$ , i.e., diversity, the network should go through an intermediate region of optimal diversity values, characterized by resonant, global oscillatory behavior, followed by a progressive decrease of collective oscillations up to an excitable state in the limit of large  $M$ . This is the DIR effect described in the literature [2–6,8,9,11,24,25,43,44].

If the  $J_i$  distribution is asymmetric, then  $\mu_3 \neq 0$  and one must use Eqs. (5). At stationarity, equating the nullclines gives  $Y = -X(1 - M) + \frac{X^3}{3} + \frac{\mu_3}{3} = \frac{J_{av}}{b} - \frac{X}{b}$ , i.e.,

$$-X(1 - M) + \frac{X^3}{3} = \left( \frac{J_{av}}{b} - \frac{\mu_3}{3} \right) - \frac{X}{b}, \quad (7)$$

so  $\mu_3$  does not alter the  $Y$ -nullcline  $Y = \frac{J_{av}}{b} - \frac{X}{b}$ ; instead it shifts the  $X$ -nullcline vertically by  $+\mu_3/3$ . Equivalently, for the purpose of determining fixed points via Eq. (7), one may define an effective mean  $J_{av}^{\text{eff}} = J_{av} - \frac{b}{3}\mu_3$ .

To connect  $\mu_3$  to the diversity parameter distribution, we linearize the single-unit steady-state equations around the synchronous equilibrium (all units identical:  $M = \mu_3 = 0$ ) and obtain the susceptibility

$$\chi \equiv \frac{\partial x^*}{\partial J} = \frac{1/b}{1/b + X^2 + C - 1}, \quad (8)$$

where  $x^*(J; X, Y)$  denotes the single-unit steady state at fixed mean field  $(X, Y)$ . This yields

$$M \approx \chi^2 \sigma^2, \quad \mu_3 \approx \chi^3 \mu_3^{(J)} = \chi^3 \gamma_1^{(J)} \sigma^3, \quad (9)$$

where  $\sigma^2$ ,  $\mu_3^{(J)}$ , and  $\gamma_1^{(J)}$  are the variance, third central moment, and skewness of the  $J$  distribution, respectively. Equations (7)–(9) therefore predict that (i) variance enters via  $M \approx \chi^2 \sigma^2$  and reduces the linear coefficient  $1 - M$  in the cubic  $X$ -nullcline (narrowing its S-shape and delimiting the DIR window), while (ii) skewness shifts the  $X$ -nullcline vertically by  $+\mu_3/3$  (leaving the  $Y$ -nullcline unchanged), thereby moving the nullcline intersections and the onset of global oscillations.

The above considerations, although qualitative, illustrate that the degree of symmetry of the diversity distribution has

a crucial impact on the network's ability to exhibit global oscillations.

#### IV. RESULTS

We now examine a series of network examples with varying diversity distributions and topologies to illustrate how the diversity distribution symmetry affects the global oscillatory activity of the network. For each diversity distribution, we study three topologies, i.e., cubic lattice, all-to-all coupling, and cubic lattice augmented with small-world features. We implement the latter according to the Newman-Watts model, with 0.1 rewiring probability [47].

##### A. Symmetry metrics

Let us first introduce some metrics to quantify the degree of symmetry of the various bias distributions we are considering. We will utilize two parameters: a "normalized center of mass" (nCOM) and a "symmetry balance score" (SBS).

We define the nCOM of a distribution as

$$\text{nCOM} \equiv \frac{|\sum_{i=1}^N (J_i - J_0)|}{N\varepsilon}, \quad (10)$$

where  $N$  is the number of elements in the distribution;  $J_0$  is the center of the oscillatory interval, which in our examples is  $J_0 = 0$  since the oscillatory interval is  $(-\varepsilon, +\varepsilon)$ ; and  $\varepsilon$ , defined in Eq. (2), provides a normalization factor that makes nCOM independent of the width of the oscillatory interval. The nCOM quantifies the aggregate shift of the distribution with respect to the center of the oscillatory range and takes values in the interval  $[0, \infty)$ . Values of  $\text{nCOM} \in [0, 1)$  correspond to a fairly symmetric (or moderately asymmetric) distribution centered in the oscillatory range  $(-\varepsilon, +\varepsilon)$ , whereas  $\text{nCOM} \in [1, \infty)$  indicates increasing asymmetry, with the mass of the distribution predominantly concentrated on one side of the center and outside the oscillatory range. Therefore, we expect that distributions with  $\text{nCOM} \in [0, 1)$  should correspond to networks characterized by sustained collective oscillations, whereas  $\text{nCOM} \geq 1$  should be indicative of the absence of global oscillatory activity.

The SBS is instead defined as

$$\text{SBS} \equiv \frac{\min(N_+, N_-)}{\max(N_+, N_-)}, \quad (11)$$

where  $N_+$  and  $N_-$  denote, respectively, the number of elements in the distribution such that  $J_i > J_0$  and  $J_i < J_0$ . The SBS, which can be viewed as an adaptation of the imbalance ratio used in classification problems [48], captures the balance in the number of components on either side of  $J_0$  and can vary between 0 and 1. A value of  $\text{SBS} = 1$  indicates a perfectly symmetric distribution with equal populations on both sides of  $J_0$ , while values equal to or close to zero correspond to highly imbalanced (asymmetric) distributions. Consequently, we expect bias distributions with very low or zero SBS to be unable to exhibit global network oscillations, while SBS values significantly higher than zero and up to 1 should give rise to collective oscillations.

Together, these two metrics provide complementary information: nCOM reflects the net displacement of the distribution's mass from the center of the oscillatory range,

while SBS evaluates whether the distribution is balanced in terms of the number of components on each side.

However, it should be noted that while nCOM can be calculated for any distribution, SBS is only applicable to distributions that have at least one element on either side of  $J_0$ . For instance, if  $J_0 = 0$  and all  $J_i$ 's are positive, SBS would always assume the same value ( $\text{SBS} = 0$ ) regardless of the shape of the distribution, therefore it is not meaningful in such cases. In addition, both nCOM and SBS do not explicitly incorporate third-moment information nor the variance-to-state mapping that sets  $M$ ; nCOM only reflects skewness via its induced mean shift, and SBS only via sign imbalance. For this reason they can fail in some specific cases, as will be discussed in Secs. IV B–IV C.

Both metrics should be experimentally observable with standard recordings. SBS only requires classifying units as spontaneously oscillatory versus quiescent at a fixed drive (e.g., from  $\text{Ca}^{2+}$  or voltage optical maps); the resulting counts yield SBS. nCOM can be estimated by applying a slow ramp of the control parameter (bias current, glucose, or pacing drive) to locate each unit within its oscillatory window and then averaging the normalized positions. Such ramp/threshold protocols are routine in cardiac optical mapping and excitable media [18,20] and in pancreatic islets with  $\text{Ca}^{2+}$  imaging under glucose ramps [22].

It should be pointed out that although all FHN networks considered in this study have an oscillatory interval centered at zero ( $J_0 = 0$ ), our conclusions regarding the effects of distribution symmetry remain valid for any value of  $J_0$  that may arise in different formulations of the FHN equations.

Table I reports the nCOM and SBS values for all the diversity distributions that will be considered in the following sections, alongside the corresponding ratios of oscillatory to nonoscillatory units, that is, the main criterion considered in previous literature. Beyond being strictly applicable only to a narrow subset of distributions, a key limitation of this criterion is the absence of a clear threshold ratio, above which global network oscillations are expected to emerge. In Table I, we have assumed this threshold to be  $\approx 0.3$ , allowing a correct prediction for the distribution shown in Fig. 4(a). However, there are examples from the literature where an oscillator/nonoscillator ratio of 0.25 resulted in collective network oscillations [24].

##### B. Half-normal diversity distributions

###### 1. Oscillatory units only

We begin our analysis by studying half-normal diversity distributions and take as a first example a truncated distribution, with  $J_{\text{av}} = 0$  and  $\sigma = 0.5$ , where  $J_i$  values are drawn exclusively from the interval  $[0, \varepsilon)$ . This means that all network units are individually in an oscillatory state and the diversity distribution is relatively asymmetric, because we are picking  $J_i$  values from the positive semiaxis only [Fig. 2(a)].

After numerically solving the FHN equations (3) for each studied topology, we compute the normalized oscillatory activity of the network,  $\rho$ , from the expression

$$\rho \equiv \frac{1}{N\sigma_*} \sqrt{\langle (S(t) - \bar{S})^2 \rangle}, \quad (12)$$

TABLE I. Comparison of symmetry metrics and oscillatory behavior for the nine bias distributions shown in the paper. Green indicates correct predictions, while red highlights discrepancies. Results for Fig. 3(b) appear in orange, indicating a borderline case. The criterion for global network oscillations is shown in parentheses in each column heading.

Figure	Distribution	Oscillator/Nonoscillator Ratio (>0.3)	Normalized Center of Mass (<1)	Symmetry Balance Score ( $\gg 0$ )	Global Oscillations? (borderline case?)
2(a)		Inf.	0.50	n.a.	Yes
2(b)		0	1.50	n.a.	No
2(c)		1	0.99	n.a.	Yes
2(d)		0.5	1.52	n.a.	No
3(a)		0	0.00	0.95	Yes
3(b)		0	1.37	0.045	Yes/No (borderline case)
3(c)		0	1.47	0.015	No
4(a)		0.25	25.15	0.00	No
4(b)		0	24.01	0.26	Yes

where  $N$  is the total number of units,  $S(t) = \sum_i x_i(t)$ , and  $\bar{S} = \langle S(t) \rangle$ , with  $\langle \dots \rangle$  denoting a time average. Here, the normalization factor  $\sigma_*$  denotes the time-standard deviation of a single, isolated unit whose diversity parameter is fixed at the midpoint of the oscillatory interval ( $J_0 = 0$  for FHN units), i.e.,  $\sigma_* \equiv \sqrt{\langle (x_*(t) - \langle x_* \rangle)^2 \rangle}$ . A strong collective oscillatory activity corresponds to  $\rho \approx 1$ , while  $\rho \approx 0$  indicates no activity.

As shown in Fig. 2(a), a network with the above diversity distribution exhibits strong collective oscillations in each studied topology. Therefore, asymmetry does not prevent a network made solely of oscillatory units from being in a globally oscillatory state.

### 2. Excitable units only

Let us now examine the behavior of a network whose constituent units are still picked exclusively from the positive semiaxis, but all of them are individually in an excitable state, since they belong to the interval  $(\varepsilon, 2\varepsilon]$ . In this case, as shown in Fig. 2(b), the asymmetry in the diversity distribution is

able to prevent collective network oscillations for all studied topologies.

### 3. Both types of units

But what happens in the case of a truncated, half-normal diversity distribution that includes both excitable and oscillatory units? For instance, let us consider the diversity distribution shown in Fig. 2(c). Here, half of the units are picked from the interval  $[0, \varepsilon)$  and are therefore individually oscillatory, while the remaining half belong to the interval  $(\varepsilon, 2\varepsilon]$  and as such are excitable. As shown in Fig. 2(c), the outcome in terms of global network oscillations is similar to that in Fig. 2(a), i.e., the network is in a resonant oscillatory state even though the diversity distribution is asymmetric and there is a substantial number of units that are individually nonoscillatory. It is worth pointing out that this outcome is consistent with previous studies reported in the literature [2,24,25], which explained this dynamics on the basis of a mechanism where the oscillatory units pull the other units, generating global oscillations. In line with this reasoning, if we now add more

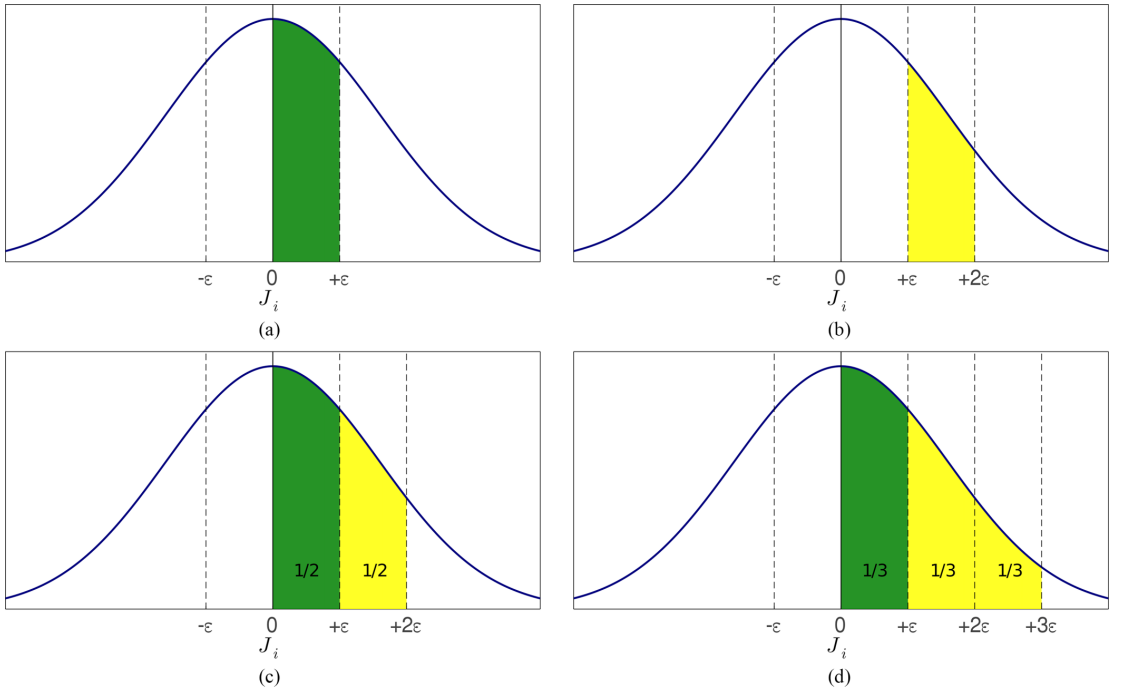


FIG. 2. Truncated half-normal diversity distributions studied in Sec. IV B. The shaded areas highlight the portions of the Gaussian that have been used to sample  $J_i$  values (green for oscillatory, yellow for excitable units). Following are the  $\rho$  values corresponding to each panel, for the lattice, all-to-all, and small-world topologies; an italicized label states whether the symmetry-based prediction matches the simulated outcome. (a) Lattice:  $\rho = 1.00$ ; All-to-All:  $\rho = 1.00$ ; Small-World:  $\rho = 1.00$ ; *Correct (Osc.)* (b) Lattice:  $\rho = 0.00$ ; All-to-All:  $\rho = 0.00$ ; Small-World:  $\rho = 0.00$ ; *Correct (Non-Osc.)* (c) Lattice:  $\rho = 0.98$ ; All-to-All:  $\rho = 0.97$ ; Small-World:  $\rho = 0.98$ ; *Correct (Osc.)* (d) Lattice:  $\rho = 0.00$ ; All-to-All:  $\rho = 0.00$ ; Small-World:  $\rho = 0.00$ ; *Correct (Non-Osc.)*.

excitable units to the diversity distribution, achieving a 2/1 ratio of excitable to oscillatory units, as shown in Fig. 2(d), we observe that global network oscillations disappear. According to the pull mechanism, this happens because the relative amount of nonoscillatory units has now become too high. However, we should also point out that the diversity distribution shown in Fig. 2(d) is more asymmetric than the one in Fig. 2(c).

Looking at the symmetry parameter values reported in Table I for the four distributions examined in this subsection, we can observe that the distributions in Figs. 2(a) and 2(c) have nCOM values lower than 1 and, as such, give rise to global network oscillations. Instead, those in Figs. 2(b) and 2(d), which are less symmetric, have nCOM  $> 1$  and, accordingly, do not produce sustained collective oscillations. Therefore, nCOM is able to correctly predict all four cases, whereas the oscillator fraction criterion fails to explain the lack of global oscillations for the distribution corresponding to Fig. 2(d).

### C. Normal diversity distributions

We now turn to examples of truncated normal distributions of  $J_i$  values, i.e., diversity distributions characterized by the

presence of  $J_i$  values on both sides of the mode of the parent, nontruncated Gaussian.

#### 1. Excitable units only: Symmetric subpopulations

The first case we analyze is an extension of the system presented in Ref. [1]. In that study, the network population was divided into two subgroups, made of identical units with  $J_i$  values below and above the oscillatory interval  $-\varepsilon < J_i < \varepsilon$ , respectively. Here, we consider a diversity distribution made of excitable units only, which are symmetrically positioned on the two sides of the mode of a Gaussian, as shown in Fig. 3(a). This distribution is fully symmetric, with nCOM = 0 and SBS = 0.95 (Table I), and produces strong collective network oscillations, just like the system in Ref. [1]. There is no way to explain or predict the oscillatory behavior of this network based on the ratio between oscillatory and excitable units, whereas the observed dynamics is fully consistent with our considerations about the symmetry of the diversity distribution.

#### 2. Excitable units only: Highly asymmetric subpopulations

We now introduce a degree of asymmetry into the diversity distribution of Fig. 3(a), by picking a different number of units

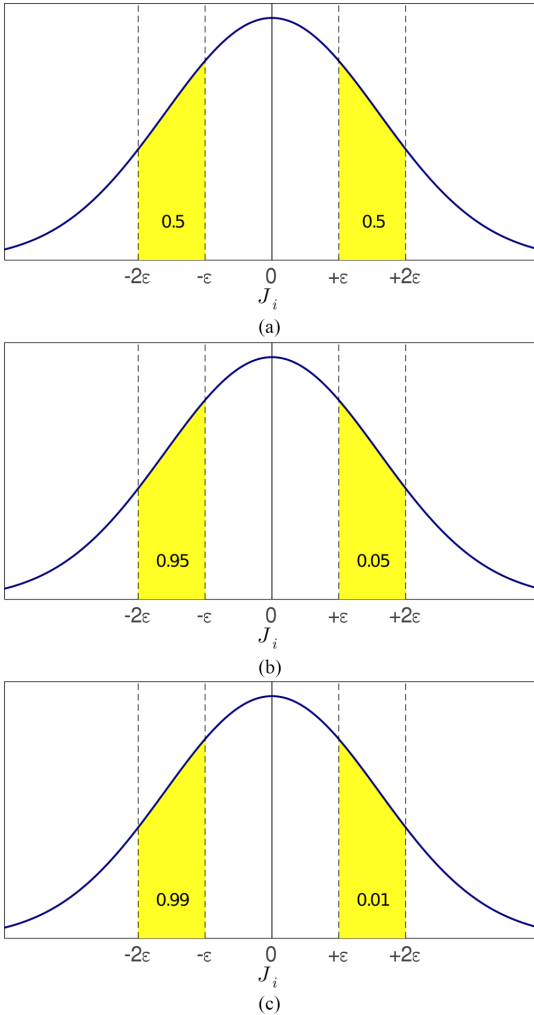


FIG. 3. Truncated normal diversity distributions studied in Sec. IV C. The shaded areas highlight the portions of the Gaussian that have been used to sample  $J_i$  values (green for oscillatory, yellow for excitable units). Following are the  $\rho$  values corresponding to each panel, for the lattice, all-to-all, and small-world topologies; an italicized label states whether the symmetry-based prediction matches the simulated outcome. (a) Lattice:  $\rho = 1.01$ ; All-to-All:  $\rho = 1.00$ ; Small-World:  $\rho = 1.01$ ; *Correct (Osc.)* (b) Lattice:  $\rho = 0.98$ ; All-to-All:  $\rho = 0.00$ ; Small-World:  $\rho = 0.98$ ; *Borderline (Metrics Predict Non-Osc.)* (c) Lattice:  $\rho = 0.00$ ; All-to-All:  $\rho = 0.00$ ; Small-World:  $\rho = 0.00$ ; *Correct (Non-Osc.)*.

from either side of the truncated Gaussian. Specifically, a fraction of the total number of units equal to 0.95 are taken from the positive side and 0.05 from the negative one [Fig. 3(b)]. In Fig. 3(c) we push this asymmetry even further, by picking 0.99 of the units from the positive side and only 0.01 from the negative one.

Simulation results show that a 95/5% ratio of positive to negative  $J_i$  values corresponds to a borderline situation, where the network is still capable of global oscillations with the lattice and small-world topologies, but not with all-to-all coupling. Instead, at the even more asymmetric 99/1% ratio there are no oscillations regardless of the topology.

Upon comparing the diversity distributions in Fig. 3(b) and Fig. 3(c) to that in Fig. 2(b), we should point out that the latter is more asymmetric than both of the former, as shown by its higher nCOM value (Table I). Among these three distributions, only the one with the lowest nCOM value, i.e., with the lowest degree of asymmetry [corresponding to Fig. 3(b)], is able to produce sustained collective oscillations in two out of three tested topologies. Notice that the nCOM parameter correctly indicates that the relative tendency to global oscillations should be in the order Fig. 3(b) > Fig. 3(c) > Fig. 2(b), in line with the increasing symmetry (i.e., decreasing nCOM values) of the distributions.

### 3. Distributions with subthreshold mode

As final examples of normal diversity distributions, we study two cases where the mode of the distribution is subthreshold, i.e., below the interval of oscillatory  $J_i$  values (in all previous cases, the mode of the distribution was positioned at the center of the oscillatory interval). In Fig. 4(a), excitable units have  $J_i$  values distributed over the range  $(-\infty, -\varepsilon)$ , while  $J_i$  values for oscillatory units are picked from  $(-\varepsilon, +\varepsilon)$ . Here we see again that the network has no collective oscillatory activity, which can be explained by both the criterion based on the numerical ratio between oscillatory and excitable units (too low in this case), and considerations related to the degree of symmetry of the diversity distribution, which is also very low (nCOM = 25.15).

However, if we consider the distribution shown in Fig. 4(b), where there are no oscillatory units but the excitable ones are now distributed over the range  $(-\infty, -\varepsilon) \cup (+\varepsilon, +\infty)$ , we observe that the network is again able to exhibit global oscillations, in spite of a diversity distribution that includes  $J_i$  values extremely far away from the oscillatory range. Rather than from the ratio between oscillatory and excitable units, this behavior can only be inferred from considerations based on the greater symmetry of the distribution in Fig. 4(b) (nCOM = 24.01, SBS = 0.26) compared to the one in Fig. 4(a) (nCOM = 25.15, SBS = 0). Here too, the nCOM parameter fails to predict the global oscillations of the network configuration corresponding to Fig. 4(b), however, it correctly ranks Figs. 4(a) and 4(b) in terms of their respective degrees of symmetry and tendencies to give rise to collective oscillations.

## V. PSEUDOPOTENTIAL ANALYSIS

To understand the mechanism through which populations of units that are all, or predominantly, in an excitable state can give rise to collective network oscillations, it is instructive to consider the case of a minimal system composed of only two coupled FHN units [49]. Although the FHN model is not a gradient system and does not possess a true potential function, it is still possible to define an effective pseudopotential for

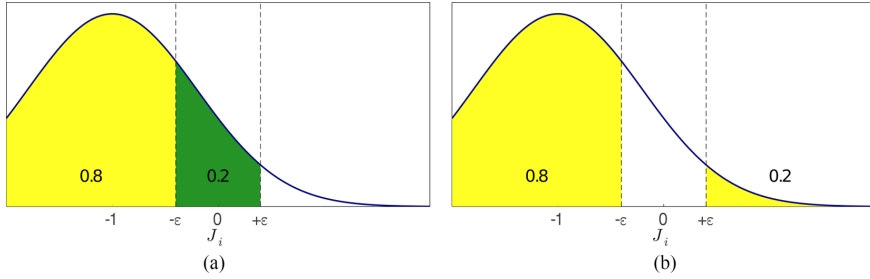


FIG. 4. Truncated half-normal diversity distributions studied in Sec. IV B. The shaded areas highlight the portions of the Gaussian that have been used to sample  $J_i$  values (green for oscillatory, yellow for excitable units). Following are the  $\rho$  values corresponding to each panel, for the lattice, all-to-all, and small-world topologies; an italicized label states whether the symmetry-based prediction matches the simulated outcome. (a) Lattice:  $\rho = 0.00$ ; All-to-All:  $\rho = 0.00$ ; Small-World:  $\rho = 0.00$ ; All-to-All:  $\rho = 0.00$ ; Correct (Non-osc.) (b) Lattice:  $\rho = 1.09$ ; All-to-All:  $\rho = 1.00$ ; Small-World:  $\rho = 1.10$ ; *nCOM incorrect, SBS correct (Osc.)*.

the fast variables under the assumption that the slow variables  $y_i$  are quasistatic over fast timescales [46]. For two coupled units, the fast variables obey

$$\dot{x}_1 = a \left[ x_1 - \frac{x_1^3}{3} + y_1 + C(x_2 - x_1) \right], \quad (13a)$$

$$\dot{x}_2 = a \left[ x_2 - \frac{x_2^3}{3} + y_2 + C(x_1 - x_2) \right], \quad (13b)$$

while the slow variables still follow Eq. (3b).

Treating  $y_1$  and  $y_2$  as quasiconstants on the fast timescale ( $a \gg 1$ ), one can define an effective pseudopotential

$$V_{\text{eff}}(x_1, x_2; y_1, y_2) = V_1(x_1; y_1) + V_2(x_2; y_2) + \frac{C}{2}(x_1 - x_2)^2, \quad (14)$$

where the local terms  $V_1$  and  $V_2$  are defined as

$$V_i(x_i; y_i) = -\frac{1}{2}x_i^2 + \frac{1}{12}x_i^4 + x_i y_i \quad (i = 1, 2). \quad (15)$$

Each term  $V_i(x_i; y_i)$  represents the local pseudopotential of a single FHN unit at fixed  $y_i$ , while the quadratic coupling term acts to reduce deviations between the two fast variables, favoring synchronization. When  $C = 0$ , the landscape consists of two independent tilted wells, and the system relaxes to a fixed point if both units are excitable ( $|J_i| > \varepsilon$ ). However, for moderate coupling, the quadratic term  $\frac{C}{2}(x_1 - x_2)^2$  deforms the landscape, lowering the barrier between the wells and creating a cyclic valley that can support a limit cycle, even though neither unit would oscillate in isolation.

This two-unit mechanism serves as a coarse-grained proxy for larger networks once units segregate into two sign-defined clusters around the excitability threshold, so that intracluster states are tight and interactions are mediated by the population mean (see below).

Importantly, this collective oscillation can only occur if the respective  $J_i$  parameters of the two excitable units are on opposite sides of the oscillatory threshold; that is, they must be positioned symmetrically with respect to the center of the oscillatory interval  $(-\varepsilon, +\varepsilon)$ . This symmetric configuration ensures that the wells of the two local pseudopotentials are tilted in opposite directions [due to the opposite signs of the  $x y$  terms in Eqs. (15)], forming a double-well-like landscape with

a cyclic saddle path that the system can move along (Fig. 5, upper panel). If instead the two  $J_i$ 's are on the same side, the landscape collapses into a single minimum and no oscillatory path can emerge, regardless of coupling (Fig. 5, lower panel).

The two-unit pseudopotential analysis extends to an  $N$ -unit system via a coarse-grained reduction based on the sign of the bias parameters  $J_i$ . Let us partition the population into two subgroups with fractions  $w_+$  and  $w_- = 1 - w_+$  (units with  $J_i > 0$  and  $J_i < 0$ ). Let us define subgroup averages  $(x_+, y_+)$  and  $(x_-, y_-)$ . For all-to-all coupling, the subgroup means obey  $\dot{x}_+ = \dots + C w_- (x_- - x_+)$  and  $\dot{x}_- = \dots + C w_+ (x_+ - x_-)$ , so their interaction has the same form as in the two-unit case with an *effective* coupling  $C_{\text{eff}} = C w_+ w_-$ . We absorb this rescaling into  $C$  below for notational simplicity. The subgroup biases are  $J_+ = \langle J_i \rangle_{J_i > 0}$  and  $J_- = \langle J_i \rangle_{J_i < 0}$ , obtained by taking the average of the  $J_i$  values for each subpopulation. The effective pseudopotential then takes the form

$$V_{\text{eff}}(x_+, x_-) = V_+(x_+; y_+) + V_-(x_-; y_-) + \frac{C_{\text{eff}}}{2}(x_+ - x_-)^2, \quad (16)$$

where

$$V_{\pm}(x_{\pm}; y_{\pm}) = -\frac{1}{2}x_{\pm}^2 + \frac{1}{12}x_{\pm}^4 + x_{\pm} y_{\pm}, \quad (17)$$

are the coarse-grained local pseudopotentials for each cluster.

In this reduction, the symmetry condition  $J_+ \approx -J_-$  corresponds in the mean-field picture to a small effective intercept shift ( $J_{\text{av}}^{\text{eff}} \approx 0$ ), while within-subgroup spreads contribute to the variance  $M$ . Thus, the existence of a cyclic valley in  $V_{\text{eff}}$  is the geometric counterpart of the mean-field regime where the  $X$ -nullcline retains its S-shape and the  $Y$ -nullcline intersects it near the cubic's central branch (see Fig. 1); as  $M$  grows, the S-shape narrows and eventually disappears, destroying the cyclic valley. This coarse-grained link is accurate when (i) the slow-fast separation holds ( $a \gg 1$ ), (ii) intrasubgroup dispersion is moderate so subgroup means are representative, and (iii) coupling is sufficiently dense that subgroup interactions are mean-field-like. Consequently, even when both subgroups are individually excitable (or contain a large excitable fraction), a limit cycle can emerge provided their average biases lie on opposite sides of the oscillatory interval, which creates opposing tilts and a cyclic valley; if the subpopulations

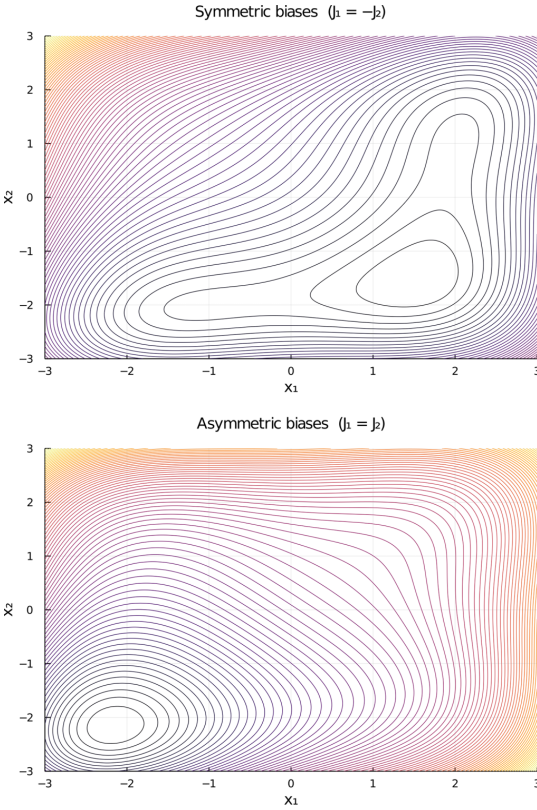


FIG. 5. Contour plots of the effective pseudopotential defined by Eq. (14) in the symmetric (upper panel) and asymmetric (lower panel) cases. In the symmetric case, a double-well-like landscape emerges from the sum of the coupling term with the two local pseudopotentials  $V_1(x_1; y_1)$  and  $V_2(x_2; y_2)$ , which are tilted in opposite directions due to the different signs of the respective  $xy$  terms. In the asymmetric case, the potential landscape collapses into a single minimum as the  $xy$  terms have the same sign. Parameter values:  $C = 0.5$ ,  $\varepsilon = 1.0$ ,  $J_2 = 1.2$  ( $J_1 = -1.2$  and  $J_1 = 1.2$  in the symmetric and asymmetric case, respectively). The slow variables  $y_1$  and  $y_2$  are kept constant and set equal to  $J_1$  and  $J_2$ , respectively.

are biased in the same direction (asymmetry), the effective landscape collapses into a single minimum and global oscillations do not arise.

## VI. EXTENSION BEYOND FHN NETWORKS

The symmetry-based analysis we applied to networks of FHN units does not rely on model-specific waveforms. It rests on two characteristics that many excitable/oscillatory models share under electrical or diffusive coupling: (i) a diversity parameter  $\theta_i$  (analogous to  $J_i$  in our FHN analysis) that shifts each unit relative to a model-specific center  $\theta_0$  of the single-cell oscillatory window, and (ii) Laplacian (diffusive) coupling. Examples include Type-II Morris-Lecar [50], Hindmarsh-Rose [51], Izhikevich [52], and reduced

conductance-based models with gap-junction-like coupling [53,54].

If we define  $h_i := \theta_i - \theta_0$ , the symmetry of the ensemble is encoded in the distribution of  $\{h_i\}$  about zero. When this distribution is balanced, i.e., it has approximately zero mean and small odd moments, positive and negative deviations cancel. When it is asymmetric, e.g., with a biased mean or a disproportion in positive versus negative signs, the cancellation is lost.

Two key mechanisms explain the advantage of symmetric  $\{h_i\}$  distributions:

(i) Close to the oscillatory threshold, many models can be simplified to a linearized dynamics, in which the initial tendency of unit  $i$ 's oscillations to grow or fade reverses when  $h_i$  changes sign; a symmetric spread of  $\{h_i\}$  therefore keeps the network, on average, close to the balance point where small oscillations neither grow nor die out, so modest coupling can push the population-average activity into self-sustained oscillations. Instead, an asymmetric spread pulls the average away from that balance and increases the cross-unit spread that coupling must overcome to induce global oscillations.

(ii) For diffusive coupling on any graph Laplacian  $L$ , the population sum  $S(t) = \sum_i x_i(t)$  satisfies

$$\dot{S}(t) = \sum_{i=1}^N f(x_i, \dots; \theta_i) + K \mathbf{1}^\top L x(t), \quad (18)$$

where  $K \geq 0$  is a scalar coupling gain multiplying the Laplacian  $L$ . We assume  $L$  has zero column sums ( $\mathbf{1}^\top L = 0$ ), hence  $\mathbf{1}^\top (KL)x = 0$  and the coupling does not contribute to  $\dot{S}$ . Thus, coupling only rebalances which units are more or less active and, on average, does not add or subtract any net tendency to oscillate at the population level. Consequently, the size of the coherent population-average signal is set by how completely the unit-specific biases (set by  $h_i$ ) cancel across the group: a symmetric distribution of  $\{h_i\}$  maximizes cancellation of opposite-sign biases and promotes synchronization, whereas an asymmetric distribution leaves a residual bias that persists in the population-mean dynamics.

These arguments depend only on the existence of a parameter  $h_i$  that determines the single-cell transition to oscillations, and the structure of diffusive coupling. Consequently, the qualitative ranking observed for the families of diversity distributions we studied is expected to carry over to other excitable models under the same coupling regime.

Obviously, quantitative thresholds will vary with model details, such as single-cell amplitudes, phase response properties, and coupling gain/topology. Deviations may occur when heterogeneity is genuinely multiparametric (not well captured by a single  $h_i$  coordinate), when coupling is nondiffusive (breaking  $\mathbf{1}^\top L = 0$ ), or far from threshold where higher-order nonlinearities dominate. Within these limits, the symmetry of the diversity parameter distribution is a key determinant of whether coupling can assemble microscopic activity into a coherent macroscopic oscillation.

## VII. CONCLUSIONS

We have shown that the symmetry of the diversity distribution is a primary determinant of global oscillations in

networks of coupled excitable units, using FHN as a prototypical model. Whereas prior work emphasized the ratio of oscillatory to excitable elements, our results reveal that symmetry of the excitability distribution is a more general predictor of oscillatory behavior, deepening our understanding of how structural and statistical properties of heterogeneity shape the collective behavior of excitable systems.

Using half-normal and truncated normal test cases, we documented that symmetric diversity robustly yields global oscillations even when all units are individually excitable, whereas asymmetric diversity suppresses collective activity. We proposed two complementary metrics—the normalized center of mass (nCOM) and the symmetry balance score (SBS)—that capture distinct aspects of symmetry and offer simple predictive diagnostics. A minimal two-unit reduction with an effective pseudopotential visualizes the mechanism: symmetry creates a cyclic valley that supports limit cycles, while asymmetry collapses the dynamics to a single equilibrium.

In biological networks, the diversity parameter is the unit-specific bias  $J_i$ , which we interpret as an effective drive/threshold. The population  $\{J_i\}$  defines the diversity distribution in our framework.  $J_i$  values can be inferred from experimentally accessible observables—including, for example, rheobase current, glucose threshold for  $\text{Ca}^{2+}$  oscillations, intrinsic pacemaker bias, ion-channel conductances, metabolic drive (e.g., glucokinase activity), and gap-junctional coupling strength.

All of these observables map, via linear susceptibilities around the operating point, to the scalar  $J$ ; hence, their population distribution is the diversity distribution in our framework. For pancreatic islets, single-cell data show broad, often skewed variability in metabolic and electrical parameters and coupling [23,55], making symmetry/asymmetry directly testable via population distributions of glucose thresholds or  $\text{Ca}^{2+}$  oscillation onsets. Our findings suggest that physiological or pathological changes that alter the balance or symmetry of cellular populations can profoundly influence the emergence or loss of coherent dynamics, with implications for tissue and network function.

Since our mean-field criteria depend on the first three moments of the effective drive distribution (through  $M$  and the skewness-induced shift of the nullcline intercept), our qualitative predictions extend beyond the specific distribution families used here to any distribution with finite variance and third moment—including moderately multimodal or heavy-tailed cases once mapped through susceptibility. However, strongly multimodal populations with weak intercluster coupling, or heavy-tailed laws with ill-defined moments, can induce additional bifurcations and fall outside the present framework. We also believe that our symmetry-based analysis should generalize to other excitable-network models with diffusive coupling, because it assumes only a unit-level bifurcation parameter governing the onset of oscillations and a symmetric cross-unit distribution of that parameter.

Exploring strongly multimodal regimes with data-driven mixture models and testing the symmetry metrics on empirically observed heterogeneity (e.g., in  $\beta$ -cell networks [55]) are natural directions for future work, together with the extension to other excitable models through numerical simulations.

#### ACKNOWLEDGMENTS

S.S., M.P., and E.H. acknowledge support from the Estonian Research Council through Grant No. PRG1059. M.E.Y. acknowledges support from the Deutsche Forschungsgemeinschaft (DFG, German Research Foundation) via Grant No. YA 764/1-1, Project No. 456989199. J.H.E.C. acknowledges support from the Spanish Ministerio de Ciencia, Innovación y Universidades through Grant No. PID2024-160443NB-I00.

#### DATA AVAILABILITY

The data that support the findings of this article are not publicly available upon publication because it is not technically feasible and/or the cost of preparing, depositing, and hosting the data would be prohibitive within the terms of this research project. The data are available from the authors upon reasonable request.

- 
- [1] J. H. E. Cartwright, *Phys. Rev. E* **62**, 1149 (2000).  
 [2] C. J. Tessone, C. R. Mirasso, R. Toral, and J. D. Gunton, *Phys. Rev. Lett.* **97**, 194101 (2006).  
 [3] R. Toral, E. Hernández-García, and J. D. Gunton, *Int. J. Bifurcat. Chaos* **19**, 3499 (2009).  
 [4] H. Chen, Z. Hou, and H. Xin, *Physica A* **388**, 2299 (2009).  
 [5] L. Wu, S. Zhu, and X. Luo, *Chaos* **20**, 033113 (2010).  
 [6] L. Wu, S. Zhu, X. Luo, and D. Wu, *Phys. Rev. E* **81**, 061118 (2010).  
 [7] M. Patriarca, S. Postnova, H. A. Braun, E. Hernández-García, and R. Toral, *PLoS Comput. Biol.* **8**, e1002650 (2012).  
 [8] C. J. Tessone, A. Sánchez, and F. Schweitzer, *Phys. Rev. E* **87**, 022803 (2013).  
 [9] M. Grace and M.-T. Hütt, *Eur. Phys. J. B* **87**, 29 (2014).  
 [10] M. Patriarca, E. Hernández-García, and R. Toral, *Chaos, Solitons & Fractals* **81**, 567 (2015).  
 [11] X. Liang, X. Zhang, and L. Zhao, *Chaos* **30**, 103101 (2020).  
 [12] C. Degli Esposti Boschi, E. Louis, and G. Ortega, *Phys. Rev. E* **65**, 012901 (2001).  
 [13] Y.-Y. Li, B. Jia, H.-G. Gu, and S.-C. An, *Commun. Theor. Phys.* **57**, 817 (2012).  
 [14] Y.-Y. Li and X.-L. Ding, *Commun. Theor. Phys.* **62**, 917 (2014).  
 [15] M. Gassel, E. Glatt, and F. Kaiser, *Phys. Rev. E* **76**, 016203 (2007).  
 [16] C. Zhou, J. Kurths, and B. Hu, *Phys. Rev. Lett.* **87**, 098101 (2001).  
 [17] E. Glatt, M. Gassel, and F. Kaiser, *Europhys. Lett.* **81**, 40004 (2008).  
 [18] R. Barrio, S. Coombes, M. Desroches, F. Fenton, S. Luther, and E. Pueyo, *Commun. Nonlin. Sci. Numer. Simul.* **86**, 105275 (2020).

- [19] J. Lebert, M. Mittal, and J. Christoph, *Phys. Rev. E* **107**, 014221 (2023).
- [20] S. Alonso, M. Bär, and B. Echebarria, *Rep. Prog. Phys.* **79**, 096601 (2016).
- [21] M. Wellner, J. Jalife, and A. M. Pertsov, *Int. J. Bifurcat. Chaos* **12**, 1939 (2002).
- [22] G. J. Félix-Martínez and J. R. Godínez-Fernández, *Islets* **15**, 2231609 (2023).
- [23] A. Stožer, R. Markovič, J. Dolenšek, M. Perc, M. Marhl, M. Slak Rupnik, and M. Gosak, *Front. Physiol.* **10**, 869 (2019).
- [24] D. Pazo and E. Montbrío, *Phys. Rev. E* **73**, 055202(R) (2006).
- [25] S. Chuan-Sheng, C. Han-Shuang, and Z. Ji-Qian, *Chinese Phys. Lett.* **25**, 1591 (2008).
- [26] H. Daido and K. Nakanishi, *Phys. Rev. Lett.* **93**, 104101 (2004).
- [27] A. Sharma, B. Rakshit, and K. Aihara, *Chaos* **35**, 011101 (2025).
- [28] K. Morino, G. Tanaka, and K. Aihara, *Phys. Rev. E* **83**, 056208 (2011).
- [29] A. Sharma and B. Rakshit, *Chaos, Solitons & Fractals* **156**, 111823 (2022).
- [30] Y. Liu, W. Zou, M. Zhan, J. Duan, and J. Kurths, *Europhys. Lett.* **114**, 40004 (2016).
- [31] S. Kundu, S. Majhi, and D. Ghosh, *Phys. Rev. E* **97**, 052313 (2018).
- [32] B. Rakshit, N. Rajendrakumar, and B. Balaram, *Chaos* **30**, 101101 (2020).
- [33] A. Sharma and B. Rakshit, *Chaos* **31**, 013114 (2021).
- [34] T. Yuan, K. Aihara, and G. Tanaka, *Phys. Rev. E* **95**, 012315 (2017).
- [35] U. Barać, M. Perc, and M. Gosak, *Chaos: Interdisc. J. Nonlin. Sci.* **33**, 043120 (2023).
- [36] D. M. Vogt Weisenhorn, F. Giesert, and W. Wurst, *J. Neurochem.* **139**, 8 (2016).
- [37] S. Efrat, *Stem Cells* **37**, 1267 (2019).
- [38] F. Leenders, E. J. P. de Koning, and F. Carlotti, *Int. J. Mol. Sci.* **25**, 4720 (2024).
- [39] J. U. Wagner and S. Dimmeler, *J. Mol. Cell. Cardiol.* **138**, 136 (2020).
- [40] R. Fitzhugh, *J. Gener. Physiol.* **43**, 867 (1960).
- [41] R. FitzHugh, *Biophys. J.* **1**, 445 (1961).
- [42] J. Nagumo, S. Arimoto, and S. Yoshizawa, *Proc. IRE* **50**, 2061 (1962).
- [43] S. Scialla, A. Loppini, M. Patriarca, and E. Heinsalu, *Phys. Rev. E* **103**, 052211 (2021).
- [44] S. Scialla, M. Patriarca, and E. Heinsalu, *Europhys. Lett.* **137**, 51001 (2022).
- [45] R. C. Desai and R. Zwanzig, *J. Stat. Phys.* **19**, 1 (1978).
- [46] M. E. Yamakou, E. Heinsalu, M. Patriarca, and S. Scialla, *Phys. Rev. E* **106**, L032401 (2022).
- [47] M. Newman and D. Watts, *Phys. Lett. A* **263**, 341 (1999).
- [48] H. He and E. A. Garcia, *IEEE Trans. Knowl. Data Eng.* **21**, 1263 (2009).
- [49] M. Patriarca, S. Scialla, E. Heinsalu, M. E. Yamakou, and J. H. E. Cartwright, *Chaos* **35**, 073115 (2025).
- [50] C. Morris and H. Lecar, *Biophys. J.* **35**, 193 (1981).
- [51] J. L. Hindmarsh and R. M. Rose, *Proc. R. Soc. B* **221**, 87 (1984).
- [52] E. M. Izhikevich, *IEEE Trans. Neural Netw.* **14**, 1569 (2003).
- [53] C. C. Chow and N. Kopell, *Neural Comput.* **12**, 1643 (2000).
- [54] M. V. L. Bennett and R. S. Zukin, *Neuron* **41**, 495 (2004).
- [55] J. M. Dwulet, J. K. Briggs, and R. K. P. Benninger, *PLoS Comput. Biol.* **17**, e1008948 (2021).

# Curriculum Vitae

## 1. Personal data

Name	Stefano Scialla
Date and place of birth	17 February 1962 - Rome, Italy
Nationality	Italian

## 2. Contact information

Address	National Institute of Chemical Physics and Biophysics, Akadeemia Tee 23, 12618 Tallinn, Estonia
Phone	+39 338 8962616
E-mail	stefano.scialla@kbfi.ee stefano.scialla@unicampus.it

## 3. Education

2022–2025	Tallinn University of Technology, School of Science, Applied Physics and Mathematics, PhD studies
1980–1986	Università “La Sapienza” di Roma (Rome, Italy), Faculty of Science, Chemistry, Laurea <i>summa cum laude</i> (5-year course equivalent to BSc + MSc)

## 4. Language competence

Italian	native
English	C2
French	B2

## 5. Professional employment

2021–Present	Univ. Campus Bio-Medico di Roma (Italy), Adjunct Professor, Dept. of Engineering
2021–Present	National Inst. of Chem. Physics and Biophysics (Estonia), Visiting Research Fellow
2015–2020	Procter & Gamble (Belgium), Senior R&D Director – Fabric & Home Care Technology
2008–2015	Procter & Gamble (Italy), Senior R&D Director – Fabric & Home Care Technology
2005–2008	Procter & Gamble (Italy), Senior R&D Director – Home Care Product Design
2002–2005	Procter & Gamble (Belgium), Senior R&D Director – Fabric Care Product Design
1998–2002	Procter & Gamble (Italy), Senior R&D Director – New Business Development
1994–1998	Procter & Gamble (Italy), R&D Director – Bleach & Laundry Additives and Home Care
1992–1994	Procter & Gamble (Italy), Senior Scientist – Bleach & Laundry Additives
1988–1992	Procter & Gamble (Italy), Scientist – Bleach & Laundry Additives
1987–1987	Queen’s Univ. of Belfast (UK), Assistant Researcher
1986–1986	Daresbury Laboratories (UK), Assistant Researcher

## 6. Voluntary work

- 2021–Present Univ. Campus Bio-Medico di Roma (Italy), Grand Challenges Scholars Program Director
- 2024–Present Association “Per la strada”, Homeless Meal Program

## 7. Computer skills

- Operating systems: Windows
- Document preparation: WfW and Office, LaTeX
- Programming languages: Julia, FORTRAN
- Scientific packages: Materials Studio, JMP

## 8. Honours and awards

- 2014, Prize “Città di Arpino”, in recognition of professional achievements
- 2023, Member of the “Accademia di Storia dell’Arte Sanitaria” (Academy of History of Healthcare Art), by appointment of the Italian Ministry of Culture

## 9. Defended theses

- 1986, *The computation of the exchange interaction in electron-molecule collisions*, MSc, supervisor Prof. Francesco A. Gianturco, Università “La Sapienza” di Roma (Rome, Italy), Department of Chemistry

## 10. Fields of research

- Complex systems
- Biophysics
- Molecular physics
- Nanomedicine
- Interfacial chemistry

## 11. Scientific work

### Papers

1. S. Scialla, M. Patriarca, E. Heinsalu, M. E. Yamakou, and J. H. E. Cartwright, “Effect of diversity distribution symmetry on global oscillations of networks of excitable units,” *Phys. Rev. E*, vol. 112, p. 054201, 2025
2. M. Patriarca, S. Scialla, E. Heinsalu, M. E. Yamakou, and J. H. E. Cartwright, “Dynamical equivalence between resonant translocation of a polymer chain and diversity-induced resonance,” *Chaos*, vol. 35, p. 073115, 2025
3. M. V. Tamm, E. Heinsalu, S. Scialla, and M. Patriarca, “Learning thresholds lead to stable language coexistence,” *Phys. Rev. E*, vol. 111, no. 2, p. 024304, 2025
4. L. Marcotullio, P. Gröb, S. Scialla, and P. Saveyn, “Understanding perfume deposition mechanisms on different textile substrates in a realistic laundering process,” *Journal of Surfactants and Detergents*, vol. 28, no. 4, pp. 731–745, 2025

5. X. Han, S. Scialla, E. Limiti, E. T. Davis, M. Trombetta, A. Rainer, S. W. Jones, E. Mauri, and Z. J. Zhang, "Nanoscope gel particle for intra-articular injection formulation," *Biomaterials Advances*, vol. 163, p. 213956, 2024
6. S. Scialla, J. K. Liivand, M. Patriarca, and E. Heinsalu, "A three-state language competition model including language learning and attrition," *Frontiers in Complex Systems*, vol. 1, 2023
7. E. Mauri and S. Scialla, "Nanogels based on hyaluronic acid as potential active carriers for dermatological and cosmetic applications," *Cosmetics*, vol. 10, no. 4, p. 113, 2023
8. M. E. Yamakou, E. Heinsalu, M. Patriarca, and S. Scialla, "Diversity-induced decoherence," *Phys. Rev. E*, vol. 106, p. L032401, 2022
9. S. M. Giannitelli, E. Limiti, P. Mozetic, F. Pinelli, X. Han, F. Abbruzzese, F. Basoli, D. D. Rio, S. Scialla, F. Rossi, M. Trombetta, L. Rosanò, G. Gigli, Z. J. Zhang, E. Mauri, and A. Rainer, "Droplet-based microfluidic synthesis of nanogels for controlled drug delivery: tailoring nanomaterial properties via pneumatically actuated flow-focusing junction," *Nanoscale*, vol. 14, no. 31, pp. 11415–11428, 2022
10. S. Scialla, M. Patriarca, and E. Heinsalu, "The interplay between diversity and noise in an excitable cell network model," *EPL*, vol. 137, p. 51001, 2022
11. E. Limiti, P. Mozetic, S. M. Giannitelli, F. Pinelli, X. Han, D. D. Rio, F. Abbruzzese, F. Basoli, L. Rosanò, S. Scialla, M. Trombetta, G. Gigli, Z. J. Zhang, E. Mauri, and A. Rainer, "Hyaluronic acid–polyethyleneimine nanogels for controlled drug delivery in cancer treatment," *ACS Applied Nano Materials*, vol. 5, no. 4, pp. 5544–5557, 2022
12. S. Scialla, A. Loppini, M. Patriarca, and E. Heinsalu, "Hubs, diversity, and synchronization in FitzHugh-Nagumo oscillator networks: Resonance effects and biophysical implications," *Phys. Rev. E*, vol. 103, p. 052211, 2021
13. K. A. Berrington, V. M. Burke, P. G. Burke, and S. Scialla, "Electron impact excitation of  $n=3$  states of C III: an application of a new R-matrix package," *Journal of Physics B: Atomic, Molecular and Optical Physics*, vol. 22, no. 4, pp. 665–676, 1989
14. F. A. Gianturco, L. C. Pantano, and S. Scialla, "Low-energy structure in electron-silane scattering," *Phys. Rev. A*, vol. 36, no. 2, pp. 557–563, 1987
15. F. A. Gianturco and S. Scialla, "Low-energy electron scattering from water molecules: A study of angular distributions," *The Journal of Chemical Physics*, vol. 87, no. 11, pp. 6468–6473, 1987
16. F. A. Gianturco and S. Scialla, "Local approximations of exchange interaction in electron-molecule collisions: the methane molecule," *Journal of Physics B: Atomic and Molecular Physics*, vol. 20, no. 13, pp. 3171–3189, 1987

### Contributed talks

1. S. Scialla, M. Patriarca, E. Heinsalu, M. E. Yamakou, and J. H. E. Cartwright. *Effect of diversity distribution symmetry on global oscillations of networks of excitable units*, Dynamics Days Europe 2025: 23–27 June 2025, Thessaloniki, Greece

2. S. Scialla, M. Patriarca, E. Heinsalu, M. E. Yamakou, and J. H. E. Cartwright. *Asymmetry in the distribution of unit properties is the key factor determining the efficiency of collective oscillations in FitzHugh-Nagumo networks*, Conference on Complex Systems CCS 2024: 2–6 September 2024, Exeter, UK
3. S. Scialla, J. K. Liivand, M. Patriarca, E. Heinsalu. *The impact of memory and heterogeneity on language competition dynamics*, Dynamics Days Europe 2023: 3–8 September 2023, Naples, Italy
4. S. Scialla, J. K. Liivand, M. Patriarca, E. Heinsalu. *The effect of memory and heterogeneity in an agent-based language competition model*, Conference on Complex Systems CCS 2022: 17–21 October 2022, Palma de Mallorca, Spain
5. S. Scialla, M. Patriarca, E. Heinsalu. *Hubs, diversity, and noise in FitzHugh-Nagumo oscillator networks: Synchronization and Resonances*, SR 40 1981-2021 Forty Years of Stochastic Resonance: 13–15 September 2021, Perugia, Italy

## Chapters

1. P. Morganti and S. Scialla, “Nanoparticles, nanofibrils, and tissues as novel carriers in cosmetic dermatology,” in *Soft Particles*, pp. 257–287, Elsevier, 2023
2. S. Scialla and O. Todini, “Liquid bleach formulations,” in *Handbook of Detergents, Part D*, pp. 179–206, CRC Press, 2005
3. S. Scialla, “The formulation of liquid household cleaners,” in *Handbook of Detergents, Part D*, pp. 153–177, CRC Press, 2005
4. F. A. Gianturco and S. Scialla, “A parameter-free theoretical model for low-energy electron scattering from polyatomic molecules,” in *Nonequilibrium Processes in Partially Ionized Gases*, pp. 323–332, Springer US, 1990
5. F. A. Gianturco and S. Scialla, “Electron scattering by polyatomic molecules: Recent advances in theory and calculations,” in *Electron-Molecule Scattering and Photoionization*, pp. 169–186, Springer US, 1988

## Patents

207 international patents. See full list on ResearchGate:

<https://www.researchgate.net/profile/Stefano-Scialla/publications>

or Google Scholar:

<https://scholar.google.com/citations?hl=it&user=gMh152EAAAAJ>

# Elulookirjeldus

## 1. Isikuandmed

Nimi Stefano Scialla  
Sünniaeg ja -koht 17.01.1962 - Rooma, Itaalia  
Kodakondsus itaalia

## 2. Kontaktandmed

Address Keemilise ja Bioloogilise Füüsika Instituut,  
Akadeemia Tee 23, 12618 Tallinn, Estonia  
Telefon +39 338 8962616  
E-post stefano.scialla@kbfi.ee  
stefano.scialla@unicampus.it

## 3. Haridus

2022–2025 Tallinna Tehnikaülikool, Loodusteaduste teaduskond,  
rakendusfüüsika ja matemaatika, doktoriõpe  
1980–1986 Rooma Ülikool “La Sapienza” (Rooma, Itaalia), Loodusteaduste teaduskond,  
keemia, Laurea *summa cum laude* (5-year course equivalent to BSc + MSc)

## 4. Keelteoskus

Itaalia keel emakeel  
Inglise keel C2  
Prantsuse keel B2

## 5. Teenistuskäik

2021–praegu Univ. Campus Bio-Medico di Roma (Itaalia), Adjunct Professor, Dept. of  
Engineering  
2021–praegu Keemilise ja Bioloogilise Füüsika Instituut (Eesti), Visiting Research Fellow  
2015–2020 Procter & Gamble (Belgium), Senior R&D Director – Fabric & Home Care  
Technology  
2008–2015 Procter & Gamble (Italy), Senior R&D Director – Fabric & Home Care Tech-  
nology  
2005–2008 Procter & Gamble (Italy), Senior R&D Director – Home Care Product De-  
sign  
2002–2005 Procter & Gamble (Belgium), Senior R&D Director – Fabric Care Product  
Design  
1998–2002 Procter & Gamble (Italy), Senior R&D Director – New Business Develop-  
ment  
1994–1998 Procter & Gamble (Italy), R&D Director – Bleach & Laundry Additives and  
Home Care  
1992–1994 Procter & Gamble (Italy), Senior Scientist – Bleach & Laundry Additives  
1988–1992 Procter & Gamble (Italy), Scientist – Bleach & Laundry Additives  
1987–1987 Queen’s Univ. of Belfast (UK), Assistant Researcher  
1986–1986 Daresbury Laboratories (UK), Assistant Researcher

## 6. Voluntary work

- 2021–praegu Univ. Campus Bio-Medico di Roma (Itaalia), Grand Challenges Scholars Program Director
- 2024–praegu MTÜ “Per la strada”, Kodutute toitlustusprogramm

## 7. Computer skills

- Operatsioonisüsteemid: Windows
- Kontoritarkvara: WfW, Office, LaTeX
- Programmeerimiskeeled: Julia, FORTRAN
- Teadustarkvara paketid: Materials Studio, JMP

## 8. Autasud

- 2014, Auhind “Città di Arpino” professionaalsete saavutuste tunnustuseks
- 2023, Liige organisatsioonis “Accademia di Storia dell’Arte Sanitaria” (Tervishoiukunsti Ajaloo Akadeemia), määratud Itaalia kultuuriministeeriumi poolt

## 9. Kaitstud lõputööd

- 1986 – *The computation of the exchange interaction in electron-molecule collisions*, magistritöö, juhendaja prof. Francesco A. Gianturco, Rooma Ülikool “La Sapienza”, Keemiaosakond (Rooma, Itaalia)

## 10. Teadustöö põhisuunad

- Kompleksed süsteemid
- Biofüüsika
- Molekulaarfüüsika
- Nanomeditsiin
- Pindade keemia

## 11. Teadustegevus

### Artiklid

1. S. Scialla, M. Patriarca, E. Heinsalu, M. E. Yamakou, and J. H. E. Cartwright, “Effect of diversity distribution symmetry on global oscillations of networks of excitable units,” *Phys. Rev. E*, vol. 112, p. 054201, 2025
2. M. Patriarca, S. Scialla, E. Heinsalu, M. E. Yamakou, and J. H. E. Cartwright, “Dynamical equivalence between resonant translocation of a polymer chain and diversity-induced resonance,” *Chaos*, vol. 35, p. 073115, 2025
3. M. V. Tamm, E. Heinsalu, S. Scialla, and M. Patriarca, “Learning thresholds lead to stable language coexistence,” *Phys. Rev. E*, vol. 111, no. 2, p. 024304, 2025
4. L. Marcotullio, P. Gröb, S. Scialla, and P. Saveyn, “Understanding perfume deposition mechanisms on different textile substrates in a realistic laundering process,” *Journal of Surfactants and Detergents*, vol. 28, no. 4, pp. 731–745, 2025

5. X. Han, S. Scialla, E. Limiti, E. T. Davis, M. Trombetta, A. Rainer, S. W. Jones, E. Mauri, and Z. J. Zhang, "Nanoscope gel particle for intra-articular injection formulation," *Biomaterials Advances*, vol. 163, p. 213956, 2024
6. S. Scialla, J. K. Liivand, M. Patriarca, and E. Heinsalu, "A three-state language competition model including language learning and attrition," *Frontiers in Complex Systems*, vol. 1, 2023
7. E. Mauri and S. Scialla, "Nanogels based on hyaluronic acid as potential active carriers for dermatological and cosmetic applications," *Cosmetics*, vol. 10, no. 4, p. 113, 2023
8. M. E. Yamakou, E. Heinsalu, M. Patriarca, and S. Scialla, "Diversity-induced decoherence," *Phys. Rev. E*, vol. 106, p. L032401, 2022
9. S. M. Giannitelli, E. Limiti, P. Mozetic, F. Pinelli, X. Han, F. Abbruzzese, F. Basoli, D. D. Rio, S. Scialla, F. Rossi, M. Trombetta, L. Rosanò, G. Gigli, Z. J. Zhang, E. Mauri, and A. Rainer, "Droplet-based microfluidic synthesis of nanogels for controlled drug delivery: tailoring nanomaterial properties via pneumatically actuated flow-focusing junction," *Nanoscale*, vol. 14, no. 31, pp. 11415–11428, 2022
10. S. Scialla, M. Patriarca, and E. Heinsalu, "The interplay between diversity and noise in an excitable cell network model," *EPL*, vol. 137, p. 51001, 2022
11. E. Limiti, P. Mozetic, S. M. Giannitelli, F. Pinelli, X. Han, D. D. Rio, F. Abbruzzese, F. Basoli, L. Rosanò, S. Scialla, M. Trombetta, G. Gigli, Z. J. Zhang, E. Mauri, and A. Rainer, "Hyaluronic acid–polyethyleneimine nanogels for controlled drug delivery in cancer treatment," *ACS Applied Nano Materials*, vol. 5, no. 4, pp. 5544–5557, 2022
12. S. Scialla, A. Loppini, M. Patriarca, and E. Heinsalu, "Hubs, diversity, and synchronization in FitzHugh-Nagumo oscillator networks: Resonance effects and biophysical implications," *Phys. Rev. E*, vol. 103, p. 052211, 2021
13. K. A. Berrington, V. M. Burke, P. G. Burke, and S. Scialla, "Electron impact excitation of  $n=3$  states of C III: an application of a new R-matrix package," *Journal of Physics B: Atomic, Molecular and Optical Physics*, vol. 22, no. 4, pp. 665–676, 1989
14. F. A. Gianturco, L. C. Pantano, and S. Scialla, "Low-energy structure in electron-silane scattering," *Phys. Rev. A*, vol. 36, no. 2, pp. 557–563, 1987
15. F. A. Gianturco and S. Scialla, "Low-energy electron scattering from water molecules: A study of angular distributions," *The Journal of Chemical Physics*, vol. 87, no. 11, pp. 6468–6473, 1987
16. F. A. Gianturco and S. Scialla, "Local approximations of exchange interaction in electron-molecule collisions: the methane molecule," *Journal of Physics B: Atomic and Molecular Physics*, vol. 20, no. 13, pp. 3171–3189, 1987

### **Ettekanded konverentsidel**

1. S. Scialla, M. Patriarca, E. Heinsalu, M. E. Yamakou, and J. H. E. Cartwright. *Effect of diversity distribution symmetry on global oscillations of networks of excitable units*, Dynamics Days Europe 2025: 23–27 June 2025, Thessaloniki, Greece

2. S. Scialla, M. Patriarca, E. Heinsalu, M. E. Yamakou, and J. H. E. Cartwright. *Asymmetry in the distribution of unit properties is the key factor determining the efficiency of collective oscillations in FitzHugh-Nagumo networks*, Conference on Complex Systems CCS 2024: 2–6 September 2024, Exeter, UK
3. S. Scialla, J. K. Liivand, M. Patriarca, E. Heinsalu. *The impact of memory and heterogeneity on language competition dynamics*, Dynamics Days Europe 2023: 3–8 September 2023, Naples, Italy
4. S. Scialla, J. K. Liivand, M. Patriarca, E. Heinsalu. *The effect of memory and heterogeneity in an agent-based language competition model*, Conference on Complex Systems CCS 2022: 17–21 October 2022, Palma de Mallorca, Spain
5. S. Scialla, M. Patriarca, E. Heinsalu. *Hubs, diversity, and noise in FitzHugh-Nagumo oscillator networks: Synchronization and Resonances*, SR 40 1981-2021 Forty Years of Stochastic Resonance: 13–15 September 2021, Perugia, Italy

### **Raamatupeatükid**

1. P. Morganti and S. Scialla, “Nanoparticles, nanofibrils, and tissues as novel carriers in cosmetic dermatology,” in *Soft Particles*, pp. 257–287, Elsevier, 2023
2. S. Scialla and O. Todini, “Liquid bleach formulations,” in *Handbook of Detergents, Part D*, pp. 179–206, CRC Press, 2005
3. S. Scialla, “The formulation of liquid household cleaners,” in *Handbook of Detergents, Part D*, pp. 153–177, CRC Press, 2005
4. F. A. Gianturco and S. Scialla, “A parameter-free theoretical model for low-energy electron scattering from polyatomic molecules,” in *Nonequilibrium Processes in Partially Ionized Gases*, pp. 323–332, Springer US, 1990
5. F. A. Gianturco and S. Scialla, “Electron scattering by polyatomic molecules: Recent advances in theory and calculations,” in *Electron-Molecule Scattering and Photoionization*, pp. 169–186, Springer US, 1988

### **Patendid**

207 rahvusvahelist patenti. Täielik loetelu ResearchGate'is:

<https://www.researchgate.net/profile/Stefano-Scialla/publications>

või Google Scholaris:

<https://scholar.google.com/citations?hl=it&user=gMh152EAAAAJ>

ISSN 2585-6901 (PDF)  
ISBN 978-9916-80-426-1 (PDF)